Functional brain networks in multiple sclerosis: linking structural pathology to clinical disability

Prejaas Tewarie

© Copyright P.K.B. Tewarie, 2014
All rights reserved. No part of this publication may be reproduced, stored in a retrieval system, or transmitted, in any form or by any means, electronically, mechanically, by photocopying, recording, or otherwise, without the prior written permission of the author.

Lay-out by: Nikki Vermeulen, Ridderprint BV, Ridderkerk, the Netherlands
Printed by: Ridderprint BV, Ridderkerk, the Netherlands

ISBN: 978-90-5335-963-1

VRIJE UNIVERSITEIT

Functional brain networks in multiple sclerosis: linking structural pathology to clinical disability

ACADEMISCH PROEFSCHRIFT

ter verkrijging van de graad Doctor aan
de Vrije Universiteit Amsterdam,
op gezag van de rector magnificus
prof.dr. F.A. van der Duyn Schouten,
in het openbaar te verdedigen
ten overstaan van de promotiecommissie
van de Faculteit der Geneeskunde
op vrijdag 19 december 2014 om 9.45 uur
in de aula van de universiteit,
De Boelelaan 1105

door

Prejaas Kavish Baldewpersad Tewarie

geboren te Amsterdam

PROMOTIECOMMISSIE

promotoren:	prof.dr. C.J. Stam prof.dr. C.H. Polman
copromotoren:	dr.ir. A. Hillebrand prof.dr. F. Barkhof

"Architect, finally I have met you. You will not rebuild your house again... Oh lord of my own ego, you are pure illusion, you do not exist. The earth is my witness"

Gautama Buddha, Dhammapada 11:154

Voor mijn ouders & grootouders

CONTENTS

Chapter 1

General introduction

MULTIPLE SCLEROSIS: A GENERAL INTRODUCTION

The brain and the central nervous system play a vital role in controlling organs throughout the human body, but are also essential for the characteristics that make us human such as our locomotion, cognitive abilities, emotions and behaviour. Multiple sclerosis (MS) is a chronic disorder of the central nervous system that can affect all these capabilities and therefore often leads to a large burden to the patient (Compston and Coles, 2008). The exact aetiology and pathophysiology of the disease remain to be elucidated, but MS is considered to be both an inflammatory demyelinating and neurodegenerative disease (Pirko et al., 2007). The relationship between inflammation and the neurodegenerative component is a matter of debate, as it has been claimed that either inflammation is the cause of neurodegeneration (outside-in-model) or that neurodegeneration induces inflammation (inside-out-model) (Stys et al., 2012). Especially in the initial phases of the disease, inflammation is often the cause of the first clinical episodes of neurological dysfunction such as optic neuritis (inflammation of the optic nerve), muscle weakness, sensory deficits, balance problems, or fatigue. Patients often fully or partially recover from these episodes, also called relapses (Compston and Coles, 2008). Apart from physical disability, MS patients also suffer from cognitive impairment which can occur at any stage during the disease. In particular information processing speed, visual memory and verbal memory are the cognitive domains that are mostly affected (Chiaravalloti and DeLuca, 2008).

MS can be categorized in different disease types (Lublin et al., 2014). The largest proportion of patients suffers from relapsing remitting (RR-) MS, characterised by relapses during the disease course. Later on in the disease the relapsing remitting course can co-occur with a slow progressive disease course of neurological disability entailing the transition to secondary progressive (SP-) MS. It is claimed that this slowly progressive phase of the disease is due to neurodegeneration rather than inflammation (Geurts and Barkhof, 2008). Apart from the RR- and SP- subtypes, the onset of MS can also be characterized by a slow progression of neurological disability, referred to as primary progressive (PP-) MS (Cottrell et al., 1999). Initial research in MS has largely focused on the mechanisms that lead to inflammation and the relationship between inflammation and clinical disability (here defined as physical disability and cognitive impairment). This has subsequently led to disease modifying therapies that efficiently slow down inflammation. However, MS patients still deteriorate even when inflammation is efficiently tackled, for which the neurodegenerative component of the disease may be responsible (Daams et al., 2013). In the context of neuro-inflammation and neurodegeneration, emphasis has largely been laid on structural measures such as white matter lesion load, grey matter lesions or volumetric measures in order to gain an understanding of the relationship between MS pathology and clinical dysfunction.

In this dissertation a different route is followed where it is hypothesized that brain functioning is important for the understanding of clinical dysfunction in MS. The rationale behind this approach stems from the notion that the brain can be considered as a hierarchical system formed by a circular and causal interplay between structure and function, and its optimal functioning underlies normal

cognition. Brain functioning here is regarded as patterns of communication between brain regions (Bullmore and Sporns, 2009). The set of all communication routes between brain regions is called a functional network, which can also be considered as the traffic of communication. As might be expected, this traffic of communication flows on 'roads and highways' in the brain (physical connections) which are referred to as the structural network. Therefore, the aim of this dissertation is to investigate if disruption of these structural and functional brain networks can explain the occurrence of clinical dysfunction in MS. Furthermore, it is highly likely that structural MS pathology may be associated with disruption or damage of these networks. Therefore, as a second step, it is further investigated how structural pathology in MS may affect these structural and functional brain networks. The potential advantage of this approach is that it could allow us to bridge the gap between structural pathology and clinical dysfunction in MS. The following sections explain the reconstruction of structural and functional networks in MS obtained from magnetoencephalography (MEG) recordings and functional magnetic resonance imaging (fMRI) scans.

Neuronal activity

In order to reconstruct functional networks, neuronal activity needs to be measured, for which functional neuroimaging modalities such as MEG and fMRI are frequently used. MEG and fMRI are complementary techniques as MEG has high temporal resolution but varying spatial resolution, in contrast to fMRI, which has low temporal resolution and high spatial resolution.

MRI is an imaging modality that picks up changes in tissue magnetization (Haacke et al., 1999). In order to measure this, a strong external magnetic field induced by a superconducting coil is used such that all nuclear spins in the tissue align, leading to a net magnetization. By applying radio frequency pulses at the desired resonant frequency, net magnetization is tilted away from the direction of the external static magnetic field. Then, the rotation of the transverse component of the magnetization, "precession", induces a current in MR pick-up coils (the MR signal). The contrast between tissues emerges from the difference in decay behavior of the net tissue magnetization in its return to the equilibrium state, i.e. aligned to the strong external magnetic field. The high spatial encoding in MRI is achieved by using gradient magnetic fields and also determined by the strength of the external magnetic field. fMRI is a technique that captures the change in tissue magnetization due to de-oxygenation or oxygenation that is called blood oxygenation level dependency (BOLD) (Ogawa et al., 1992). It is assumed that that changes in blood oxygenation are especially related to changes in post-synaptic activity as quantified by local field potentials (LFPs) (Ojemann et al., 2013). Therefore, this allows us to indirectly estimate neuronal activity with fMRI (Buxton et al., 1998; Logothetis, 2008; Logothetis et al., 2001).

MEG is a technique that directly assesses neuronal activity by measuring fluctuations in magnetic fields originating from synchronous activity from large neuronal populations (Hamalainen et al., 1993). The generation of these magnetic fields can be understood by considering Maxwell's equations, and especially Ampere's law

$$\vec{\nabla} \times \vec{B} = \mu\left(\vec{J} + \varepsilon \frac{\partial \vec{E}}{\partial t}\right) \quad (1)$$

that describes how a magnetic field $\vec{B}$ is induced by a current density $\vec{J}$ and a fluctuating electric field $\partial\vec{E}/\partial t$, and where μ and ε refer to the permeability and permittivity of brain tissue. The induced magnetic fields $\vec{B}$ are circular around $\vec{J}$ denoted by the curl of $\vec{B}$, i.e. $\left(\vec{\nabla} \times \vec{B}\right)$. Induced magnetic fields in the brain can be understood under the assumption of the quasi-static Maxwell equations which entails that the contribution of fluctuating electric fields $\partial\vec{E}/\partial t$ is negligible in inducing magnetic fields, i.e. $\left|\varepsilon \cdot \partial\vec{E}/\partial t\right| << \left|\vec{J}\right|$ (generally holds for frequencies < 100Hz) (Hamalainen et al., 1993). This leaves us with the current density $\vec{J}$ as the source for fluctuating magnetic fields in the brain. These sources are predominantly currents induced by post-synaptic potentials and thus form the main contribution to the signal measured by MEG (Murakami and Okada, 2006). The fluctuating magnetic fields predominantly originated from post-synaptic potentials are generally very weak (in the order of femto-Tesla) and therefore require very sensitive magnetic detectors. To this end, the MEG apparatus uses superconducting quantum interference devices (SQUIDs). To enhance the detection of the magnetic field captured by SQUIDs additional superconducting coils *(flux transformers*) are coupled to the SQUIDS: magnetometers and gradiometers. The former detects the magnetic field from especially nearby sources, whereas the latter detects a spatial gradient of the magnetic field rather than the magnetic field itself and is therefore less sensitive for noise from distant non-neuronal sources (Hansen et al., 2010). Finally, SQUIDS convert the magnetic fields into electrical signals that are subsequently digitized.

Unfortunately, MEG is affected by the ill-posed nature of the inverse problem, i.e. there is no unique solution of reconstructing the spatial distribution of neuronal activity in the brain based on the extra-cranial recordings (source localization) (Helmholtz, 1853). However, by introducing assumptions it is possible to solve the inverse problem. A widely accepted method to reconstruct neuronal activity at the source level, and one that has been used in this dissertation is beamforming. Compared to other source localization methods such as Loreta or minimum norm estimation, the beamformer approach uses a minimum amount of assumptions that at the same time have a physiological basis (Hillebrand and Barnes, 2005). Beamforming can be considered as a spatial filtering approach that reconstructs the neuronal activity at a source as a weighted sum of the activity at all the sensors. The main assumption behind the beamformer approach is that spatially distinct neuronal sources are linearly independent (Hillebrand and Barnes, 2005). This linear independence is achieved by using two constraints, the unit gain constraint and the minimum variance constraint, together leading to a spatial filter that is an approximation of an ideal filter. A more in-depth explanation of the beamforming approach can be found in subsequent chapters and particularly in (Hillebrand et al., 2005; Hillebrand et al., 2012; Hillebrand and Barnes, 2005).

Functional connectivity

Functional connectivity refers to the existence of any statistical interdependency between the activation profiles of distinct neuronal populations, with the assumption that this interdependency is a reflection of communication between these neuronal populations (Aertsen and Preissl, 1991). Functional connectivity measures can be divided into linear and non-linear measures (Pereda et al., 2005). For fMRI linear measures are most often used, since it is assumed that these linear measures adequately capture the information contained in the fMRI BOLD signals (Hlinka et al., 2011).

However, for MEG, linear measures fail to take into account the non-linear information contained in the time-series and, moreover, these measures are highly sensitive to volume conduction and field spread (Vindiola et al., 2014). Volume conduction refers to the magnetic fields that are induced by *ohmic return currents* in surrounding tissue. In a perfect sphere these volume conduction effects cancel out, however, the head is not a perfect sphere and therefore MEG measurements still slightly suffer from volume conduction (Nunez et al., 1997). Field spread refers to the problem that the signal from one source spreads over multiple MEG sensors. Unfortunately, many linear and non-linear measures for functional connectivity fail to correct for volume conduction or field spread. Therefore, in this dissertation functional connectivity is estimated with a measure that is largely insensitive to volume conduction or field spread, the phase lag index (PLI) (Stam et al., 2007). This measure takes into account the information contained in the phases of the time-signals, formally defined as "the fractional part of a period through which an oscillating signal has moved, as measured at any point in time from an arbitrary time origin" (Licker, 2002). From non-linear dynamics it is well known that two dynamical systems interact if they are weakly coupled. Weak coupling implies that there is an interaction between one state variable of the two systems without causing the dynamical systems to become identical. For example, there can be a stable phase-shift between two time-signals while their amplitudes can remain irregular and uncorrelated. Phase synchronization is a form of weak coupling and entails that the phase difference between two time-signals is *bounded* (Pikovsky et al., 2001). In our case, estimation of the instantaneous phase of every time signal $x(t)$ is obtained by first computing the analytical signal $a(t)$, given by

$$a(t) = x(t) + \frac{i}{\pi} p.v. \int_{-\infty}^{\infty} \frac{x(\tau)}{t-\tau} d\tau \ . \tag{2}$$

Here i refers to the imaginary unit and p.v. (Cauchy principal value) ensures that the integral is defined even in the case for improper integrals. The second term on the right hand-side of Eq. 2 refers to the Hilbert transform of $x(t)$. The instantaneous phase is then deduced by

$$\phi(t) = \arctan\left(\frac{\mathrm{Re}\{a(t)\}}{\mathrm{Im}\{a(t)\}}\right) \tag{3}$$

where *Re* and *Im* correspond to the real and imaginary part of the analytical signal respectively. Subsequently, the PLI is computed based on the instantaneous phase differences between time-series (Stam et al., 2007)

$$PLI = |< sign[\sin(\Delta\varphi(t_k))] >| . \quad (4)$$

Here the phase difference $\Delta\varphi$ is defined in the interval $[-\pi, \pi]$, <> denotes the mean value, sign stands for signum function and ffIffI indicates the absolute value. The PLI is a measure that calculates the asymmetry of the distribution of instantaneous phase differences between two time-series. The rationale behind this approach is that field spread/volume conduction causes a zero phase lag between two time-series, and that a uniform distribution of phases occurs when there is no coupling at all. The presence of a consistent, non-zero, phase lag between two time-series therefore reflects true interactions that are unaffected by field spread or volume conduction (Stam et al., 2007). Recent findings suggest that this method is capable of removing spurious coupling between time-series at the expense of discarding any physiological interactions with zero lag (Hillebrand et al., 2012). A more detailed explanation of the PLI can be found in subsequent chapters and especially in (Stam et al., 2007).

Structural and functional networks

Modern network theory is a new field that has emerged from the combination of graph theory, statistical mechanics and dynamical systems theory. Networks are formed by a set of nodes interconnected to each other by links. Many systems found in nature and daily life can be described in terms of networks, such as the World Wide Web, collaborations, financial transactions on a stock market, co-authorship, gene expression but also the brain, which can be considered as a network at different scales. At the micro-scale the connections between individual neurons form a network whereas at the meso-scale connections between groups of neurons within a cortical column form a network that can be considered as a functional unit (Ohki et al., 2005). At the macro-scale, structural and functional networks are formed by brain areas consisting of several cortical columns connected by white matter tracts. One of the advantages of network theory is that its rules and principles are general and can be applied to any network, irrespective of its origin and nature. The organization of these networks is called network topology, and it is the topology that determines the stability, efficiency, robustness, and synchronization properties (and many other properties) of these networks.

Network theory has rapidly developed since the advent of network models as these models were able to explain many properties that had been observed in real world networks. Random graphs were one of the first network models that described large-scale networks. The most novel aspect of this model was the stochastic element: the presence of a link in this network was determined by a probability *p* which was independent from any other link in the network (Erdos and Renyi, 1959). Even these random graphs showed non-trivial behaviour with respect to several properties, including robustness. Another reason why random graphs were of particular interest to network scientists was the possibility of analytical treatment of these graphs. However, many realistic networks displayed properties that could not be explained by random network models, for example the occurrence of high clustering, which indicates that neighbours of a node are also interconnected among themselves.

Chapter 1

Discoveries of two models have led to further development within network theory, the small-world model by Watts and Strogatz (1998) and the scale-free model by Barabasi and Albert (1999) (Barabasi and Albert, 1999; Watts and Strogatz, 1998). A small-world network is characterized by high clustering and short path length, where the latter indicates that there is a path between any two nodes via a small number of links. Scale-free networks are networks were some nodes have a much higher degree (number of connections of a node) compared to the other nodes in the network. More specifically, the degree distribution of scale-free networks is characterized by a power law. The main difference between the small-world model and the scale-free model is that only the former is capable of explaining the observed clustering in real networks, whereas only the latter is able to explain the occurrence of high degree nodes as observed in real networks. Another difference between the small-world model and the scale-free models is the way in which they are constructed; the small-world model is based on a rewiring procedure applied to a regular network (a network where all nodes have the same degree) as its starting point. In contrast, scale-free networks were especially constructed by growth models, such as the preferential attachment model, where new nodes are preferentially attached to those 'old' nodes that have a high degree (Barabasi and Albert, 1999). Unfortunately, there is still no suitable network model that explains scale-free and small-world characteristics of large-scale networks at the same time, in a single framework. However, such a model may be crucial for further explaining realistic and real world networks and needs to be a focus for future studies on complex networks. One of the hypotheses is that a combination of scale-free and small-world characteristics may give rise to hierarchical modular networks which are a better resemblance of brain networks (Stam and van Straaten, 2012).

Other important network properties are assortative mixing and community structure (Newman, 2002). Assortativity quantifies the relationship of the degrees between connected nodes. A positive assortativity value indicates that high degree nodes tend to connect to high degree nodes, whereas a negative assortativity value indicates that high degree nodes tend to connect to low degree nodes. Community structure refers to sub-networks within larger networks that consist of sets of nodes with a higher density of connections between them than with nodes outside the set (Girvan and Newman, 2002).

Brain networks can be divided into structural and functional networks. Nodes in both types of networks generally refer to brain regions. Links in functional networks are based on functional connectivity between regions (Bullmore and Sporns, 2009; Stam, 2004), whereas links in structural networks are based on physical connections between brain regions or on the co-variance of regional properties such as cortical thickness between brain regions (Bullmore and Sporns, 2009; He et al., 2007; Tijms et al., 2012). Brain networks can be considered analogous to transportation networks, where the structural network forms the (road/railway) infrastructure upon which information is allowed to flow (functional connections) (Bullmore and Sporns, 2009). Similar to transportation networks, in brain networks there is a mutual relationship between structural and functional networks as functional connections are constrained by the structural topology. At the same time

Hebbian learning mechanisms can strengthen those structural connections that are widely used for functional interactions as opposed to structural connections that are minimally used (Song et al., 2000). Thus, the relation between structural and functional connectivity represents an example of circular causality (Le van Quyen, 2003; Lloret-Climent and Nescolarde-Selva, 2014; Thomas, 2006).

Both structural and functional networks robustly show a highly non-random organization that is characterized by both small-world as well as scale-free characteristics (Bullmore and Sporns, 2012). However, the quantification and comparison of their network topologies is accompanied by several methodological problems (Fornito et al., 2013; van Wijk et al., 2010). Conventional network measures mix information about network topology with other network aspects such as the size of the network (i.e the number of nodes), network density (percentage links present) or the average degree. Normalization procedures are often used to correct for these biases. However, even these normalization procedures do not solve the dependence of size, degree and density effects of conventional network measures and may even exaggerate it (van Wijk et al., 2010). Even the use of weighted networks instead of un-weighted networks does not provide an optimal solution since measures computed on these networks are influenced by (the large number of) noisy connections and by the average functional connectivity or weight strength (van Wijk et al., 2010). Computation of a minimum spanning tree (MST), an acyclic sub-network containing the strongest connections, may enable comparison of the different types of networks without biases as the MST has always a fixed density and is unique if the weights in the original network are unique (Stam et al., 2014). In this dissertation, the capabilities of the MST as an unbiased approach to compare networks are also explored.

AIMS AND OUTLINE

Classical structural pathology, such as white matter lesion load, fails to fully explain clinical disability in MS. To bridge this so-called clinico-radiological paradox, several other structural characteristics have recently received attention, varying from gray or white matter atrophy, reduced gray or white matter integrity, gray matter lesions or deep gray matter damage such as thalamic atrophy. If we assume that there is circular causality between structural and functional brain networks, it can be hypothesized that any form of structural damage (focal or global) could be related to disruption of functional brain networks and thus to clinical dysfunction (Figure 1).

Therefore, in the present dissertation, three research questions are addressed:

1. Can clinical disability be explained by disruption of functional network topology?
2. How is this disruption of functional network topology related to structural network topology and other forms of structural pathology, such as (deep) gray matter atrophy?
3. How can computational modelling help to investigate the relationship between structural and functional networks?

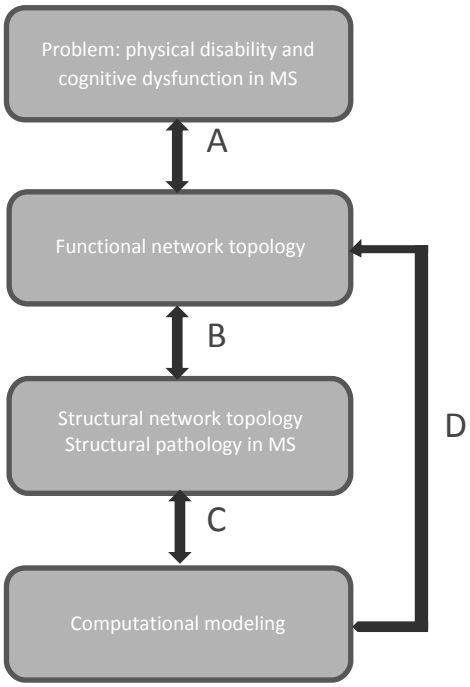

Figure 1: The aim of this dissertation is to investigate the relationship between functional network topology and clinical disability in MS on one hand (A) and at the same time to investigate the link between structural pathology and functional network topology (B). The letters in the figure correspond to relationships between the boxes. The letters C and D correspond to the use of computational models to study the effect of structural pathology on neuronal dynamics and functional network topology.

This dissertation is divided into two sections. The first section consists of methodological and computational approaches that allow us to develop a theoretical framework in order to investigate the relationship between structural and functional networks. In the second section the methodology that has been developed in section one is applied to structural and functional networks in MS.

Theoretical neuroscience and computational modelling may be helpful to investigate the emergence of functional networks and even the disruption of these networks in pathology such as MS. Manipulations during network simulations may mimic the independent contribution of several types of pathology (global or regional atrophy, gray or white matter lesions) and their effect on functional network topology. The most common computational models to simulate neuronal activity and functional networks are neural mass models. These models are based on mean-field approximations that are only valid when the underlying system is homogenous. In **chapter 2** it is investigated to what extent neural mass models based on mean-field approximations capture the mean activity of a neuronal population when the underlying population is in-homogenous, as expected in MS (Figure 1*C* and *D*). To this end, the spectral densities of neural mass signals and the average network signals are compared. In **chapter 3** the aim is to investigate how properties of the structural network allow us to predict functional network connectivity based on both fMRI and MEG data (Figure 1*B*). In order to estimate the relationship between the two types of networks, first modality-invariant functional connections are quantified that serve as the basis for further analysis. We then hypothesized that the functional connections can be understood near a phase transition for functional connectivity and as the weighted sum of the Euclidean distance and the structural degree product. In **chapter 4** a methodological analysis is performed that forms the very basis for the subsequent functional network studies in MS. Here, it is investigated if an MST approach is able to overcome methodological difficulties with respect to network comparison by analysing if MST metrics are equally sensitive for changes in mean connectivity and network density as conventional network measures. Secondly, it is investigated if topological changes in this sub-network are also related to conventional network measures computed on the underlying network since this would increase the interpretability of MST studies compared to conventional network studies.

Section two starts with **chapter 5**. From **chapter 5** on the theoretical framework developed in section one is applied to structural and functional brain networks in MS. In **chapter 5** it is investigated how changes in local oscillatory activity in MS patients are related to cognitive problems (Figure 1*A*). These analyses are followed in **chapter 6** where the aim is to bridge the gap between structural pathology, in particular thalamic atrophy, and cognitive and clinical dysfunction by considering functional connectivity as an intermediate (Figure 1*A* and *B*). We hypothesized that especially disruption of MEG resting-state networks, and in particular the default mode network, would be a good correlate for clinical disability in MS rather than global functional connectivity. In **chapter 7** it is argued that by merely investigating functional connectivity one may miss the crucial information that is contained in the network topology to understand clinical disability in MS. Due to limitations of conventional network measures, the MST approach is then applied to investigate functional network

topology in MS and at the same time to control for biases such as differences in mean connectivity or network density. Subsequently, associations between network properties computed on the MST and cognitive performance in MS patients is analyzed (Figure 1*A*). The last two chapters can be regarded as test-retest analyses for the obtained MST results from chapter *7* in order to investigate if our MST results for functional networks in MS are robust and reproducible. Furthermore, it is tested if disruption of functional network topology in MS as quantified by the MST is related to the underlying structural pathology. For example, **chapter 8** combines functional networks obtained with MEG and structural co-variance networks in MS and analyzes their relationship in order to bridge the gap between gray matter atrophy and functional network disruption (Figure 1*B*). Both networks are thus analyzed using an MST approach. Lastly, **chapter 9** combines fMRI and MEG to study the topology of functional networks in relation to thalamic atrophy and clinical disability (Figure 1*A* and *B*). The main difference between chapter 6 and chapter 9 is that in the former functional connectivity is studied, in contrast to functional network topology in the latter. Additionally, thalamo-cortical functional connectivity is quantified in chapter 9 to investigate the relationship between thalamic atrophy and cortical functional network topology. Finally, this dissertation is concluded with a summary and a general discussion of the main findings.

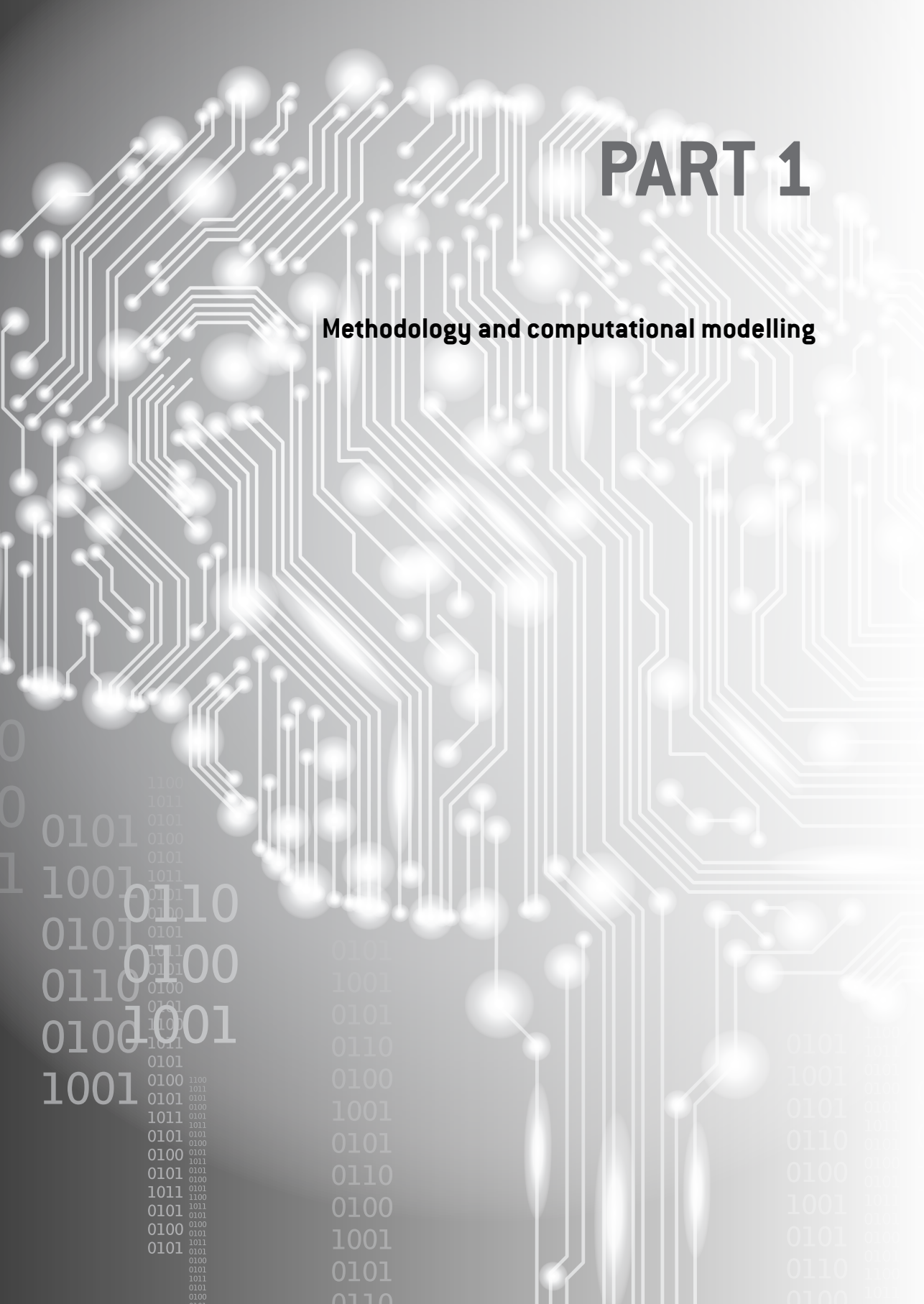

PART 1

Methodology and computational modelling

Chapter 2

Comparing average network signals and neural mass signals in systems with low-synchrony

P. Tewarie, A. Daffertshofer, B.W. van Dijk

In preparation

ABSTRACT

Neural mass models are accepted as efficient modelling techniques to model empirical observations such as disturbed oscillations or neuronal synchronization. Neural mass models are based on the mean-field assumption, i.e. they capture the mean-activity of a neuronal population. However, it is unclear if neural mass models still describe the mean activity of a neuronal population when the underlying neural network topology is not homogenous. Here, we tested whether the mean activity of a neuronal population can be described by neural mass models when there is neuronal loss and when the connections in the network become sparse. To this end, we derived two neural mass models from a conductance based leaky integrate-and-firing (LIF) model. We then compared the power spectral densities of the mean activity of a network of inhibitory and excitatory LIF neurons with that of neural mass models by computing the Kolmogorov-Smirnov test statistic. Firstly, we found that when the number of neurons in a fully connected LIF-network is larger than 300, the neural mass model is a good description of the mean activity. Secondly, if the connection density in the LIF-network does not exceed a critical value, this leads to desynchronization of neurons within the LIF-network and to failure of the neural mass description. Therefore we conclude that neural mass models can be used for analysing empirical observations if the neuronal network of interest is large enough and when neurons in this system synchronize.

1. INTRODUCTION

There is an increasing need in neuroscience to comprehend the enormous amount of empirical data obtained with neuroimaging modalities such as fMRI and MEG/EEG by means of theoretical analysis. Computational approaches such as neural mass models are widely used in this context (Deco et al., 2008). The advantage of neural mass models is that they simulate the average activity of all neurons in a neuronal population, and thereby avoid the overwhelming detailed behaviour of all individual neurons in a neuronal population. However, neural mass models are based on a mean-field approximation, which assumes homogeneity of the underlying neuronal population. As realistic neuronal populations are naturally inhomogeneous, it is unclear to what extent neural mass models are able to capture the average activity of these realistic populations.

The mean field approximation has its roots in statistical physics where it is often applied to reduce many body systems to low dimensional systems (Landau and Lifshitz, 1968). For instance, mean-field theory has been used in ising spin systems to replace individual interactions between atomic spins by an effective mean-field which accounts for the average interaction over all local atomic spins. However, it is known from these systems that a mean-field description fails when this average interaction term is dependent on spatial location (e.g. inhomogeneity), when fluctuations around this average are large or when the size of the system becomes too small.

Mean-field theory has been widely applied in neuroscience where the underlying assumption is it that each neuron in a neuronal population can be described by equivalent statistics and that each neuron converges to the same attractor in phase space (Deco et al., 2008). This allows to describe the dynamics of neuronal population by a limited number of time dependent variables corresponding to the average dynamics of the population (Baladron et al., 2012). The very first studies in neuroscience demonstrated analytically that the mean-field approximation was valid for homogenous neural networks when the numbers of neurons tend to infinity (Amari, 1972; Amari et al., 1977). Ever since, numerous studies have analysed the mean-field in neural networks under diverse conditions such as in finite neural networks (Mattia and Del Giduice, 2002; Touboul and Ermentrout, 2011), with different connectivity patterns (Brunel and Hakim, 1999; Cessac, 1995; Cessac and Vieville T, 2013; Moynot and Samuelides, 2002; Samuelides and Cessac, 2007), using different single-cell neuronal models (Abbott and van Vreeswijk, 1993; Cessac, 2008; Treves, 1993), using realistic parameter regimes (Grabska-Barwinska and Latham, 2013), or as a function of time (Molgedey et al., 2013; Moynot and Samuelides, 2002), the so-called dynamic mean-field approaches.

Despite the large number of previous studies on mean-field approaches in neural networks, both the derivation of neural mass models from single-cell neuronal models and the effect of mean-field approximations involved in this derivation to describe the average activity of realistic inhomogeneous neuronal populations are not fully elucidated (Breakspear et al., 2003; Faugeras et al., 2009; Wong and Wang, 2006). In notable work by Rodrigues and colleagues (2010), two mappings between conductance based leaky integrate-and-fire (LIF) neurons and a commonly used neural mass model

were introduced that allowed for an interpretation of model characteristics between the two scales (Rodrigues et al., 2010). The two models were based on different assumptions with regard to the time scales of the membrane and synaptic activities of neurons, as these time scales were either considered similar or dissimilar. Irrespective of the assumption related to these time-scales, both models resulted in a neural mass model similar to that of the well-known Freeman model (Freeman, 1975). Although these findings form a basis for future research, neurons in the simulated neuronal populations in this study were kept in a non-spiking regime which is not a realistic representation of the underlying physiology as spiking is a prerequisite for neuronal populations to communicate between each other.

In the present study we build upon the work of this previous study and compare neural mass signals with the average signal of inhomogeneous neuronal populations in which individual neurons operate in the spiking regime (Rodrigues et al., 2010). Our main objective is to analyse what the effect of mean-field approximations are for neural mass models when the underlying neuronal population is inhomogeneous. In addition, we investigate the lower limit of neuronal network size for which a neural mass description is still valid. In this study, we use a network of conductance based inhibitory and excitatory LIF neurons to model a neuronal population and we derive two neural mass models from the LIF model. Since it is extremely challenging to solve this comparison problem analytically, we adopt a numerical approach to compare average signals from neuronal populations with neural mass signals. During these analyses, we either decrease the number of neurons or decrease the number of connections in the neuronal population for different network topologies. Lastly, we hypothesize that a discrepancy between the average signal of a neuronal population and the neural mass signal can potentially be explained by desynchronization between neurons in the neuronal population.

2. NEURONAL MODELS

2.1 Network of leaky integrate-and-fire neurons

We consider a population of N LIF neurons (Rudolph-Lilith et al., 2012). A LIF neuron can be regarded as a parallel electric circuit with a resistor, capacitor C and an external input current J_{ext}. Every neuron is described in terms of the dynamics of its membrane potential V_j with $j = 1,E,N$ and its time-dependent synaptic conductances. Conductances are denoted as $g_j^{(\alpha)}$ for every neuron j, which alter due to incoming spikes. Synapses are either excitatory or inhibitory and can be discriminated by α, where $\alpha \in \{E,I\}$. We assume that V_j obeys the stochastic dynamics

$$dV_j = -\frac{1}{\tau}\left[\left(V_j - V_{mem}\right) + \sum_{\alpha}\frac{g_j^{(\alpha)}}{g_0}\left(V_j - V_{syn}^{(\alpha)}\right) - \frac{J_{ext,j}}{C}\right]dt + \sigma\sqrt{2\tau}dW_j \qquad (1)$$

with fixed resting state potential V_{mem} and reversal potentials $V_{syn}^{(\alpha)}$. g_0 is the leak conductance that is considered constant and τ is the membrane time constant. Both constants are assumed to be

identical for all neurons. The membrane time constant τ is related by $\tau = C/g_0$ to the capacitor and membrane conductance constant g_0. τ determines the rise and decay of the membrane potential and $J_{ext,j}$ refers to an external current on neuron j. Every neuron j is under influence of zero-centered, δ correlated, Gaussian white noise W_j with unit variance, i.e. that is $E[W_j] = 0$ and $E[W_j(t)W_k(t')] = \delta_{jk}\delta(t-t')$ where δ_{jk} is the Kronecker's delta function and $\delta(t-t')$ refers to Dirac's delta-function. The noise strength σ is considered identical for all neurons – see Table 1 for values of all constants (Vogels and Abbott, 2005). To simplify our approach and to increase the interpretability of our analyses with previous LIF studies we assume that conductances $g_j^{(\alpha)}$ have an infinitely fast rising time (Yger et al., 2011). This can be assumed when the neurons of interest operate in the high frequency regime which is usually the case for excitatory neurons and often also for inhibitory neurons (Creutzfeldt and Ito, 1968). Therefore, the dynamics of the conductances are described by a first order response and depend on the incoming spikes as follows

$$dg_j^{(\alpha)} = -\frac{1}{\tau^{(\alpha)}}\left[g_j^{(\alpha)} - g_0^{(\alpha)}\left(\phi_{\text{int},j}^{(\alpha)} + \phi_{ext,j}^{(\alpha)}\right)\right]dt \tag{2}$$

Here $g_0^{(\alpha)} \in \{g_0^{(\varepsilon)}, g_0^{(1)}\}$ refer to constants related to the maximal conductance that serves to discriminate between excitatory and inhibitory neurons. $\tau^{(\alpha)}$ determines the decay of synaptic activity which is in general different for inhibitory and excitatory neurons. $\varphi_{int,j}^{(\alpha)}$ and $\varphi_{ext,j}^{(\alpha)}$ corresponds to incoming firing rates from respectively internal and external sources. Due to variation in synaptic conductances the membrane potential of neurons will fluctuate. If these membrane fluctuations reach the threshold potential, the membrane potential is set to a reset potential and kept in a short refractory state of 5 ms.

2.2 Neural mass models

We derive two neural mass mappings from the LIF neuronal model. See appendix B for a detailed derivation of both neural mass mappings. Here, we briefly mention the assumptions and subsequent approximations that are necessary to obtain both neural mass models.

For the first neural mass mapping we follow an approach introduced by Rodrgues et al. 2010 (Rodrigues et al., 2010). Based on experimental indications, the starting assumption here is that we assume that membrane and synaptic time scales are of the same order of magnitude (Destexhe and Sejnowski, 2001; Gerstner and Kistler, 2002). We consider the expectation value of the mean membrane potential V (from Eq. 1), main variable of interest, and the expectation values of the synaptic conductances g_j and firing rates φ_{ij} for inhibitory and excitatory neurons separately (from Eq. 2). Subsequently, we assume that fluctuations of driving forces $g_j^{(\alpha)}(V_j - V_{syn}^{(\alpha)})$ for synaptic currents (in eq. 1) are relatively small which allows for a mean-field approximation $(V_j - V_{syn}^{(\alpha)}) \approx (\hat{V} - V_{syn}^{(\alpha)})$ and simplifies the expression for V. Then, the next assumption entails that time scales of synaptic activity are of the same order irrespective their type, which allows us to combine excitatory and inhibitory synaptic activity into one description. These assumptions lead to modified first order

differential equations (for Eqs. 1 and 2 describing *V* and *g*) and combining these yield a second order differential equation as description for our first neural mass model

$$\left[\tau_{syn}\frac{d}{dt}+1\right]\left[\tau\frac{d}{dt}+1\right]V = V_{mem} - \sum_{\alpha}\frac{g_0^{(\alpha)}}{g_0}\left(\phi_{\text{int}}^{(\alpha)}+\phi_{ext}^{(\alpha)}\right)\left(\hat{V}-V_{syn}^{(\alpha)}\right)+\frac{J_{ext}}{C} \tag{3}$$

Note that the index *j* is omitted in the equation as variables *V* and *g* do not correspond to single neurons anymore but to the expectation value of *Vj* and *gj* and hence the neural mass. We further ignored the reset-rule and the presence of a refractory period, incorporated in the initial LIF equations, as we assume that the most important characteristics that need to be captured are sub-threshold post-synaptic potentials of neurons in the neuronal population. Notice that our first neural mapping model is identical to the widely known neural mass model of Freeman (see Appendix B) (Freeman, 1975). $\varphi_{int,j}^{(\alpha)}$ and $\varphi_{ext,j}^{(\alpha)}$ in Eq. 3 refer to average incoming firing from neurons within and external to the population. Both are assumed to be deterministic and defined as

$$\phi_{\text{int}}^{(\alpha)} = \frac{1}{N}\sum_{j=1}^{N}\sum_{k=1}^{N}\sum_{m}A_{jk}^{(\alpha)}\delta\left(t-t_{k,m}\right) \qquad \text{and} \qquad \phi_{ext,j}^{(\alpha)} = \sum_{j=1}^{N}\sum_{k=1}^{N}\sum_{m}\delta\left(t-t_{ext,j,k,m}^{(\alpha)}\right). \tag{4}$$

Here, $\delta(t\text{-}t')$ refers to the Dirac's delta-function. $t_{k,m}$ is the time of the *m*-th spike of neuron *k* and synapse $\{j,k,\alpha\}$ may also receive external input in the form of spikes at times $t_{ext,j,k,m}^{(\alpha)}$. $A_{j,k}^{(\alpha)}$ is the adjacency matrix describing whether neuron *k* targets neuron *j*.

For the second mapping we question some of the assumptions made in the first mapping and therefore follow a different route. First of all, we question the assumption that driving currents should be considered as constants. Related to this, it is not entirely clear in the former approach why this assumption only applies to synaptic driving currents but not to the leaky driving current. In the second neural mass mapping we follow neural-field like approach. Here, we again consider the expectation values of *V*, $g^{(\alpha)}$, $\varphi_{int}^{(\alpha)}$ and $\varphi_{ext}^{(\alpha)}$ and similarly assume that time scales of synapses agree irrespective of their type. We now combine both first order differential equations of *V* and $g^{(\alpha)}$, which results in a second order differential equation. The main approximation related to neural field-theory is that we follow the assumption that the time scale of the membrane potential is much smaller than the time scale of the synaptic conductivity. This indicates that the membrane potential instantly follows changes at the synapse. Therefore, the dynamics of the membrane potential can be eliminated adiabatically which eventually yields for the mean membrane potential of the second neural mass mapping

$$\left[\tau_{syn}\frac{d}{dt}+1\right]\left[\tau\frac{d}{dt}+1\right]V = V_{mem} - \sum_{\alpha}\frac{g_0^{(\alpha)}}{g_0}\left(\phi_{\text{int}}^{(\alpha)}+\phi_{ext}^{(\alpha)}\right)\left(V-V_{syn}^{(\alpha)}\right)+\frac{J_{ext}}{C}. \tag{5}$$

Qualitative difference to Eq. 4 is that Eq. 5 contains an extra parametric force term $[\varphi_{int,j}^{(\alpha)} + \varphi_{ext,j}^{(\alpha)}]V$ on the RHS due to which this no longer agrees with Freeman's model. We again assume that $\varphi_{int}^{(\alpha)}$ and $\varphi_{ext}^{(\alpha)}$ are considered to be deterministic and are defined similarly as in Eq. 4.

3. THE LIF-NETWORK VS NEURAL MASS MODELS

3.1 Simulation of average LIF-network signals

Simulation of a neuronal population of *N* LIF neurons was performed using Eqs. 1, 2, 12 and 15 with parameters defined as in Table 1. Eqs. 12 and 15 can be found in the appendix and describe the incoming firing rates to each neuron, and the reset and refractory rule, respectively. See appendix C for the algorithm that was used for this purpose. For all simulations we used a ratio of *5:1* for excitatory versus inhibitory neurons (Yger et al., 2011). We consider a 1D network topology where connections between neurons were established using an adjacency matrix which is based on the network configuration of interest (see below). Simulations were executed for *50* seconds with an integration time step of *0.1ms* (i.e. a sample frequency of 10 kHz). We used an initial transient current to all neurons of $J_{ext,j} = 20nA$ during the first *20ms* of the simulations to trigger network activity. We choose not add a constant external current input $J_{ext,j}$ or an external firing input $\varphi^{(\alpha)}_{ext,j}$ during the whole simulation time since such an external input would refer to neuronal influence from other populations or experimental stimuli which needed to be excluded. Subsequently, we used an Euler forward method to solve the coupled first order differential equations for synaptic conductances g_j and an Euler forward method with additive white noise in the Stratonovich picture to solve the stochastic differential equations for the individual membrane potentials V_j. At the end of the simulations we stored all individual spike times $t_{j,m}$ to compute the average firing and subsequently computed the average network activity $\bar{V} = \frac{1}{N}\sum_{j=1}^{N} V_j$. The average network activity was main variable of interest for the LIF populations and their average firing rates were stored and used in subsequent neural mass simulations.

We compared average network activity with our neural mass mapping for different network conditions:

1. Effect of network size: We ran simulations for different network sizes given a fully connected network configuration. Simulations were executed in steps of $\Delta N = 100$ for $100 < N < 1000$ and in steps of $\Delta N = 500$ for $1000 < N < 10000$.
2. Effect of network density: We ran simulations for three different network topologies: regular networks, small-world networks and random networks for networks with a size of *N=10000*. Regular networks were defined as networks were the numnber of connections was equal for every node. Small-world networks were obtained by randomly rewiring a regular network with a probability of *0.1* and random networks were obtained by simulating Erdos Renyi networks (Erdos and Renyi, 1959; Watts and Strogatz, 1998). For each network configuration we ran simulations for different network densities between $0 < density < 1.0$. Networks were reconstructed using the contest toolbox for Matlab (http://www.mathstat.strath.ac.uk/outreach/contest/).

3.2 Simulation of neural mass signals

We simulated neural mass signals by solving Eqs 3 (neural mass model 1) and 5 (neural mass model 2) by using a conventional Euler forward method. To this end, parameters in Table 1 were used and the synaptic time constant in the LHS of these equations was defined as $\tau_{syn}=(\tau^{(E)}+\tau^{(i)})/2$. We used $\hat{V}=\frac{1}{T}\int_0^T \bar{V}dt$ for the mean potential´s temporal average in the RHS of Eq. 3. The input to both neural mass models was achieved by using the average firing rates of the simulated LIF population in the RHS of Eqs 3 and 5 ($\varphi_{int}^{(\alpha)}$). Similar to the simulations of the LIF-network activity we ignored external firing input $\varphi_{ext}^{(\alpha)}$ and the external input current $J_{ext,j}$. We again simulated 50 seconds of data for both neural mass models with an integration time step of 0.1ms.

Table 1: Constants used in simulations.

τ	Membrane time constant	20 ms
V_{mem}	Resting state potential	-60 mV
$V_{syn}^{(\varepsilon)}$	Reversal potential for excitatory synapses	0 mV
$V_{syn}^{(i)}$	Reversal potential for inhibotory synapses	-80 mV
G_0	Leak conductance	10 nS
Σ	Noise strength	0.6 mV
$\tau^{(\varepsilon)}$	excitatory synaptic time constant	5 ms
$\tau^{(i)}$	Inhibitory synaptic time constant	10 ms
g_0^{ε}	Excitatory synaptic conductance	3 nS
g_0^{I}	Excitatory synaptic conductance	50 nS
V_{thres}	Threshold potential	-50 mV
V_{reset}	Reset potential	-60 mV
$\Delta t_{refract}$	Refractory period	5 ms

3.3 Comparing average LIF-network signals and neural mass signals

The neural mass signal V and the average network signal $\bar{V}$ were compared by testing whether the spectral contents of the signals differed. To this end, we compared the power spectral densities of the two signals by means of the two-sided Kolmogorov-Smirnov (KS) test. The two sided KS-test quantifies the distance between two empirical distibution functions and is sensitive for differences in location and in the shape of the distribution functions. In order to compare both signals, both signals were filtered using a Chebyshev low pass filter with a stop frequency of *80Hz* and a pass frequency of *70Hz*. Subsequently, both signals were z-transformed to ensure that the mean was zero-centered and sealing to unit variance. Power spectral densities were computed using the Welch's periodogram method with a window of *3* seconds and an overlap of *0.4*. See appendix C for the pseudo-code that was used to compare average network signals with neural mass signals.

3.4 Synchronization properties of the LIF-network

We computed the phase locking value (PLV) between neurons in the LIF-networks to test whether a discrepancy between average network signals and the neural mass signals could be explained by desynchronization between neurons in the LIF-network (Mardia, 1975). For this purpose we filtered the individual membrane potentials of neurons in the LIF-network with a Chebyshev band-pass filter between 8-13 Hz. Subsequently, we computed the analytical signal $a(t)$ to extract the phase φ of the signals

$$\varphi(t) = \arctan\left(\frac{\mathrm{Re}\{a(t)\}}{\mathrm{Im}\{a(t)\}}\right) \tag{6}$$

The PLV was then computed between neurons j and k in time interval T to determine the amount of phase synchronization between signals of individual neurons

$$PLV_{j,k,t} = T^{-1}\left|\sum_{t=1}^{T} e^{i\left[\varphi_j(t)-\varphi_k(t)\right]}\right|. \tag{7}$$

The PLV value between 1000 random pairs of neurons in the network was calculated. The mean PLV and standard error was then computed and used for further analyses. All analyses were executed using Matlab R2011b (Natick, Massachusetts: The MathWorks Inc., 2011).

4. RESULTS

4.1 Effect of network size

We simulated fully connected LIF-networks for a range of network sizes. For the first neural mass model, we observed that there was discrepancy between the average network signal and the neural mass signal when the number of neurons was less than 300 (Fig. 1C), i.e. in the lower limit. Below the limit of 300 neurons, the Kolmogorov-Smirnov test statistic had a significant p-value ($p\text{-}value < 0.05$), indicating a difference between power spectral densities of the average network signal and the neural mass signal. In Fig. 1E we show the power spectral densities with confidence intervals belonging the neural mass signal (dashed lines) and the average network signal (normal lines) for a LIF-network with 100 neurons. There is still an overlap between the two in the higher alpha band and beta band regime but it can be observed that the neural mass model failed for especially higher frequencies. For a LIF network of 2000 neurons it can be observed that there was a large overlap between the confidence intervals of the power spectral densities of the average network signal and the neural mass signal for a wide range of frequencies (Fig. 1F). Only for the highest frequencies we observe a slight shift between the two.

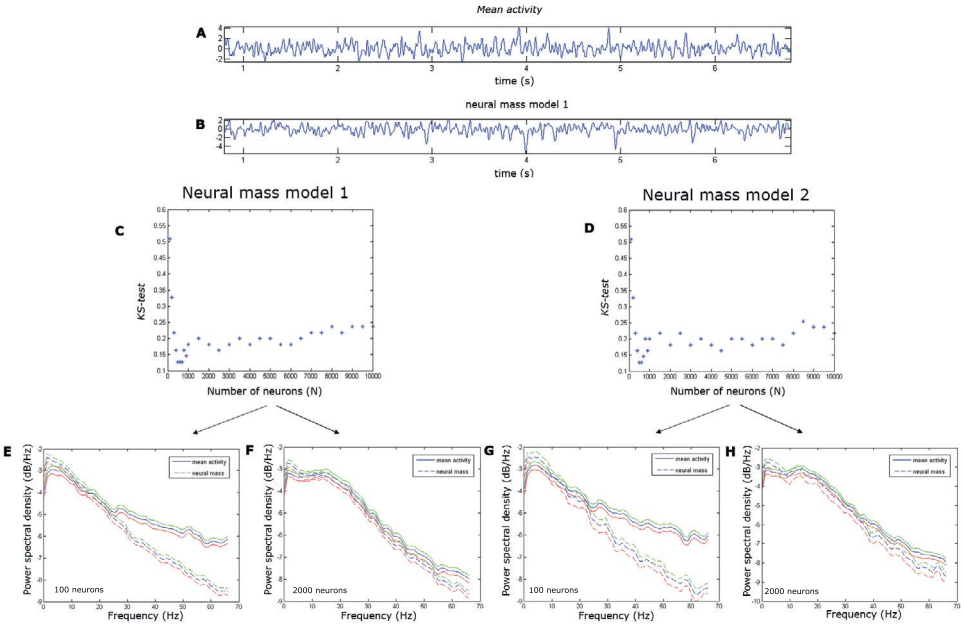

Figure 1: Effect of network size. Simulations were done for fully connected LIF-networks, starting with 10000 neurons down to 100 neurons. For each network size we estimated the average network signal, example shown for 1000 neurons (A). We calculated neural mass activity for both neural mass models with the mean spike train of the LIF-network as input, example shown for neural mass model 1 with 1000 neurons (B). The Kolmogorov-test statistic was used to compare the power spectral densities of the average network signals with signals from neural mass model 1 (C) and neural mass model 2 (D) for networks with increasing number of neurons. We further show conditions where neural mass models are capable (F and H) and not capable (E and G) of describing the average network signal. In each of these plots the power spectral densities with confidence intervals (red and green lines) of the average network signal (normal lines) and the neural mass signals (dashed lines) are plotted for a given frequency range, for 100 neurons (F and H) and 2000 neurons (E and G). Figure E and F correspond to neural mass model 1 and G and H to neural mass model 2.

For the second neural mass model, we again observe that there was a discrepancy between the average network signal and the neural mass signal when the number of neurons was less than 300 (Fig 1D). Again we plotted the power spectral densities with confidence intervals below the limit of 300 neurons and observe a discrepancy between the average network signal and the neural mass signal for a large amount of the frequency range (Fig 1G.). There was overlap only in the alpha frequency range. For a LIF network of 2000 neurons we again observed a large overlap between the confidence intervals, except for the highest frequencies.

For both neural mass models we observe that the Kolmogorov-Smirnov test statistic has local minima for networks between 500 and 1000 neurons. For larger network sizes, we observed that the Kolmogorov-Smirnov test statistic increased as a function of number of neurons, though not reaching significance.

4.2 Effect of network density

For three different network configurations (regular, small world and random network topology) we assessed the effect of decreasing the density of connections in the LIF-network on the ability of the neural mass model to describe the average network signal. Since we obtained similar results for neural mass model 1 and neural mass model 2 in the previous analyses, we continued these analyses by using neural mass model 1 only due to less computational expense of neural mass model 1.

For the LIF-network with a regular network topology we observed that there was a significant difference between the average network signal and the neural mass signal when the density of connections in the LIF-network was smaller than 0.9 (Fig. 2A). For LIF-networks with small world and random network topology we also observed a critical density below which there is a discrepancy between the average network signal and the neural mass model. These critical densities were 0.85 and 0.05 for the small world and random LIF networks respectively (Fig 2B & 2C). By analyzing the PLV in the LIF-networks as a function of connection density we also observed that there was an instantaneous shift to larger PLVs if the densities were higher than the aforementioned critical densities. Note that the increase in PLV beyond these thresholds was relatively small (in order of 0.1-0.2), but appeared to be instantaneous.

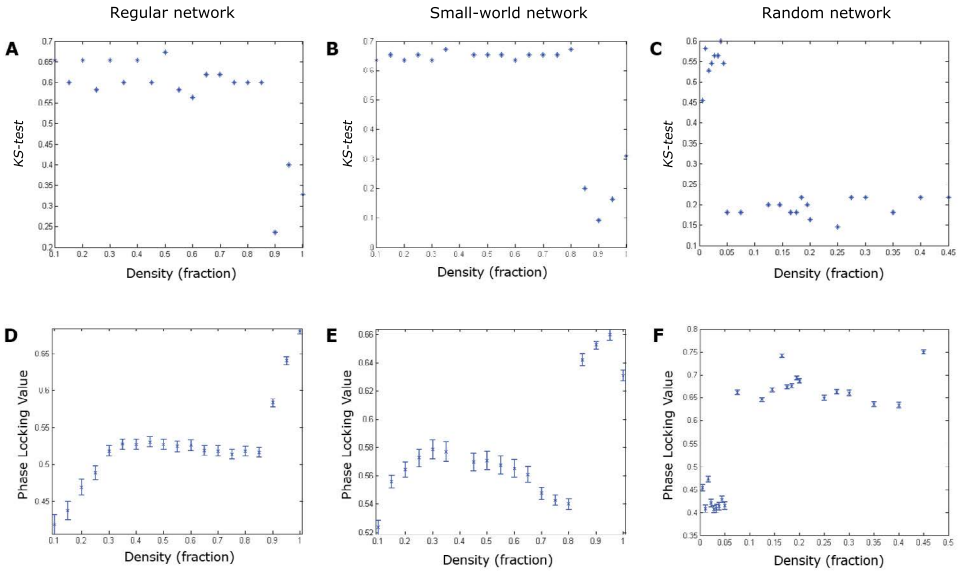

Figure 2: Effect of network density. Simulations were done for regular, small-world and random networks given a network size of 10000 neurons. For each network configuration we decreased the density of connections and the Kolomogorov-Smirnov test statistic was used to compare the power spectral densities of the average network signals with the first neural mass model (ABC). For each network configuration we computed the mean PLV between neurons in the neuronal network. We plotted this mean PLV (with standard error) as a function of density (DEF) for each network configuration. Note the critical thresholds for density for mean PLV values and the Kolomogorov-Smirnov test statistic for each network configuration.

When inspecting the power density spectra of the average network signal and neural mass signal we observed a large overlap between the confidence intervals of the average network signal and neural mass signal after the critical densities for any network configuration (Fig. 3BDF). Before the critical densities we again observed a small overlap especially in the alpha band for regular and random networks (Fig. 3AE). However, for small world LIF-networks we found that there can be still overlap between the confidence intervals up to frequencies in the beta band (Fig. 3C). For higher frequencies we again observed that the confidence intervals diverge. For all network configurations, there is higher prominence of higher frequencies in the average network signal which is not captured by the neural mass signal.

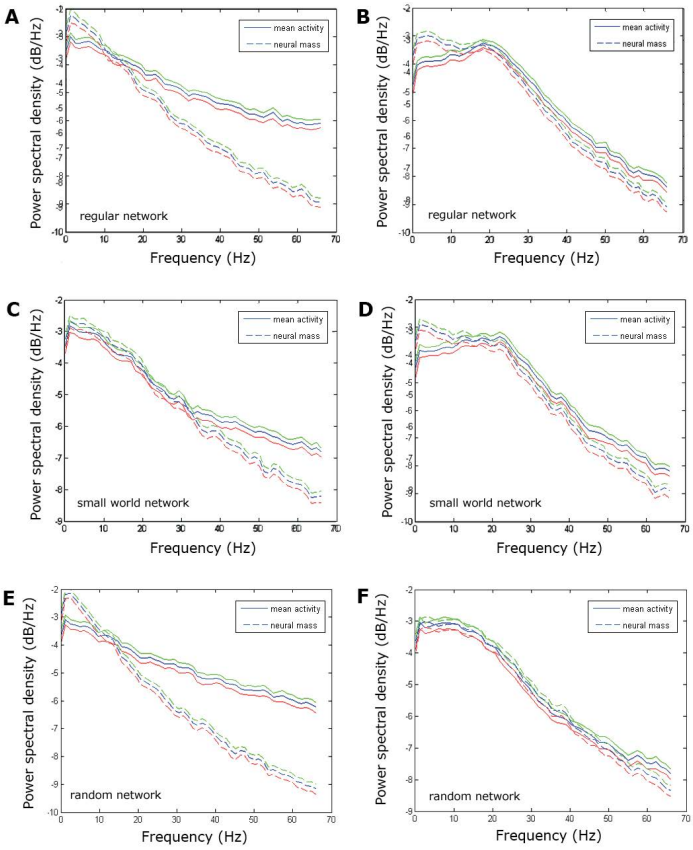

Figure 3: Power spectral densities. Elaboration of the simulations shown in figure 2. We have plotted the power spectral densities with confidence intervals (green and red lines) of the average network signal (normal lines) and neural mass model 1 (dashed lines) before (ACE) and after the critical thresholds (BDF) (see Figure 2 for explanation). This was done for each network configuration, regular network (AB), small-world network (CD) and a random network (DF). Note that before the threshold there is mostly overlap found for the alpha band range, except for the small world network, where this extents to the beta band. After the threshold there is a large overlap between the average network signal and the neural mass model.

5. DISCUSSION

In the present study we aimed to investigate whether the average network signal of a neuronal poulation can be described by a neural mass signal when the underlying neuronal population is inhomogeneous. Our main findings are: (1) for a fully connected neuronal network there is a threshold for network size above which the neural mass model is capable of describing the average network signal; (2) By decreasing the connection density in the neuronal network we observed that for any topological configuration, there is a critical density below which there is a discrepancy between the average network signal and the neural mass signal accompanied with lower PLV values between neurons in the neuronal network; (3) this change in behaviour of the average network signals was abrupt.

Firstly, we found that there is threshold for network size, 300 neurons, above which the neural mass model is still a good description of the average network signal. We reproduced this finding with both neural mass models. These present findings are in accordance with the concept of a mean-field description, which is only valid when the number of elements in a system becomes large. However, even for large network sizes, the neural mass model has difficulty in capturing higher frequency components of the average network signal. When the number of neurons in the fully connected neuronal network increased, the firing rate also increased, leading to higher frequency components in the average network signal. However, fully connected neuronal networks are often used in computational studies (Borgers et al., 2005; Deco et al., 2013b; Nakagawa et al., 2013), but do not resemble realistic neurobiological networks often characterized by sparsity of connections.

In our second analyses we found that if connections in neuronal network become too sparse there was discrepancy between the average network signal and the neural mass model. There was a critical density for all topological configurations, albeit these densities differed for the different topological configurations as for random network topology this density was around 5\% in contrast to regular networks where this was 90\% for a given network size. As this discrepancy between the average network signal and neural mass around this critical density coincided with a drop in PLV, we interpret these findings in the following way: synchronization of neurons in a neuronal network is a prerequisite for a valid mean-field description by a neural mass model. In all our simulations we obtained significantly different power spectral densities when we also found low PLV values. This can be understood by the notion that a decrease of synchronization between neurons in the neuronal network leads to a loss of simultaneous firing in the neuronal network and the influence of noise for the behavior of individual neurons becomes relatively larger. This leads to higher contribution of higher frequency components in the average network signal which cannot be captured by the neural mass model. Our interpretation for a requirement of a minimum amount of synchronization also explains why the density threshold for random networks was much lower than for regular networks since it is well-known that random networks are much easier to synchronize than regular networks (Barahona and Pecora, 2002). Our hypothesis was further underpinned by the finding that for a larger random network the critical density was a few percent lower. This can be explained by the fact that synchronizability of a network scales with network size (Belykh et al., 2005).

The neural mass models had especially difficulty in describing high frequency components of the average network signal, especially when there was a drop in synchronization between neurons in the neuronal network. This can be understood by the notion that neural mass models can be considered as low-pass filters whose qualities are determined by the time constants (τ and τ_{syn}). Changing these parameters will lead to a change in slope of the power density spectra of the neural mass models. However, the range for which these time constants make physiologically sense is limited and therefore this restricts possible parameter values.

In the present study we used two neural mass models derived from the same LIF model, but based on different assumptions. In the first neural mass model we assumed that time scales of the membrane potential and synaptic activity were of the same order and that driving currents $g_j^{(\alpha)}(V_j - V_{syn}^{(\alpha)})$ could be considered constant. This is based on the idea that fluctuations of the membrane potential around a reference value are small (Rodrigues et al., 2010). In the second neural mass model we questioned the assumption that driving currents should be considered constant and instead assumed that the time scale of the membrane potential was smaller than the time scale of synaptic activity. This led to an extra force term in Eq. 5. During our simulations we observed that the behaviour of both neural mass models was highly similar when we compared them to the average network signals, probably indicating that fluctuations of this extra force in the second neural mass model were negligible. Another assumption in both neural mass models was that communication between neurons was instantaneous and we ignored delays involved in action potential propagation and in the time course of neurotransmitter transport in synaptic clefts. The impact of delays was beyond the scope of the present paper and needs to be analysed in future studies.

The present study has implications for future model studies that try to elucidate biophysical mechanisms of disturbed oscillatory activity in neurodegenerative disorders. If the system of interest is large enough and not too sparse one can use neural mass models without concern that the neural mass model will not be a good description of the mean-field. However, when one is modelling relatively small networks and there is an indication of loss of connections between neurons, one should first check if the neurons in the underlying neuronal network are synchronized. An exception for this rule is when one is interested in alpha band activity, as we demonstrated that neural mass models were robust for this frequency range. Importantly, neural masses are generally considered to simulate activity from cortical columns. A cortical column consists of approximately 60.000-90.000 neurons/mm^3 with a connection density of $11.05 \cdot 10^8$/mm^3 (Boucsein et al., 2011; Peter, 1979). Note that this connection density may be around the critical threshold for networks with random network topology.

To conclude, we have used two mappings between a LIF-neuron and reduced neural mass models. Average network signals based on activity of LIF-networks can be described by neural mass models if the neurons in the network synchronize. Caution is needed when modelling neurodegenerative diseases since it is not a priori certain that synchrony is unaltered by the disease.

APPENDIX A: A NETWORK OF LEAKY INTEGRATE-AND-FIRE NEURONS

We consider a population of N neurons. Every neuron is described in terms of the dynamics of its membrane potential V_j with $j = 1,E,N$ and with time-dependent synaptic conductances. The latter alter due to incoming spikes. Conductances are denoted as $g_{jk}^{(\alpha)}$, i.e. every neuron j can be connected up to N other neurons by its synapses with $k = 1,...,N$. Synapses are either excitatory or inhibitory and can be discriminated by α, where $\alpha \in \{E, I\}$. We assume that V_j obeys the stochastic dynamics

$$dV_j = -\frac{1}{\tau}\left[\left(V_j - V_{mem}\right) + \sum_{\alpha}\sum_{k} A_{jk}^{(\alpha)} \frac{g_{jk}^{(\alpha)}}{g_0}\left(V_j - V_{syn}^{(\alpha)}\right) - \frac{J_{ext,j}}{C}\right]dt + \sigma\sqrt{2\tau}\,dW_j \qquad \text{(A.1)}$$

with fixed resting and reversal potentials $Vmem$ and $V_{syn}^{(\alpha)}$, respectively. g_0 is the leak conductance that is constant considered and τ is the membrane time constant. Both constants are identical for all neurons. The membrane time constant τ is related by $\tau = C/g_0$ to the capacitor and membrane conductance constant g_0 and τ determines the rise and decay of the membrane potential. $A_{jk}^{(\alpha)}$ is the adjacency matrix describing whether neuron k targets neuron j:

$$A_{jk}^{(\alpha)} = \begin{cases} 1 \text{ if neuron targets neuron} \\ 0 \text{ otherwise} \end{cases} \qquad \text{(A.2)}$$

$J_{ext,j}$ may be some external current on neuron j. Every neuron j is also under influence of zero-centered, δ correlated, Gaussian white noise W_j with unit variance, i.e. we have $E[W_j] = 0$ and $E[W_j(t)W_k(t')] = \delta_{jk}\,\delta(t-t')$ where δ_{jk} is the Kronecker's delta function and $\delta(t-t')$ refers to Dirac's delta-function. The noise 'strength' σ is also considered identical for all neurons – see table below for values of the constants. The corresponding conductances $g_{jk}^{(\alpha)}$ are mere low-pass filters that depend on the incoming spikes as follows

$$dg_{jk}^{(\alpha)} = -\frac{1}{\tau^{(\alpha)}}\left[g_{jk}^{(\alpha)} - g_0^{(\alpha)}\left\{\sum_m A_{jk}^{(\alpha)}\delta\left(t - t_{k,m}\right) + \sum_m \delta\left(t - t_{ext,j,k,m}^{(\alpha)}\right)\right\}\right]dt\,. \qquad \text{(A.3)}$$

$g_0^{(\alpha)}$ is a constant related to the maximal conductance that may serve to discriminate between excitatory and inhibitory neurons. $t_{k,m}$ is the time of the m-th spike of neuron k and, furthermore, synapse $\{j,k,\alpha\}$ may also receive external input in the form of spikes at times $t_{ext,j,k,m}^{(\alpha)}$. $\tau^{(\alpha)}$ determines the rise and decay of synaptic activity which is in general different for inhibitory and excitatory neurons. Fortunately, we can simplify Eqs. (A.1 & A.3) when defining the total activity of the α-synapse of neuron j as $g_j = \sum_{k=1}^{N} A_{jk}^{(\alpha)} g_{jk}^{(\alpha)}$. Multiplying Eq. A.3 with $A_{jk}^{(\alpha)}$ and summation over k yields for neuron j's total synapse dynamics

$$dg_j^{(\alpha)} = -\frac{1}{\tau^{(\alpha)}}\left[g_j^{(\alpha)} - g_0^{(\alpha)}\sum_{k=1}^{N}\left\{\sum_m A_{jk}^{(\alpha)}\delta\left(t - t_{k,m}\right) + \sum_m \delta\left(t - t_{ext,j,k,m}^{(\alpha)}\right)\right\}\right]dt \qquad \text{(A.4)}$$

because $A_{jk}^{(\alpha)}$ is nilpotent, i.e. $A_{jk}^{(\alpha)}\,A_{jk}^{(\alpha)} = A_{jk}^{(\alpha)}$ For the sake of legibility we introduce abbreviations for the incoming firing rates, namely

$$\phi_{\text{int},j}^{(\alpha)} = \sum_{k=1}^{N}\sum_{m} A_{jk}^{(\alpha)}\delta\left(t - t_{k,m}\right) \qquad \text{and} \qquad \varphi_{ext,j}^{(\alpha)} = \sum_{k=1}^{N}\sum_{m}\delta\left(t - t_{ext,j,k,m}^{(\alpha)}\right) \tag{A.5}$$

with which Eq. A.4 can be rewritten as

$$dg_j^{(\alpha)} = -\frac{1}{\tau^{(\alpha)}}\left[g_j^{(\alpha)} - g_0^{(\alpha)}\left(\phi_{\text{int},j}^{(\alpha)} + \phi_{ext,j}^{(\alpha)}\right)\right]dt\,. \tag{A.6}$$

With the substitution of $g_j = \sum_k A_{jk}^{(\alpha)} g_{jk}^{(\alpha)}$ into Eq. A.1 reduces the membrane dynamics of neuron *j* into

$$dV_j = -\frac{1}{\tau}\left[\left(V_j - V_{mem}\right) + \sum_{\alpha}\frac{g_j^{(\alpha)}}{g_0}\left(V_j - V_{syn}^{(\alpha)}\right) - \frac{J_{ext,j}}{C}\right]dt + \sigma\sqrt{2\tau}dW_j\,. \tag{A.7}$$

Finally, the capacitor is charged until the membrane potential $V_j(t)$ reaches a threshold, after which spikes are emitted and at which we define

$$t_{k,m} : \left\{V_j \geq V_{thres}\right\} \rightarrow \left\{V_i = V_{reset} \text{ for } t_{i,m} < t \leq t_i^{(m)} + \Delta t_{refract}\right\}. \tag{A.8}$$

Threshold and reset potential, Vt_{hres} and V_{reset}, respectively, as well as the refractory time $\Delta t_{refract}$, are considered identical for all neurons.

APPENDIX B: DERIVATION OF THE NEURAL MASS MODELS

For the macro-scale we derive two neural mass models. Aim is to find the dynamics of the expectation value of the mean membrane potential

$$V = \mathrm{E}\left[\frac{1}{N}\sum_{j=1}^{N} V_j\right] = \frac{1}{N}\sum_{j=1}^{N}\mathrm{E}\left[V_j\right]. \tag{B.1}$$

We define the expectation value of the mean synaptic conductivity as well by

$$g^{(\alpha)} = \mathrm{E}\left[\frac{1}{N}\sum_{j=1}^{N} g_j^{(\alpha)}\right] = \frac{1}{N}\sum_{j=1}^{N}\mathrm{E}\left[g_j^{(\alpha)}\right]. \tag{B.2}$$

We assume that $\mathrm{E}\left[\frac{d}{dt}\sum_j f_j(t)\right] = \frac{d}{dt}\mathrm{E}\left[\sum_j f_j(t)\right]$ holds for all functions $f_j = V_j$ *and* $f_j = g_{jk}^{(\alpha)}$. If we now combine Eq. A.7, B.1 & B.2 we obtain an equation describing the dynamics of the mean membrane potential *V*

$$\left[\tau\frac{d}{dt} + 1\right]V = V_{mem} - \mathrm{E}\left[\sum_{\alpha}\frac{1}{N}\sum_{j=1}^{N}\frac{g_j^{(\alpha)}}{g_0}\left(V_j - V_{syn}^{(\alpha)}\right)\right] + \frac{J_{ext}}{C} \tag{B.3}$$

where we assumed $J_{ext} = N^{-1}\sum_{j=1}^{N} J_{ext,j}$ to be deterministic. Similarly, we can derive the mean dynamics of the synaptic conductivity if we define the expectation value of spiking behaviour

$$\begin{aligned}\phi_{\text{int}}^{(\alpha)} &= \mathrm{E}\left[\frac{1}{N}\sum_{j=1}^{N}\phi_{int,j}^{(\alpha)}\right] = \frac{1}{N}\sum_{j=1}^{N}\mathrm{E}\left[\phi_{\text{int,j}}^{(\alpha)}\right] \text{ and} \\ \phi_{ext}^{(\alpha)} &= \mathrm{E}\left[\frac{1}{N}\sum_{j=1}^{N}\phi_{ext,j}^{(\alpha)}\right] = \frac{1}{N}\sum_{j=1}^{N}\mathrm{E}\left[\phi_{ext,j}^{(\alpha)}\right]\end{aligned} \tag{B.4}$$

such that for we obtain an equation for the mean synaptic conductivity by

$$\left[\tau^{(\alpha)}\frac{d}{dt}+1\right]dg^{(\alpha)} = g_0^{(\alpha)}\left(\phi_{\text{int}}^{(\alpha)}+\phi_{ext}^{(\alpha)}\right). \tag{B.5}$$

Aim of what follows is to substitute the $g_j^{[\alpha]}$ in the equation for the mean membrane potential (Eq. B.3). From here we follow two separate approaches to derive neural mass models.

Neural mass derivation 1:

In this derivation we follow an approach by Rodrgues and co-workers where it is assumed that driving forces $g_j(V_j - V_{syn})$ for all channels are constant (Moreno-Bote and Parga, 2005; Rodrigues et al., 2010). This based on the assumption that fluctuations of these driving forces are relatively small. Therefore, we use a general, finite value for $\hat{V}$ and formalize this approximation by $(V_j - V_{syn}^{[\alpha]}) \approx (\hat{V} - V_{syn}^{[\alpha]})$. Now the mean membrane potential's dynamics (Eq. B.3) reduces to

$$\begin{aligned}\left[\tau\frac{d}{dt}+1\right]V &\approx V_{mem} - \mathrm{E}\left[\sum_{\alpha}\frac{1}{N}\sum_{j=1}^{N}\frac{g_j^{(\alpha)}}{g_0}\left(\hat{V}-V_{syn}^{(\alpha)}\right)\right] + \frac{J_{ext}}{C} \\ &= V_{mem} - \sum_{\alpha}\frac{\mathrm{E}\left[\frac{1}{N}\sum_{j=1}^{N}g_j^{(\alpha)}\right]}{g_0}\left(\hat{V}-V_{syn}^{(\alpha)}\right) + \frac{J_{ext}}{C} \\ &= V_{mem} - \sum_{\alpha}\frac{g_j^{(\alpha)}}{g_0}\left(\hat{V}-V_{syn}^{(\alpha)}\right) + \frac{J_{ext}}{C}\end{aligned} \tag{B.6}$$

We further assume that the time scales of the membrane potential and synaptic activity are of the same order irrespective their type (Destexhe and Sejnowski, 2001; Gerstner and Kistler, 2002). That is $\forall\alpha{:}\tau^{[\alpha]} \approx \tau_{\text{syn}}$ holds. This leads to

$$\left[\tau_{syn}\frac{d}{dt}+1\right]g^{(\alpha)} \approx \left[\tau^{(\alpha)}\frac{d}{dt}+1\right]g^{(\alpha)} = g_0^{(\alpha)}\left(\phi_{\text{int}}^{(\alpha)}+\phi_{ext}^{(\alpha)}\right). \tag{B.7}$$

The only remaining difference between inhibitory and excitatory neurons/synapses is given through $V_{syn}^{[\alpha]}$ and $g_0^{[\alpha]}$. We further adopt the external current to be constant by which $\left[\tau_{syn}\frac{d}{dt}+1\right]J_{ext}=J_{ext}$ holds. By combining Eq. B.6 with Eq. B.7 we derive for our first neural mass model the following equation

$$\left[\tau_{syn}\frac{d}{dt}+1\right]\left[\tau\frac{d}{dt}+1\right]V=V_{mem}-\sum_{\alpha}\frac{g_0^{(\alpha)}}{g_0}\left(\phi_{\text{int}}^{(\alpha)}+\phi_{ext}^{(\alpha)}\right)\left(\hat{V}-V_{syn}^{(\alpha)}\right)+\frac{J_{ext}}{C} \tag{B.8}$$

We further ignored the reset-rule and the presence of a refractory period, incorporated in the initial LIF equations, as we assume that the most important characteristics that need to be captured are sub-threshold post-synaptic potentials of neurons in the neuronal population. By inspection we find that our first neural mass model is identical to the widely known neural mass model of Freeman (Freeman, 1975)

$$\left[\frac{d^2}{dt^2}+(\alpha+\beta)\frac{d}{dt}+\alpha\beta\right]V=J \tag{B.9}$$

when substituting $a=\tau^{-1}$, $\beta=\tau_{syn}^{-1}$ and $J=(\tau\tau_{syn})^{-1}rhs\{\text{Eq.B.8}\}$.

Neural mass derivation 2:

Since we are not entirely certain about the validity of all assumptions made in the first neural mass derivation, especially the assumption that the driving forces $g_j(V_j-V_{syn})$ are constant, we search for an alternative derivation. Now we start again with the equation describing the dynamics of *V*, Eq. B.3

$$\left[\tau\frac{d}{dt}+1\right]V=V_{mem}-\mathrm{E}\left[\sum_{\alpha}\frac{1}{N}\sum_{j=1}^{N}\frac{g_j^{(\alpha)}}{g_0}\left(V_j-V_{syn}^{(\alpha)}\right)\right]+\frac{J_{ext}}{C} \tag{B.3}$$

We now assume that the synaptic time scales of the excitatory and inhibitory conductances for individual neurons are again in the same order of magnitude. This indicates that we can write

$$\left[\tau_{syn}\frac{d}{dt}+1\right]g_j^{(\alpha)}\approx\left[\tau^{(\alpha)}\frac{d}{dt}+1\right]g_j^{(\alpha)}=g_0^{(\alpha)}\left(\phi_{\text{int,j}}^{(\alpha)}+\phi_{ext,j}^{(\alpha)}\right). \tag{B.10}$$

If we now multiply Eq. B.3 by the LHS of Eq. B.10 then we can write

$$\left[\tau_{syn}\frac{d}{dt}+1\right]\left[\tau\frac{d}{dt}+1\right]V=V_{mem}-\sum_{\alpha}\frac{1}{N}\sum_{j=1}^{N}\mathrm{E}\left[\left[\tau_{syn}\frac{d}{dt}+1\right]\frac{g_j^{(\alpha)}}{g_0}\left(V_j-V_{syn}^{(\alpha)}\right)\right]+\frac{J_{ext}}{C} \tag{B.11}$$

Subsequently, by using the product rule for differentiation this leads to

$$\begin{aligned}\left[\tau_{syn}\frac{d}{dt}+1\right]\left[\tau\frac{d}{dt}+1\right]V=V_{mem}&-\sum_{\alpha}\frac{1}{N}\sum_{j=1}^{N}\mathrm{E}\left[\left[\tau_{syn}\frac{d}{dt}+1\right]\frac{g_j^{(\alpha)}}{g_0}\left(V_j-V_{syn}^{(\alpha)}\right)\right]\\&-\sum_{\alpha}\frac{1}{N}\sum_{j=1}^{N}\mathrm{E}\left[\tau_{syn}\frac{g_j^{(\alpha)}}{g_0}\frac{dV_j}{dt}\right]+\frac{J_{ext}}{C}\end{aligned} \tag{B.12}$$

Furthermore, by substituting the RHS of Eq. B.10 in Eq. B.12 we obtain

$$\left[\tau_{syn}\frac{d}{dt}+1\right]\left[\tau\frac{d}{dt}+1\right]V = V_{mem} - \sum_{\alpha}\frac{1}{N}\sum_{j=1}^{N}\mathrm{E}\left[\frac{g_0^{(\alpha)}}{g_0}\left(\phi_{\mathrm{int},j}^{(\alpha)}+\phi_{ext,j}^{(\alpha)}\right)\left(V_j - V_{syn}^{(\alpha)}\right)\right] - \sum_{\alpha}\frac{1}{N}\sum_{j=1}^{N}\mathrm{E}\left[\tau_{syn}\frac{g_j^{(\alpha)}}{g_0}\frac{dV_j}{dt}\right] + \frac{J_{ext}}{C} \tag{B.13}$$

Next we assume the ring rates to be deterministic. This allows for a mean-field approximation such that $\frac{1}{N}\sum_{j=1}^{N}\mathrm{E}\left[\left(\phi_{\mathrm{int},j}^{(\alpha)}+\phi_{ext,j}^{(\alpha)}\right)\left(V_j - V_{syn}^{(\alpha)}\right)\right] = \left(\phi_{\mathrm{int},j}^{(\alpha)}+\phi_{ext,j}^{(\alpha)}\right)\left(V - V_{syn}^{(\alpha)}\right)$ can be replaced in the first term of RHS of Eq. B.13. To treat the final term of Eq. B.13 we compare the time scale of the membrane potential vis-á-vis with the synaptic conductivity. If the first is considered to be much smaller than the latter, meaning that the membrane potential instantly follows changes at the synapse, the dynamics of the membrane potential can be eliminated adiabatically that might be formalized as

$$\left|\frac{dV_j}{dt}\middle/V_j\right| \ll \left|\frac{dg_j^{(\alpha)}}{dt}\middle/g_j^{(\alpha)}\right| \Rightarrow \left|g_j^{(\alpha)}\frac{dV_j}{dt}\right| \ll \left|\frac{dg_j^{(\alpha)}}{dt}V_j\right|. \tag{B.14}$$

This allows for reducing Eq. B.13 to

$$\left[\tau_{syn}\frac{d}{dt}+1\right]\left[\tau\frac{d}{dt}+1\right]V = V_{mem} - \sum_{\alpha}\frac{g_0^{(\alpha)}}{g_0}\left(\phi_{\mathrm{int,j}}^{(\alpha)}+\phi_{ext,j}^{(\alpha)}\right)\left(V - V_{syn}^{(\alpha)}\right) + \frac{J_{ext}}{C} \tag{B.15}$$

which gives us the equation for the second neural mass model. Qualitative difference to Eq. B.8 is that Eq. B.15 contains an extra parametric forcing term $(\varphi_{int,j}^{(\alpha)} + \varphi_{ext,j}^{(\alpha)})V$, which no longer agrees with Freeman's model.

Chapter 3

Structural degree predicts functional network connectivity: a multimodal resting-state fMRI and MEG study

P. Tewarie, A. Hillebrand, E. van Dellen, M.M. Schoonheim, F. Barkhof, C.H. Polman, C. Beaulieu, G. Gong, B.W. van Dijk, C.J. Stam

Neuroimage. 2014 Aug 15;97:296-307

ABSTRACT

Communication between neuronal populations in the human brain is characterized by complex functional interactions across time and space. Recent studies have demonstrated that these functional interactions depend on the underlying structural connections at an aggregate level. Multiple imaging modalities can be used to investigate the relation between the structural connections between brain regions and their functional interactions at multiple timescales. We investigated if consistent modality-independent functional interactions take place between brain regions, and whether these can be accounted for by underlying structural properties. We used functional MRI (fMRI) and magnetoencephalography (MEG) recordings from a population of healthy adults together with a previously described structural network. A high overlap in resting-state functional networks was found in fMRI and especially alpha band MEG recordings. This overlap was characterized by a strongly interconnected functional core network in temporo-posterior brain regions. Anatomically realistically coupled neural mass models revealed that this strongly interconnected functional network emerges near the threshold for global synchronization. Most importantly, this functional core network could be explained by a trade-off between the product of the degrees of structurally-connected regions and the Euclidean distance between them. For both fMRI and MEG, the product of the degrees of connected regions was the most important predictor for functional network connectivity. Therefore, irrespective of the modality, these results indicate that a functional core network in the human brain is especially shaped by communication between high degree nodes of the structural network.

INTRODUCTION

The brain is a highly complex system consisting of a large-scale functional and structural network, together called the connectome (Bullmore and Sporns, 2009). The functional network reflects communication between spatially remote brain regions and is partially shaped by the underlying connections of the structural network. Communication between brain regions is crucial for proper cognitive functioning, and neuropsychiatric diseases are associated with disturbed structural and functional networks (Stam and van Straaten, 2012b). Understanding the principles that determine the topology of both the structural and functional network, as well as their interdependencies is therefore crucial. However, functional networks as estimated from neuroimaging data depend on the choice of the functional neuroimaging modality (e.g. functional Magnetic Resonance Imaging (fMRI) or magneto/electro-encephalography (MEG/EEG)), as well as on the metric that is used to quantify functional interactions. This raises two fundamental questions: 1) is a multimodal imaging approach capable of identifying modality invariant functional interactions that are not the result of artifacts induced by the applied tools or metrics, and 2) how are these modality invariant functional interactions related to the underlying structural network?

Functional interactions or connectivity refers to the existence of any statistical interdependency between the activation profiles of distinct neuronal populations (Friston, 1994). For the estimation of functional connectivity, we rely on functional neuroimaging modalities such as blood-oxygenation-level-dependent (BOLD) fMRI and MEG/EEG. Although fMRI is a widely used modality with a high spatial resolution, BOLD signals are an indirect measure of neuronal activity, are affected by non-neuronal physiological signals, and suffer from limited temporal resolution (Logothetis, 2008). MEG directly measures the magnetic fields induced by currents in locally synchronous neuronal populations with high temporal resolution. However, MEG is affected by the ill-posed nature of the inverse problem, i.e. there is no unique solution of reconstructing the spatial distribution of neuronal activity in the brain based on the extra-cranial recordings (Helmholtz, 1853; Singh, 2012). A multimodal imaging approach employing both fMRI and MEG to reduce these uni-modal confounds has been applied by several groups (Brunetti et al., 2008; Muthukumaraswamy et al., 2009; Singh, 2012; Zumer et al., 2010). Previous studies have either quantified the spatial overlap of responses during tasks (Brunetti et al., 2005; Grummich et al., 2006; Kawakami et al., 2002), or used both modalities in an integrative framework in order to optimize MEG source reconstruction through the utilization of the high spatial resolution of fMRI (Dale et al., 2000; Liu et al., 1998; Liu et al., 2006). Estimation of joined functional networks by both modalities has gained less attention (Brookes et al., 2011a; de Pasquale F. et al., 2010), despite recent success in revealing a large overlap between resting-state networks (RSNs) – semi-independent clusters of correlated brain activity during rest – obtained with both modalities (Brookes et al., 2011b). Moreover, there is a need for a more sophisticated mathematical framework exceeding merely comparative analyses between fMRI and MEG, that is capable of understanding the similarities or dissimilarities between fMRI and MEG obtained functional networks and their relation with the underlying structural network.

The relation between functional interactions and underlying structural connections has been studied by using combined tractography and fMRI, revealing a strong overlap between the two and demonstrating that strong functional interactions among brain regions often coexist with structural connections (Hermundstad et al., 2013; Honey et al., 2009a; Skudlarski et al., 2008; van den Heuvel et al., 2009a). Nevertheless, strong functional interactions can exist even in the absence of structural connections, which is insufficiently explained by indirect structural connections (Honey et al., 2009b). The anatomical (Euclidean) distance between brain regions may account for some of the functional connectivity as short distance connections predominate and brain regions located close to each other tend to be strongly functionally connected (Alexander-Bloch et al., 2013c). However, the existence of long range functional interactions cannot merely be explained by distance penalization (Vertes et al., 2012), and here we hypothesize that functional interactions may be strongly dependent on the number of structural connections of the brain regions involved (the structural degree). The importance of the degree of a region has been shown in other complex networks such as airline infrastructure, where the degree product of airports is crucial for explaining air-traffic ("functional connectivity") between airports (Barrat et al., 2004). In addition, in theoretical models for the generation of random graphs, such as configuration models, the probability of a connection being present between two regions is proportional to the product of their structural degrees (Newman, 2010b). Despite these considerations, brain dynamics have often been put forward as an important missing link between structural and functional topology (Deco et al., 2011; Deco et al., 2013a). In this context, a large number of computational brain models have been applied, ranging from neural mass models (Deco et al., 2009; Honey et al., 2007; Ponten et al., 2010), neural field models (Jirsa and Kelso, 2000; Pinotsis et al., 2013; Robinson, 2012), the Kuramoto model (Cabral et al., 2011; Cabral et al., 2013) and spiking models (Deco and Jirsa, 2012; Ghosh et al., 2008; Nakagawa et al., 2013; Zemanova et al., 2006; Zhou et al., 2006) to link structural and functional networks through neuronal dynamics. A common finding is that global anatomical connection strength[1] is tuned such that the best fit for empirical functional connectivity is found near a bifurcation, which allows for a flexible access between dynamical states (Deco et al., 2013b). In this paper we aim to find modality invariant functional interactions by using the Phase Lag Index and Pearson's correlation coefficient as functional connectivity metrics for respectively MEG and fMRI BOLD time-series (Friston, 1994; Stam et al., 2007). We compare MEG and fMRI functional networks by computing the overlap between high weight connections since these high weight connections are associated with high traffic load of neuronal communication and may be linked to the core of the brain's functional network (Collin et al., 2013; van den Heuvel et al., 2012). We use a literature based structural network obtained by tractography from a large cohort of healthy individuals and a realistically coupled neural mass model to explain these modality invariant functional interactions. We hypothesize that these strong functional connections appear near a

1 Global anatomical connection strength refers to a control parameter in computational models for the scaling of global inter-regional coupling.

phase transition for functional connectivity and that they can be explained by a combination of the degree product and Euclidean distance between areas in the structural network, irrespective of the modality.

METHODS

Data acquisition and postprocessing

We used data obtained from two datasets. The first dataset was used for comparative analyses between fMRI and MEG. This first dataset consisted of healthy subjects that were scanned and recorded under resting-state conditions with fMRI and MEG on the same day. For the second dataset, only the MEG recordings were available and were used to inspect if MEG functional network findings were robust and dataset independent. The first dataset contained data from seventeen healthy subjects of age 39.8 ± 9.8 (mean and standard deviation) from a previous study, who underwent both fMRI and MEG (Meer et al., 2013; Tewarie et al., 2013d). The second dataset contained MEG data from 68 healthy individuals (see SI for further information about the second dataset). Both studies were approved by the institutional ethics review board of the VUmc and all subjects gave written informed consent prior to participation.

MRI scans were executed using a 3T-MRI system (GE SignaHDxt) with a 3D-T1 weighted fast spoiled gradient-echo (FSPGR, TR 7.8 ms, TE 3.0 ms, TI 450 ms, FA 12, 0.9x0.9x1 mm voxel size), and a resting-state fMRI sequence containing 202 volumes, of which the first two were discarded (EPI, TR 2200 ms, TE 35 ms, FA 80, 3 mm contiguous axial slices covering the entire brain, in-plane resolution 3.3x3.3 mm). Pre-processing was performed by an experienced rater (MMS) using FSL 5 (FMRIB's Software Library, http://www.fmrib.ox.ac.uk/fsl), and included brain extraction for the 3D-T1 sequence. The fMRI data was processed as part of the pipeline of MELODIC (part of FSL) using default settings, including masking, motion correction, smoothing and high-pass filtering (100 s cut-off). All preprocessed fMRI images were kept in subject space; the AAL atlas was non-linearly registered back to each subject using nearest-neighbour interpolation. This was done by inverting the registration steps calculated by a boundary-based registration (BBR, part of FSL) between fMRI and 3D-T1 sequences, and non-linear registration between 3D-T1 and standard space using FNIRT (part of FSL). After registration, the average time-series were calculated for each individual AAL region, which were used in the connectivity analyses.

MEG data were recorded using a 151-channel whole-head MEG system (CTF Systems; Port Coquitlam, BC, Canada) while participants were in a supine position in a magnetically shielded room (Vacuumschmelze, Hanau, Germany). Magnetic fields were recorded during a no-task, eyes-open condition for three minutes (not analysed here) and eyes-closed condition for five consecutive minutes. A third-order software gradient (Vrba J, 1999) was used with a recording passband of 0– 150 Hz and a sample frequency of 625 Hz. Participants had to be free of any metal objects. At the beginning and end of each recording, the head position relative to the coordinate system of

the helmet was determined by leading small alternating currents through three head position coils attached to the left and right pre-auricular points and the nasion. Changes in head position of <0.5 cm during a recording condition were accepted. Each original dataset consisted of a continuous resting-state recording from which artefact-free segments were subsequently selected for further analysis. Each segment or epoch had a duration of 6.555 seconds (total number of segments or epochs was 45). Channels and epochs were visually inspected. Epochs and channels were rejected based on system related artefacts (SQUID jumps, noisy, broken or saturated channels), physiological artefacts (eye movements, eye blinks, muscle artefacts), external artefacts (magnetized dental fillings) and environmental noise (Gross et al., 2012), as well as for representing an alert eyes-closed state. A minimum of 25 eyes-closed epochs was considered sufficient for further beamformer analysis (Brookes et al., 2008). On average 5.7 channels (range: 2-14) and 8.4 epochs (range 3-20) were discarded.

We used the beamformer approach known as Synthetic Aperture Magnetometry (SAM) (Robinson and Vrba, 1999) to reconstruct neural activity at labelled AAL voxels *(see SI)* (Hillebrand et al., 2012). In order to represent a ROI by a single time-series, we selected, for each ROI and frequency band separately, the voxel with maximum pseudo-Z value in that frequency band (Hillebrand et al., 2012; Robinson and Vrba, 1999). This resulted in 78 time-series for each frequency band: delta (0.5–4 Hz), theta (4–8 Hz), alpha1 (8–10 Hz), alpha2 (10–13 Hz), beta (13–30 Hz), and gamma bands (30–48 Hz).

The present study used a structural network which has been published before (Gong et al., 2009). In summary, 80 healthy subjects of age 18-31 years were included who did not have any history of neurological or psychiatric disorders. Diffusion tensor images for all subjects were obtained with a 1.5T-MRI system using 6 diffusion directions (Siemens Medical Systems, Erlangen, Germany), see (Gong et al., 2009) for details on MRI-sequences and parameters. First, each structural (T_1-weighted MP-RAGE) image was coregistered to DTI native space using a linear transformation. Secondly, the transformed structural image was mapped onto a T1 template space (ICBM152) using a non-linear transformation. Applying an inverse transformation to the anatomical automatic labelling (AAL) template in MNI space led to a subject specific AAL mask in DTI space. In this AAL template, the cerebral cortex is parcellated into 78 cortical areas (Tzourio-Mazoyer et al., 2002). Subsequently, white matter fiber tracking was reconstructed using deterministic tractography. For each subject, two cortical areas were considered to be connected if the end points of white matter fibers were located in these specific cortical regions. Lastly, a population based structural network was obtained by identifying connections that were most consistent across subjects by applying a nonparametric sign test to every pair of cortical regions.

MODALITY INVARIANT FUNCTIONAL INTERACTIONS

Functional connectivity analyses

For each subject and MEG epoch separately, we used the phase lag index (PLI) to calculate the functional connectivity between time-series of separate ROIs (nodes) to obtain a 78x78 connectivity matrix for each frequency band (Stam et al., 2007). The PLI is a metric for phase synchronization and calculates the asymmetry of the distribution of (instantaneous) phase differences between two time-series. The PLI ranges between 0 (no phase locking) and 1 (total synchronization) *(see SI)*. In addition, we applied the average envelope correlation (AEC) metric to estimate functional connectivity for each subject and MEG epoch separately (Brookes et al., 2011a). Time series were filtered in each frequency band. Before computing the Hilbert transform to obtain the analytical signal we orthogonalized time-series by means of linear regression analysis in order to reduce the effects of volume conduction (Hipp et al., 2012). The absolute value of the analytical signal was used as power envelope between which Pearson correlation coefficients were computed. For comparison, we also computed an older version of the AEC (where the orthogonalization procedure was not applied), which has previously been compared successfully to fMRI (Brookes et al., 2011a). For fMRI we used Pearson's correlation coefficients to estimate functional connectivity between time-series. To all functional connectivity values (based on Pearson correlation coefficients) we added one and subsequently divided by two to avoid issues with negative correlations. This also resulted in a 78x78 connectivity matrix for each subject. Connectivity matrices were subsequently averaged over epochs (MEG) and subjects (MEG and fMRI) to obtain one grand average functional connectivity matrix for each modality. For MEG, this was done for each frequency band and dataset separately.

Overlap of fMRI and MEG networks

Only for the first dataset we computed the overlap of strong connections between fMRI and each MEG frequency band using the PLI and AEC. To this end, we adjusted a measure that has been used for synonym extraction and web searching (Blondel et al., 2006). If **A** and **B** are two functional connectivity matrices, than the overlap of nodes with high degree is given by a similarity matrix **S** which is obtained after iterating:

$$\mathbf{S}_{q+1} = \mathbf{A}^T \mathbf{S}_q \mathbf{B} + \mathbf{B}^T \mathbf{S}_q \mathbf{A} \qquad (1)$$

where **S** is normalized after each iteration q using the matrix norm and $\mathbf{S}_0$ is initialized as a matrix with all entries one. As our functional connectivity values vary between one and zero, iterations may lead to an artificially high contrast between strong and weak connections. Even subtle regions showing relatively strong connections may be missed by an iterative process. To correct for this we did not iterate, but multiplied **S** by the element wise product matrix of **A** and **B**. To ensure that

MEG functional connectivity values across frequency bands, as well as MEG and fMRI functional connectivity values, contribute equally to the similarity values we normalized every matrix (**A** or **B**). Normalization was performed by transforming the matrices **A** and **B** into $\mathbf{A}_R$ and $\mathbf{B}_R$ where all elements in the functional connectivity matrices were replaced by their rank number. These ranked matrices were used to compute the similarity matrix (**Sim**) which is given by

$$\mathbf{Sim} = \frac{\mathbf{A}_R{}^T\mathbf{B}_R + \mathbf{B}_R{}^T\mathbf{A}_R}{\left\|\mathbf{A}_R{}^T\mathbf{B}_R + \mathbf{B}_R{}^T\mathbf{A}_R\right\|} \circ \frac{\mathbf{A}_R \circ \mathbf{B}_R}{\left\|\mathbf{A}_R \circ \mathbf{B}_R\right\|} . \quad (2)$$

Here, T corresponds to the transpose, $||...||$ indicates that each term is range normed and $\circ$ to the element wise product or Hadamard product.

STRUCTURAL AND FUNCTIONAL NETWORKS

Neural mass model

Aiming to understand the relation between the functional networks as observed by fMRI and MEG (Figure 2C) and the underlying structural network, we implemented a neural mass model which simulates alpha band oscillations (for details, see *SI* and (Ponten et al., 2010; Stam et al., 1999; van Dellen E. et al., 2013) for details). In summary: one neural mass model (NMM) describes the mean dynamics of a large neuronal population. Each NMM is characterized by the membrane potentials (simulated MEG time-series) and firing rates of its (excitatory and inhibitory) neuronal populations. Inhibitory and excitatory populations in each NMM are mutually coupled and coupling between two NMMs is reciprocal and excitatory. Neural masses were coupled using the literature based structural network described above. This structural network is an unweighted network with an equal number of nodes as our empirical functional connectivity analyses (see Figure 2). The overall coupling strength between neural masses is given by S. We varied S between 0-1.8 with steps of 0.1 and for each value of S 100 simulations were executed. To obtain fMRI BOLD-like time-series neural dynamics were transformed using a hemodynamic response function *(see SI)* (de Munck et al., 2007). Subsequently, the PLI and Pearson correlations were applied on simulated MEG and fMRI time-series, respectively, to obtain simulated functional networks. In both cases we averaged the functional connectivity matrices over all 100 simulated epochs. This average simulated functional connectivity matrix was used as a determinant to predict an empirical functional connectivity matrix using linear regression analysis. We used adjusted R-squared as a measure for goodness of fit to allow for interpretability of our results within the context of previous studies and to minimize potential overestimation of the variance that may be explained by a model (Deco et al., 2013b; Harel, 2009; Honey et al., 2007; Honey et al., 2009b).

Distance vs degree model

This distance vs degree model can be regarded as a reconfiguration model that aims to mimic functional connectivity as a trade-off between two rules: 1) the physical distance between two nodes, where distance is defined as Euclidean distance between the centroids of AAL regions (Alexander-Bloch et al., 2013b), and 2) the product of the structural degrees of two regions. Subsequently, the applied distance vs degree model entails that functional connectivity is regarded as a weighted sum of the degree product and the inverse distance. Based on findings in other fields of complex networks and the economical preferential attachment model we assumed that both the degree product and the inverse distance follow a power law (Yook et al., 2002). Taken together, for the functional connectivity ($\tilde{y}$) this yields

$$\tilde{y}_{ij} = a \cdot dis_{ij}^{-m} + b \cdot \left(k_i k_j\right)^n + c \text{, where } \tilde{y}_{ij} \in \{PLI_{ij}, Pearson_{ij}\}. \quad (3)$$

Here, for nodes *i* and *j*, the distance and degree product values are represented by dis_{ij} and $(k_i k_j)$, respectively. PLI_{ij} and $Pearson_{ij}$ are the PLI and Pearson based values of the connectivity matrices. The coefficients a, b, c, m and n were estimated using a non-linear least squares method using the Trust-Region algorithm (Byrd et al., 1987) to obtain estimates for functional connectivity for both fMRI and MEG.

Based on the distance vs degree model we follow a three step approach to predict functional connectivity (MEG, fMRI and the similarity between fMRI and MEG). First, we predict functional connectivity on the basis of the inverse distance, the degree product and the structural connectivity matrix separately (Figure 6). We also include the structural connectivity matrix for the prediction since it is known that there exists an overlap between structural and functional connectivity (Honey et al., 2007). Thus step 1 includes three predictions

$$\tilde{y}_{ij} = \begin{cases} a \cdot SC_{ij} + b & step\ 1a \\ a \cdot \left(k_i k_j\right)^m + b & step\ 1b \\ a \cdot dis_{ij}^{-m} + b & step\ 1c \end{cases} \quad (4)$$

Here SC_{ij} refers to a structural connection between node *i* and *j*. For the inverse distance and the degree product we also estimate the exponents such as in Eq. 3In the second step, we use the weighted sum of any two of the independent variables to predict functional connectivity which also leads to three predictions

$$\tilde{y}_{ij} = \begin{cases} a \cdot SC_{ij} + b \cdot dis_{ij}^{-m} + c & step\ 2a \\ a \cdot SC_{ij} + b \cdot \left(k_i k_j\right)^m + c & step\ 2b \\ a \cdot dis_{ij}^{-m} + b \cdot \left(k_i k_j\right)^n + c & step\ 2c \end{cases} \quad (5)$$

In the last and third step, we us the weighted sum of all three dependent variables to predict functional connectivity

$$\tilde{y}_{ij} = a \cdot dis_{ij}^{-m} + b \cdot (k_i k_j)^n + c \cdot SC_{ij} + d \quad (6)$$

In all equations *a, b, c* and *d* refer to constants or coefficients which are estimated using the aforementioned non-linear least squares method.

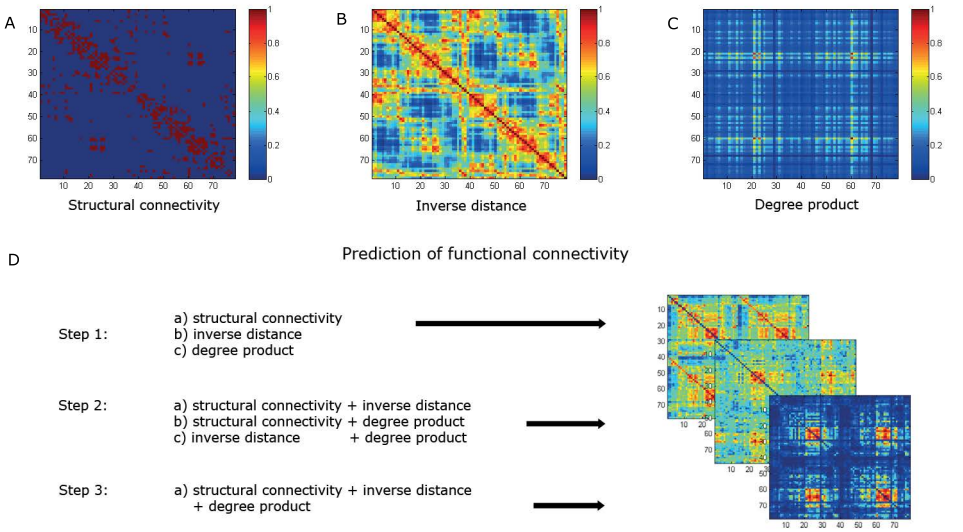

Figure 1: The flow chart of the distance vs degree analysis is depicted. (A) the unweighted structural connectivity matrix; (B) the inverse distance matrix which is defined as the Euclidian distance between the centroids of AAL regions; (C) the degree product matrix. (D). We follow a step by step approach: step 1: we predict functional connectivity by the structural connectivity matrix, inverse distance matrix or degree product matrix separately; step 2: we predict functional connectivity by a weighted sum of any two of these matrices; step 3: we predict functional connectivity by the weighed sum of all three matrices. In these analyses we predict MEG and fMRI functional connectivity as well as the similarity between the two.

Assortativity of the structural network

Lastly, we quantified assortativity of the literature based structural network to analyze how nodes with a certain degree tend to be connected to each other (see SI) (Newman, 2002). Assortativity quantifies the relationship of the degrees between nodes which is related by measuring the pearson correlation coefficient between the degree of nodes. An assortativity value higher than zero indicates that high degree nodes tend to connect to high degree nodes, whereas an assortativity value less than zero indicates that high degree nodes tend to connect to low degree nodes. All analyses were performed using Matlab v2012a and Brainwave (versions 0.9.101. available from http://home.kpn.nl/stam7883/brainwave.html)

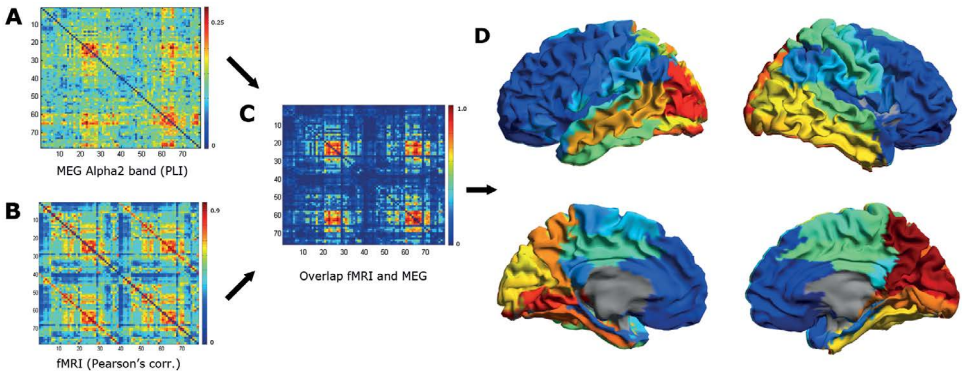

Figure 2: Overlap of strong functional connections between MEG and fMRI. (A) MEG functional connectivity in the alpha2 band; (B) fMRI functional connectivity; strong functional connections are depicted in red, weak functional connections are depicted in blue; (C and D) The overlap of strong functional connections (equation 1) is dominated by four strongly connected blocks of brain regions in posterior and temporal areas, including the precuneus and superior parietal gyrus. These four blocks correspond to one group of regions in the brain that are strongly connected within one hemisphere and at the same time have many interhemispheric homologous connections. Panel D shows a colour coded map of the average similarity for each ROI: red indicates high overlap and blue low overlap.

RESULTS

Modality invariant functional interactions

We computed the functional connectivity matrices for MEG by computing the PLI (see Figure S1) and for fMRI by computing Pearson correlation coefficients. MEG functional connectivity matrices in the alpha1, alpha2 and beta band displayed structure in the form of strongly connected brain regions in posterior and temporal areas, also involving the precuneus (AAL regions 20-28 and 59-67 in Figure 2A and S1, see Table S1 for AAL regions), that appeared as four red blocks in the functional connectivity matrix. The two blocks that appeared around the diagonal of the matrix correspond to temporal and posterior connections within the two hemispheres, i.e. short distance functional connections. The two off-diagonal blocks correspond to the homologous interhemispheric and long distance connections between these same temporal and posterior areas. Thus these four blocks correspond to one group of regions in the brain that are strongly connected within one hemisphere and at the same time have many interhemispheric homologous connections. Also, note that the four red blocks were almost joined by vertical and horizontal 'stripes', which indicates that these brain regions were not only strongly interconnected with each other but also with the rest of the brain. In addition, we observed that these four blocks were less well bounded for the beta band, where also regions such as the right postcentral gyrus, inferior and superior parietal gyrus are incorporated (AAL 56, 56, 57) (Figure S1). In a larger dataset, the same patterns of blocks can also be seen in the alpha1, alpha2, beta and delta band as well (Figure S1), indicating that these blocks are robust

properties of functional connectivity matrices obtained by PLI. These observations were confirmed in plots (not shown) of similarity between CTF MEG data and Elekta MEG data. In the fMRI functional connectivity matrix there were also four large blocks apparent, at exactly the same temporal and posterior locations (Figure 2B). Apart from these four large red blocks there were four smaller red blocks (between AAL regions 12-17 and 51-56 in Figure 2B) in the fMRI functional connectivity matrix. These latter blocks were formed by functional connections with frontal and parietal areas such as the precentral gyrus, postcentral gyrus and superior parietal gyri. Additionally, the fMRI functional connectivity matrix showed strong homologous inter-hemispheric functional connections, the two lines parallel to the diagonal (Figure 2B), which were not observed with MEG.

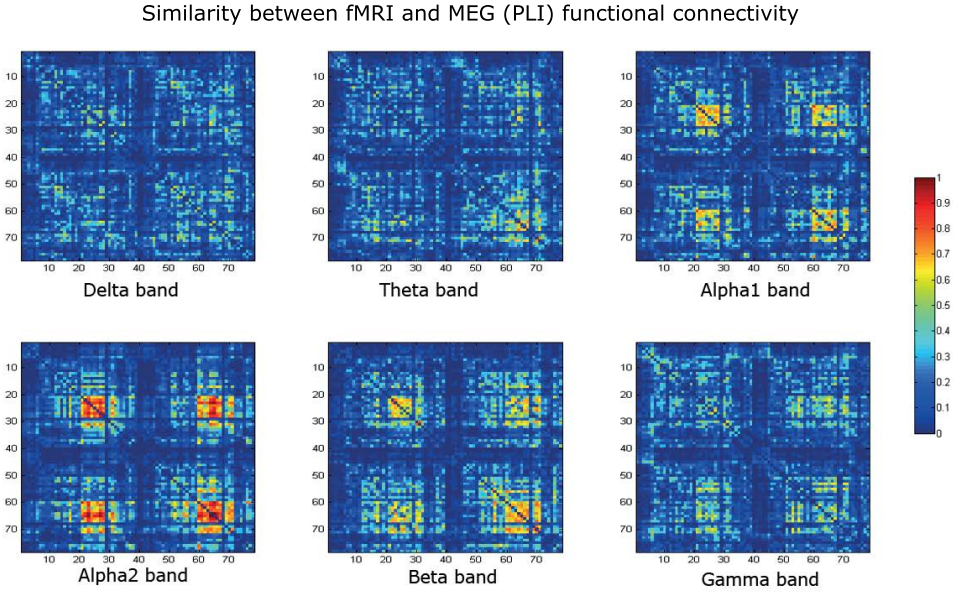

Figure 3: The similarity or overlap between MEG functional networks obtained with the PLI metric and fMRI. Similarity is computed by Eq. 2. Note the appearance of four blocks in the matrices for several frequency bands. The color bar indicates the amount of similarity which can range between 0 and 1.

To test the overlap of strong modality invariant functional connections we computed the similarity between fMRI and MEG functional connectivity matrices. Figure 3 and 4 show the similarity matrices for each frequency band separately, where we again observed the four red blocks in the alpha1, alpha2 and beta band, indicating that these temporal and posterior connections are stable connections with respect to both fMRI and MEG and thus modality-invariant. In the plots of the distribution of all similarity values for each frequency band (all elements from the similarity matrices) we observed that especially the alpha2 band showed high similarity (kruskal-wallis, $\chi^2 = 25.97$, df = 5, $p < 0.001$) (Figure 5). As the similarity values were the highest for the alpha2

band, we only illustrate the overlap of strong connections between fMRI and alpha2 MEG functional connectivity matrices in more detail (Figure 2C). The aforementioned four large red blocks were formed especially by connections between the precuneus, superior-, medial- and inferior occipital gyri, calcarine gyri, cuneus, lingual gyri, fusiform gyri, superior parietal gyri, medial cingulate gyri, and medial and inferior temporal gyri (Figure 2C and D).

In addition to the analyses based upon the PLI, we repeated the same analyses for the MEG dataset, but this time using the average envelope correlation (AEC) as functional connectivity metric (Brookes et al., 2012b; Hipp et al., 2012). MEG functional connectivity matrices based on the AEC showed similar large blocks in temporal and posterior regions in the alpha1, alpha2, beta and also in the theta band (Figure S2). For the AEC metric strong functional connections in the beta band appeared again in four blocks in the matrix, however, compared to the other frequency bands these blocks were shifted towards more parietal regions, including the precentral, postcentral and inferior and superior parietal gyrus (AAL 14, 16, 17, 18). If we now again compute the overlap of connections between fMRI and MEG we still observe (figure S3) four blocks of areas in the similarity matrices for the theta, alpha1, alpha2 and beta band just as in our previous analysis (Figure 2). For the beta band, the strongest overlap occurred more in parietal areas as compared to the other frequency bands, which showed highest similarity for the superior parietal gyrus. Furthermore, there seemed to be homologous inter-hemispheric functional connections, as two lines parallel to the diagonal could be discerned for most frequency bands (Figure S3). By plotting the distribution of the similarity values we observed that the MEG functional connections in the alpha2 and beta band had the highest level of similarity with fMRI (kruskal-wallis, $\chi^2 = 16.25$, df = 5, $p = 0.006$) (Figure S4).

An older version of the AEC has previously been compared to fMRI (Brookes et al., 2011a), and we therefore computed MEG functional matrices based on this previous AEC version as well (Figure S5). Functional connectivity patterns for this measure were highly similar across frequency bands and had a high overlap with the Euclidean distance matrix (which is defined as the Euclidian distance between the centroids of AAL regions) (Figure 1). The difficulty with MEG is that many short distance connections, abundantly found in the distance matrix and in these AEC matrices, are difficult to distinguish from volume conduction (Winter et al., 2007).

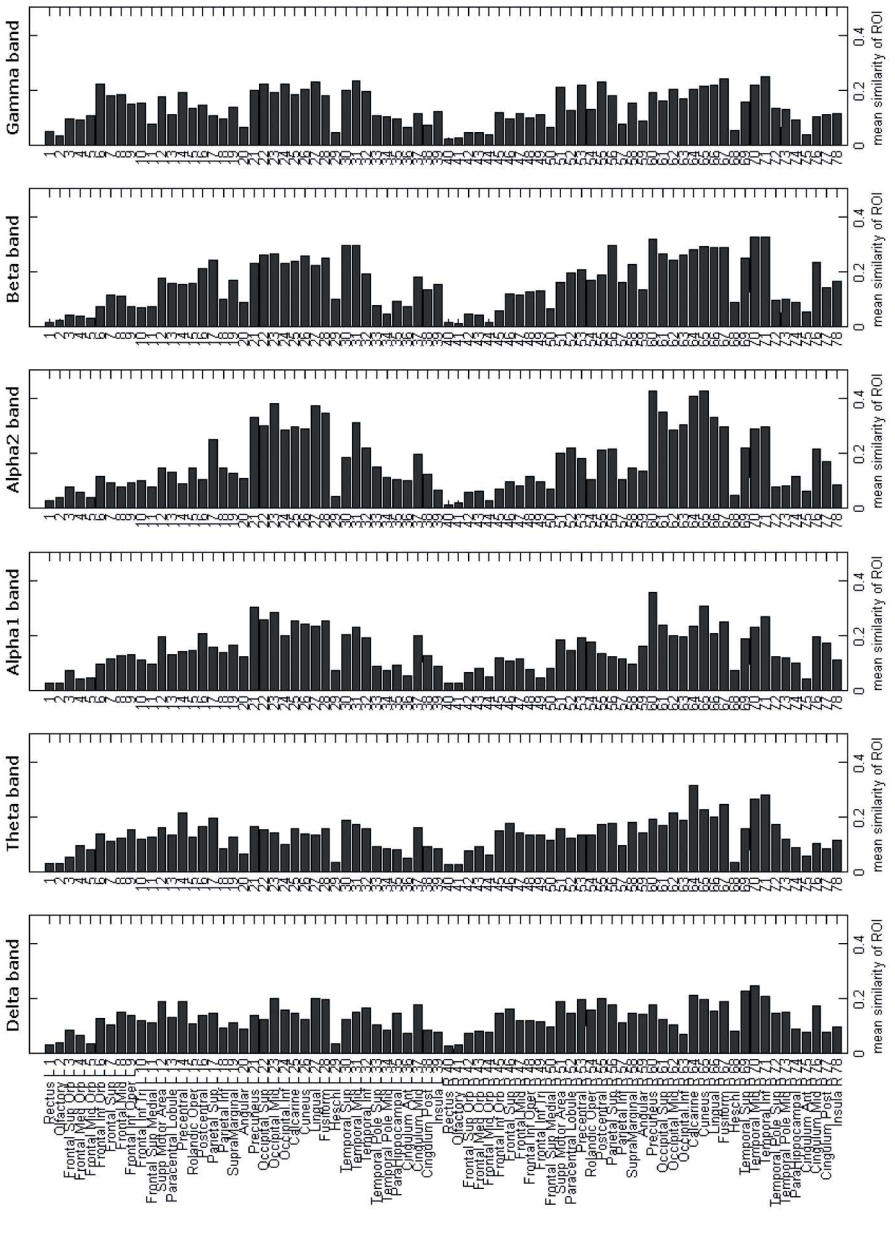

Figure 4: Similarity regionwise. For each MEG frequency band we computed the average similarity per region with fMRI. Each bar corresponds to the average over rows in the corresponding matrix in Figure 2.

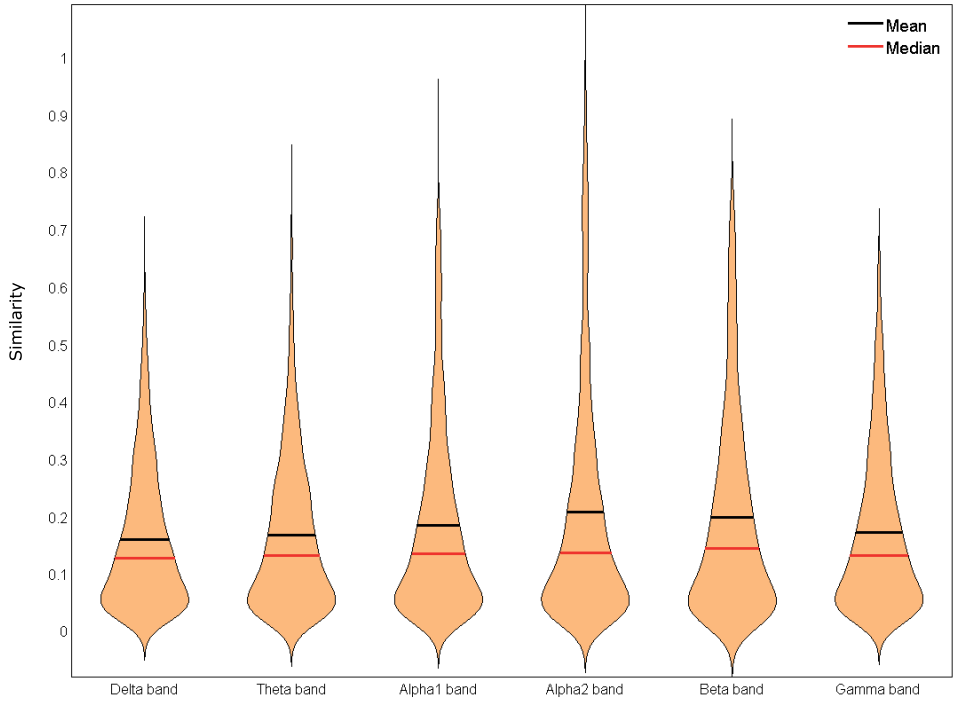

Figure 5: distribution plots for the similarity between fMRI and each MEG frequency band. Similarity values were not normally distributed and therefore depicted using violin distribution plots.

Structural and functional networks

In the previous section we have demonstrated the presence of modality invariant functional connections between posterior and temporal brain areas in the theta, alpha1, alpha2 and beta band using both the PLI and the AEC as functional connectivity metrics for MEG. In subsequent analysis we analysed the relationship between these functional connections and the underlying structural network, where for MEG we only performed analysis for the PLI in the alpha2 band. The rationale behind this is that the similarity between the alpha2 band and fMRI was the highest and, moreover, we subsequently used a specific neural mass model that was developed to simulate alpha band oscillations. It should be noted though that, apart from the neural mass modelling, the subsequent results generally could also hold for the other frequency bands as the same modality invariant functional connections were also found for other frequency bands.

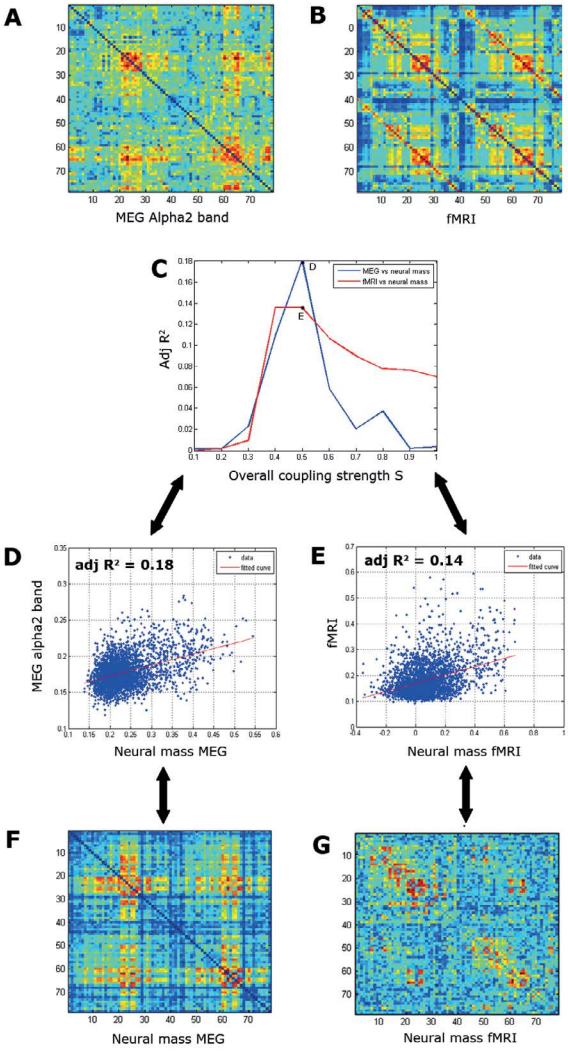

Figure 6: Prediction of empirical functional connectivity based on simulated functional connectivity, for MEG and fMRI separately. Neural mass models were used to simulate MEG and fMRI-like functional networks. (A) empirical MEG functional connectivity in the alpha2 band; (B) empirical fMRI functional connectivity; (C) Global strength of structural coupling S was increased with steps of 0.1 and for each value of S a simulated functional network was obtained. Empirical functional networks were predicted based on these simulated networks using a linear regression analyses. For both fMRI and MEG the best match between empirical and simulated functional networks was found for S = 0.5; (D) Scatter plot of empirical MEG functional connectivity (alpha2 band) versus simulated functional connectivity and linear fit for the optimum structural coupling strength (S=0.5); (E) Scatter plot of empirical fMRI functional connectivity versus simulated functional connectivity and linear fit for the optimum structural coupling strength (S=0.5); (F) Simulated MEG functional connectivity that was obtained for the optimum structural connection strength (S=0.5). Note the reappearance of the four blocks of strongly connected brain regions in temporo-posterior regions along with horizontal and vertical stripes as in the empirical MEG connectivity matrix; (G) Simulated fMRI functional connectivity that was obtained for the optimum structural connection strength (S=0.5). Note the reappearance of the same four blocks as in B and F, but also other blocks near the diagonal (as in the experimental data (B)).

In the first analysis, we varied the global strength of coupling between neural masses and used the obtained average simulated functional connectivity matrix to predict the empirically observed functional connectivity matrices, for fMRI and MEG separately. We observed that for both fMRI and MEG the best fit between the simulated and experimental functional connectivity was obtained for an overall structural coupling strength of $S = 0.5$ (Figure 6C). For $S < 0.5$ we observed average simulated functional connectivity matrices (fMRI and MEG) that showed only weak patterns and for $S > 0.5$ the simulated functional connectivity matrices more resembled the structural connectivity matrix (Figure S6). The mean PLI for the MEG simulated functional networks also increased as a function of global coupling strength for $0 < S < 0.8$ (Figure S7). There was a rapid increase of mean PLI between $0.2 < S < 0.5$ and the derivative of the mean PLI had a clear maximum at $S = 0.4$. Together, this indicates that the optimal fit for the functional network is found near a phase transition for global synchronization. Note that especially for the MEG simulated functional connectivity matrix we again observed four blocks, indicating strong functional connectivity for exactly the same temporo-posterior regions as for the empirical MEG data (AAL regions 20-28 and 59-67) (Figures 6A&F). Similarly, these four blocks in the matrix were again almost joined by vertical and horizontal 'stripes', as was the case for the empirical data. For simulated fMRI, we also saw strongly connected regions, including the strongly connected temporo-posterior regions, however the resemblance with the empirical functional connectivity matrix was weaker (adj $R^2 = 0.14$) (Figure 6E).

In the second analysis we used a distance vs degree model in order to predict functional connectivity on the basis of the underlying structural network characteristics by a three step approach. In the first step, we observed that for both modalities and for the similarity matrix the degree product matrix seemed to be the best predictor of functional connectivity when the degree product, the inverse distance and the structural connectivity were all used as separate predictors for functional connectivity (Table 1). Especially for the similarity matrix the amount of variance that could merely be explained by the degree product matrix was relatively large compared to the inverse distance or structural connectivity matrix (adj $R^2 = 0.24$). For the degree product the exponent had a value close to one, whereas for the inverse distance this exponent was around 2 or larger (Table 2) indicating that the amount of functional connectivity that could be explained by distance drops off fast with distance. In the second step, we combined any two predictors for explaining functional connectivity. The best fit for functional connectivity for each modality and the similarity matrix was obtained by the weighted sum of distance and the degree product (i.e. distance vs degree model). The corresponding fits and the derived matrices are depicted in Figure 7. The optimal ratio for inverse distance vs degree product coefficients was 0.36 for MEG and 1.1 for fMRI. The degree product contributed more than distance in explaining empirical functional connectivity for MEG, whereas the contribution in explaining empirical functional connectivity for fMRI was almost equal between the distance and the degree product. The estimated power exponent for the distance was 2.3 and 5.8 for MEG and fMRI, respectively, indicating again that there was a tendency that large distances contribute little to functional connectivity values. Also note that the adj R^2 was higher for

the fMRI data than for the MEG data (adj R^2 fMRI = 0.33 vs adj R^2 MEG = 0.12). This was not only the case for the specific distance vs degree model but for all used models. In the estimated functional connectivity matrices (Figures 7E&F), we again observed the modality invariant functional core network (Figures 7A&B). In the estimated functional connectivity matrix for fMRI (Figure 7F) we also observed homologous inter-hemispheric connections and other regions as seen with empirical fMRI (Figure 7B) such as the left anterior and posterior cingulate gyri (AAL 36, 39), the left and right medial superior frontal gyri (AAL 11, 50) and the pre- and post-central gyri (AAL 14, 16, 53, 55). In the last step, we predicted functional connectivity on the basis of structural connectivity, the inverse distance and the degree product. The obtained fits were slightly better than for the distance vs degree product (Table 1). Also for this estimation, the exponents for the inverse distance were consistently higher than for the degree product for all modalities and the similarity matrix.

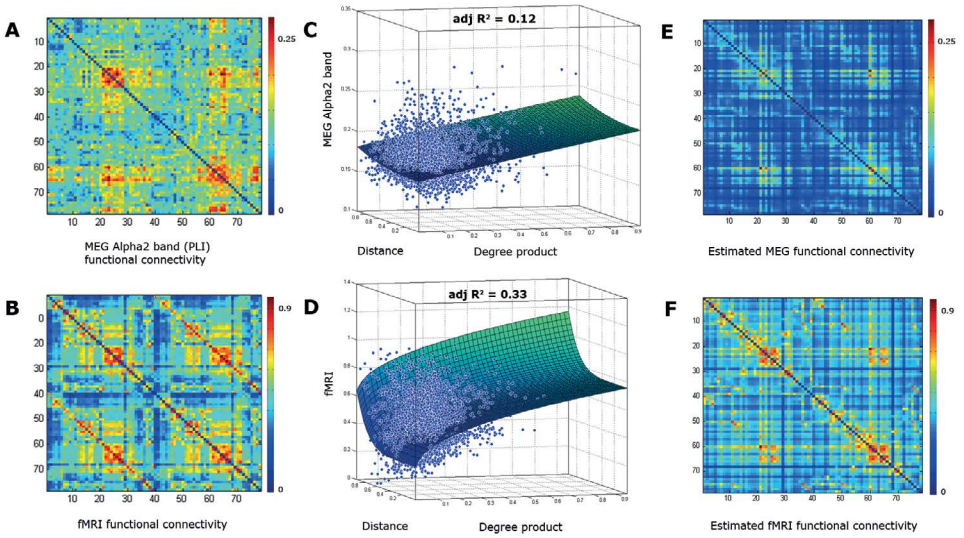

Figure 7: Prediction of empirical functional connectivity based on the distance vs degree model: trade-off between distance penalization and the degree product of nodes in the structural network, both described as a power law. Five parameters corresponding to the coefficients and powers of distance and the degree product were estimated to fit a plane (equation 2). (A) empirical MEG functional connectivity in the alpha2 band; (B) empirical fMRI functional connectivity; (C) fit for MEG, the plane is mostly influenced by the coefficients for the degree product; (D) fit for fMRI, there is again a linear trend present caused by the coefficients for the degree product. The power coefficient for the distance contribution causes the steep increase of the plane for shorter distances; (E) estimated MEG functional connectivity characterized by reappearance of the four strongly connected temporo-posterior blocks, i.e. one group of regions in the brain that are strongly connected within one hemisphere and at the same time have many interhemispheric homologous connections.; (F) estimated fMRI functional connectivity shows even more similarity with the empirical fMRI functional connectivity (B), such as the appearance of homologous interhemispheric connections and strong connections for other regions, including the left anterior and posterior cingulate gyri (AAL 36, 39), the left and right medial superior frontal gyri (AAL 11, 50) and the pre- and post-central gyri (AAL 14, 16, 53, 55).

The above results demonstrated that the degree product (i.e. high degree nodes) was important to explain empirical functional connectivity for both fMRI and MEG (PLI), and we therefore computed the assortativity coefficient for the structural network. This was found to be 0.08 (positive), indicating that high degree nodes tend to be connected to each other.

DISCUSSION

Analysis of resting-state functional connectivity between brain regions derived from MEG and fMRI recordings revealed a modality invariant functional core network in the human brain. For MEG data, the core network was most prominently found in the upper alpha frequency band. This functional core network consists mainly of temporo-posterior regions. With an anatomically realistic coupling of neural mass models we demonstrated that this functional core appears near a phase transition for functional connectivity. Most importantly, we could predict this modality invariant functional core network with a simple yet powerful analytical model that takes into account the degree product of nodes in the structural network and the Euclidean distance between these nodes.

To our knowledge this is the first paper that analyzed the overlap between MEG and fMRI functional networks on the same subjects using the same anatomical AAL atlas. The largest overlap between functional interactions estimated by fMRI and MEG was found for temporo-posterior regions including the precuneus and superior parietal gyrus. These areas are considered to be part of a densely connected structural network of high degree nodes, also known as the "rich-club" (Collin et al., 2013; van den Heuvel and Sporns, 2011). Other areas in the observed temporo-posterior core network (Figure 2) such as the lingual gyrus, cuneus, fusiform gyrus and calcarine gyrus are also known to be high degree nodes and are sometimes also considered to be part of the rich-club (van den Heuvel and Sporns, 2011). The medial superior frontal cortex and subcortical regions make up the rest of the rich-club, but these regions did not show much overlap between MEG and fMRI. In our analysis subcortical regions were not included as ROIs. The fact that the medial superior frontal cortex and other frontal connections were not found could be caused by more variability across subjects or less stability of frontal connections. Nevertheless, the absence of these frontal connections requires further investigation as previous large scale studies did find important frontal connections, however only using an uni-modal approach (Power et al., 2013; Yeo et al., 2011). Compared to the phase lag index, the average envelope correlation showed similar patterns in the functional connectivity matrices across several frequency bands. Therefore the current findings do not seem to depend highly on the functional connectivity metric for MEG as long as one corrects for signal leakage. Therefore, the observed temporo-posterior core network can certainly be regarded as modality invariant as it was observed with MEG by applying two metrics in two different datasets (Figure S1, S2, S3), in more than one frequency band (delta, theta, alpha1, alpha2, and beta band, Figure S1), was also observed with fMRI and even reproduced by a realistically coupled neural mass model. This finding is consistent with recent studies that also reported strongly functionally

connected areas in temporo-posterior parts of the brain (Liao et al., 2013; Power et al., 2013). Also another MEG study found that posterior regions may play an important role in temporal dynamics of resting state networks and even in switching between on and off status of these networks (de Pasquale F. et al., 2012). However, in the present study modality invariant functional interactions could be regarded as stationary spatial patterns of functional connectivity as functional networks were obtained after averaging over MEG epochs, i.e. small fluctuations of functional interactions were discarded.

Table 1: Prediction of functional connectivity matrices. Adjusted R^2 are listed for each modality (MEG alpha2 band PLI, fMRI and similarity between fMRI and MEG). Prediction is performed based on the independent variables (model) listed on the left.

model	MEG PLI alpha2	fMRI	Similarity
Step 1			
structural connectivity	0.037	0.150	0.104
inverse distance	0.035	0.147	0.078
degree product	0.087	0.183	0.236
Step 2			
structural connectivity + inverse distance	0.044	0.184	0.117
structural connectivity + degree product	0.104	0.276	0.285
inverse distance + degree product	0.120	0.334	0.317
Step 3			
structural connectivity + inverse distance + degreeproduct	0.121	0.340	0.322

The observed temporo-posterior core network was reproduced by using realistically coupled neural mass models. The optimal structural model, i.e. the one for which the coupled neural masses produced a functional network that was most similar to the empirical data, was determined by varying the global structural connectivity strength. For this optimal structural network, the functional network was found to be near the threshold for global synchronization. These findings are in agreement with a recent computational modelling approach which revealed that the best agreement between empirical and simulated functional connectivity is found near a bifurcation in a multi-stable regime where a spontaneous state (i.e. resting-state) coexists with states of high activity (Deco et al., 2013b). Small linear fluctuations around the spontaneous state were able to explain resting-state dynamics and re-occurring functional connectivity patterns. Other models also found that functional connectivity emerged due to noise induced fluctuations near instability (Cabral et al., 2013; Deco et al., 2009; Deco and Jirsa, 2012; Ghosh et al., 2008; Honey et al., 2007) or at criticality (Haimovici et al., 2013). Previous studies have performed sophisticated analysis of neural mass models for single modalities. The present study is the first study that employed a multi-modal approach to demonstrate that the optimal fit for functional networks near a phase

transition is independent of the modality, indicating that these findings can be generalized. In the present study, functional networks characterized by low average synchronization and a more-or-less random topology were obtained when global structural connectivity strength was low. When increasing global structural connectivity strength, the first regions that start to synchronize were mostly located in the functional core network (Figure S6). Especially for the simulated and empirical MEG data there was high similarity in terms of reappearance of the temporo-posterior core network in combination with co-occurring 'stripes' in the functional connectivity matrices (Figure 6). The relatively low overall match between simulated functional connectivity and empirical functional connectivity (adj $R^2 = 0.18$ for MEG and adj $R^2 = 0.14$) could be due to the fact that the empirical functional connectivity matrices contain a lot of noise, since many elements in the matrix correspond to functional connections that occur with low probability.

We further explored the relation between functional and structural networks by using different models based on the distance vs degree model and demonstrated that functional networks emerge due to a trade-off between distance penalization and the product of the structural degree of nodes. First, we separately estimated the contribution of inverse distance, the degree product and structural connections to functional connectivity. The degree product was for all modalities the best predictor for functional connectivity. When we allowed two or three predictors in our model we found that the distance vs degree model and the distance vs degree plus structural connection model were the best models that could predict functional connectivity. However, the addition of structural connections to the distance vs degree model only slightly improved prediction. This could be explained by the observation that the structural connectivity matrix and the inverse distance seem to be highly similar (Figure 1), except for the fact that the former is unweighted and the latter weighted. The importance of the degree product of structural nodes for explaining functional connectivity was evident in our brain networks. This concept has first been used for explaining air-traffic between airports and social networks (Barrat et al., 2004). The exponent of the degree product in air-traffic networks was estimated at around 0.5, which is similar to our findings for fMRI. This exponent depends on the scale-free properties or degree distribution of the nodes in the network as for networks with larger scale-free exponents the degree product exponent is also larger (Barrat et al., 2004). As this degree product exponent was higher for MEG than fMRI this could indicate that MEG functional networks are more shaped by scale-free characteristics of the structural network than is the case for fMRI. Furthermore, in particular for MEG, the contribution of the structural degree product to functional connectivity was more dominant than anatomical distance. Moreover, the estimated exponents for distance were much larger than for the degree product in both cases, demonstrating that the relative differences in anatomical distance (anatomical connections over large distances contribute less than short distance connections) are of less importance for functional connectivity than is the case for the variability in degree product. This suggests that two remote brain areas are still able to communicate, but the probability at which this occurs is higher if these areas are high degree nodes in the structural network. As the structural

network was assortative (high degree nodes tend to be connected to high degree nodes), this also suggests that high degree nodes are necessary for long distance communication. Under the assumption that these long distance connections provide for efficient network topology (Bullmore and Sporns, 2012), this indicates as well that high degree nodes are necessary for maintaining efficient functional network topology.

Table 2: Prediction of functional connectivity matrices. Estimated parameters for each model.

model	MEG PLI alpha2	fMRI	Similarity
Step 1			
$a \cdot SC_{ij} + b$	a = 0.013 b = 0.177	a = 0.196 b = 0.454	a = 0.204 b = 0.147
$a \cdot (k_i k_j)^m + b$	a = 0.068 b = 0.169 m = 1.167	a = 0.574 b = 0.286 m = 0.615	a = 0.944 b = 0.005 m = 1.008
$a \cdot dis_{ij}^{-m} + b$	a = 0.024 b = 0.017 m =2.804	a = 0.726 b = 0.445 m = 6.309	a = 0.297 b = 0.101 m = 2.139
Step 2			
$a \cdot SC_{ij} + b \cdot dis_{ij}^{-m} + c$	a = 0.009 b = 0.012 c = 0.174 m = 1.947	a = 0.124 b = 0.540 c = 0.446 m = 7.613	a = 0.163 b = 0.186 c = 0.028 m = 0.481
$a \cdot SC_{ij} + b \cdot (k_i k_j)^m + c$	a = 0.009 b = 0.060 c = 0.169 m = 1.145	a = 0.159 b = 0.486 c = 0.276 m = 0.534	a = 0.144 b = 0.833 c = 0.001 m = 0.974
$a \cdot dis_{ij}^{-m} + b \cdot (k_i k_j)^n + c$	a = 0.022 b = 0.060 c = 0.162 m = 2.304 n = 0.947	a = 0.652 b = 0.580 c = 0.195 m = 5.698 n = 0.466	a = 0.284 b = 0.980 c = 2.24×10^{-10} m = 2.561 n = 1.222
Step 3			
$a \cdot dis_{ij}^{-m} + b \cdot (k_i k_j)^n + c \cdot SC_{ij} + d$	a = 0.002 b = 0.059 c = 0.019 d = 0.162 n = 0.959 m = 2.105	a = 0.051 b = 0.552 c = 0.564 d = 0.207 n = 0.464 m = 5.902	a = 0.075 b = 0.932 c = 0.189 d = 1.18×10^{-10} n= 1.212 m = 1.961

Abbreviations: dis_{ij} = Euclidean distance between two nodes *i* and *j*; k_i = degree of node *I*; SC_{ij} = structural connection between nodes *i* and *j*. *a, b, c, d* are parameters that are fitted. Likewise, *m* and *n* refer to exponents that are fitted.

Generative models such as the economical preferential attachment model or economical clustering model have also been used to explain emergent functional networks (Vertes et al., 2012; Yook et al., 2002). Although these growth models are able to describe and model features of realistic functional networks, the emergent degree distribution of these networks become stable only when network size is very large (Foster et al., 2006; Klemm and Eguiluz, 2002). Therefore, growth models

might not be suitable for functional brain networks given the small sizes of these networks as a result of current parcellation schemes for atlases of the cortex (Tzourio-Mazoyer et al., 2002). The current approach differs with respect to these generative models in the sense that our model is not a growth model, but utilizes information about high degree nodes of the underlying structural network. Furthermore, we assumed that the product of two nodal degrees in the structural network and distance penalty may contribute independently to functional network connectivity as both may correspond to independent processes.

By using the distance vs degree model we were able to estimate functional connectivity matrices that again were characterized by the appearance of the temporo-posterior core network. This core network could even be identified merely based on the degree product matrix where especially the precuneus seemed important in shaping its structure (Figure 1). Adding distance to this degree product matrix ensures 'smearing out' of functional connections towards the diagonal. This phenomenon was more evident for fMRI functional networks than for MEG functional networks, i.e. fMRI functional networks contain more distance based information than MEG functional networks. In the estimated fMRI functional networks we observed, besides the temporo-posterior core network, other strongly connected brain regions, that were also observed in the empirical fMRI network. These included homologous inter-hemispheric functional connections and important hub areas such as the medial superior frontal gyri and the left posterior cingulate gyrus, supporting the hypothesis that the mentioned distance vs degree model is important to understand function in terms of structure (van den Heuvel and Sporns, 2011). The explanation for appearance of the temporo-posterior core network is that high degree nodes in our structural network tend to be more distributed in the posterior part of the brain which also has been demonstrated by an early structural network study (Gong et al., 2009; Hagmann et al., 2008). This also explains why even in the neural mass simulations this temporo-posterior core network was present as neural masses were coupled using the given structural network with high degree nodes in temporo-posterior regions.

We need to mention some methodological considerations. Although an in-depth comparison of the performance, in experimental data, of different types of MEG metrics of functional connectivity, i.e. those based on phase relationships and those based on amplitude modulations, was beyond the scope of the current paper, we do believe that this is an important topic for future research. This relationship was only partially studied previously (Hipp et al., 2012), where it was shown that the amplitude correlation between two signals is monotonically related to the magnitude of the phase difference between the carrier oscillations. Furthermore, in the present study we have also demonstrated that both measures are able to correct for volume conduction effects as functional network matrices obtained by both measures were not merely a reflection of the inverse distance matrix. Therefore it may seem that for experimental data methodological differences between AEC and PLI might have little effect at the group level.

The present study does have some limitations. Firstly, we investigated the relation between structural and functional networks while the structural network we used for analyses was not

derived from the same subjects as the functional network analyses, but instead we used a literature-based structural network obtained from a large population. We therefore predict that usage of structural and functional data originating from the same subjects would increase the predictive power of structural networks with regards to the functional connectivity on the network. Biases and limitations related to construction of the structural network itself may also have contributed to the imperfect prediction of functional networks from the structural network. The structural network that we used was obtained by deterministic tractography which is known to have difficulties in resolving crossing fibers and thus may lead to missed connections, especially long distance and interhemispheric connections (Gong et al., 2009; Mori and van Zijl, 2002; Sotiropoulos et al., 2010). Related to this point, we used an unweighted structural network to predict functional networks, whereas taking into account the weights of the connections in the structural network may lead to different results. Future studies will need to explore these issues further when a weighted structural network for a healthy population becomes available. Secondly, we described a functional core network consisting of strongly connected regions in temporal and posterior regions. However, the boundaries of this core network were not analyzed by sophisticated methods such as core decomposition or modularity analysis. Future studies will need to investigate this functional core network in more detail as was done by (de Pasquale F. et al., 2012; Hagmann et al., 2008; Shanahan, 2012). Thirdly, we used a relatively simple hemodynamic response function for simulating fMRI data, which may have resulted in a relatively low adj R^2. However, even with the empirically derived hemodynamic response function that we used, we were able to demonstrate that the best fit for empirical fMRI was obtained near the transition to global synchronization. This is in agreement with earlier studies (Deco et al., 2009; Ghosh et al., 2008), hence we do not expect that the use of a more complicated hemodynamic response function would affect our results qualitatively. Fourthly, the neural mass model used in this study does not include conduction delays. It is known that including delays in neural mass models allows for studying more complex and realistic temporal patterns of brain dynamics and properties such as multi-stability of states (Deco et al., 2011). However, in the present study we were interested in stationary spatial patterns of functional networks, and these are not altered by the introduction of delays (Deco et al., 2013a). Finally, we used a relatively straightforward matrix manipulation to compare the strongest connections in two connectivity matrices (equation 2), which may not capture all the relevant information in the two matrices (i.e. similarity in weak connections are ignored). However, there is still no consensus on the best way to objectively quantify the similarity of two networks. Theoretical studies are needed to investigate this issue further.

We have investigated modality invariant functional interactions which revealed a temporo-posterior core network obtained by fMRI and MEG. We have demonstrated that this temporo-posterior core network emerges near a modality invariant phase transition for functional connectivity. Most importantly, this modality invariant temporo-posterior core network could be predicted by especially the degree product between nodes in the underlying structural network.

SUPPLEMENTARY INFORMATION

MEG: Beamforming

We used the beamformer approach as described by (Hillebrand et al., 2012). In summary, a co-registered MRI was spatially normalized to a template MRI. The AAL atlas was used to label the voxels in a subject's normalized co-registered MRI (Tzourio-Mazoyer et al., 2002). Subcortical structures were removed, and the voxels in the remaining 78 cortical regions of interest (ROIs) were used for further analysis (Gong et al., 2009), after inverse transformation to the patient's co-registered MRI. Neuronal activity for the labeled voxels in the ROIs was reconstructed using a beamforming approach known as Synthetic Aperture Magnetometry (SAM) (Robinson and Vrba, 1999). Neuronal activity VE at each voxel was reconstructed as the weighted sum of the recorded time-series **B** at sensor locations:

$$VE = \mathbf{C}_j \mathbf{L}^T \mathbf{C}_b^{-1} \mathbf{B} = \mathbf{W}\mathbf{B} \quad (1)$$

The beamformer weights, **W**, are determined by the lead field **L,** the data covariance matrix $\mathbf{C}_b$ (based on, on average, 307s (range: 164-282s) of data), and the source current covariance matrix $\mathbf{C}_j$. The crux of the beamformer approach is the estimation of **W**, which can be done analytically under the assumption that any two sources in the brain are linearly independent (Hillebrand et al., 2012). Subsequently, in order to represent a ROI by a single time-series, we selected, for each ROI and frequency band separately, the voxel with maximum pseudo-Z value in that frequency band (1, 4). For the computation of the pseudo-Z values we used $\mathbf{C}_b$ and a unity matrix for the noise covariance. The broad-band (0.5–48 Hz) time-series for these selected voxels were used for further analysis. This resulted in 78 time-series for each frequency band. Six frequency bands were analyzed: delta (0.5–4 Hz), theta (4–8 Hz), alpha1 (8–10 Hz), alpha2 (10–13 Hz), beta (13–30 Hz), and gamma bands (30–48 Hz). For each subject, five artefact free epochs of 4096 samples (6.555s) were selected to obtain stable results (5-13). BrainWave software was used for this purpose and further analyses (version 0.9.101 available from http://home.kpn.nl/stam7883/brainwave.html).

Functional Connectivity analysis

For each subject and MEG epoch separately, we used the phase lag index (PLI) to calculate the functional connectivity between time series of separate ROIs (nodes) to obtain a 78x78 weighted connectivity matrix **A**. The PLI calculates the asymmetry of the distribution of (instantaneous) phase differences between two time-series:

$$PLI = |< \mathrm{sign}[\sin(\Delta\varphi(t_k))] >| . \quad (2)$$

Here the phase difference $\Delta\varphi$ is defined in the interval $[-\pi, \pi]$, <> denotes the mean value, sign stands for signum function and ffffl indicates the absolute value. The PLI ranges between 0

(completely symmetric phase distribution) and 1 (completely asymmetric phase distribution). The rationale behind this approach is that field spread/volume conduction causes a zero phase lag between two time-series, and that a uniform distribution of phases occurs when there is no coupling at all. The presence of a consistent, non-zero, phase lag between two time-series therefore reflects true interactions that are unaffected by field spread/volume conduction or common sources (Stam et al., 2007).

Graph measure: Assortativity

Assortativity calculation was based on (Newman, 2002). Assortativity was estimated by a correlation function that quantifies whether nodes in the network that have many connections also tend to be connected to other nodes with many connections. This correlation function is zero, negative or positive. Positive values for a given network correspond to assortativity, whereas negative values correspond to disassortativity, meaning that high degree nodes tend to be connected to low degree nodes. Assortativity is given by:

$$r = \frac{H^{-1}\sum_i j_i k_i - \left[H^{-1}\sum_i \tfrac{1}{2}(j_i + k_i)\right]^2}{H^{-1}\sum_i \tfrac{1}{2}(j_i^2 + k_i^2) - \left[H^{-1}\sum_i \tfrac{1}{2}(j_i + k_i)\right]^2} \qquad (3)$$

where j_i , k_i are the degrees of the nodes at the ends of the *i*th link, with i = 1,Ɛ.H (H = number of links in the network). This correlation function is actually a modified Pearson's correlation coefficient.

Neural mass model

We used the well known alpha rhythm model described by Lopes da Silva (Lopes da Silva et al., 1974; Zetterberg et al., 1978) to simulate EEG/MEG like signals. We consider a network of neural masses where each neural mass is defined by a set of two coupled inhibitory and excitatory neuronal populations. In short, a neural mass model (NMM) is a mean field model which describes the mean dynamics of a large neuronal population. Each NMM is characterized by the membrane potentials ($V_i(t)$, $V_e(t)$) and firing rates ($E(t)$, $I(t)$) of its neuronal populations (e = excitatory and i = inhibitory). The membrane potential $V_m(t)$ and the corresponding firing of the same population are related by a sigmoid function (Zetterberg et al., 1978):

$$S(V_m - V_d) = g \cdot \exp(q(V_m - V_d)) \qquad \text{for } V_m \le V_d \qquad (4a)$$

$$S(V_m - V_d) = g[2 - \exp(q(V_m - V_d))] \qquad \text{for } V_m > V_d \qquad (4b)$$

and

$$E(t) = \lambda_e S(V_m - V_d)$$
$$I(t) = \lambda_i S(V_m - V_d) \qquad (5a,b)$$

Here g, λ_e, λ_i and V_d refer to constants (see below) and $V_m \in \{V_i(t), V_e(t)\}$. Inhibitory and excitatory populations in each NMM are mutually coupled by c1 and c2 (see below). Coupling between two NMMs is reciprocal and excitatory. The sum of firing outputs $\mathcal{E}_{ext}(t)$ of excitatory populations of other NMMs is used as the input for the receiving NMM. The membrane potential of each NMM population was computed by a convolution of the incoming firing rates with a kernel $h_s(t)$, resembling the shape of the postsynaptic potentials (PSP) where $s \in \{i,e\}$. Given the shape of the kernel

$$h_s(t) = A_s[\exp(-a_s t) - \exp(-b_s t)] \qquad \text{for } t \geq 0 \tag{6a}$$

$$h_s(t) = 0 \qquad \text{for } t < 0\ , \tag{6b}$$

this leads to the following convolution for the membrane potential of the inhibitory population in an NMM

$$V_i(t) = \int_0^\infty [c_1 E(t-\tau) h_e(\tau) d\tau \quad \text{and} \tag{7a}$$

and

$$V_e(t) = \int_0^\infty [\sum E_{ext}(t-\tau) + P(t-\tau)] h_e(\tau) d\tau - \int_0^\infty [c_2 I(t-\tau) h_i(\tau) d\tau \tag{7b}$$

for excitatory population in an NMM. For inhibitory PSPs and excitatory PSPs the constants in $h(t)$ such as A_s, a_s, b_s are defined below. We added subcortical input P(t) consisting of a firing rate of 550 s^{-1} with a firing rate variation realized using Gaussian white noise with standard deviation of 0.1 s^{-1}. The membrane potentials of the excitatory populations of NMM are the MEG-like time series of interest and used for further analyses.

Parameters for the neural mass model are: A_e = 1.6 mV, a_e = 55 s^{-1}, b_e = 605 s^{-1}, A_i = 32 mV, a_i = 27.5 s^{-1}, b_i = 55 s^{-1}, q = 0.34 mV^{-1}, Vd = 7mV, g = 25 s^{-1}, C1 = 32 and C2 = 3.

Simulated fMRI time series

To simulate fMRI-like time series we convoluted the firing rate of the excitatory neuronal population of an NMM, E(t), with a known hemodynamic response function (HRF) similar to the one used by SPM (de Munck et al., 2007):

$$BOLD_{sim} = \int_0^\tau E(t-\tau)\left[\left(t/d_1\right)^{b_1} e^{-t/d_1} - c\left(t/d_2\right)^{b_2} e^{-t/d_2}\right] d\tau\ . \tag{8}$$

Here d1, d2, b1 and b2 correspond to rise and decay times for the HRF. Parameter values for this HRF are: d1 = 1.26, b1 =4.20, c =1.70, d2 = 2.82, b2 = 2.56 (17, 18, 20).

SECOND LARGER MEG DATASET

Subjects

In the second larger dataset, only MEG recordings were available. A total of 70 healthy subjects were included. 2 subjects were excluded from the analysis because during the study radiological features of neurological diseases were identified. 68 healthy subjects remained in the study (mean age of 53.7 ± 10.2 years) and 65% of the study population was female. Subjects were recruited from the VU University Medical Center. The study protocol was approved by the Local Research Ethics Committee (Medical Ethical Review Committee of VU University Medical Center), whose ethics review criteria conformed to the Helsinki declaration. All subjects had given written informed consent prior to participation.

Data acquisition

MEG recordings were made in a magnetically shielded room (VacuumSchmelze GmbH, Hanua, Germany) using a 306-channel whole-head neuromagnetometer (Elekta Neuromag Oy, Helsinki, Finland). Five minutes of MEG data were recorded during a resting-state eyes-closed condition with a sample frequency of 1250 Hz. An anti-aliasing filter and high-pass filter of 410 Hz and 0.1 Hz were applied, respectively. Other artifacts were removed from the data with an offline spatial filter, namely the temporal extension of Signal Space Separation (tSSS) (Taulu and Hari, 2009; Taulu and Simola, 2006) in MaxFilter software (Elekta Neuromag Oy, version 2.2.10). A sliding window of 10 s was used. Channels that were malfunctioning during the recording, for example due to excessive noise, were automatically discarded before estimation of the SSS coefficients. Additionally, malfunctioning channels were identified by visual inspection of the data, and excluded before applying tSSS. The number of excluded channels varied between one and twelve. The tSSS-filter was then used to remove noise signals that SSS failed to discard, typically from noise sources near the head, using a subspace correlation limit of 0.9. The head position relative to the MEG sensors was recorded continuously using the signals from four head-localization coils. The head-localization coil positions were digitized, as well as the outline of the participants scalp (ff500 points), using a 3D digitizer (3Space FastTrack, Polhemus, Colchester, VT, USA). This scalp surface was used for co-registration with the patient's anatomical MRI using surface-matching software developed by one of the authors (AH), resulting in an estimated co-registration accuracy of approximately 4 mm (Whalen et al., 2008). A single best fitting sphere was fitted to the outline of the scalp as obtained from the co-registered MRI, which was used as a volume conductor model for the beamformer analysis described above.

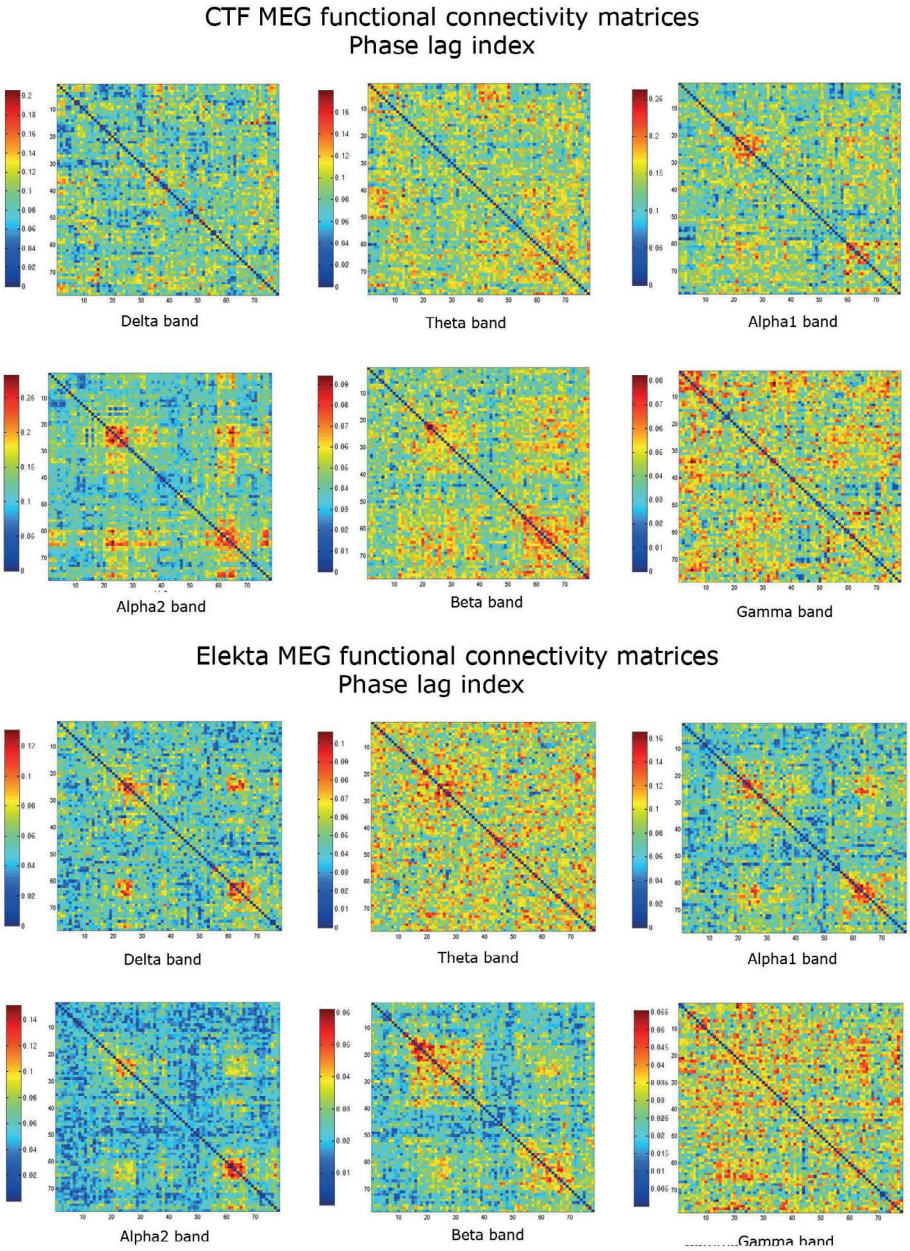

FIgure S1: MEG functional networks (connectivity matrices) for each frequency band obtained with PLI. The top two rows show data obtained with a CTF MEG system, whereas the bottom two rows show data for the larger dataset obtained with an Elekta MEG system. Note the appearance of four clusters in temporo-posterior regions in several frequency bands, for both datasets. A colorbar on the left of each connectivity matrix indicates the strength of functional connectivity (PLI in this case).

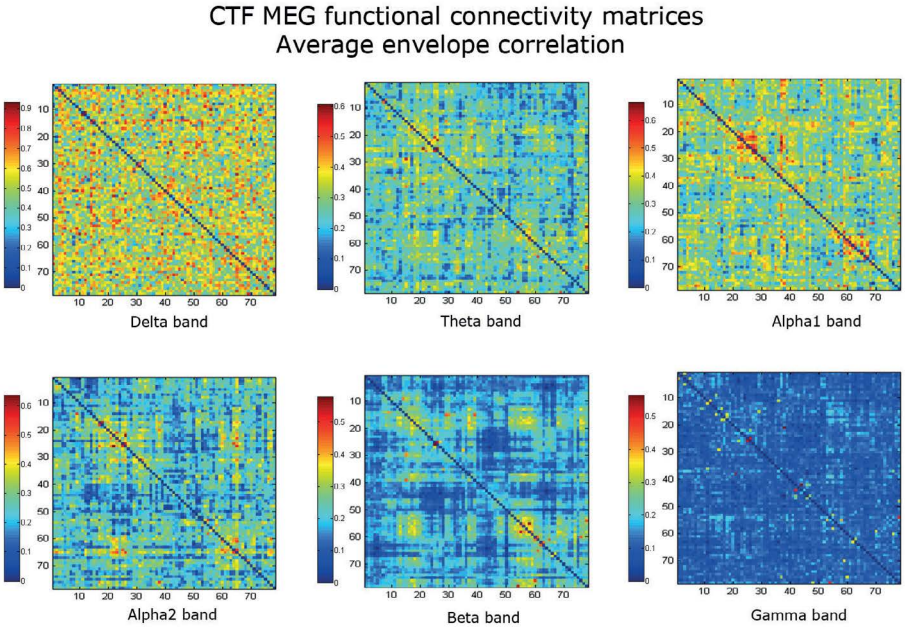

Figure S2: MEG functional networks (connectivity matrices) for each frequency band obtained with the improved AEC metric for the first dataset using a CTF MEG system. Note the appearance of four blocks in temporo-posterior regions in several frequency bands. A colorbar on the left of each connectivity matrix indicates the strength of functional connectivity (AEC in this case).

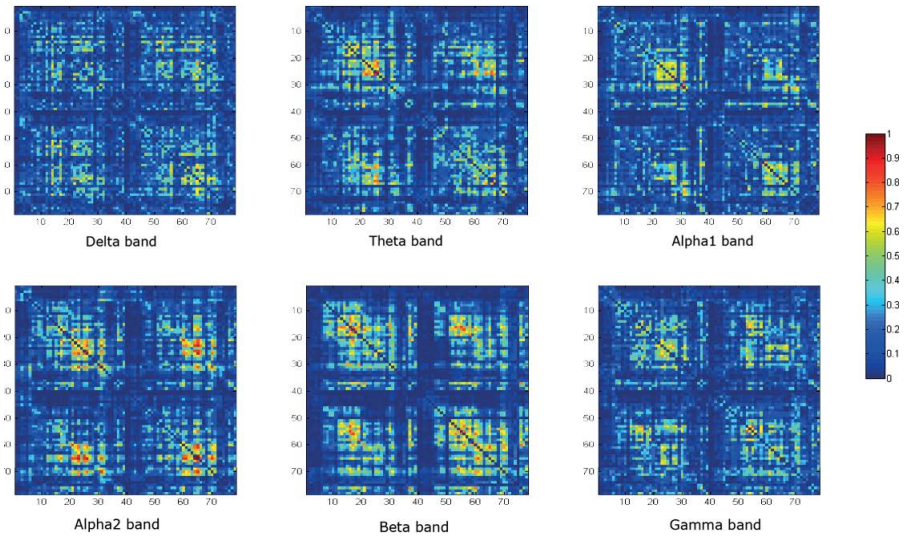

Figure S3: The similarity or overlap between MEG functional networks obtained with the AEC metric and fMRI. Again note the appearance of four blocks in the matrices for several frequency bands. The color bar indicates the amount of similarity which can range between 0 and 1.

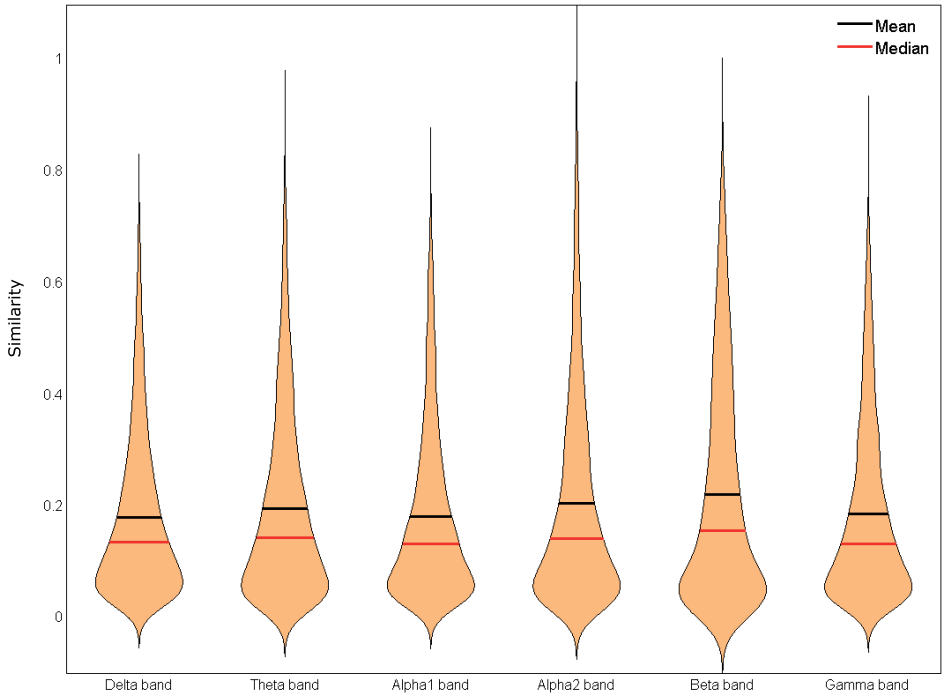

Figure S4: Distribution plots of similarity values for each frequency band (AEC) with fMRI. The similarity values for each frequency band with fMRI are depicted in distribution plots. The distributions correspond to all values of the similarity matrices of figure S3.

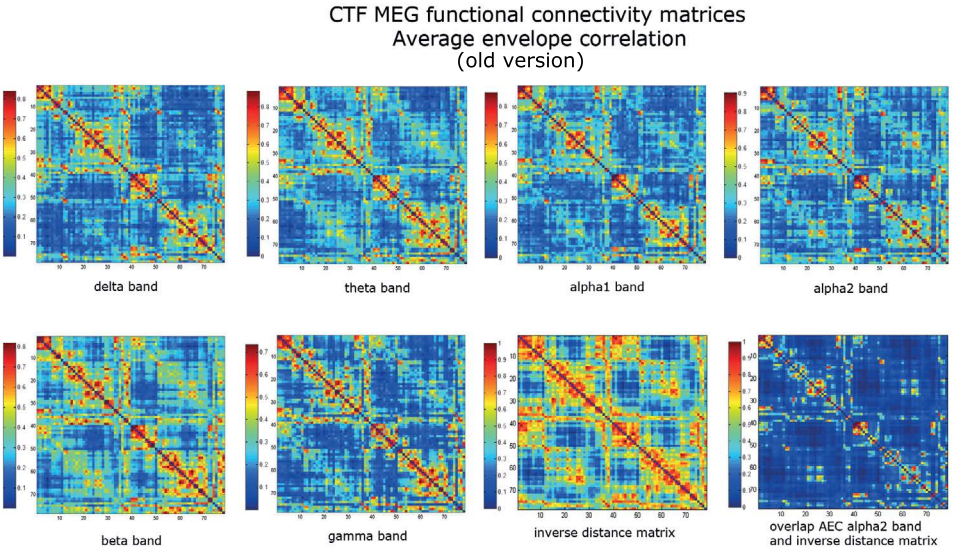

Figure S5: MEG Functional networks (connectivity matrices) for each frequency band obtained with old AEC metric. The matrices correspond to a dataset obtained with a CTF MEG system. A colorbar on the left of each connectivity matrix indicates the strength of functional connectivity (old AEC metric in this case). The inverse distance matrix is displayed next to the connectivity matrices (bottom row middle right). The color bar next to this matrix indicates the inverse distance normalized between 0 and 1. Note the overlap of connections in the old AEC obtained matrices with the inverse distance matrix (bottom row on the right). The colorbar on the left of this panel indicates the amount of overlap.

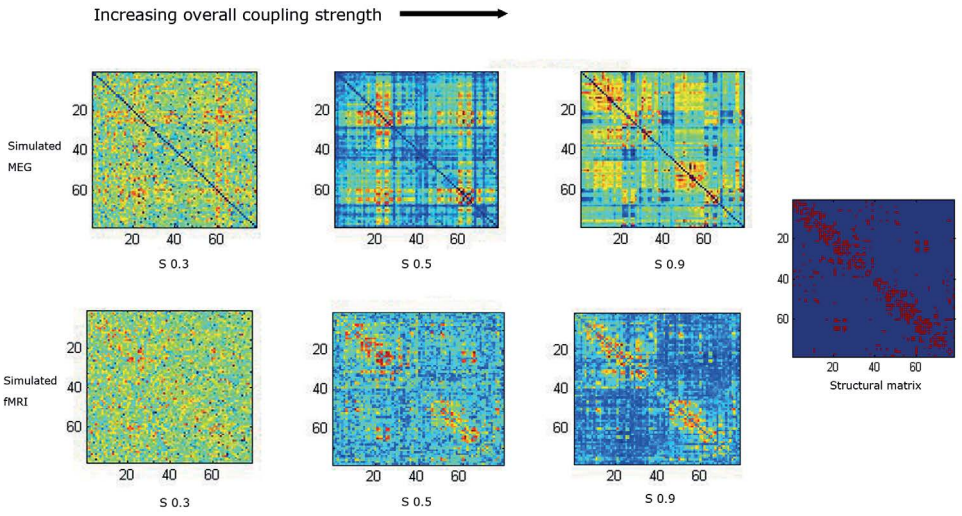

Figure S6: Simulated MEG and fMRI functional connectivity for increasing global structural coupling strength. For S <0.5 the functional connectivity matrices have a more random appearance. For S > 0.5 the simulated functional networks start to resemble the unweighted structural white matter network (right –(Gong et al., 2009)).

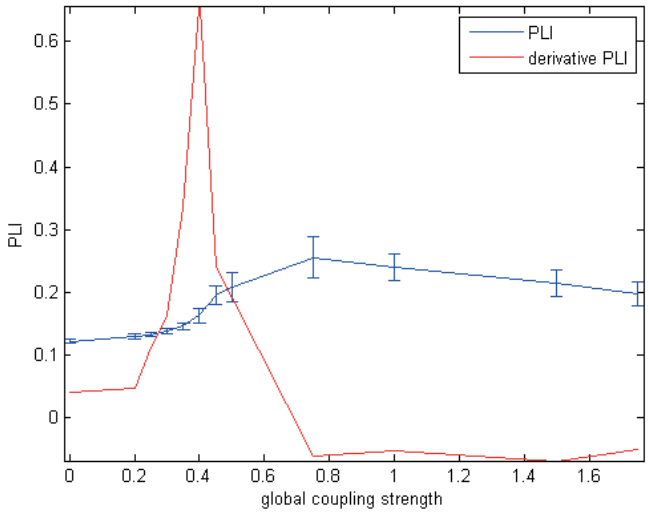

Figure S7: Average simulated functional connectivity (PLI) as a function of global coupling strength (blue line). There is a steep increase in average functional connectivity between $0.2 < S < 0.6$, with a maximum increase at $S = 0.4$ (peak of the red line). The red line corresponds to the derivative of the average functional connectivity.

Chapter 4

The minimum spanning tree: an unbiased method for brain network analysis

P. Tewarie, E. van Dellen*, A. Hillebrand, C.J. Stam*

** equal contribution*

Neuroimage 2014 accepted

ABSTRACT

The brain is increasingly studied with graph theoretical approaches, which can be used to characterize network topology. However, studies on brain networks have reported contradictory findings, and do not easily converge to a clear concept of the structural and functional network organization of the brain. It has recently been suggested that the minimum spanning tree (MST) may help to increase comparability between studies. The MST is an acyclic sub-network that connects all nodes and may solve several methodological limitations of previous work, such as sensitivity to alterations in connection strength (for weighted networks) or link density (for unweighted networks), which may occur concomitantly with alterations in network topology under empirical conditions. If analysis of MSTs avoids these methodological limitations, understanding the relationship between MST characteristics and conventional network measures is crucial for interpreting MST brain network studies. Here, we firstly demonstrated that the MST is insensitive to alterations in connection strength or link density. We then explored the behaviour of MST and conventional network-characteristics for simulated regular and scale-free networks that were gradually rewired to random networks. Surprisingly, although most connections are discarded during construction of the MST, MST characteristics were equally sensitive to alterations in network topology as the conventional graph theoretical measures. The MST characteristics diameter and leaf fraction where very strongly related to changes in the characteristic path length when the network changed from a regular to a random configuration. Similarly, MST degree, diameter, and leaf fraction were very strongly related to the degree of scale-free networks that were rewired to random networks. Analysis of the MST is especially suitable for the comparison of brain networks, as it avoids methodological biases. Even though the MST does not utilise all the connections in the network, it still provides a, mathematically defined and unbiased, sub-network with characteristics that can provide similar information about network topology as conventional graph measures.

1. INTRODUCTION

1.1 General introduction

Brain functioning requires both specialization and global integration of information (Tononi et al., 1998). The brain is organized as a complex network, and neural functioning can only be fully understood when activity is studied in the context of this network (Bullmore and Sporns 2009;Stam and van Straaten 2012;Park and Friston 2013). Major graph theoretical advances have provided elegant tools for systems neuroscience (Rubinov and Sporns 2010). Graph theory makes it possible to fully characterize structural and functional brain networks, which provides insights in fundamental properties of the structural and dynamical organization of neural communication (Bullmore and Sporns 2009; Bullmore and Sporns 2012).

Early studies used the small-world and scale-free model to describe structural and functional networks (Sporns and Zwi 2004;Bullmore and Sporns 2009). A small-world topology efficiently combines local specialization and global integration(Watts and Strogatz, 1998). A scale-free topology is characterized by a power law degree[1] distribution with an important role for hub nodes (Barabasi and Albert, 1999). Human structural and functional networks have both small-world and scale-free characteristics that have often been correlated to optimal cognitive functioning (Bullmore and Sporns, 2012; van den Heuvel et al., 2009). Importantly, a deviation from this optimal topology has been linked to cognitive and clinical symptoms in neuropsychiatric diseases (Stam and van Straaten, 2012). In recent years, other aspects of complex brain networks have also attracted attention, such as modularity, hierarchy, and mixing properties such as degree correlations and the 'rich-club' of strongly interconnected hub nodes (Bullmore and Sporns, 2009; Bullmore and Sporns, 2012; van den Heuvel et al., 2012).

1.2 Problem definition

Although findings obtained with conventional graph metrics such as the clustering coefficient, shortest path length and degree distribution (see section 2.1) have increased our understanding of the complexity of the brain's architecture, methodological issues have limited comparability between experimental conditions, cohorts and studies. Brain network studies are typically based on neuroimaging data (such as functional MRI (fMRI), similarity in cortical structure or Diffusion Tensor Imaging) or neurophysiological recordings (such as electroencephalography (EEG), magnetoencephalography (MEG), or corticography) (Bullmore and Sporns, 2012). Especially for this type of empirical data, the underlying network topology is often topic of interest and apriori unknown. A connectivity matrix containing information on all possible structural or functional connections can be converted into a network, which can then be analyzed with graph theoretical approaches. For this purpose, connections can be either unweighted (i.e. they either exist or do not

1 Degree refers to the number of connections to a node. A node with a high number of connections is considered to be a hub.

exist) or weighted (i.e. they have a weight that characterizes its strength). Both the comparison of unweighted and weighted networks based on neuroimaging data is accompanied by methodological hurdles. For thorough studies on this topic we refer to(Fornito et al., 2013; van Wijk et al., 2010). Here we will briefly discuss this topic.

Let us first consider unweighted networks, where the problem is to decide whether a connection is present or absent; this decision involves arbitrary choices that influence the network properties of interest. To construct unweighted networks one has to apply a threshold on the connectivity values of the original weighted network of interest. This results in scaling of the network properties as a function of the threshold (Fornito et al., 2010). Moreover, the threshold can be chosen in a variety of ways, for example based on an arbitrary choice, or using statistical criteria of connectivity strength, based on the average degree, or based on the density of the network. The main problem with choosing a threshold based on connectivity strength is that a difference in the distribution of connectivity values in two connectivity matrices may result in two unweighted networks having different densities. Subsequently, these differences in densities affect the estimated network characteristics even when the actual underlying network topology is the same. This problem cannot be solved by simply using different threshold values for each network (van Wijk et al., 2010). When the threshold is based on a fixed average degree or average density, the number of connections in the network is fixed. However, this may result in either inclusion of spurious or noisy connections in networks (for too high density values or too high average degree) or the exclusion of relevant connection in networks (for too low density values or too low average degree) (van Wijk et al., 2010).

The analysis of weighted networks is similarly accompanied by methodological problems, despite the fact that it does not suffer from threshold problems. Graph measures on these networks are influenced by average connection strength, the range of connectivity values and by the noisy and spurious connections contained in these weighted networks.

Proposed normalization procedures to correct for these biases in both unweighted and weighted network analyses do not provide an adequate solution (van Wijk et al., 2010). Normalization typically involves comparison of estimated network characteristics to those for a reference network with the same density, and sometimes also the same degree distribution. This normalization step may reduce the bias but does not solve it completely. Furthermore, the choice for a specific random network as surrogate data is arbitrary as one could use a random network obtained by reshuffling the original link weights, either with or without preserving the degree distribution, or by using the configuration model (Maslov and Sneppen, 2002; Newman et al., 2001). Therefore, analyses of both unweighted and weighted networks involve arbitrary choices that in itself affect the network properties. This may partly explain why studies on network alterations in brain diseases describe contradictory findings for specific patient populations, as has been reported for Alzheimer's disease and epilepsy (Diessen et al., 2013; Tijms et al., 2013).

1.3 The minimum spanning tree

Analysis of the minimum spanning tree (MST) may be helpful as it avoids methodological biases when comparing networks. The MST is mathematically defined as the sub-network that connects all nodes while minimizing the link weights and without forming loops (Kruskal, 1956; Prim, 1957). The link weights in neuroimaging data typically represent the connectivity strength (which can be considered as an inverse distance; an MST based on connectivity strength formally is a maximum spanning tree). Two assumptions underlying the MST analysis are that all nodes in the original weighted network are connected, and that all link weights are unique. Theoretically, the MST is insensitive to scaling effects since its topology only depends on the ordering of the weights in the original network and not on the absolute values or the distribution of these weights (Jackson and Read, 2010). Furthermore, every transformation of the weights which preserves weight ordering does not affect the MST (Dobrin and Duxbury, 2001). Apart from being insensitive to scaling effects, the MST may also efficiently capture the essential properties of complex networks, as found for many fields of science. The MST has been used as dimension reduction method in genetic linkage maps, as a method to partition highways and roads in transport networks, or as way to find the state with the lowest energy or disorder in physical systems (Dussert et al., 1986; Jackson and Read, 2010; King and Tidor, 2009; Wu et al., 2008; Wu et al., 2006).

MST analysis was first applied to brain networks by (Lee et al. 2006), and has been used in several recent studies on development and neuropsychiatric diseases (Boersma et al., 2012; Demuru et al., 2013; Olde Dubbelink et al., 2014; Ortega et al., 2008; Tewarie et al., 2013a; van Dellen E. et al., 2014). However, it is unclear how the MST relates to conventional measures of network organization such as clustering and path length. Furthermore, it has been stated that the MST is biologically unlikely to be a realistic representation of brain networks because the MST, in contrast to real brain networks, contains no loops (Meunier et al., 2009). Here, we use simulations to demonstrate 1) how analysis of the MST overcomes scaling effects; 2) how topological changes of the MST relate to topological changes of the original graph in terms of the measures that describe its small-worldness and scale-freeness. Indeed, we show that several MST characteristics are very strongly related to the conventional graph theoretical measures, such as the path length and node degree. Finally, we discuss how these insights can be used to interpret data from empirical MST studies.

2. SIMULATIONS

2.1 Network characteristics

Formal definitions and explanations of all network characteristics used in this paper are given in Table 1. Empirical networks often display non-random organization, characterized by local specialization (i.e. local clusters of connections) and global integration (through relatively sparse long range connections). This local specialization is usually quantified by computing the clustering coefficient

C, which is the fraction of triangles in the network (Rubinov and Sporns, 2010). The average shortest path length *L* is often considered as a measure for global integration and is defined as the average number of links in the shortest path between any two nodes, subsequently just referred to as path length. Both measures are often compared to a random reference network of the same size and density by computing the normalized clustering coefficient = $C/\langle C_{random} \rangle$ and the normalized path length = $L/\langle L_{random} \rangle$ (<> indicates the average). Here $\langle C_{random} \rangle$ and $\langle L_{random} \rangle$ refer to the average clustering coefficient and path length computed on an ensemble of surrogate data. In our case, we computed random networks by reshuffling the original link weights and preserved the degree distribution of the original network (Maslov and Sneppen, 2002). For this purpose, 1000 random networks were generated for each computation. For both the clustering coefficient and path length there also exists weighted versions in case that the network is weighted, C_w and L_w respectively (see (Rubinov and Sporns, 2010) for a more detailed description of conventional network measures).

2.2 The minimum spanning tree

The MST is a sub-network of the original weighted network that connects all nodes in the network without forming loops and has the minimum total weight of all possible spanning trees. MSTs are constructed based on the weighted networks with Kruskal's algorithm (Kruskal, 1956). In our case we start the algorithm with the largest link weights since we are interested in the strongest connections in the network. This algorithm first orders the weights of all links in a descending order and starts the construction of the minimum spanning tree with the largest link weight and adds the following largest link weight until all nodes N are connected in an acyclic sub-network that consists of M=N-1 links, i.e. a fixed density. When in the process, addition of a link forms a loop, this link is ignored. After construction of the MST, all link weights are assigned a value of one. We characterize and compare the topology of the MSTs using the MST overlap, MST leaf fraction, MST diameter and MST degree (Stam and van Straaten 2012;Boersma et al. 2012). The MST overlap is defined as the fraction of links that two MSTs have in common (the overlap of the MST links across time has previously been described as 'survival ratio' (Lee et al., 2006)). MST leaf fraction is the fraction of nodes with a degree of one and MST diameter refers to the longest shortest path of an MST (see Table 1 for a detailed explanation of all MST metrics). MST degree is the maximum degree within the MST. MST diameter and degree were normalized by network size *N*.

2.3 Simulated networks

In our analyses we construct weighted- and unweighted networks, as well as the MST. Each network is formed by a set of nodes connected to each other by links. The link weights in the weighted networks ranged between 0 and 1; the link weights in unweighted networks were either 0 or 1. Networks were constructed based on $N = 78$ nodes. The rationale for this is that many empirical studies use parcellation schemes based on the Automated Anatomical Labeling (AAL) atlas, which (without sub-cortical regions) contains 78 nodes (Gong et al., 2009; Tzourio-Mazoyer et al., 2002).

In the first analysis (section 'the MST and the thresholding problem'; Figure 1) we illustrate the problem with regard to computation of metrics on unweighted and weighted networks. To this end, we constructed regular and small-world networks with an average degree of 26 (arbitrarily chosen). We defined regular networks as a network where all nodes in the network had a degree of 26. Small-world networks were constructed based on these regular networks by rewiring every link of the regular network with a probability of $p = 0.1$. In order to be able to compute weighted network metrics and the MST for these networks, we then assigned random weights by taking random numbers from a standard uniform distribution for each link with strength > 0. For the unweighted networks described in Figure 1, we applied a range of thresholds to these matrices to obtain networks with different densities. For each threshold we constructed two networks: 1) the MST and 2) an unweighted network based on the links that remained after thresholding. Subsequently, after each threshold we computed the clustering coefficient, path length, normalized clustering, normalized path length and the overlap between successive MSTs. For the weighted network analysis we followed a similar approach. However, instead of applying a range of thresholds we multiplied the link weights by increasing values between 1 and 2. Furthermore, instead of C and L, we computed the weighted versions C_w and L_w (see Table 1 for formulas and formal definitions). These analyses were performed using Matlab R2012a (The Mathworks, Inc., Natick, MA, United States), together with the brain connectivity toolbox (https://sites.google.com/site/bctnet/).

In the second analysis (sections 'The MST of small-world and scale-free networks' and 'MST metrics behave similarly to conventional metrics; Figures 2-5) we illustrate how MST metrics behave in relation to conventional metrics. To this end, we constructed a regular network with 78 nodes and 658 links, for which the link density of the network was based on a structural brain network obtained from a large population of healthy subjects as described by (Gong et al., 2009). We then followed a rewiring procedure that randomly rewired a link in the networks with probability p, with p ranging from $p = 0.01$ to $p = 0.9$ in steps of 0.01 (Watts and Strogatz, 1998). During this rewiring process, rewired links were only accepted if the network was still connected and thus disconnected sub-networks or nodes were not allowed. For each rewiring probability we rewired the initial network 300 times to obtain 300 realizations for a given p to obtain stable results. After rewiring, we computed the clustering coefficient, path length and the degree. We then again assigned random weights by taking random numbers from a standard uniform distribution for each link with strength > 0 (and in addition also by taking random numbers from an empirical functional connectivity distribution obtained by MEG from a previous dataset (Tewarie et al., 2013b)). Based on this matrix we calculated the MST and subsequently computed MST metrics as described above (see Table 1). In addition to the regular network we also used a scale-free network as a starting configuration for subsequent rewiring. First, a degree sequence was constructed with a degree distribution that followed a power law with an exponent of 1.5. Brain networks are generally characterized by higher exponents. However, we imposed a density constraint for the scale-free networks which limits the value of the exponent. The rationale behind this is that the density of these scale-free networks needed to be equal to that of the regular networks that we used for the comparative analysis.

However, it is highly likely that use of a degree distribution characterized by a larger exponent would not qualitatively affect our results.Subsequently, the degree sequence was then used to construct a scale-free network using a configuration model (Newman, 2010). The number of links and nodes were the same as for the regular network, as were the rewiring approach and computed network metrics. As a last step we repeated the same analysis for regular and scale-free networks of larger size (N = 200 and N = 300) to investigate the effect of network size on MST metrics. Here, we used only 100 realizations for each p, and increased p in steps of 0.1, due to computational limitations.

3. THE MST AND THE THRESHOLDING PROBLEM

3.1 Unweighted networks are affected by arbitrary thresholding

We briefly illustrate the problem of applying thresholds based on the density for the construction of unweighted networks and compare this with an analysis of the MST (Figure 1). For this purpose we started with a regular network or small-world network to which thresholds were applied to obtain unweighted networks with different densities. As expected, we observed that both the path length and clustering coefficient change as a function of density (i.e. threshold) in unweighted networks (Figure 1A). The path length decreased as a function of density and decreased slightly faster for the small-world networks compared to the regular networks, whereas the clustering coefficient increased almost linearly as a function of density. A common approach that aims to correct for these effects of link density is to normalize network properties by the averages of these network properties obtained for random surrogate networks. However, even normalized path length and clustering changed as a function of density (Figure 1A), and a divergence between the behavior of normalized clustering and path length was even observed when comparing small-world and regular networks (see middle panel in Figure 1A). Hence, the use of normalized measures does not solve the dependence of graph measures on density, as was also reported in van Wijk et al. (2010). In contrast to conventional measures, we observed that the MST overlap did not change for different densities, irrespective of the underlying topology. This behavior was expected, since, given N nodes, the density of the MST is fixed by definition. The MST remains therefore unaltered, despite any thresholds, as long as the original network remains connected and the weight ordering preserved (Jackson and Read, 2010). Generally, unconnected networks are not of interest in empirical studies in neuroscience.

The reader may notice that the effect of density on the unweighted network is slightly different from the behaviour shown by van Wijk et al. (2010) (see their Figure 3). This is due to the difference between the approaches that were used to construct the networks, where we sub-sampled a given network by using a threshold and they constructed true regular and small-world networks for each density (see Figure S1). Although initial regular and small-world networks can convert to non-regular or non-small-world networks by using our sub-sampling approach, empirical studies usually obtain one network for one condition that is then sub-sampled to gain knowledge about the underlying topology.

Table 1: Explanation of concepts and terminology

Symbol	Concept	Explanation	Formula
N	Nodes	Number of nodes	
M	Links	Number of links / maximum leaf number	
k	Degree	Number of links for a given node	$k_i = \sum_{j \in N} a_{ij}$
C	Clustering coefficient	C is a measure of the local connectedness of a network, which is defined as the fraction of triangles in the network	$C = \frac{1}{N}\sum_{i \in N} \frac{\sum_{j,h \in N} a_{ij}a_{ih}a_{jh}}{k_i(k_i-1)}$ a corresponds to links connecting node i, j or h
C_w	Weighted clustering coefficient	C_w is the clustering coefficient for weighted networks	$C_w = \frac{1}{N}\sum_{i \in N} \frac{\sum_{j,h \in N} \left(w_{ij}w_{ih}w_{jh}\right)^{\frac{1}{3}}}{k_i(k_i-1)}$ w corresponds to links connecting node i, j or h
L	Path length	L is defined as the average shortest path between any two nodes in the network. The paths are based on the topological distance between nodes d_{ij}, where distance is defined as the inverse of the link weights	$L = \frac{1}{N}\sum_{i \in N} \frac{\sum_{j \in N, j \neq i} d_{ij}}{n-1}$
L_w	Weighted path length	L_w is the weighted form of the path length in case that the network of interested is weighted	$L_w = \frac{1}{N}\sum_{i \in N} \frac{\sum_{j \in N, j \neq i} d_{ij}^w}{n-1}$
L_f	Leaf fraction	Fraction of leaf nodes (L) in the MST where a leaf node is defined as a node with degree one	$L_f = L/M$
D	Diameter	Longest shortest path d of an MST. The diameter is also related to the leaf number. The upper limit of the diameter is defined as $d_{max} = m - L + 2$, which implies that the value of the largest possible diameter decreases when the leaf number increases	$D = d/M$
	Eccentricity	Longest shortest path from a reference node to any other node in the MST. The eccentricity of the whole MST is the difference between the eccentricity values of the nodes with the largest and smallest eccentricity in the tree	
BC	Betweenness Centrality	Fraction of all shortest paths that pass through a particular node	$BC_i = \frac{1}{(n-1)(n-2)} \sum_{\substack{h,j \in N \\ h \neq j, h \neq i, \neq i}} \frac{\rho_{hj}^{(i)}}{\rho_{hj}}$ ρ_{ih} is the number of shortest paths between h and j, and $\rho_{ih}^{(i)}$ is the number of shortest paths between h and j that pass through i.
κ	Degree divergence	Measure of the broadness of the degree distribution. Related to resilience against attacks, epidemic spreading and the synchronizability of complex networks	$\kappa = \frac{\langle k^2 \rangle}{\langle k \rangle}$
Th	Tree hierarchy	Quantifies the trade-off between large scale integration in the MST and the overload of central nodes	$T_H = \frac{L}{2MBC_{\max}}$
	Overlap	The fraction of links that two MSTs (MST_x and MST_y) have in common. This value can range between 0 and 1.	$Overlap = \frac{MST_x \cap MST_y}{M}$

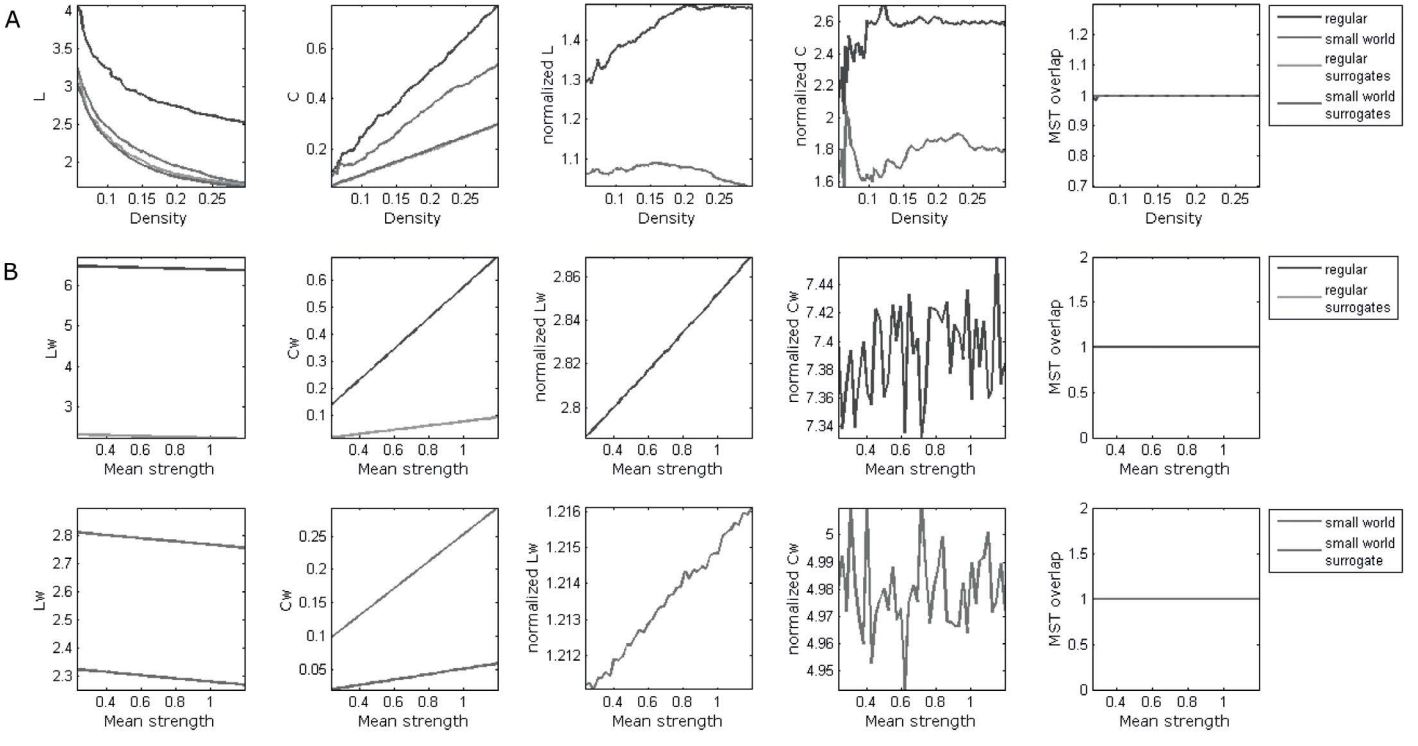

Figure 1: Network characteristics as a function of link density and connection strength. Network characteristics are given as a function of link density (***A***, unweighted networks) and mean connection strength (***B***, weighted networks). Two network types were constructed, being regular networks and small-world networks (rewiring probability p is 0.1) with size $N = 78$. Note that the path length and clustering coefficient change as a function of density in unweighted networks, and as a function of mean connection strength in weighted networks. This problem is not solved after normalization by comparison to the path length and clustering coefficient for random networks with similar density/strength. In contrast, the minimum spanning tree is not affected by changes in link density or mean connection strength (right column).

3.2 Weighted networks are affected by spurious connections and link density effects

We illustrate the shortcomings of weighted network analysis by demonstrating the dependency of graph metrics on mean connectivity strength and compare it to the behavior of metrics computed for the MST. Now, instead of thresholding, we multiplied each link weight in the weighted network by increasing values ranging between 1 and 2, and subsequently computed the weighted versions of the clustering coefficient, C_w, and path length, L_w, as a function of increasing mean connectivity strength. We observed the expected behavior for both the clustering coefficient and the path length: the clustering coefficient increased as a function of mean connectivity strength, while the path length decreased (Figure 1B). Normalizing both measures did not entirely solve the dependency on mean connectivity strength. This was especially the case for the normalized path length, which showed a positive dependency on mean connectivity strength (even though the increases were small) in contrast to the negative dependency for the weighted path length itself. This flipping in sign was caused by the fact that there was a steeper decline of the mean path length of the random network surrogate data when mean connectivity strength increased compared to the path length of the original networks. For the clustering coefficient, we observed a pattern that seems to fluctuate around a stable point, therefore normalization may be appropriate for this metric. In contrast to the weighted graph metrics, we again see that the MST overlap remains unaltered when mean connection strength is increased. The explanation for this steady behavior is the fact that the ordering of the weights remains intact when their scale changes and thus the MST does not change (Braunstein et al., 2013). Importantly, this steady behavior is valid for any metric that is derived from the MST as the MST as a whole does not change.

4. THE MST OF SMALL-WORLD AND SCALE-FREE NETWORKS

Both the small-world and scale-free model are important models to help understand the architecture of complex networks (Barrat et al., 2008). Here, we study the ability of the MST to capture the characteristics of these models by testing two hypotheses: 1) the MST can accurately pick up alterations related to changes in the level of "small-worldness" or "scale-freeness" of a network; 2) conventional metrics and MST metrics are related to each other in a straightforward manner when such changes occur. We tested these hypotheses by computing MST characteristics and measures of small-worldness and scale-freeness for a range of networks with known topology, and subsequently calculated correlations between them. We used Spearman's correlation coefficients since the relationship between the two can be non-linear.

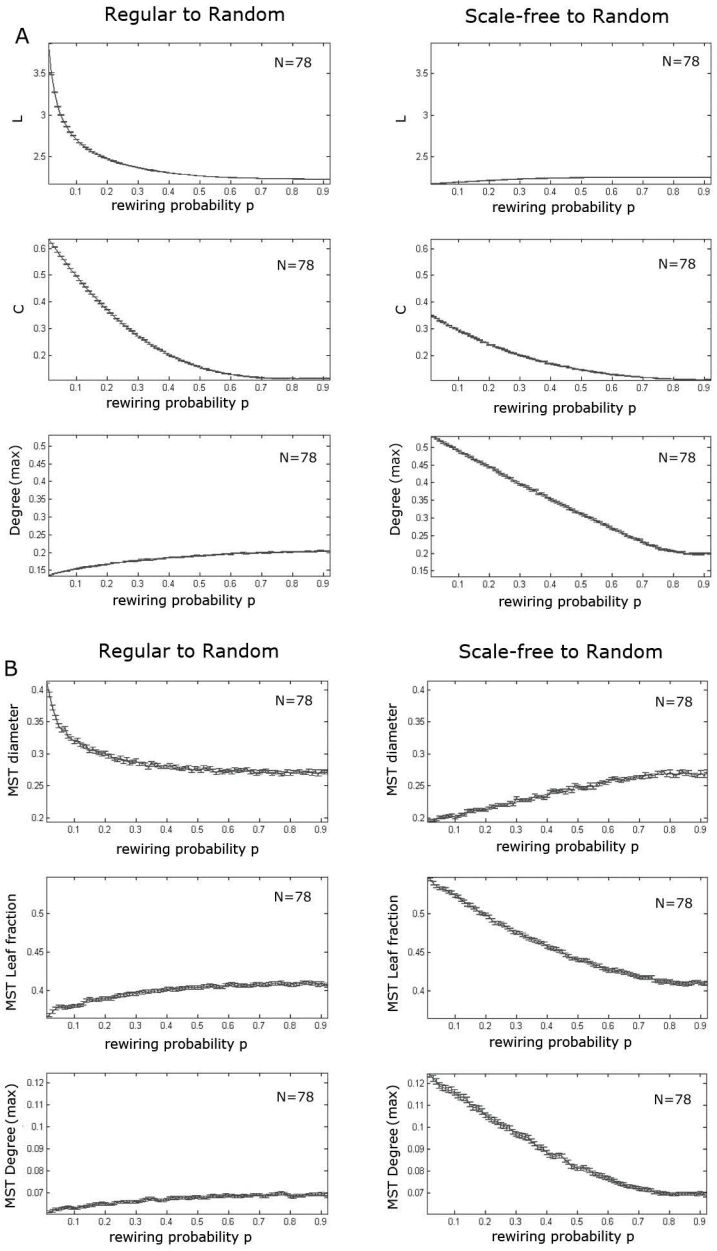

Figure 2: Network characteristics as a function of rewiring probability for regular and scale-free networks. Network characteristics are presented for networks that were rewired with probability *p*, starting with either a regular network or a scale-free network of size *N = 78*. Note the similarity in the slopes of the maximum MST diameter and the path length, and degree and the maximum MST degree, irrespective of whether a regular or a scale-free network was taken as a starting point (see Figure 4 for further quantification).The error bars correspond to the standard error based on 300 network realizations for each rewiring probability.

As expected we observed that path length and clustering coefficient decreased as a function of *p* when rewiring a regular network to a random network, while the maximum degree increased during this rewiring (Figure 2A). When the scale-free network was rewired to a random network, a drop-off of the maximum degree was found, while the path length increased slightly and the clustering coefficient showed a decrease. MST diameter scaled similarly to the path length for both network types (Figure 2B). MST leaf fraction was low for MSTs constructed from regular networks, which increased when networks were rewired to random networks, and, as expected, was much larger for scale-free networks. Interestingly, both MST diameter and leaf fraction have extreme values for regular and scale-free networks, while their values are in between those extremes for random networks. Lastly, the MST degree scales almost identical to the maximum degree in the unweighted networks, irrespective whether a regular or scale-free network was taken as a starting point. The effect of rewiring on the MST betweenness centrality, MST eccentricity, MST hierarchy and MST degree divergence (Figure 3; see Table 1 for explanation of these metric) showed similar behaviour to that of the previous metrics. Again, these measures have extreme values for regular and scale-free networks.

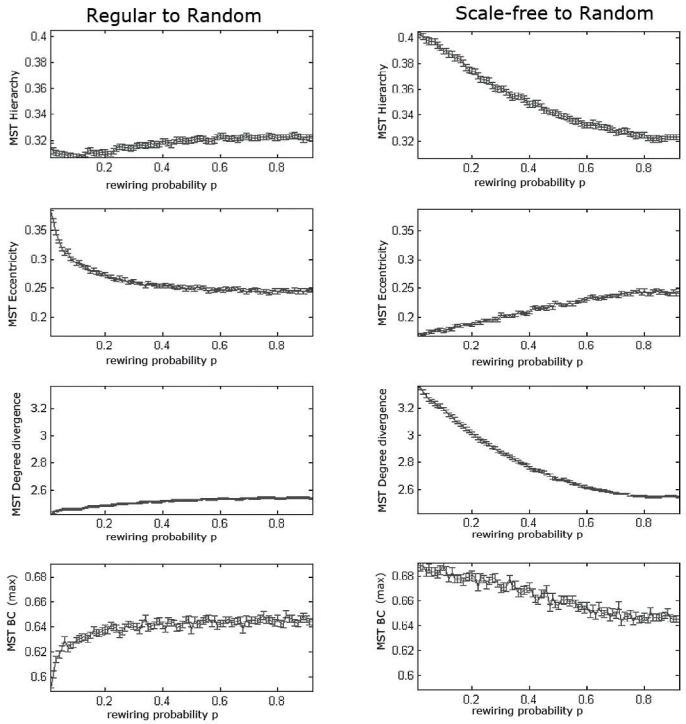

Figure 3: MST metrics as a function of network rewiring probability for regular and scale-free networks. As figure 2. Changes in network topology were most sensitively picked up by MST eccentricity and MST BC (Betweenness Centrality, maximum values) when regular networks were randomized, whereas MST hierarchy and degree divergence were more sensitive to changes in the topology of rewired scale-free networks.

In addition to the previous analysis, where we assigned random weights obtained from a uniform distribution, we repeated the same analysis except that the random weights were taken from an empirical distribution of MEG functional connectivity data (from one of our previous studies (Tewarie et al., 2013b). We found that for both the regular to random rewiring process and for the scale-free to random rewiring process all topological metrics behaved highly similar or almost identically compared to the behaviour of those metrics as seen in previous analysis (compare Figure S2 and S3 with Figure 2 and 3). The reason for this is that the MST is insensitive to the shape of the link weight distribution, and only dependents on the ranking of the link weights (Dobrin and Duxbury, 2001).

5. MST METRICS BEHAVE SIMILARLY TO CONVENTIONAL METRICS

In order to analyze the relationship between MST metrics and conventional measures in more detail we computed spearman correlations between the mean values (i.e. averaged over realizations) of these measures (Figure 2). For the regular to random rewiring scheme, main interests are correlations between MST measures and path length or clustering coefficient, as these measures typically characterize small-world characteristics. MST diameter scaled linearly with path length and the two were strongly positively correlated ($R = 0.95$ $p < 0.001$) (Figure 4A). Thus, the average shortest path length of a network scales linearly with the longest shortest path the MST of that original network. For MST leaf fraction we observed a negative but strong correlation with path length ($R = -0.94$ $p < 0.001$). The clustering coefficient we also strongly related to MST measures as 1) MST diameter increased monotonically and non-linearly when the clustering coefficient increased ($R = 0.95$ $p < 0.001$), and 2) MST leaf fraction steeply decreased when clustering increased ($R = -0.94$ $p < 0.001$) (Figure 4B). The maximum MST degree was linearly and positively related to the maximum degree of the unweighted networks ($R = 0.91$ $p < 0.001$).

We repeated the same analyses for the scale-free to random rewiring scheme. Here, main interest was the relation between maximum degrees for both types of networks, as this is the most important characteristic of scale-free networks (Figure 5A). In addition, we also computed correlations between MST measures and path length (Figure 5B). Firstly, we observed a strong, positive correlation between the maximum degree of the unweighted networks and the maximum degree of the MST ($R = 0.99$ $p < 0.001$). Again, this relationship appears to be linear. Also note a strong positive correlation between MST leaf fraction and the maximum degree of the unweighted networks ($R = 0.99$ $p < 0.001$). For path length we observed that, although the shape of the correlation plots differed, the sign of the relationship with MST measures was similar to the observed relationship when regular-to-random rewiring was performed. For example, we again observed a strong positive correlation between MST diameter and path length ($R = 0.87$ $p < 0.001$), although the exact curve of this relationship was different.

The scatter plots in the previous paragraphs suggest that there could be simple functions that describe the relationships between conventional and MST metrics. However, note that the

relationships between conventional metrics and MSTs metric may be different on the regular to random or scale-free to random rewiring axis. For instance, the relationship between path length and MST diameter seems completely linear on the regular to random rewiring axis, in contrast to non-linear behaviour on the scale-free tor random axis. This would lead for two different functions for the relationship between path length and MST diameter which may not be very helpful.

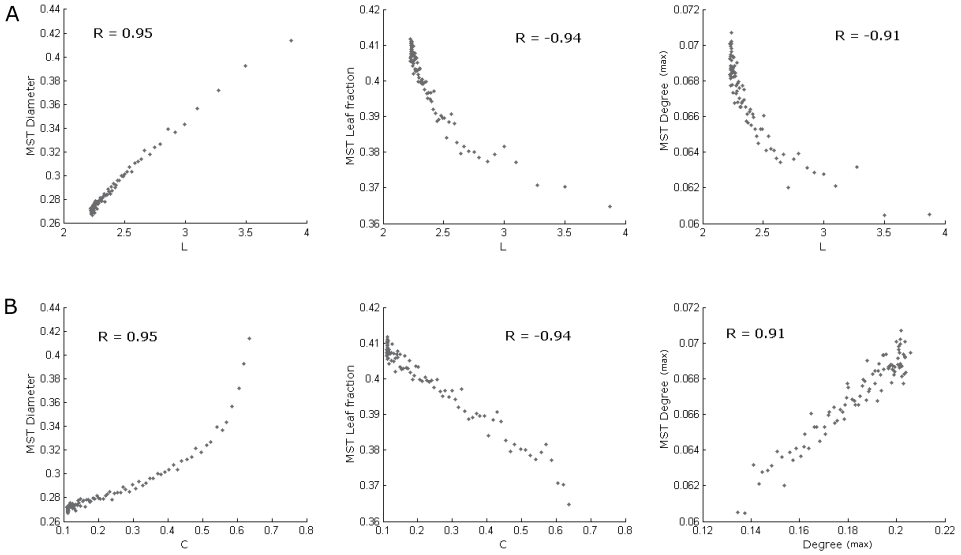

Figure 4: Correlations between path length, clustering coefficient and MST measures for the rewired regular networks. Spearman's correlations between MST measures and path length (***A***) or clustering coefficients (***B***) for the rewired regular networks (as shown in figure 2). Note that MST diameter scaled linearly with path length and the two were strongly positively correlated. MST leaf fraction shows a strong negative linear relationship with the clustering coefficient. Furthermore, the maximum degree and the maximum MST degree were strongly and linearly related. These scatter plots suggest that there may be a function that maps conventional metrics to MST metrics, however the relationships between the same metrics are different on the scale-free to random rewiring axis (see Figure 5).

We demonstrated that by averaging over 300 samples the correlations between MST metrics and conventional metrics are very high. However, these high correlations could possibly have been achieved by averaging out fluctuations in the network characteristics of individual network samples. To investigate this effect of averaging, we have done exactly the same analysis for individual samples. We then fitted non-linear curves for each relationship between conventional measures and MST metrics. Depending on the shape of the scatter plot, for each relationship we either fitted a polynomial function, power function or an exponential function. Although Spearman correlations for individual samples are still high (the absolute values of R range from 0.5 to 0.9), we observed variability among realizations, depending on the relationship of interest (Figure S4 and S5). This is especially true for the relationship between MST diameter and clustering and path length on the regular-random axis, where the shape of the fitted function can be different among realizations.

Therefore, the average correlations and relationships shown in Figure 4 and 5 do not necessarily correspond exactly to individual realizations, which impedes quantifying the exact relationship between conventional and MST measures. However, in every case the sign of the relationship (negative or positive) is always equal between individual realizations and the average result.

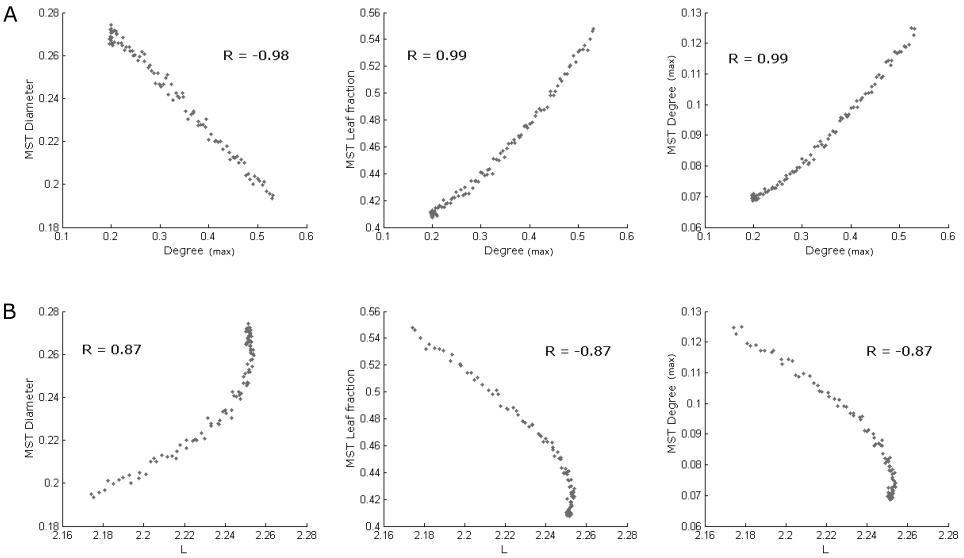

Figure 5: Correlations between path length, clustering coefficient and MST measures for the rewired scale-free networks. Spearman's correlations between MST measures and the maximum degree (***A***) or path length (***B***) for the rewired scale-free networks (as shown in figure 2). Note that MST diameter was strongly anti-correlated to the maximum degree, while MST leaf fraction and MST degree scaled almost identical to the degree of the original network. The correlation between MST measures and path length L was linear for a range of values until the network approached the random topology, where L reached a limit while MST measures could still take on a range of values.

In addition to the analysis of global measures, we also investigated the relationship between local, node-level measures of the MST and the original network. To this end, we computed spearman correlations between the degree and betweenness centrality sequences of the original networks with their corresponding sequences of the MSTs (Figure 6). We found that for both the degree and betweenness centrality the correlations start low for regular networks but monotonically increase when these networks are rewired towards random networks (Figure S6). The highest correlation between local measures of the original networks and the MST is found for scale-free networks, where the correlation monotonically decreases when these networks are rewired towards random networks (Figure 6 and S5). Note that the correlation values in both conditions converge towards the same correlation value for random networks (R = 0.4). Although the correlation between local measures of the MST and the original network are generally lower than for global measures, the characteristics of the MST still capture local features of the original networks. This is especially

true for networks that are characterized by the presence of high degree or central nodes, which is certainly the case for structural and functional brain networks (Hagmann et al., 2008; Tewarie et al., 2014; van den Heuvel and Sporns, 2011). The best match in degree and centrality sequence is found for nodes with a high degree or centrality, which suggests that the MST is most fit to identify local characteristics of hub nodes. This is also the type of nodes that are of increasing interest in brain network analysis.

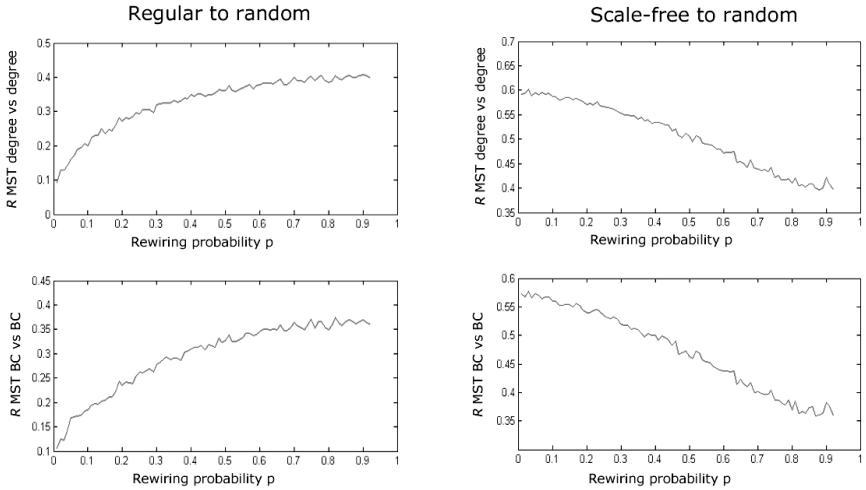

Figure 6: Correlations between node degree and centrality and MST degree and centrality for the rewired regular and scale-free networks. Spearman correlations between the degree and betweenness centrality sequences of the original networks with their corresponding sequences of the MSTs (networks as shown in figure 2). Local network metrics correlate strongest with metrics of the original networks for scale-free networks, which is less for random networks and lowest for regular networks.

6. THE MST AND NETWORK SIZE

In order to investigate the effect of network size on conventional and MST metrics we constructed regular and scale-free networks of larger sizes (N = 200, N = 300). We found that for the regular to random as well as for the scale-free to random rewiring both conventional and MST metrics scaled similarly as for the network with 78 nodes (compare Figure 7 with 2). However, several MST and also conventional metrics were affected by network size. Hence differences in network topology could be confused with size effects when comparing the MST for networks with different sizes.

In addition, Figure S6 illustrates that local MST properties reflect the underlying weighted network properties best for nodes with a high degree and/or centrality. When network size increases, the relative number of nodes with a low degree and/or centrality will also increase, and therefore lead to a lower correlation between nodal characteristics of the weighted network and MST nodal characteristics. These effects could well be inflated by the use of random edge weights in this study, and be less outspoken in empirical data.

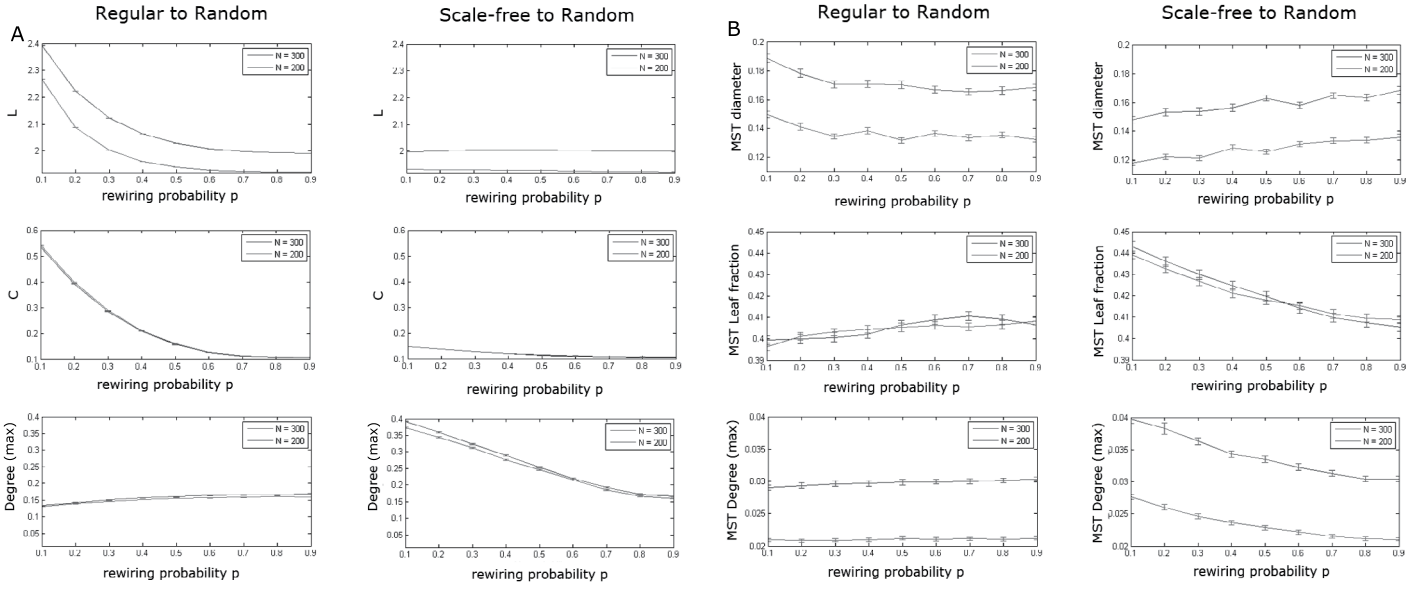

Figure 7: Network characteristics as a function of rewiring probability for regular and scale-free networks of different sizes. Network characteristics are presented for networks that were rewired with probability *p*, starting with either a regular network or a scale-free network. Network size $N = 200$ and $N = 300$. Note the similarity in the scaling of MST diameter and the path length, and degree and MST degree for both network sizes. However, the absolute values of several MST metrics were affected by network size. The error bars correspond to the standard error based on 100 network realizations for each rewiring probability.

7. NEAR DEGENERACY OF THE MST

The MST is the spanning tree with the maximum amount of weight (in our case). As mentioned earlier, its construction is merely based on the ordering of the connectivity values in the original network. A slight change in ordering, for example due to noise or different epoch selection in an experimental situation, may result in different links being selected for the MST. It is therefore important to investigate how spanning trees based on slightly different rankings differ from the MST. If the topology of spanning trees with near-optimum total weight vastly differ from the MST than this would impede the practical use of the MST due to its large sensitivity to fluctuations.

In order to construct spanning trees with near-optimal total weight we again ordered the link weights in a descending order and then randomly permuted the ordering of the link weights. During each step we permuted the highest x-percentage of link weights. For this analysis, we only included links with a weight equal to or higher than that of the weakest link within the MST. Subsequently, we construct a spanning tree by adding link weights to the tree while again discarding links that would create loops (similar to Kruskal's algorithm). For each new spanning tree we computed the overlap with the MST and its total weight, i.e. the sum of all link weights. For each x-percentage, 100 permutations were performed. For this analysis we used the same regular and scale-free networks as in the previous analyses.

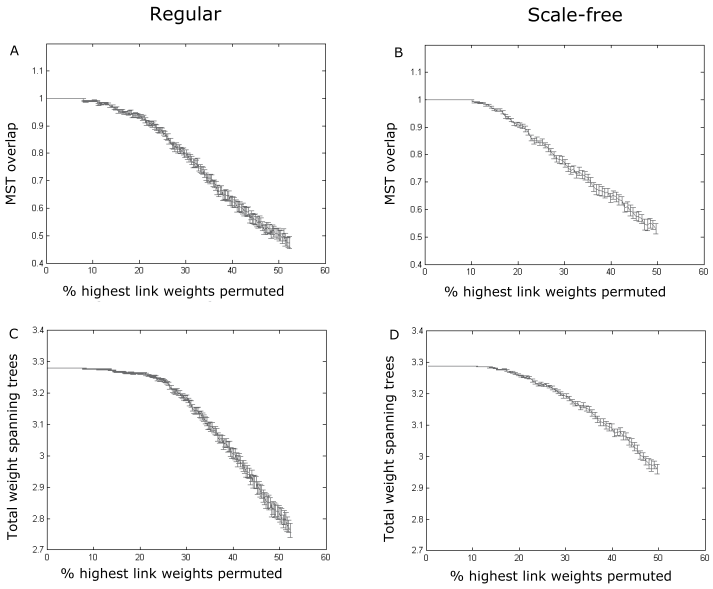

Figure 8: Minimum Spanning Tree Near-Degeneracy. Figures show overlap with the MST and cost for spanning trees with an increasing percentage of links permuted. For regular networks, reordering leads to different spanning trees only when more than 8% of the highest link weights are permuted (A). The overlap between the MST and permuted spanning trees is high and close to one for spanning trees with slightly less costs (C). Similar behaviour is observed for scale-free networks (B and D),

For regular networks, we observed that reordering leads to different spanning trees only when more than 8% of the highest link weights are permuted (Figure 8A), i.e. before this threshold reordering does not affect the MST. In addition, even after this threshold, the overlap between spanning trees with near-optimum total connectivity strength and the MST is high and close to one (Figure 8C). When 23% of the highest link weights are permuted the overlap of the spanning trees with the MST is still 0.9. The general observation is that both the overlap with the MST and the total connectivity strength of spanning trees monotonically decrease when the percentage of highest link weights is permuted, but they both remain relatively high. Similar behaviour is observed for scale-free networks, albeit with the difference that the threshold after which reordering results in different spanning trees occurs at 10% (Figure 8C). Also the total connectivity strength within the spanning trees decreases more slowly than for the regular networks (Figure 8D). This is probably due to the fact that the original scale-free networks contain fewer loops and triangles, which would lead to less frequent discarding of links in the process of constructing a spanning tree.

8. IMPLICATIONS FOR EMPIRICAL FINDINGS

Our results show that MST characteristics are unaffected by changes in density or average connectivity of a network. Moreover, MST metrics behave similarly to several conventional network metrics. Importantly, this only holds when it is the underlying topology of the full network that changes, and not the density or average connectivity, since, in contrast to MST metrics, conventional metrics mix such changes with changes in network topology.

This is the first study that revealed that metrics computed on an MST are very strongly associated with conventional graph metrics computed on the original network (Figure 9). Only one earlier study has revealed that spanning trees for large-scale networks generally contain scale-free characteristics, i.e. power law degree distributions, similar to that of the original network (Kim et al., 2004). Together, these studies indicate that although the MST contains merely a fraction of the links in the original network, this relatively small and mathematically well-defined sub-network, contains important information about the underlying network. Therefore, adding links to the MST in order to obtain a, supposedly, realistic representation of the underlying network may not be necessary, and in fact introduces an arbitrary element as one would have to make a decision on the number of links that should be added.(Hagmann et al., 2008).

The similarities between MST and conventional metrics have consequences for the interpretation of network alterations observed in previous studies on functional brain networks. For example, work by Boersma and others showed that EEG functional connectivity (using the Synchronization Likelihood (Stam et al., 2003) decreased in children between the ages of 5 and 7 years, while the clustering and path length both increased, indicating that the networks became more regular (Boersma et al., 2011). The MST diameter and eccentricity increased and the leaf fraction decreased in the same dataset (Boersma et al., 2012) – as would be expected from our simulations (Figure 4). Taken together, the finding that networks became more regular between the age of 5 and 7

was confirmed by the MST analysis, which showed that networks became more line-like during maturation. However, the study also described that mean functional connectivity was higher in girls than in boys, while the clustering was higher in girls as well (in the alpha and beta frequency band). MST analysis did not show any difference in network topology between boys and girls for these frequency bands, indicating that the observed difference in clustering may simply have been due to the higher connectivity levels in girls. In addition, boys had a more star-like topology than girls in the theta band, while no network differences were found in this frequency range with conventional network metrics. This again can be explained by the observation that the mean connectivity in girls was higher than in boys in this frequency band, thereby obscuring the change in network topology when conventional metrics were used.

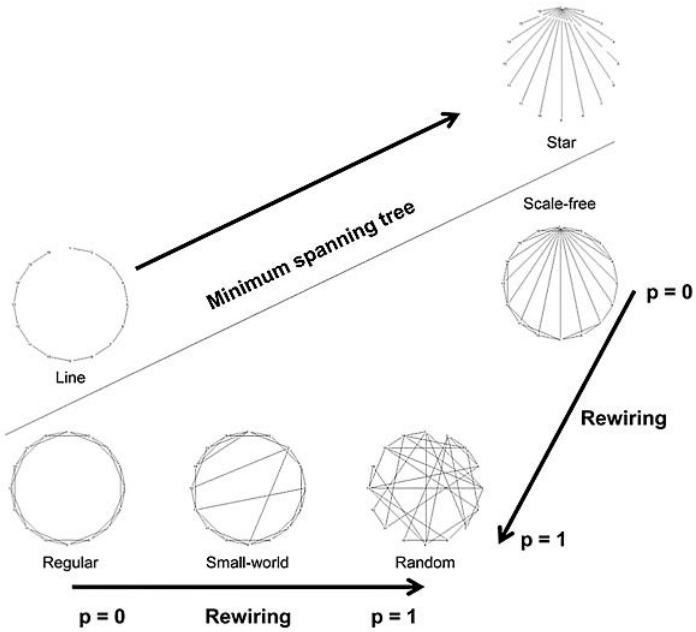

Figure 9: Schematic presentation of MST topology in relation to the topology of well known network models. The schema shows how the MST reflects the underlying network topology for regular, small-world, random, and scale-free networks. Our analyses indicate that MST metrics are strongly related to the underlying network topology. For alterations on the scale of regular to random networks, MST diameter and leaf number change similarly to the path length for the underlying network; MST diameter is positively correlated to the path length, and MST leaf number is negatively correlated to the path length. When a scale-free network is randomized, the degree of the MST reflects the degree of the underlying network.

It should be noted that the spatial embedding of the network may affect the topology of the MST, depending on the modality and type of connectivity measure that is used to determine edge weights. For example, in EEG data, it is known that linear functional connectivity measures overestimate local connectivity, which will lead to more line-like MSTs (see Figure S7 and 9). In contrast, non-zero

phase-lag based measures are more biased towards long-distance connections, which will lead to more star-like MSTs (see Figure S7). Similarly, DTI/DWI-based tractography is thought to be biased towards local connections, and thus towards a more line-like MST. However, such (modality specific) effects of connectivity measures are also present in traditional graph analytical approaches.

9. STRENGTHS, LIMITATIONS AND PERSPECTIVES

The strengths of using the MST for brain network analysis are that it is a mathematically defined, unbiased sub-network that reflects the most fundamental network properties, while its characteristics are strongly related to conventional network metrics. Importantly, this allows for unbiased comparison between networks of equal size in empirical studies.

At the same time, the MST is unique if the link weights of the underlying network are also unique. This uniqueness is also an advantage of the MST over other approaches to compute the backbone of the network, such as k-core decomposition (Hagmann et al, 2008), as the construction of the MST is independent of arbitrary thresholds or dependency on link weight transformations. However, there are some methodological issues that need to be discussed. Firstly, the fact that the MST discards all connections that form loops makes it impossible to study clustering directly. However, it has previously been shown that the clustering coefficient and path length in the small-world model are highly correlated and therefore contain redundant information; the computation of the clustering coefficient is therefore not very informative (Li et al., 2011).

Secondly, estimation of modular network organization on the basis of the MST is challenging. However, previous studies revealed that even trees can contain information about hierarchical modularity (Bagrow, 2012; Ciftci, 2011; Lee et al., 2006). Furthermore, in the present study we considered the MST as the end product of Kruskal's algorithm. However, for large size networks it is known that amid the growth process of an MST during Kruskal's algorithm a distribution of disconnected modules occurs, that enlarge and eventually connect to each other to form an MST (Braunstein et al., 2013). Therefore, apart from the MST itself, processes that lead to the MST might also provide information about modularity.

Thirdly, the MST is a sub-network based on the ordering of connectivity values. If the connectivity values of a network are unique and if the ordering of the connectivity values does not alter, the solution of the MST is always unique, irrespective of the used algorithm. One of the advantages of the use of an MST is that these methodological issues about the uniqueness, stability of the MST solution and test-retest reliability have been thoroughly studied in basic mathematical papers (Cheriton and Tarjan, 1976; Graham and Hell, 1985; Michailidis, 2005; Moret and Shapiro, 1993). However, measuring a same network twice could lead to slight modulations in the ordering of connectivity values which would lead to a different MST. However, our findings suggest that spanning trees with near-optimal total weight obtained by link re-ordering have a large of overlap with the MST, indicating that the topologies of these nearly-optimal spanning trees are highly similar to the topology of the MST. The results obtained from an analysis of the MSTs can thus be considered

as robust to (experimental) fluctuations in link weights. Also, when dynamical data are studied, such as from EEG, MEG or fMRI recordings, ordering may vary between states, which may contain information about the stability of specific links in the MST. It is demonstrated that there is a set of links that remain stable over time and are complemented by more peripheral links that change over time (Lee et al., 2006; Lee et al., 2010).

Fourthly, although we demonstrated that the MST is insensitive to effects related to arbitrary thresholds, average strength of connectivity, and network density, the MST metrics are still sensitive to network size. Therefore, to minimize size-effects we normalized MST metrics by network size. However, this did not solve the effect of network size. Future studies need to address this point and until a solution is provided we encourage usage of standard atlases to keep network size and thus results comparable between studies.

Finally, we chose to study the MST in the context of small-world and scale networks which were rewired to random networks, since the characteristics of these network models have been studied in most detail. However, some other characteristics also shape brain networks, such as hierarchical modularity, rich club organization, economical clustering, and, in the case of functional brain networks, the degree product of the underlying structural network ((Tewarie et al., 2014; van den Heuvel and Sporns, 2011; Vertes et al., 2012). These characteristics do not easily fit to the models studied in the current work. However, we suggest that interpretation of MST characteristics in relation to the most fundamental network models is an important step for interpretation of the increasing number of empirical studies using the MST.

10. CONCLUSION

MST analysis is shown to be a feasible, unbiased method for brain network analysis, as it avoids methodological biases due to the mixing of information about topology with information about functional connectivity. Furthermore, changes in MST topology reflect changes in the underlying network topology, and MST characteristics can be interpreted along the lines of the familiar small-world and scale-free model. Future work should elucidate how the MST relates to other network characteristics such as modularity, hierarchy, and rich club phenomena.

SUPPLEMENTARY FIGURES

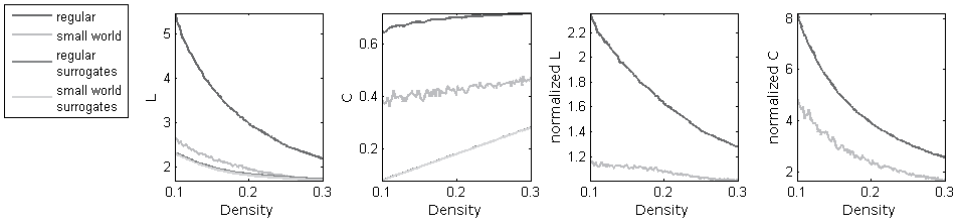

Figure S1: Network characteristics as a function of link density and connection strength (not using a sub-sampling approach). Network characteristics are given as a function of link density (unweighted networks). In contrast to figure 1, no threshold was used for sub-sampling the original network. Instead, for each network density a new regular and small-world network (rewiring probability *p* is 0.1 with size *N* = 78) was constructed. Note that the path length and clustering coefficient change as a function of density in unweighted networks. This problem is not solved after normalization by comparison to the path length and clustering coefficient for random networks with similar density/strength. Results are similar to Figure 3 in the paper of van Wijk et al. (2010).

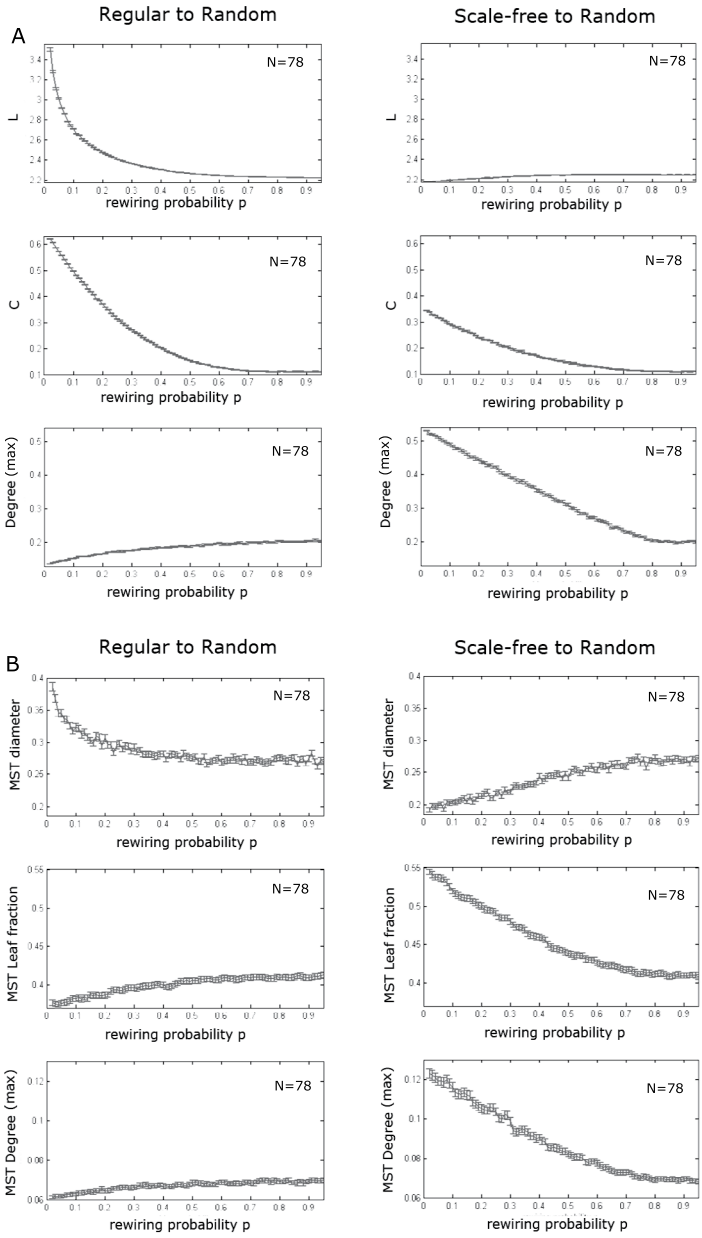

Figure S2: Network properties as a function of network rewiring probability for regular and scale-free networks with an empirical edge weight distribution. Network characteristics are presented for networks that were rewired with probability *p*, starting with either a regular network or a scale-free network of size *N* = 78. Figure similar to figure 2, but now the edge weight distribution was obtained from MEG functional connectivity described by(Tewarie et al., 2013b). All topological metrics behave highly similar or almost identically compared to the behaviour of those metrics as seen in previous analysis.

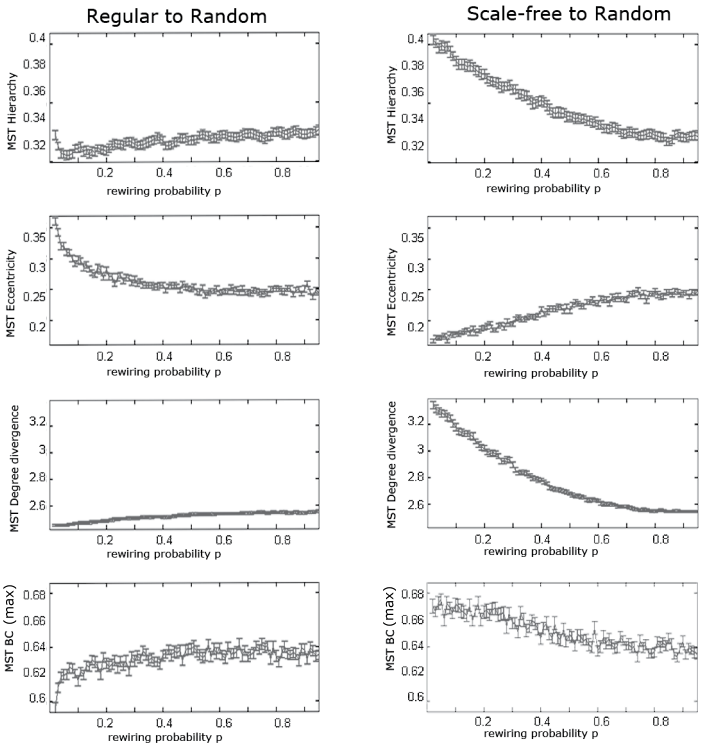

Figure S3: MST metrics as a function of network rewiring probability for regular and scale-free networks with an empirical edge weight distribution.
MST characteristics are presented for networks that were rewired with probability *p*, starting with either a regular network or a scale-free network of size *N* = 78. Figure similar to figure 3, but now the edge weight distribution was obtained from MEG functional connectivity described by(Tewarie et al., 2013b). All topological metrics behave highly similar or almost identically compared to the behaviour of those metrics as seen in previous analysis. The reason for this is that the MST is insensitive to the shape of the link weight distribution, but is only dependent on the ordering or ranking of the link weights(Dobrin and Duxbury, 2001).

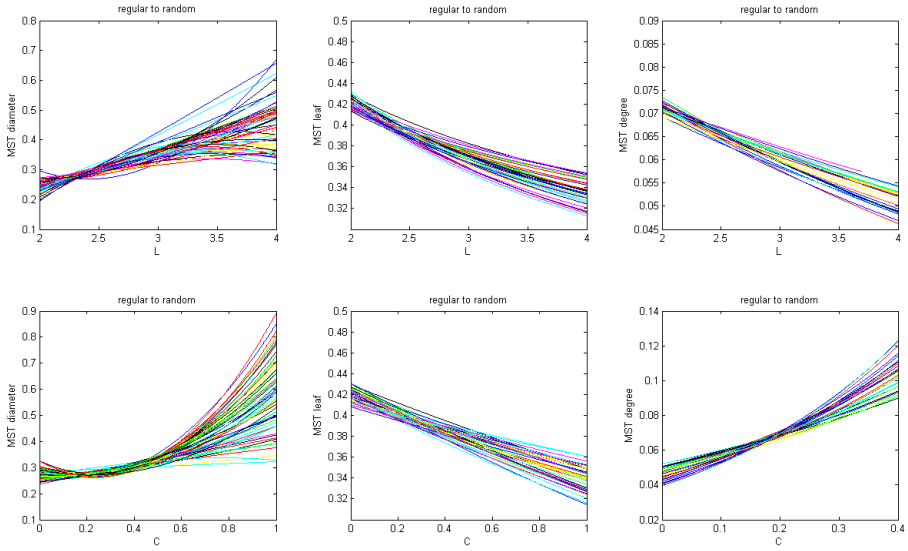

Figure S4: Fitted functions for the relationships between conventional and MST measures on the rewired regular networks.
Figure is similar to figure 4, but now displaying the fit for individual realizations (50 realizations) on the regular vs random axis. Depending on the shape, we used a polynomial, power or exponential functions to fit individual realizations. Note the variability in the relationship between MST diameter and path length and clustering.

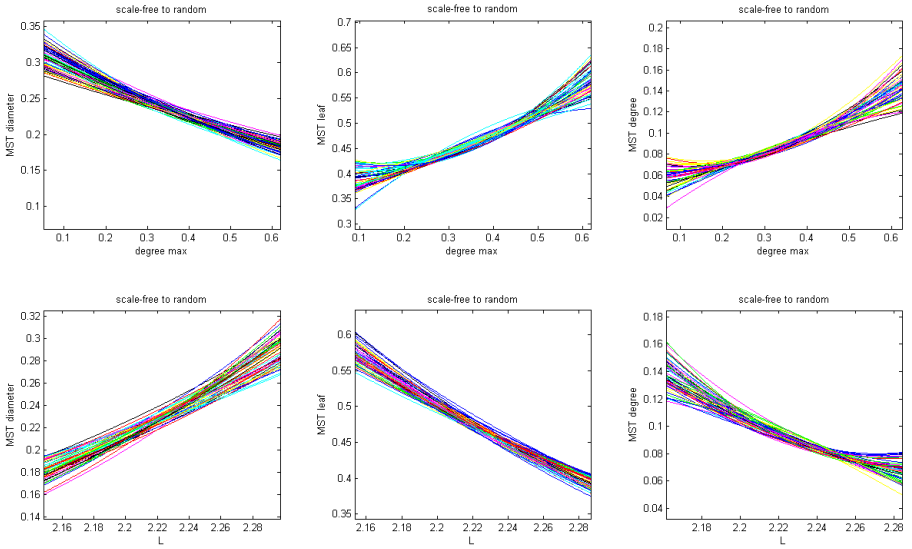

Figure S5: Fitted functions for the relationships between conventional and MST measures on the rewired scale-free networks.
Figure is similar to figure 5, but now displaying the fit for individual realizations (50 realizations) on the scale-free random axis. Depending on the shape, we used a polynomial, power or exponential functions to fit individual realizations.

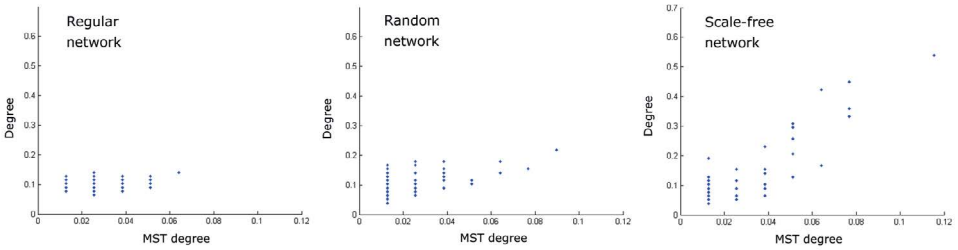

Figure S6: Scatter plot for node degree in the MST and the degree of the original regular, random, and scale-free graphs. Note that especially for scale-free graphs, the MST and original degree ranks seem to become more strongly correlated for nodes with a high degree, suggesting that the MST is especially capable of picking up characteristics of hub nodes.

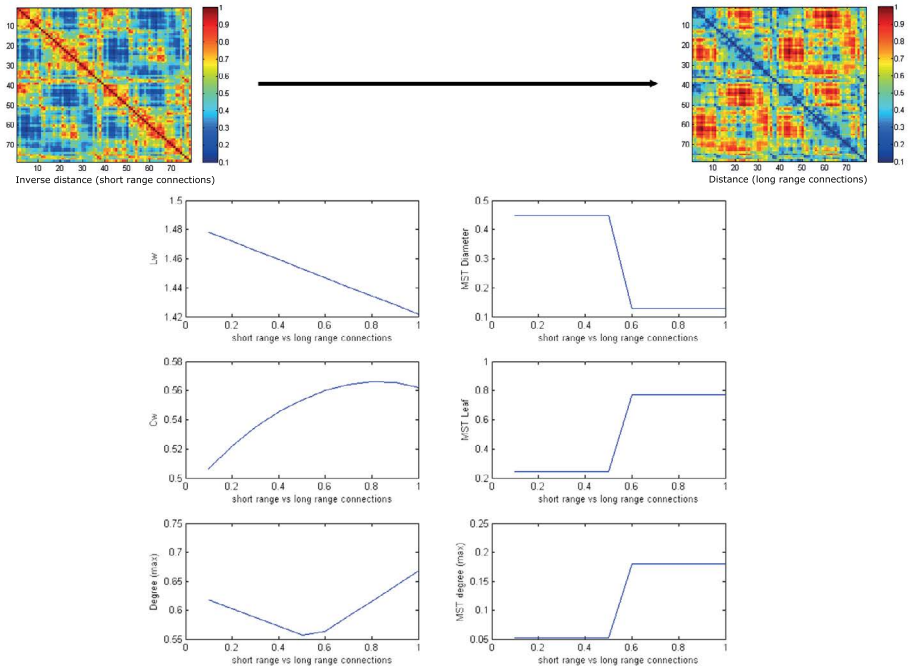

Figure S7: Effect of distance dependent connection strength on global network properties. Simulations were performed to study the effects of strong short-range connections on global MST properties in comparison to traditional network characteristics, as such bias may be present in empirical datasets, for example in DTI recordings. Edge weights were assigned according to the inversed Euclidian distance between all node pairs (Figure S7), such that strongest links were present for short-range connections. We also computed a Euclidian distance matrix, where the highest link weights represented longest distance between nodes. We computed the weighted sum of these matrices using a step function: New_matrix = a * [inverse Euclidean distance matrix] + b * [Euclidean distance matrix], where $0<a<1$ and $0<b<1$ and $a+b=1$.This new_matrix was subsequently normalized by the range of values. Weighted network characteristics gradually change when longer distance connections become stronger, leading to a lower path length and higher clustering. MST characteristics change in the same direction as traditional measures, but only at the transition point b>a, while it remains stable for all other points. These findings indicate that the MST is quite robust to changes in distance between nodes as long as the ordering of the links weights remains unchanged.

PART 2

Applications in multiple sclerosis

Chapter 5

Cognition in MS correlates with resting-state oscillatory brain activity: An explorative MEG source-space study.

M.L. van der Meer, P. Tewarie, M.M. Schoonheim, L. Douw, F. Barkhof, C.H. Polman, C.J. Stam, A. Hillebrand

Neuroimage Clin. 2013 May 13;2:727-34

ABSTRACT

Clinical and cognitive dysfunction in Multiple Sclerosis (MS) is insufficiently explained by structural damage as identified by traditional magnetic resonance imaging (MRI) of the brain, indicating the need for reliable functional measures in MS. We investigated whether altered resting-state oscillatory power could be related to clinical and cognitive dysfunction in MS. MEG recordings were acquired using a 151-channel whole-head MEG system from 21 relapsing remitting MS patients and 17 healthy age-, gender-, and education-matched controls, using an eyes-closed no-task condition. Relative spectral power was estimated for 78 regions of interest, using an atlas-based beamforming approach, for classical frequency bands; delta, theta, alpha1, alpha2, beta and gamma. These cortical power estimates were compared between groups by means of permutation analysis and correlated with clinical disability (Expanded Disability Status Scale: EDSS), cognitive performance and MRI measures of atrophy and lesion load. Patients showed increased power in the alpha1 band and decreased power in the alpha2 band, compared to controls, mainly in occipital, parietal and temporal areas, confirmed by a lower alpha peak-frequency. Increased power in the alpha1 band was associated with worse overall cognition and especially with information processing speed. Our quantitative relative power analysis of MEG recordings showed abnormalities in oscillatory brain dynamics in MS patients in the alpha band. By applying source-space analyses, this study provides a detailed topographical view of abnormal brain activity in MS patients, especially localized to occipital areas. Interestingly, poor cognitive performance was related to high resting-state alpha1 power indicating that changes in oscillatory activity might be of value as an objective measure of disease burden in MS patients.

INTRODUCTION

Multiple Sclerosis (MS) is an acquired progressive neurological disease with a highly variable course, leading to both physical symptoms and cognitive impairment. Clinical and cognitive decline in MS is insufficiently explained by classical MRI measures such as lesion load or atrophy of the white matter (Barkhof, 2002). However axonal damage and demyelination in the gray matter seem to correlate with clinical and cognitive deficits in MS (Geurts and Barkhof, 2008).

In physiological conditions modulations in neuron population firing probability occur preferentially during a certain phase of the oscillatory activity (Schnitzler and Gross, 2005). Demyelination and axonal damage could lead to altered firing probability and therefore to altered oscillatory cortical activity in MS. Neurophysiological techniques, such as EEG and MEG, can be used to detect such changes in activity, as has been demonstrated for neurological diseases such as Alzheimer's disease (de Haan W. et al., 2008; Jeong, 2004; Stam et al., 2006a), Parkinson's disease (Bosboom et al., 2006; Ponsen et al., 2013; Stoffers et al., 2007), low-grade glioma (Bosma et al., 2008), traumatic brain injury (Kumar et al., 2009), and stroke (van Putten and Tavy, 2004). Up to 70% of patients with MS suffer from cognitive impairment (Rao et al., 1991); attention, information processing speed and memory being the most commonly affected domains (Chiaravalloti and DeLuca, 2008). There is increasing evidence that changes in oscillatory brain activity may be related to cognitive dysfunction in neurological disease (Schnitzler and Gross, 2005; Stam and van Straaten, 2012b; Uhlhaas and Singer, 2006). We therefore hypothesize that cognitive impairment in MS patients might be partially explained by pathological changes in oscillatory brain activity.

To date, literature on EEG or MEG in MS is scarce. Visual inspection of EEG recordings from MS patients revealed more focal EEG abnormalities (slow activity) in patients with relapses compared to patients with a progressive course (Feng, 1981). A 5-year follow-up study did not show a significant correlation between visual EEG abnormalities and neurological disability (Quattrini et al., 1981). Yet, another group used computerised spectral analysis to demonstrate a positive relation between patients' disability and increased theta power over the temporal regions and increased beta power over the frontal regions, where visual interpretation of the EEG failed to demonstrate any correlations (Colon et al., 1981). Power spectral density analysis of EEG data, obtained during an auditory oddball task, revealed increased power in beta and gamma bands (especially over midfrontal areas) in MS patients compared to healthy controls (Vazquez-Marrufo et al., 2008). Similarly, for a visuo-spatial task, more beta and gamma power was found over occipital and right-frontal regions in relapsing remitting MS patients compared to a group of healthy controls, but no differences were found in the high frequency bands during resting-state, nor were there any significant correlations between quantitative EEG (QEEG) scores and Expanded Disability Status Scale (EDSS) (Vazquez-Marrufo et al., 2008).

Compared to EEG, MEG provides a reference free method and the magnetic fields are much less disturbed by the skull. MS research using EEG and MEG has recently focussed on altered functional connectivity, which referrers to statistical interdependencies between physiological time series

(Cover et al., 2006a; Leocani et al., 2000; Schoonheim et al., 2011; Tecchio et al., 2008), and changes in functional network topology (Hardmeier et al., 2012; Schoonheim et al., 2011). A more basic characterisation, including for example global and local spectral analysis of the rhythmic MEG activity in MS patients has not been performed to date. Yet, knowledge of changes in local spectral power seems fundamental in comprehending the outcome of connectivity research. Additionally, the aforementioned studies were performed at the sensor level, i.e. results were estimated based on the extracranial recordings directly, making interpretation of these results in terms of the specific anatomical brain regions that are involved more difficult. In addition, investigation of abnormal MEG activity at the source-level facilitates comparison with other neuroimaging techniques, notably structural and functional MRI.

The aim of the present MEG study was therefore to explore differences in resting-state oscillatory brain activity in MS patients compared to healthy controls, and to relate these differences to cognitive performance, physical disability and structural deficits measured with MRI. A recently developed technique, projecting sensor-based data onto an atlas-based source-space using beamforming, was applied (Hillebrand et al., 2012) in order to provide a detailed anatomical mapping of cortical rhythms for 78 regions of interest (ROIs).

METHODS

General study design

In this cross-sectional study MS patients and healthy controls underwent MEG, MRI, neurological examination and neuropsychological assessment on the same day. Outcome measures were global relative power, relative power per ROI (regional relative power), peak frequency, anterior-posterior gradients, diffuse slow-wave activity and the presence of asymmetry. These outcome measures were associated with cognition and MRI measures.

Subject characteristics

MS patients and healthy volunteers were recruited from an ongoing large clinical study at the Multiple Sclerosis Center of the VU University Medical Center, as described in a previous MEG study in the same subjects (Schoonheim et al., 2011). Our project involved 34 MS patients (17 women, mean age 41.4 ± 8.0 years, disease duration 8.1 ± 1.6 years) and 28 healthy controls (14 women, mean age 39.8 ± 10.5 years), matched for age, gender and educational level (using a Dutch classification system ranging from 1 (only primary education) to 7 (university degree)). Twenty four participants were excluded from further analysis due to unavailability of an anatomical MRI (n=2), failed MEG/MRI co-registration (n=10) and too many artefacts in the raw MEG data (n=12). Consequently, 21 MS patients (mean age 41.9 ± 7.7, disease duration 6.8 ± 0.9 years) and 17 controls (mean age 39.8 ± 9.8) remained in the present study, who were still gender-, age- and education-matched. Patients were diagnosed with MS according to the revised McDonald Criteria (Polman et al., 2005). None of the healthy controls suffered from a neurological or psychiatric disease, nor did they use

any medication or drugs. Eight patients were treated with interferon β since diagnosis, one of them switched to glatiramer acetate and two to natalizumab, which they received during this study. No other medication was used. Patients were assessed according to a clinical protocol, involving history taking, neurological examination, blood tests, neuropsychological tests, MRI of the brain and MEG. Physical disability was measured using the Expanded Disability Status Scale (EDSS) (Kurtzke et al., 1983). The study protocol was approved by the Local Research Ethics Committee, whose ethics review criteria conformed to the Helsinki declaration. All subjects had given written informed consent prior to participation.

MRI

An MRI scan was obtained from all subjects, using a 3T-MRI system (GE Signa HDXT V15m). A 2D dual-echo T2-weighted sequence (TR 9680 ms, TE 22/112 ms) and T1-weighted sequence (TR 475 ms, TE 9 ms) were obtained with 48 slices of 3 mm and 3D-T1 heavily T1-weighted sequence (FSPGR , TR 7.8 ms, TE 3.0 ms, TI 450 ms) with 1 mm, slices covering the entire brain. All scans were inspected by an experienced rater (MMS). T1-hypointense and T2-hyperintense lesions in MS patients were marked and their volumes were measured using a local-threshold technique. Total normal gray matter volume (NGMV), total normal white matter volume (NWMV), and normal whole brain volumes (NBV), corrected for head size, were estimated using FSPGR images and SIENAX (Smith et al., 2002) version 2.5 (part of FSL 4.1, FMRIB's Software Library, http://www.fmrib.ox.ac.uk/fsl). Thalamic volumes were outlined and volumes measured using FIRST (part of FSL), as described before for this cohort (Schoonheim et al., 2012). Left and right volumes were summed to give the total volume.

Neuropsychological evaluation

Cognitive function in all subjects was assessed according to the protocol used and described before (Schoonheim et al., 2012). A Brief Repeatable Battery of Neuropsychological Tests (BRB-N), the selective reminder test (SRT), the 10/36 spatial recall test (SPART), the symbol digit modalities test (SDMT), the word list generation test (WLG), the concept shifting test (CST), the Stroop color-word test and the memory comparison test (MCT) were administered. Individual patients' test scores were converted to z-scores, using the means and standard deviations of the entire group of participants. The z-scores for all tests were averaged for each subject, creating overall cognition z-score. Subsequently, individual scores on the tests were summarized into seven cognitive domains, namely (1) executive functioning (CST, WLG) , (2) information processing speed (SDMT), (3) psychomotor speed (CST, SDMT), (4) attention (Stroop), (5) verbal memory (SRT), (6) working memory (MCT), and (7) visuospatial memory (SPART). Construction of these domains with comparable cognitive tests has been reported previously and was based on a principal component analysis using varimax rotation with Kaiser normalization performed on the z-scores for a large group of healthy controls (Klein et al., 2003), and these domains are commonly used in neurocognitive practice and research.

MEG recordings

MEG data were acquired using a 151-channel whole-head MEG system (CTF Systems Inc., Port Coquitlam, BC, Canada), while subjects were seated inside a magnetically shielded room (Vacuumschmelze GmbH, Hanau, Germany). A third-order software gradient (Vrba et al., 1999) was used with a recording passband of 0–150 Hz and a sample frequency of 625 Hz. At the beginning and end of the measurement, the head position relative to the coordinate system of the helmet was determined by leading small currents through three position coils situated at the left and right pre-auricular points and the nasion. Changes in head position smaller than 0.5 cm during the recording were accepted. The MEG recordings were performed in a no task, eyes-closed and-eyes open condition. Only data from the eyes-closed condition were analysed here. For each participant, five minutes of the continuous resting-state, eyes-closed recording was divided into 45 epochs of 6.555 seconds. Channels and epochs were visually inspected. Epochs and channels were rejected based on system related artefacts (SQUID jumps, noisy, broken or saturated channels), physiological artefacts (eye movements, eye blinks, muscle artefacts), external artefacts (magnetized dental fillings) and environmental noise (PT, AH) (Gross et al., 2012), as well as for representing an alert eyes-closed state, leading to discarding on average 5.7 channels (range: 2-14) and 8.4 epochs (range: 3-20). The selected epochs were subsequently projected to source-space.

Beamforming: time-series estimation for regions-of-interest

The technique used in this study was recently described (Hillebrand et al., 2012). A brief overview is given below. First, a subject's MRI was co-registered with the MEG data through identification of the same anatomical landmarks in the MRI that were also used for the placement of the MEG head-localization coils (i.e. left and right pre-auriculars and nasion). Only data from subjects where the estimated co-registration error was smaller than 0.8 cm were accepted for further analysis. The co-registered MRI was then spatially normalized to a template MRI using the SEG-toolbox in SPM8 (Friston et al., 2004). The new segmentation toolbox is an extension of the unified segmentation algorithm, which incorporates additional tissue priors for improved matching of the subject's MRI to the template (Ashburner and Friston, 2005; Weiskopf et al., 2011). The automated anatomical labelling (AAL) atlas was used to label the voxels in a subject's normalized co-registered MRI (Tzourio-Mazoyer et al., 2002). Subcortical structures were removed, and the voxels in the remaining 78 cortical ROIs were used for further analysis (Gong et al., 2009), after inverse transformation to the patient's co-registered MRI.

Neuronal activity for the labeled voxels in the ROIs was reconstructed using a beamforming approach known as Synthetic Aperture Magnetometry (SAM) (Robinson and Vrba, 1999). SAM works in a sequential fashion, where the activity for each voxel is reconstructed by selectively weighting the contribution from each MEG sensor to a voxel's time-series. This weighting is done such that the activity at a voxel is reconstructed without distortion, and at the same time the contribution from external (noise) sources is minimized (Hillebrand et al., 2005; Hillebrand and Barnes, 2005).

The beamformer weights are based on the covariance of the data and the forward solution (lead field) of a dipolar source at the voxel location, where data were band-pass filtered from 0.5-48 Hz. To correct for non-uniform projection of sensor noise each beamformer weight was normalised by its vector norm. A time-window of, on average, 238 seconds (range: 164-282 sec.) was used for the computation of the data covariance matrix, which was considered sufficient for accurate estimation of the data covariance, and therefore for the accuracy of the reconstructed source power (Brookes et al, 2008). We used broadband data for the estimation of the beamformer weights, as this avoids overestimation of covariance between channels (Barnes and Hillebrand 2003). The sensor-level data were subsequently projected through the beamformer weights, resulting in a time-series for each voxel. Each ROI contains many voxels and the number of voxels per ROI differed. In order to represent a ROI by a single time-series, we selected, for each ROI and frequency band separately, the voxel with maximum absolute power in that frequency band (Hillebrand et al., 2012). The time-series for this voxel was used for further analysis, resulting in a total of 6 sets of 78 time-series (one for each frequency band, using six classic frequency bands: delta (0.5-4 Hz), theta (4-8 Hz), alpha1 (8-10 Hz), alpha2 (10-13Hz), beta (13-30 Hz), and gamma (30-48 Hz)). Like our previous studies we selected five artifact-free epochs of 4096 samples (6.555 seconds) from these time-series, based on careful visual inspection (PT) to obtain stable results (Bosboom et al., 2006; Bosma et al., 2008; Douw et al., 2008; Douw et al., 2009; Douw et al., 2010; Schoonheim et al., 2011; Stam et al., 2006; Stam et al., 2009; Stoffers et al., 2007; van Dellen et al., 2013). BrainWave software packing was used for this purpose and also for further analyses (version 0.9.58 available from http://home.kpn.nl/stam7883/brainwave.html).

The relative power, averaged over the selected 5 epochs, in every ROI for every subject was calculated using the Fast Fourier Transformation. In addition, the mean power over all ROIs was calculated to yield one mean power value per frequency band in every subject (global relative power). The peak frequency was determined as well. Other properties of the MEG background rhythm were also computed such as anterior posterior gradients, the amount of diffuse slow wave activity and asymmetry (Lodder and van Putten, 2013). Anterior posterior gradient is the ratio between power in frontal regions and power in all regions for a specific frequency range, often the alpha band. Here we calculated the anterior posterior gradient for both the alpha1 and alpha2 band separately. This gradient is within normal range if it is smaller than 0.4. Diffuse slow wave activity is calculated by the power ratio (Q_{slow}) between $P_{low} = \{2...8\}$ Hz and $P_{wide} = \{2...25\}$ Hz. Too much or abnormal diffuse slow-wave activity is present when this ratio exceeds 0.6. Asymmetry is obtained by calculating a left-right power ratio for each ROI pair in the frequency range 0.5-12 Hz, yielding 39 values (1 for each pair) (Lodder and van Putten, 2013).

Statistical analysis

To compare group differences between MS patients and healthy controls independent t-tests and in absence of normality Mann-Whitney tests were used for all global relative power values,

MRI parameters and cognition. Obtained p-values for global relative power values were corrected for multiple comparisons with the false detection rate (i.e. correcting for 6 tests (6 frequency bands)) (Benjamini and Hochberg, 1995). Normality was checked using histogram inspection and Kolmogorov-Smirnov tests of normality. Whenever there were significant differences in global relative power values, power in ROIs were compared between groups by means of permutation analysis as a post-hoc analysis (Nichols and Holmes, 2002). Here a null distribution for between-group differences (independent t-test) is derived by permuting group assignment and calculating a t-statistic after each permutation. Other global properties of the MEG rhythm were also statistically analysed as mentioned above. For analysing asymmetry differences we used permutation analyses as well.

As another post-hoc analysis, if there were significant differences in global relative power values between MS patients and healthy controls in a specific frequency band, then correlations between mean power and other parameters (EDSS, MRI, and cognition) were computed by means of Spearman's coefficients (2-tailed) for that specific frequency band. These statistical analyses were performed using SPSS for windows v.15. and the permutation analyses were performed in Matlab (R2008b).

Table 1: Descriptive variables for controls and patients

	Controls (N=17)			Patients (N=21)			p value
	Mean	±	SD	Mean	±	SD	
Age	39.8	±	9.8	41.9	±	7.7	0.49
Education(1-7)	5.9	±	1.36	5.4	±	1.33	0.52
Disease Duration				6.8	±	0.9	-
NGMV (l)	0.84	±	0.05	0.81	±	0.04	0.037*
NWMV[a] (l)	0.69	±	0.03	0.66	±	0.03	-
NBV (l)	1.53	±	0.07	1.47	±	0.05	0.006*
Total thalamic volume	0.021	±	0.001	0.019	±	0.002	0.004*
Cognition	0.04	±	0.64	-0.19	±	0.84	0.36
EDSS (1-10)[b]				2		(0-4.5)	-
T1 lesion load (mL)				1.05	±	0.81	-
T2 lesion load (mL)				2.48	±	2.03	-

NGMV, normalized gray matter volume; NWMV, normalized white matter volume; NBV, normalized brain volume; EDSS, expanded disability status scale.[a] NWMV was not used for further analyses: lesion filling was not performed and therefore NWMV was not reliably estimated. [b] indicates median and range.* indicates significant differences between the two groups.

RESULTS

Subject characteristics

Characteristics for the 21 MS patients and 17 healthy controls whose data were used for analysis in the present study are summarized in Table 1. There were no significant differences in age, gender,

or educational level between the two groups. Disease duration, EDSS score and MRI lesion load did not differ significantly between male and female patients. Neuropsychological test outcome was not significantly different between MS patients and controls. However, overall cognition Z-scores were significantly lower in male patients compared to female patients (Mann Whitney U: $Z = -2.2$, $p = 0.02$).

MRI: Atrophy measures

NBV and NGMV were significantly lower in the patient group ($t(36) = -3.01$, $p = 0.006$, $t(36) = -2.2$, $p = 0.037$, respectively) (Table 1). Mann-Whitney test revealed significantly lower total thalamic volumes ($Z = -2.9$, $p = 0.004$) in MS patients compared to healthy controls.

Global Relative Power

Global relative power (averaged over all 78 ROIs) in all the different frequency bands is shown in figure 1. Patients showed more mean relative power in the alpha1 band compared to controls (mean patients = 0.15 and mean controls = 0.11, $Z = -2.7$, $p = 0.006$) and less mean relative power in the alpha 2 band (mean patients = 0.15 and mean controls = 0.21, $Z = -2.7$, $p = 0.007$). The global relative power in the other bands did not differ significantly between groups. Differences in peak alpha frequency are illustrated in figure 2, which shows a significant shift in peak frequency from 9.92 Hz in controls to 9.15 Hz in patients ($t(36) = 2.138$, $p = 0.039$).

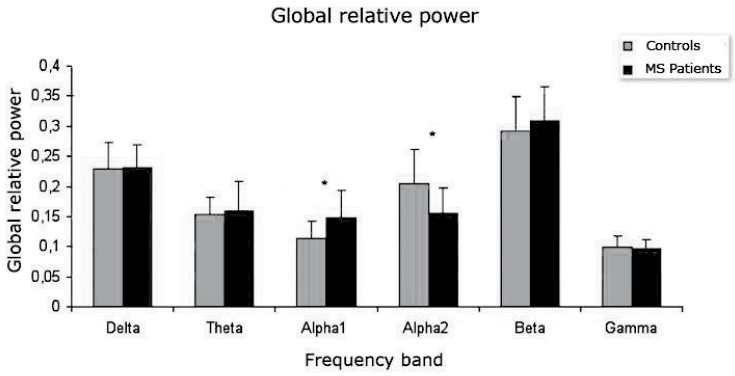

Figure 1: Relative power in the different frequency bands, averaged over all cortical areas (78 AAL ROIs), for patients and healthy controls. Error bars indicate standard deviations. * Indicates significant total power differences between the two groups, which occurred in the alpha1 and alpha2 band. The patients showed higher alpha1 power and lower alpha2 power. These results were corrected for multiple comparisons with the false detection rate.

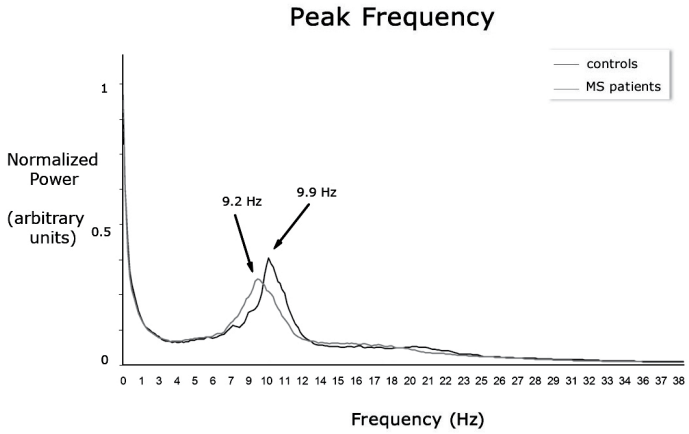

Figure 2: Normalised power spectra, with peak frequency for patients (9.15 Hz) and for controls (9.92 Hz).

Regional relative power

Only if global relative power differences were present in a specific frequency band, we compared regional power differences between MS patients and healthy controls as a post hoc analysis. There were significant differences in relative power between patients and controls in the lower and upper alpha band. Figure 3 displays the results of the post hoc permutation analysis in respectively the alpha1 and alpha2 band. The nomenclature for the different areas based on automated anatomical labelling (AAL) is given in Appendix A1. Compared to healthy controls, MS patients showed more relative power in the alpha1 band in right and left occipital regions (AAL 22-27, 61-66), inferior temporal regions (AAL 28, 32, 35, 67, 71, 74), medial parietal regions (AAL 21, 56, 59, 60), right frontal regions (AAL 51, 52) and midposterior cingulate regions (37, 38, 76, 77). Additionally, for the alpha2 band, significantly less power was found in MS patients in very similar regions, namely left and right occipital regions (AAL 22-27, 61-66), medial and inferior temporal regions (AAL 28, 31-33, 35, 67, 69-71, 74), parietal regions (AAL 20, 21, 59, 60), midposterior cingulate (AAL 38, 76, 77) and frontal regions (AAL 2, 3, 6, 12, 40, 41).

Other MEG background properties

There was no difference in diffuse slow-wave activity between MS patients and healthy controls nor between asymmetry and anterior-posterior gradients in the alpha1 band. In both MS patients and healthy controls the diffuse slow-wave activity ratio (Q_{slow}) was lower than 0.6. In the alpha2 band there was a higher anterior-posterior gradient in MS patients (healthy controls median = 0.25, range = (0.15-0.44), MS patients median = 0.3, range = (0.19-0.42), Z = -1.48 p = 0.036).

Correlations between power and cognition, physical disability and MRI

In MS patients, a negative correlation between global relative power in the alpha1 band and overall cognition was found ($r(19)$= -0.46, p = 0.03), driven by information processing speed ($r(19)$ = -0.44, p = 0.047). There were no correlations between alpha1 or alpha2 band global relative power and physical disability or MRI parameters in MS patients.

DISCUSSION

The aim of the present study was to investigate if changes in oscillatory resting-state activity were present in MS and whether these changes were clinically relevant. For this purpose we reconstructed the relative power in several frequency bands for 78 atlas-based regions. Subsequently, relations between relative power and clinical-, cognitive-, and structural-measures were assessed. We found higher mean relative power in the alpha1 band and lower mean relative power in the alpha2 band in MS patients compared to healthy controls. Moreover, cognition and more specifically information processing speed correlated with mean relative power in the alpha1 band.

Here we report for the first time that in early MS there is a shift of the alpha peak towards the slower frequencies. Apart from the power differences at the global level in both lower and upper alpha bands, regional power differences in the same frequency bands were present, mainly localised to occipital, parietal and temporal areas. The observed lower power in the alpha2 band was also strengthened by the finding of a higher anterior-posterior gradient, indicative of a loss of alpha2 power in posterior regions in MS patients. So far, limited research on EEG and MEG power spectra has been performed in MS. Some earlier EEG studies at the sensor-level did find changes in MS spectra compared to controls, namely increased theta power over temporal regions and increased beta power over frontal regions (Colon et al., 1981), increase or hemispheric asymmetry of alpha band power (Facchetti et al., 1994) and increase of beta and gamma band activity over occipital and right frontal areas during an odd-ball task (Vazquez-Marrufo et al., 2008). However the latter study used a small 13-electrode EEG system and subsequently only used the midline electrodes (Fz, Cz, Pz) for analyses. More recent MEG and EEG studies were not able to find resting-state power changes in MS (Cover et al., 2006a; Leocani et al., 2000). The use of MEG compared to EEG, in combination with analyses in source-space (which gives an increased signal-to-noise ratio) and a larger sample size, could explain some of the differences between our results and the results from these previous studies.

The power changes in the alpha band seem to be clinically relevant. Power in the alpha1 band correlated negatively with overall cognition and, more specifically, with information processing speed. It has been observed that information processing speed is one of the first affected cognitive domains in MS (Chiaravalloti and DeLuca, 2008). In line with our results, another study on MS revealed that increase of mean alpha frequency was associated with improvement in clinical status (Colon et al., 1981). Therefore it seems relevant to elucidate this relation further in larger MS cohorts

and compare power changes in the alpha band between MS patients with preserved information processing speed and impaired information processing speed. Another argument to support further investigation in this relation is the observation that in healthy conditions alpha frequency is related to information processing speed or reaction time (Klimesch, 1999).

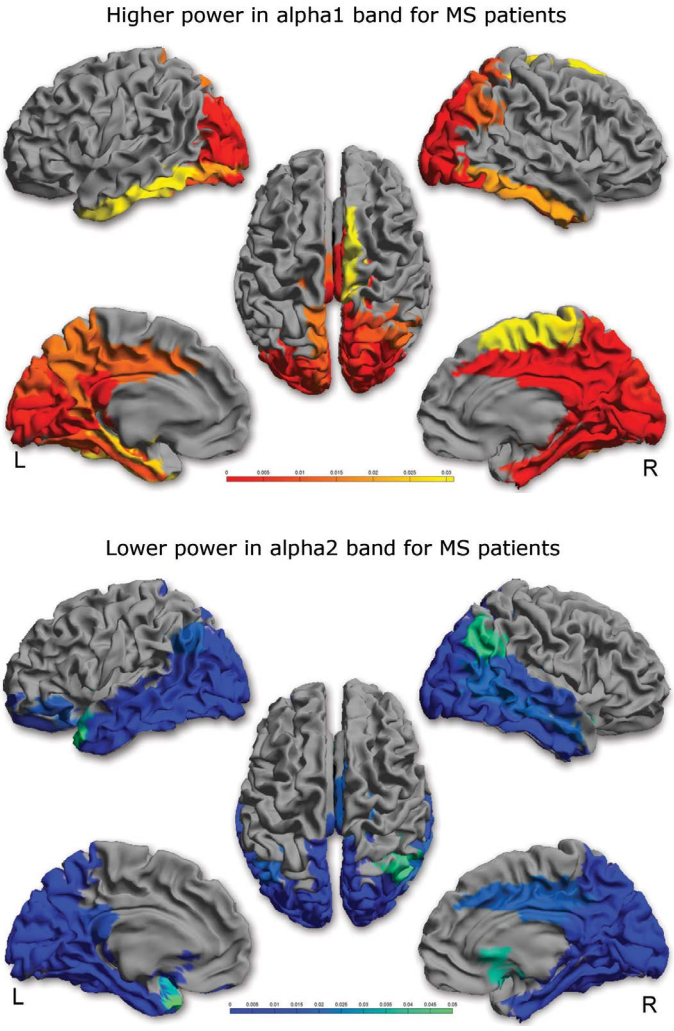

Figure 3: Significant power differences between patients and controls are shown as a colour-coded map on a template mesh. Red areas indicate higher power in patients in the alpha1 band (3A), blue areas indicate lower power in patients in the alpha2 band (3B). A scale bar is added to indicate the significance.

We observed a minor but significant slowing of the peak frequency of oscillatory brain activity. The mechanism underlying this slowing remains to be elucidated, particularly since there was no relation between alpha band power changes and structural damage (as determined from MRI measures of NBV, NGMV and T2 lesion load). However, slowing of oscillatory activity has been found for several other neurodegenerative neurological diseases, such as Alzheimer's disease (de Haan W. et al., 2008; de Waal H. et al., 2012) and Parkinson's disease (Bosboom et al., 2006; Olde Dubbelink et al., 2012; Stoffers et al., 2007). Therefore slowing of oscillatory activity might be a common pathway in neurodegenerative neurological diseases.

Oscillatory activity at the macroscopic level, such as measured with MEG/EEG, is the result of neuronal interactions at the micro-scale (between individual neurons) and macro-scale (between cortical regions), and involves different types of connections (excitatory and inhibitory). This makes it difficult to elucidate the exact origins of extracranially observed alterations in band-limited oscillatory power (Lopes da Silva F., 1991). However, some insight may be gained from computational studies. Two recent studies have used neural mass models in order to explain empirical observations in patients with Alzheimer's disease, and revealed that increased inhibition (Bhattacharya et al., 2011) or disinhibition (de Haan W. et al., 2012a) can cause slowing of oscillatory activity. Therefore a shift in the balance of inhibition/excitation could be of importance in slowing of oscillatory activity in MS as well. Such a shift in the balance of inhibition/excitation can be regarded as a problem of cortical origin.

However white matter changes measured with more advanced and sophisticated MRI measures such as DTI could also be of importance in MS. It has been shown that the integrity (fractional anisotropy values) of white matter tracts such as the corona radiata, posterior thalamic radiation and inferior longitudinal fascicle are positively correlated with the alpha peak frequency (Valdes-Hernandez et al., 2010). In MS we know that the integrity of these tracts are often affected (Harrison et al., 2012; Li et al., 2012). Furthermore, these white matter tracts are predilection sites for white matter lesions (Li et al., 2012). Therefore, the location of white matter lesions (located at white matter tracts going to occipital cortex) could be of more relevance for changes in the alpha peak frequency than overall white matter lesion load itself. Further studies are therefore warranted to elucidate the relation between white matter integrity changes, lesion probability maps and alpha band power changes. Demyelination has also been studied in a computational model of single cell neurons using modified Hodgkin and Huxley models (Coggan et al., 2010). In demyelinated neurons four types of spike behaviour could occur after an initial stimulus: delay of a spike, no spike (spike failure), stimulus dependent afterdischarge and spontaneous spiking. This behaviour can be explained in terms of the ratio between sodium conductance and the conductance for leakage charge. When leakage out of the neuron is too large due to demyelination this ratio becomes too small which results in spike failure. Increasing this ratio can lead to the other aforementioned behaviours. Failure of spike activity could be responsible for our observed lowering of the frequency of oscillatory activity. Unfortunately, it is still not fully understood how spike observations relate to

post synaptic activity observations (main source of LFP/EEG/MEG), therefore future studies are warranted to verify this possible explanation.

The present study has some limitations. Sample size of our study was limited which hampered analysis of medication and gender effects. Limited sample size was partially caused by exclusion of subjects due to inaccurate co-registration and artefacts in the raw data. Future studies will use improved co-registration procedures, as well as a sophisticated artefact removal approach (temporal extension of Signal Space Separation (tSSS) in order to address these issues (Gross et al., 2012; Taulu and Hari, 2009; Taulu and Simola, 2006; van Dellen et al., 2013). The present study had a cross-sectional design, and we therefore do not know if slowing of oscillatory activity is specific for short disease duration and is still present, or progresses, later on in the disease.

To conclude, slowing of alpha band oscillatory activity occurs in early MS. This seems to be of clinical relevance since these changes were related to information processing speed changes which is one of the first affected cognitive domains in MS. Future larger studies should verify the relation between changes in alpha power and information processing speed, and subsequently with structural changes as well.

Chapter 6

Cognitive and clinical dysfunction, altered MEG resting-state networks and thalamic atrophy in Multiple Sclerosis.

P. Tewarie, M.M. Schoonheim, C.J. Stam, M.L. van der Meer, B.W. van Dijk, F. Barkhof, C.H. Polman, A. Hillebrand

PLoS One. 2013 Jul 31;8(7):e69318

ABSTRACT

The relation between pathological findings and clinical and cognitive decline in Multiple Sclerosis remains unclear. Here, we tested the hypothesis that altered functional connectivity could provide a missing link between structural findings, such as thalamic atrophy and white matter lesion load, and clinical and cognitive dysfunction. Resting-state magnetoencephalography recordings from 21 MS patients and 17 gender- and age matched controls were projected onto atlas-based regions-of–interest using beamforming. Average functional connectivity was computed for each ROI and literature-based resting-state networks using the phase-lag index. Structural measures of whole brain and thalamic atrophy and lesion load were estimated from MRI scans. Global analyses showed lower functional connectivity in the alpha2 band and higher functional connectivity in the beta band in patients with Multiple Sclerosis. Additionally, alpha2 band functional connectivity was lower for the patients in two resting-state networks, namely the default mode network and the visual network. Higher beta band functional connectivity was found in the default mode network and in the temporo-parietal network. Lower alpha2 band functional connectivity in the visual network was related to lower thalamic volumes. Beta band functional connectivity correlated positively with disability scores, most prominently in the default mode network, and correlated negatively with cognitive performance in this network. These findings illustrate the relationship between thalamic atrophy, altered functional connectivity and clinical and cognitive dysfunction in MS, which could serve as a bridge to understand how neurodegeneration is associated with altered functional connectivity and subsequently clinical and cognitive decline.

INTRODUCTION

Multiple Sclerosis (MS) is an inflammatory demyelinating and neurodegenerative disease leading to clinical and cognitive decline to varying degree. Despite much progress in the MS field in recent years, the relation between pathological findings and clinical and cognitive decline remains unclear. The discrepancy between classical MRI findings such as white matter lesion load on the one hand and clinical decline on the other hand has been called the clinico-radiological paradox (Barkhof, 2002). To overcome this paradox the emphasis of research has shifted from white matter pathology to gray matter pathology (Filippi et al., 2012). Gray matter pathology such as atrophy and cortical lesions seem to correlate better with physical disability and cognitive impairment than white matter pathology [3,4]. Thalamic atrophy in particular seems to be present even in the earlier phases of the disease and is a strong predictor of cognitive decline (Audoin et al., 2010; Batista et al., 2012; Houtchens et al., 2007; Schoonheim et al., 2012b; Tao et al., 2009).

Other insights that may help to solve the clinico-radiological paradox may be gained by studying functional connectivity (FC). Functional MRI (fMRI) studies have revealed a link between altered FC and cognitive symptoms in MS (Cader et al., 2006; Hawellek et al., 2011; Helekar et al., 2010; Leavitt et al., 2012; Parisi et al., 2012). Both higher and lower FC has been observed in MS, where higher FC is often interpreted as a "compensatory mechanism" for structural deficits (Cader et al., 2006; Helekar et al., 2010). Alternatively, an higher FC could also be maladaptive and contribute to cognitive worsening (Hawellek et al., 2011), or excessive FC could simply be due to pathological disinhibition.

Additional insights may be gained by estimating FC in resting-state networks (RSNs). These RSNs are semi-independent networks that can be captured from the brain's activity during rest and in the absence of goal directed neural activity (Damoiseaux et al., 2006). One of these networks, the default mode network, may be of special interest here since seems to play a crucial role in cognitive decline in several disorders (Broyd et al., 2009; Hafkemeijer et al., 2012), including MS (Bonavita et al., 2011a; Hawellek et al., 2011; Rocca et al., 2010). In MS, higher FC has also been related to physical disability in other resting-state networks (RSNs), such as the frontoparietal network and the prefronto-insular network (Faivre et al., 2012).

Although fMRI is a powerful tool, its application has some drawbacks. These include its low temporal resolution and, despite progress in understanding the mechanisms that lead to the BOLD (Blood oxygen level dependent) signal, a not-entirely-understood relation with the underlying electrophysiology (Logothetis, 2008; Singh, 2012). Magnetoencephalography (MEG) and Electroencephalography (EEG) are direct measures of neuronal activity with high temporal resolution and thus provide complementary information to fMRI studies (Singh, 2012), and also allow for the investigation of specific RSNs (de Pasquale F. et al., 2012). Task activation MEG studies in MS have revealed lower FC, which has led to the interpretation of MS as a disconnection syndrome (Dell'Acqua et al., 2010; Tecchio et al., 2008). A relatively small resting-state MEG study found lower interhemispheric FC in the alpha band in MS patients with mild disability (Cover et al., 2006b). The

same group partly reproduced these findings but now higher FC in the theta, alpha1, and beta band was found as well (Schoonheim et al., 2011). Another study characterised the topology of the functional network as a whole, using a measure that quantifies the "hub-status" of an area (eigenvector centrality, or EC) (Hardmeier et al., 2012). Using MEG, lower EC over temporal regions in the alpha2 and beta band and higher EC in the theta band over parietal regions were found. Analyses in these studies were performed at the sensor-level, which are difficult to interpret and may suffer from problems with FC estimation due to field spread (Hillebrand et al., 2012; Peraza et al., 2012). Even approaches where sensor data is projected to source- space may suffer from widespread correlations between reconstructed source elements, leading to similar problems of overestimated FC (David et al., 2002; Hui et al., 2010). An atlas-based MEG beamformer approach in combination with an FC metric that is insensitive to the effects of field spread and volume conduction, i.e. the phase lag index (PLI), has the ability to overcome these problems (Hillebrand et al., 2012; Stam et al., 2007).

Here we used the atlas-based beamformer approach to investigate resting-state MEG FC in the whole brain and in literature based resting-state networks in relation to clinical and cognitive status, and in relation to whole brain- and thalamic atrophy.

METHODS

General study design

In this cross-sectional study, two independent groups, MS patients and healthy controls, underwent MEG, MRI, neurological examination and neuropsychological assessment on the same day. As outcome measures we used FC estimated from resting-state MEG data, whole brain-, gray matter- and thalamic volumes, clinical status and cognition. FC was assessed between atlas-based ROIs and in literature-based resting-state networks.

Participants

All subjects from a previous study were included (Schoonheim et al., 2011): 34 MS patients (mean age 41.4 ± 8.0 years, disease duration since the first symptom 8.1 ± 1.6 years) and 28 age- and gender matched controls (mean age 39.8 ± 10.5 years). In the present study a number of subjects were excluded due to various reasons: no MRI available (n=2), too many artefacts and noise in the raw MEG data (see below) (n=12) and inaccurate MEG/MRI co-registration (n=10). Consequently, 21 MS patients (mean age 41.9 ± 7.7, disease duration 6.8 ± 0.9 years) and 17 controls (mean age 39.8 ± 9.8) remained in the present study which were still gender- and age matched. All patients were diagnosed with clinically-definite multiple sclerosis (Polman et al., 2005), specifically the relapsing remitting form of MS (RRMS) (Lublin and Reingold, 1996). Patients were recruited from the VU University Medical Center. All patients were part of the six-year follow-up of an early inception cohort, in which patients were included at diagnosis and subsequently followed annually (Schoonheim et

al., 2012b). Physical disability was measured using the Expanded Disability Status Scale (EDSS) (Kurtzke, 1983) and found to be relatively mild (median 2, range 0-4.5). Eight patients received interferon treatment since diagnosis. One of these patients switched to glatimere acetate and two to natalizumab which they were receiving during the study. The study protocol was approved by the Local Research Ethics Committee (Medical Ethical Review Committee of VU University Medical Center), whose ethics review criteria conformed to the Helsinki declaration. All subjects had given written informed consent prior to participation.

All subjects underwent a set of neuropsychological tests as described earlier (Schoonheim et al., 2011). In summary, the brief repeatable battery for neurological disease (BRB-N), consisting of the selective reminding test (SRT), the 10/36 spatial recall test (SPART), the symbol digit modalities test (SDMT), the word list generation test (WLG), the concept shifting test (CST), the stroop color-word test and the memory comparison test (MCT) were administered. Z-scores were summarized into seven cognitive domains: executive functioning (CST, WLG), verbal memory (SRT), information processing speed (SDMT), visuospatial memory (SPART), working memory (MCT), attention (Stroop) and psychomotor speed (CST, SDMT). In addition a Z–score for overall cognition was calculated. This was overall cognition was calculated by averaging Z-scores of all seven cognitive domains and was used in further analyses (Schoonheim et al., 2012b).

Magnetic Resonance Imaging

An MRI scan was obtained from all subjects, using a 3T-MRI system (GE Signa HDXT V15m). A 2D dual-echo T2-weighted sequence (TR 9680 ms, TE 22/112 ms) and T1-weighted sequence (TR 475 ms, TE 9 ms) were obtained with 48 slices of 3 mm and 3D-T1 heavily T1-weighted sequence (FSPGR , TR 7.8 ms, TE 3.0 ms, TI 450 ms) with 1 mm, slices covering the entire brain. All scans were inspected by an experienced rater (MMS). Subsequently, lesion volumes were quantified. All lesion volumetric analyses were performed using Alice (Perceptive informatics Inc.) applying a local thresholding technique. Total gray matter (NGMV), total white matter (NWMV), and whole brain volumes (NBV), corrected for head size, were measured using the FSPGR images and SIENAX (Smith et al., 2002) version 2.5 (part of FSL 4.1, FMRIB's Software Library, http://www.fmrib.ox.ac.uk/fsl). Thalamic volumes were measured using FIRST (part of FSL), providing left and right volumes for the thalamus and were corrected for head size. Left and right thalamic volumes were summed to give the total thalamic volume.

Magnetoencephalography

MEG data were recorded using a 151-channel whole-head MEG system (CTF systems; Port Coquitlam, BC, Canada) while participants were in a supine position in a magnetically shielded room (Vacuumschmelze, Hanau, Germany). A third-order software gradient (Schoonheim et al., 2012b; Vrba J, 1999) was used with a recording passband of 0–150 Hz and a sample frequency of 625 Hz. Participants had to be free of any metal objects. Magnetic fields were recorded during a no-task,

eyes-open condition for three minutes and eyes-closed condition for five consecutive minutes. At the beginning and end of each recording, the head position relative to the coordinate system of the helmet was determined by leading small alternating currents through three head position coils attached to the left and right pre-auricular points and the nasion. Changes in head position of <0.5 cm during a recording condition were accepted. Each original dataset consisted of a continuous resting-state recording from which artefact-free segments were subsequently selected for further analysis. Each segment or epoch had a duration of 6.555 seconds (total no. of segments or epochs was 45). Channels and epochs were visually inspected. Epochs and channels were rejected based on system related artefacts (SQUID jumps, noisy, broken or saturated channels), physiological artefacts (eye movements, eye blinks, muscle artefacts), external artefacts (magnetized dental fillings) and environmental noise (PT, AH) (Gross et al., 2012), as well as for representing an alert eyes-closed state. A minimum of 25 eyes-closed epochs was considered sufficient (Brookes et al., 2008) for further beamformer analysis. On average 5.7 channels (range: 2-14) and 8.4 epochs (range 3-20) were discarded.

Beamforming: time-series estimation for regions-of-interest

The technique used in this study was recently described (Hillebrand et al., 2012). A brief overview is given below. First, a subject's MRI was co-registered with the MEG data through identification of the same anatomical landmarks in the MRI that were also used for the placement of the MEG head-localization coils (i.e. left and right pre-auriculars and nasion). Only data from subjects where the estimated co-registration error was smaller than 0.8 cm were accepted for further analysis. The co-registered MRI was then spatially non-linearly registered (normalized) to a template MRI using the SEG-toolbox in SPM8 (Friston et al., 2004). The new segmentation toolbox is an extension of the unified segmentation algorithm, which incorporates additional tissue priors for improved matching of the subject's MRI to the template [36,37]. The AAL atlas was used to label the voxels in a subject's normalized co-registered MRI (Tzourio-Mazoyer et al., 2002). Subcortical structures were removed, and the voxels in the remaining 78 cortical regions of interest (ROIs) were used for further analysis (Gong et al., 2009), after inverse transformation to the patient's co-registered MRI.

Neuronal activity for the labeled voxels in the ROIs was reconstructed using a beamforming approach known as Synthetic Aperture Magnetometry (SAM) (Robinson and Vrba, 1999). SAM works in a sequential fashion, where the activity for each voxel is reconstructed by selectively weighting the contribution from each MEG sensor to a voxel's time-series. This weighting is done such that the activity at a voxel is reconstructed without distortion, and at the same time the contribution from external (noise) sources is minimized (Hillebrand et al., 2005; Hillebrand and Barnes, 2005). The beamformer weights are based on the covariance of the data and the forward solution (lead field) of a dipolar source at the voxel location, where data were band-pass filtered from 0.5-48 Hz. A time-window of, on average, 238 seconds (range: 164-282 sec.) was used for the computation of the data covariance matrix. We used broadband data for the estimation of the beamformer weights, as this

avoids overestimation of covariance between channels (Barnes and Hillebrand, 2003). The sensor-level data were subsequently projected through the beamformer weights, resulting in a time-series for each voxel. Each ROI contains many voxels and the number of voxels per ROI differed. In order to represent a ROI by a single time-series, we selected, for each ROI and frequency band separately, the voxel with maximum power in that frequency band (Hillebrand et al., 2012). The time-series for this voxel was used for further analysis, resulting in a total of 6 sets of 78 time-series (one for each frequency band, using six classic frequency bands: delta (0.5-4 Hz), theta (4-8 Hz), alpha1 (8-10 Hz), alpha2 (10-13Hz), beta (13-30 Hz), and gamma (30-48 Hz)). As in our previous studies we selected the first five artifact-free epochs of 4096 samples (6.555 seconds) from these time-series, based on careful visual inspection (PT) to obtain stable results (Bartolomei et al., 2006; Bosma et al., 2008; Douw et al., 2008; Douw et al., 2009; Douw et al., 2010; Schoonheim et al., 2011; Stam et al., 2006b; Stam et al., 2009; van Dellen et al., 2013).

BrainWave software packing was used for this purpose and also for further analyses (version 0.9.58 available from http://home.kpn.nl/stam7883/brainwave.html).

Functional Connectivity analysis

As a measure of FC, the phase lag index (PLI) was used (Stam et al., 2007), which calculates the asymmetry of the distribution of (instantaneous) phase differences between two time-series:

$$PLI = |< sign[\sin(\Delta\varphi(t_k))] >| . \quad (1)$$

Here the phase difference is defined in the interval $[-\pi, \pi]$, $< >$ denotes the mean value, sign stands for signum function and ffIffI indicates the absolute value. The PLI ranges between 0 (completely symmetric phase distribution) and 1 (completely asymmetric phase distribution). The rationale behind this approach is that field spread/volume conduction causes a zero phase lag between two time-series, and that a uniform distribution of phases occurs when there is no coupling at all. The presence of a consistent, non-zero, phase lag between two time-series therefore reflects true interactions that are unaffected by field spread/volume conduction or common sources (Stam et al., 2007). Recent findings suggest that this method is capable of removing spurious coupling between ROIs at the expense of discarding any physiological interactions with zero lag (Hillebrand et al., 2012).

The mean PLI over 5 epochs for every patient was computed for all ROIs, i.e. the full 78x78 adjacency matrix was estimated. All row elements in this adjacency matrix were averaged yielding 78 PLI values, one for each ROI. This is a measure of the overall connectivity of a region with all other regions (in the language of graph theory: weighted degree or node strength). Subsequently, these 78 mean PLI values were averaged in order to obtain one mean (whole brain) PLI for each subject. In addition, the mean PLI between ROIs within literature-based resting-state networks (RSN) was estimated for each subject. The rationale for this latter approach was that i) previous work (Bonavita et al., 2011b; Rocca et al., 2012) has demonstrated that the integrity of RSNs is of importance for

cognitive performance, and ii) one of our aims was to link altered functional connectivity in MS to cognitive performance. If A_{ij} is an element in the adjacency matrix for the RSN, then the mean PLI within a RSN that contains N ROIs is defined as:

$$<PLI>_{rsn} = \frac{2}{N(N-1)} \sum_{i,j}^{N} A_{ij} \text{ , with } i \neq j, i > j \quad (2)$$

Here i are row indices and j are column indices. Indices i and j denote the ROIs involved within the RSN of interest. Thus only PLI values in the adjacency matrix corresponding to connections between ROIs *within* a RSN were included for calculation of $<PLI>_{rsn}$. The selection of RSNs and the ROIs selected for specific RSNs were based on a review paper (Rosazza and Minati, 2011). For our analysis we included the default mode network (DMN), left and right fronto-parietal network (FPN), the executive function network, the sensorimotor network, the temporo-parietal network and the visual network (Table S1). We applied the rationale that connections within RSNs should be unique, and therefore made two modifications to the definition of the RSNs from the review (Rosazza and Minati, 2011): the precuneus was substituted with the superior parietal gyrus in the FPN (van den Heuvel and Hulshoff Pol, 2010), and the inferior frontal gyrus was split into two parts, where inferior frontal gyrus pars operculis was assigned to the temporo-parietal network and inferior frontal gyrus pars triangularis was assigned to the FPN [56,57].

Statistical analysis

Firstly, mean whole brain PLI values were compared between groups with Mann-Whitney tests. Subsequently, as post-hoc analysis, mean PLI values per ROI were compared between groups by means of permutation analysis (Nichols and Holmes, 2002), where a null distribution for between-group differences (independent t-test) is derived by permuting group assignment and calculating a t-statistic after each permutation. If mean whole brain PLI values significantly differed between MS patients and healthy controls, as another post-hoc analyses, we used Mann-Whitney tests to determine whether there were differences in mean PLI values of RSNs ($<PLI>_{rsn}$) between MS patients and healthy controls.

MRI atrophy parameters were compared between MS patients and healthy controls with independent t-tests and in absence of normality with the Mann-Whitney test. Normality was checked using histogram inspection and Kolmogorov-Smirnov tests of normality. Whenever the mean PLI or $<PLI>_{rsn}$ was significantly different between MS patients and controls, correlations between these PLI values and cognition, EDSS, lesion load and MRI atrophy parameters were calculated using non parametric spearman's coefficients in the MS group and control group separately (Rousselet and Pernet, 2012). After correlation analyses and in case of normality, multiple regression analyses were used to determine if the association between volumes and PLI values were different between MS patients and controls. In these analyses volumes were regarded as effect modifiers and PLI values as outcome measures. These statistical analyses were performed using SPSS for windows v.18.

Table1: Descriptive variables for controls and patients

	Controls (N=17)			Patients (N=21)			p value
	Mean	±	SD	Mean	±	SD	
Age	39.8	±	9.8	41.9	±	7.7	0.49
Education(1-7)	5.9	±	1.36	5.4	±	1.33	0.52
Disease Duration				6.8	±	0.9	-
NGMV (l)	0.84	±	0.05	0.81	±	0.04	0.037*
NWMV[a] (l)	0.69	±	0.03	0.66	±	0.03	-
NBV (l)	1.53	±	0.07	1.47	±	0.05	0.006*
Total thalamic volume	0.021	±	0.001	0.019	±	0.002	0.004*
Cognition	0.04	±	0.64	-0.19	±	0.84	0.36
EDSS (1-10)[b]				2		(0-4.5)	-
T1 lesion load (mL)				1.05	±	0.81	-
T2 lesion load (mL)				2.48	±	2.03	-

NGMV, normalized gray matter volume; NWMV, normalized white matter volume; NBV, normalized brain volume; EDSS, expanded disability status scale.[a] NWMV was not used for further analyses: lesion filling was not performed and therefore NWMV was not reliably estimated. [b] indicates median and range.* indicates significant differences between the two groups.

RESULTS

Characteristics of MS patients and healthy controls are listed in Table 1.

MRI: Atrophy measures

NBV and NGMV were significantly lower in the patient group (independent t-tests $t(36) = -3.0$, $p = 0.006$, $t(36) = -2.2$, $p = 0.037$, respectively) (Table 1). Mann-Whitney test revealed significantly lower total thalamic volumes ($U(36) = 75.0$, $p = 0.004$) in MS patients compared to healthy controls.

Functional connectivity: ROI analysis

For each frequency band separately, mean (whole brain) PLI values were compared between MS patients and controls. Mean (whole brain) PLI was lower in the alpha2 ($U(36) = 89.0$, $p = 0.008$) and higher in the beta band ($U(36) = 94.0$, $p = 0.012$) in MS patients. Post-hoc analyses were performed in order to find out which ROIs were causing the global effect, which revealed significantly lower PLI values in 40 ROIs for the alpha2 band in MS patients (Figure 1 and see Table S2 for AAL regions), whereas in the beta band PLI values in 16 ROIS were significantly higher in MS patients (Figure 2 and see Table S2 for AAL regions).

Only mean (whole brain) beta PLI and EDSS correlated positively ($r(19) = 0.47$, $p = 0.031$) in MS patients. There were no correlations between whole brain PLI and T1-, T2 lesion load or atrophy measures.

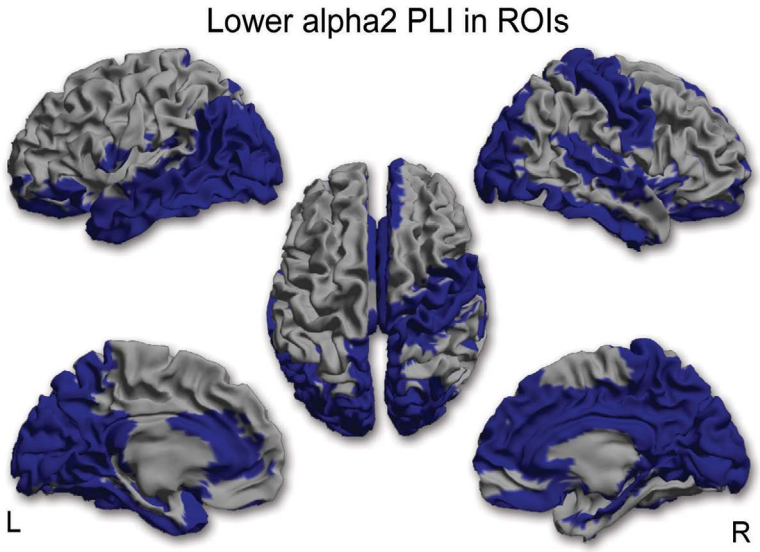

Figure 1: ROI analysis in the alpha2 band. In 40 ROIs corresponding PLI values in the alpha2 band were significantly lower in MS patients compared to healthy controls. This lower functional connectivity in the alpha2 band occurred in occipital, temporal, medial-parietal and medial frontal regions (L=left hemisphere, R=right hemisphere).

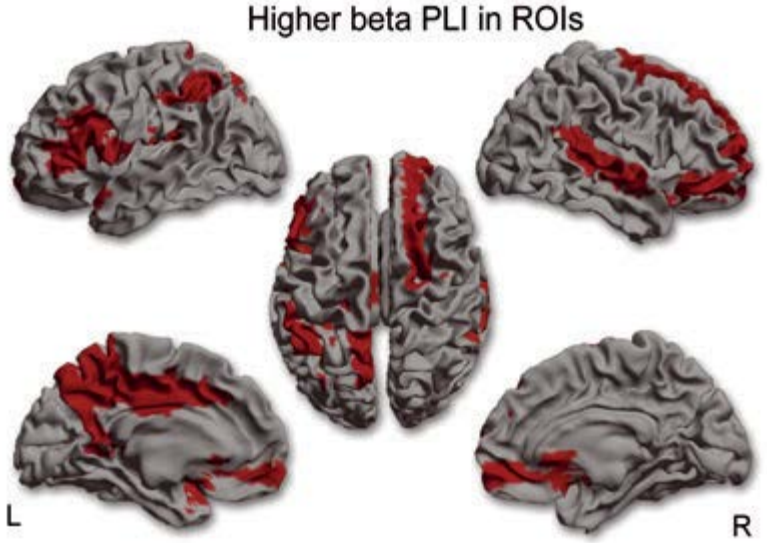

Figure 2: ROI analysis in the beta band. In 18 ROIs corresponding PLI values in the beta band were significantly higher in MS patients compared to healthy controls. This higher functional connectivity in the beta band occurred mainly in fronto-parietal and temporal regions (L=left hemisphere, R=right hemisphere).

Functional connectivity: resting-state networks

If mean (whole brain) PLI values differed in a specific frequency band between MS patients and healthy controls we calculated for each RSN the mean PLI within the network ($<PLI>_{rsn}$) and compared these between MS patients and controls (see method section and (Rosazza and Minati, 2011) for definition of RSNs). Correlations with EDSS, cognition, T1-,T2 lesion load, thalamic volumes and global measures of atrophy were only computed when there were significant group differences for $<PLI>_{rsn}$ in that frequency band.

In the alpha2 band two RSNs showed a significantly lower PLI value in MS patients: the DMN ($U(36) = 71.0$, $p=0.001$) (Figure 3a) and the visual network ($U(36) = 92$ $p=0.01$) (Figure 3b). The PLI value in the visual network in MS patients correlated positively with total thalamic volume ($r(19) = 0.58$, $p = 0.006$) (Figure 3c and Table 2). After discarding outliers this relation remained significant ($r(19) = 0.7$ $p = 0.001$). In the control group a positive, yet non-significant, correlation between total thalamic volume and PLI within the visual network was found as well.

Higher beta PLI values were found in the DMN ($U(36) = 93$, $p=0.012$) (Figure 4a) and the temporo-parietal network in MS patients ($U(36) = 106$, $p=0.033$) (Figure 4c). In the control group a negative correlation was found between beta band PLI in the temporo-parietal network and total thalamic volume ($r(15) = -0.73$ $p = 0.001$) (Figure 4d), NGMV ($r(15) = -0.52$ $p = 0.040$), and NBV ($r(15) = -0.74$ $p = 0.001$). In contrast, for the MS patient group, positive, yet non-significant, correlations were found between resting-state network beta band PLI and volumetric measures. Multiple regression analyses for the temporo-parietal network revealed that total thalamic volume had a significant different effect on beta PLI between MS patients and controls: Total thalamic volume in healthy controls was negatively associated with beta PLI within the temporo-parietal network ($B = -2.8x10^{-6}$, standardized $\beta = -0.7$, $p = 0.002$) whereas total thalamic volume was positively, yet non significantly associated with beta PLI within the temporo-parietal network ($B = 1.5x10^{-7}$, standardized $\beta = 0.05$, $p = 0.8$). No correlations were found between $<PLI>_{rsn}$ of any RSN and T1-, T2 lesion load.

For every RSN for which there was a significant group difference in $<PLI>_{rsn}$, correlations with EDSS and cognition were calculated. Significant correlations were only found in the DMN: beta PLI within this network correlated positively with EDSS ($r(19) = 0.57$ $p = 0.007$) and showed a negative correlation with cognition ($r(19) = 0.47$ $p = 0.031$) (Figure 4b). The correlation between cognition and beta PLI remained significant ($r(19) = -0.45$ $p = 0.043$) after discarding outliers. There were no significant correlations between EDSS, age, education, cognition and T1-, T2 lesion load, NBV, or NWMV.

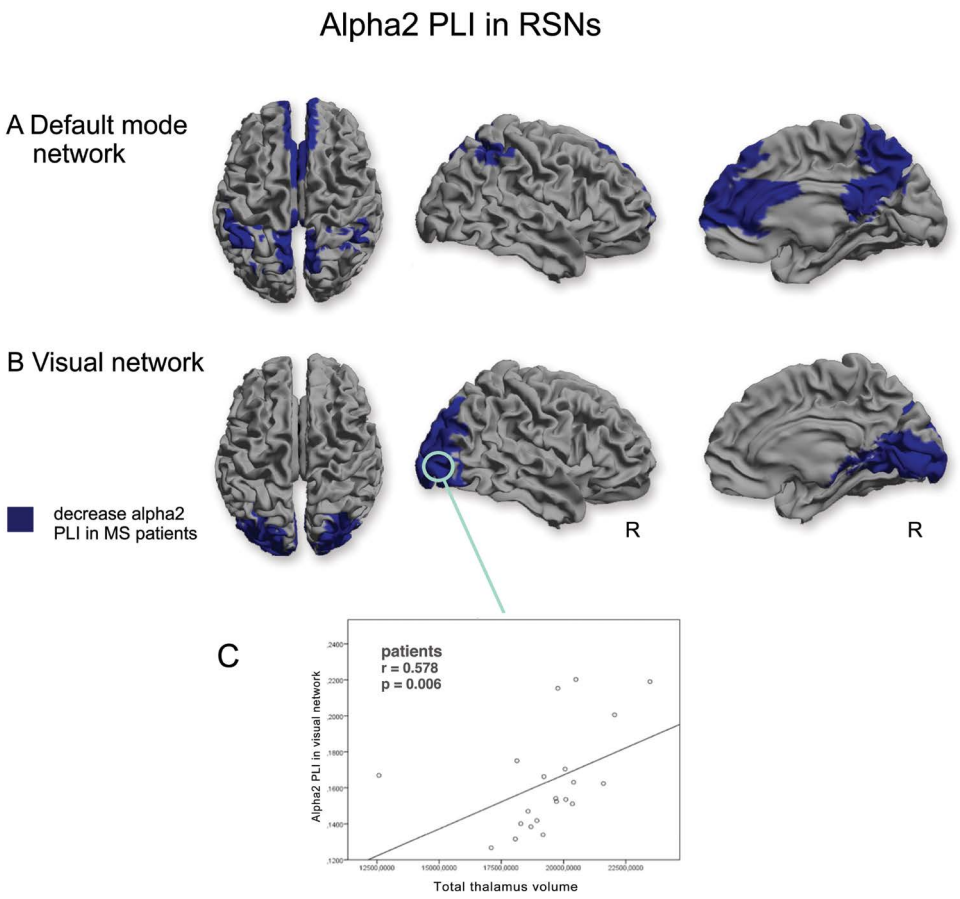

Figure 3: RSN analysis in the alpha2 band. Lower PLI values in the alpha2 band were found in the default mode network (a) and the visual network (b). Spearman correlation analysis in MS patients revealed a positive correlation between alpha2 PLI values in the visual network and thalamic volumes. (R=right hemisphere). Correlations are shown with (blue) and without (red) outlier (red dot).

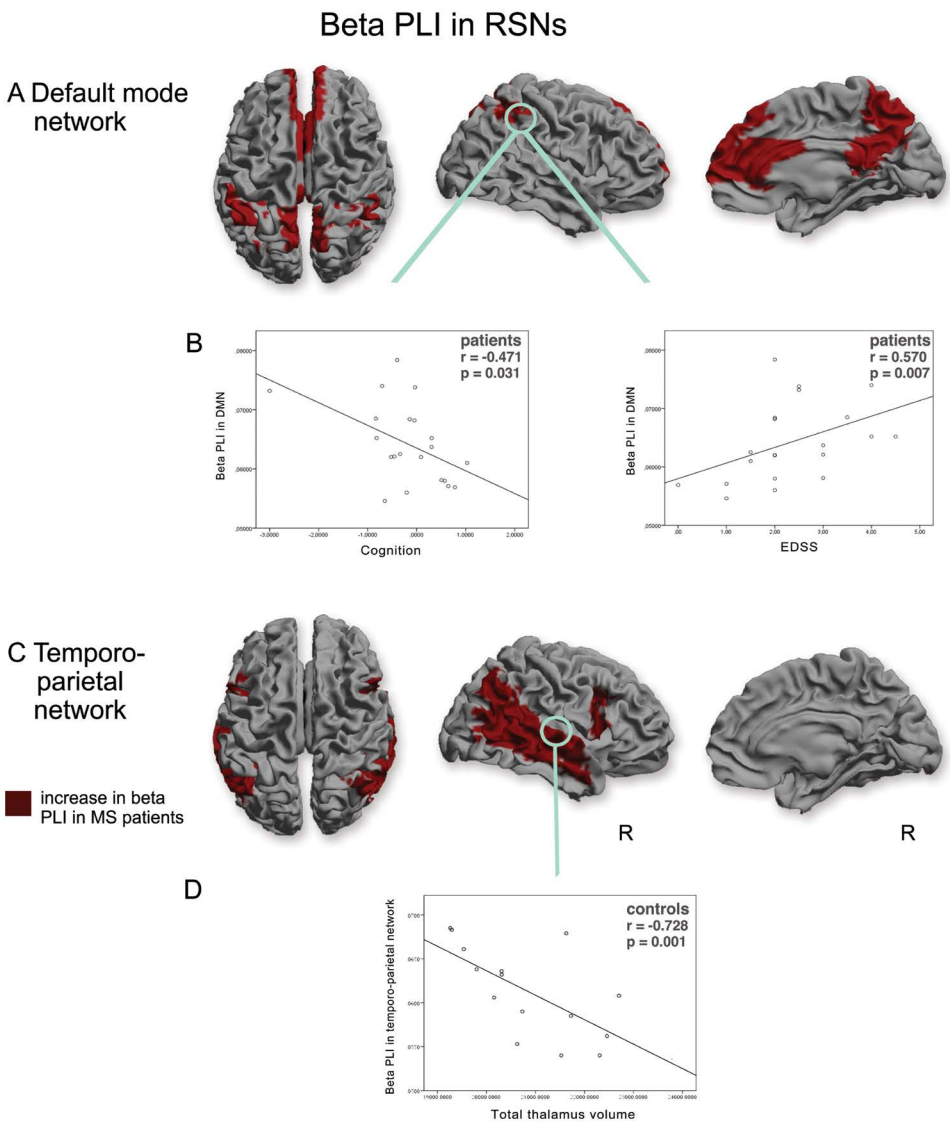

Figure 4: RSN analysis in the beta band. Higher PLI values in the beta band were found in the default mode network (a) and the temporoparietal network (c). Beta band PLI values in the default mode network correlated positively with physical disability (EDSS) and negatively with cognition in MS patients (b). Beta band PLI values in the temporoparietal network correlated negatively with thalamic volumes in healthy controls (d) but not in MS patients. (R=right hemisphere). Correlations are shown with (blue) and without (red) outlier (red dot).

DISCUSSION

We used an atlas-based MEG beamformer approach to assess FC changes in early MS in relation to cognitive and clinical dysfunction, and in relation to MRI-based measures of structural integrity such as whole brain-, thalamic atrophy and lesion load. We observed the following changes: Firstly, whole brain FC analyses revealed lower FC in the alpha2 band and higher FC in the beta band in MS patients. Secondly, RSN analyses in MS patients revealed lower FC in the alpha2 band in two RSNs, the DMN and the visual processing network, and higher FC in the beta band in two RSNs, the DMN and the temporo-parietal network. Thirdly, changes in whole brain, and more specifically thalamic atrophy was related to altered FC in the visual network and the temporo-parietal network in respectively the alpha2 and beta band. Finally, most strikingly and clinically relevant was the observed correlation between higher beta band FC in the DMN and higher EDSS scores and poorer cognition.

Whole-brain FC was lower in the alpha2 and higher in the beta band for the MS patients. Both these rhythms are involved in top-down processing of rhythmic activity which is important for the integration of information in the cortex (Engel et al., 2001; Palva and Palva, 2007). Lower FC in the alpha2 band occurred in occipital, temporal, medial-parietal and medial-frontal regions. Higher FC in the beta band occurred mainly in fronto-parietal and temporal regions. In some regions, such as the right superior temporal gyrus and the precuneus, there was both higher FC in the beta band and lower FC in the alpha2 band. An explanation for this observation of a simultaneous change in different frequency bands could be that different sub-populations within a region (i.e. beyond the resolution of our approach) are involved in the generation of the different rhythms. Alternatively, we know from pharmacological MEG/EEG studies that increased inhibitory activity may lead to increased amplitude for beta oscillations and simultaneous decreased amplitude for alpha oscillations (Jensen et al., 2005; Liley et al., 2003). Additionally, previous MEG/EEG studies in healthy controls revealed that cross-frequency phase synchrony between alpha and beta rhythms does appear in mainly parietal-occipital areas (Nikulin and Brismar, 2006; Palva et al., 2005). Furthermore its has been suggested that cross-frequency phase synchrony could reflect coordination between different functional networks (Nikulin and Brismar, 2006). This is an important notion since our findings point out that the precuneus, an important hub region that is part of the DMN, displays both higher and lower FC in respectively the beta and alpha2 band. These interactions between frequency bands are therefore very interesting and possibly clinically important and warrant future exploration using cross-frequency phase synchrony analysis.

Previous MEG studies in early MS patients have also reported lower FC in the alpha (Cover et al., 2006b) and alpha2 band (Schoonheim et al., 2011), as well as higher FC in the beta band (Schoonheim et al., 2011). However, the latter study reported in addition higher FC in the theta and alpha1 band as well, using partially the same (but larger) patient group as used in the present study. The differences between this previous study and ours could possibly be explained by factors such as analysis level (sensor-space versus source-space), a different parcellation (sensor-

groups versus atlas-based ROIs), a different FC metric (synchronization likelihood versus PLI), and therefore different sensitivity to spurious estimates of FC. An earlier EEG study in progressive MS patients found similarly a lower FC in the alpha band but also lower FC in the theta band (Leocani et al., 2000). As the study used progressive MS patients with higher disability scores and longer disease duration, it is difficult to compare these results. Indeed, it has been hypothesized that at different stages of the disease different patterns of functional reorganization occur (Schoonheim et al., 2010). Moreover, the aforementioned EEG study used coherence as a FC metric, which is sensitive to the amplitude of the timeseries (Leocani et al., 2000; Peraza et al., 2012) and therefore to the effects of field spread/volume conduction.

In addition to group differences between whole brain average connectivity, we also found prominent differences for specific resting-state networks, and these differences correlated with structural measures and clinical and cognitive status. MS patients showed changes in the DMN, where, compared to the controls, both lower FC in the alpha2 band and higher FC in the beta band was seen. Both lower and higher FC in the DMN have been reported previously in an fMRI study in relatively late MS, with the anterior cingulate gyrus displaying lower FC, and the posterior cingulate gyrus showing lower FC in the core and higher FC at the periphery (Bonavita et al., 2011a). Another study that included relatively late MS patients found lower FC in the DMN (Rocca et al., 2012). Interestingly, in this latter study interactions between RSNs were analysed as well, which revealed lower FC between the DMN and the executive control network in MS patients. In our study, higher and lower FC in respectively the beta and alpha2 band in the DMN, as well as in other RSNs, could imply that these FC changes are linked between different RSNs, or between frequency bands within a single RSN. However interpreting this simultaneous higher and lower FC as a compensatory mechanism requires additional (longitudinal) data, and warrants caution at this time.

Apart from FC changes in the DMN, lower alpha2 FC in the visual network and higher beta FC in the temporo-parietal network were observed in MS patients. This is in partial agreement with recent fMRI studies that also reported lower FC in the visual network in MS (Gallo et al., 2012; Rocca et al., 2012). In our study altered FC in RSNs was only found in the alpha2 and beta band, which seems to be in line with results from a MEG study in healthy controls where they described that RSNs could be recovered from MEG recordings, especially in the alpha and beta band, and that these RSNs showed similar segregated topography as in fMRI (de Pasquale F. et al., 2012).

An interesting finding in the present study is the relation between FC changes in RSNs and thalamic atrophy in MS, due to the ubiquitous connectivity of the thalamus with other regions throughout the brain. It has been reported previously that the thalamus is involved in many RSNs, including the DMN, sensorimotor network, visual network and the fronto-temporal network (De Luca M. et al., 2006; Mantini et al., 2007). Patients in the early phases of RRMS already show thalamic atrophy, as was also observed in this study. Importantly, we found correlations between thalamic atrophy and alpha2 band FC in the visual network in MS patients. Furthermore the effect of thalamic volume on beta FC in the temporo-parietal network was significantly different between MS patient

and controls, again indicating an important role for the thalamus in relation to altered resting-state FC. Our observed association between thalamic atrophy and altered alpha band resting-state FC seems to be in agreement with the well-known role of the thalamus as co-generator of global alpha rhythms, and to a lesser extent of the beta rhythm in physiological conditions [67-71]. The exact neurophysiological and histopathological mechanisms that link altered FC and thalamic changes require further investigation, but could possibly relate to altered expression of cortico-thalamic metabotropic glutamate receptors in subcortical white matter in MS, as these are involved in generation of alpha rhythms (Geurts et al., 2003; Hughes and Crunelli, 2005), a disbalance between inhibitory and excitatory neurons within the thalamus due to damaged interneurons in this structure in MS (Bo, 2009), alterations to parallel feedforward cortico-thalamo-cortical routes (Sherman, 2007), or even vice versa: altered FC may lead to thalamic atrophy.

Two important clinically relevant findings from our study were the observed positive correlation between beta band FC in the DMN with physical disability (EDSS) and the negative correlation with cognition. Or, in other words, higher FC in the beta band is associated with a poorer clinical status, both regarding disability and cognition. It has been hypothesized that increases in beta band oscillations are associated with maintaining the present cognitive or sensorimotor status (Engel and Fries, 2010). In the same way the authors predict that pathological enhancement of beta band synchrony is associated with a loss in flexibility of sensorimotor and cognitive processing. It has also been predicted that enhancement of beta band synchrony would predominantly occur in RSNs, as the default mode of the brain constitutes a state which seems to be distinguished by low expectation of ensuing change in the sensorimotor set (Engel and Fries, 2010). Our findings seem to fit to both these predictions. A negative relationship between FC and cognition has also been found in an fMRI study (Hawellek et al., 2011), and these authors have suggested that a higher FC might be maladaptive and contribute to worsening of cognitive functions. In a computational study on Alzheimer's disease it has been shown that higher FC could reflect pathological disinhibition of cortical networks (de Haan W. et al., 2012a). This mechanism could be a general common pathway in some stage of neurological diseases leading to higher FC. Taken together it seems questionable whether higher FC is always a compensatory mechanism to maintain cognitive abilities (Schoonheim et al., 2010). Model studies, using e.g. neural mass models, could help to clarify possible mechanisms of our observed increased FC in the beta band, combined with larger experimental and longitudinal patient studies.

When performing whole brain analyses, we only observed a weak correlation between mean beta PLI and EDSS, whereas stronger correlations were observed between beta PLI in the DMN and clinical parameters.-Studying RSN FC with MEG seems therefore to have an advantage over whole-brain analyses. We expected to find a relation between FC in the sensorimotor network and physical disability, but this was not found. It is important to note that in this study there was no association between clinical parameters and volumetric MRI measures or lesion load. The observed relation

between physical disability and FC within the DMN is difficult to interpret. Only one previous study has revealed a relationship between physical disability and altered FC in the DMN (Rocca et al., 2012). As the DMN seems to have such a central and vital role in the brain, it is considerable that damage to this network has an effect on many functions beyond cognition. If future studies are able to verify that physical disability is associated with higher FC in the beta band in the DMN, this may provide an objective assessment of clinical disability.

Table 2: Correlations between functional connectivity within resting state networks and volumetric MRI measures in MS patients.

	Spearman correlation coefficients							
	DMN alpha2		DMN beta		Temporo-parietal network beta		Visual network alpha2	
	R	p value	R	p value	R	p value	R	p value
NGMV	0.31	0.18	-0.13	0.58	-0.26	0.25	0.34	0.13
NBV	0.15	0.52	0.03	0.99	-0.024	0.92	0.42	0.059
Total thalamic volume	0.11	0.62	0.18	0.43	0.14	0.53	**0.58**	**0.006**

NGMV, normalized gray matter volume; NBV, normalized brain volume; NWMV, normalized white matter volume (NWMV was not used for further analyses since lesion filling had not performed and therefore NWMV was not reliably estimated); DMN alpha2, FC within the default mode network in the alpha2 band; DMN beta, FC within the default mode network in the beta band; temporo-parietal network beta, FC within the temporo-parietal network in the beta band; visual network alpha2, FC within the visual network in the alpha2 band.

Methodological considerations

RSN analyses of resting-state MEG source-space data is a relatively new approach. In our study regions attributed to each RSN were based on previous fMRI literature (Rosazza and Minati, 2011; van den Heuvel and Hulshoff Pol, 2010) and RSNs we used are known to be highly robust, especially the DMN (Rosazza and Minati, 2011; van den Heuvel and Hulshoff Pol, 2010). Previous MEG beamforming studies using amplitude correlations revealed that MEG RSNs obtained after independent component analysis show strong overlap with fMRI obtained RSNs (Brookes et al., 2011b; de Pasquale F. et al., 2012; Hipp et al., 2012). In contrast to these studies we used the PLI to quantify functional interactions between brain regions. The relation between amplitude correlation analyses (after application of an orthogonalisation step to remove spurious correlations) and phase synchronization methods has already been studied through simulations (Hipp et al., 2012). Importantly, the amplitude correlation between two signals was monotonically related to the magnitude of the phase difference between the carrier oscillations. This means that amplitude correlations could be less sensitive in picking up relations between two time series with small phase differences. In contrast, even when phase differences are small yet consistent, the PLI will capture such interactions. Moreover, PLI does not mix information about the magnitude of phase differences and the consistency of phase differences, enhancing the interpretability of observed interactions. Despite these differences the occurrences of spatial patterns obtained with both

methods were largely overlapping. It remains an open, yet interesting, question how these different approaches relate in experimental data. Many more metrics of functional connectivity are available (Pereda et al., 2005), yet the majority of these are sensitive to the effects of field spread and volume conduction. As mentioned above, novel approaches have been described to remove these biases before performing functional connectivity analyses (Brookes et al., 2012a; Hipp et al., 2012). However, perhaps a more convenient approach is to use metrics that are inherently insensitive to these biases, such as the PLI or phase slope index (Nolte et al., 2008).

The present study has some limitations. First of all, fMRI studies have previously revealed regional connectivity changes within the DMN in MS (Bonavita et al., 2011a; Rocca et al., 2010). In this first exploratory MEG study, such detailed regional differences were not studied yet. Secondly, the number of included subjects here was limited, possibly masking further MS-induced effects due to issues of statistical power. This also hampered the study of medication and gender effects. In addition, in such small datasets outliers could have a larger influence in the statistical outcome such as correlation or regression coefficients, although in the present study, removing outliers did not lead to significantly different results. Limited sample size was partially caused by exclusion of subjects due to sub-optimal MEG/MRI co-registration procedures and artefacts in the raw data. Future studies will use improved co-registration procedures (van Dellen et al., 2013), as well as a sophisticated artefact removal approach (temporal extension of Signal Space Separation (tSSS) (Taulu and Hari, 2009; Taulu and Simola, 2006), in order to address these issues (Gross et al., 2012). Thirdly, in this study RSN and regional FC were considered as post-hoc analyses after a main effect of disease had been found for a particular frequency band. Although it can be argued that such an explorative approach is justified, future studies are necessary to confirm our results, using an independent study sample in a hypothesis-driven study design that uses a more stringent statistical approach to the issue of multiple testing. Finally, the applied FC metric, PLI, is not influenced by power of the time series directly. However like any other FC metric, the PLI is influenced by the signal to noise ratio of the time series, and therefore indirectly depends on power (Muthukumaraswamy and Singh, 2011). Importantly though, the correlations between PLI and clinical parameters that we observed in this study, were not found for measures of relative power in the same data (Meer et al., 2012).

To conclude, changes in resting-state functional connectivity in MS were shown to be linked to neurodegenerative changes, as well as to clinical and cognitive status. This exploratory study could serve as a bridge to understand the effect of thalamic atrophy on clinical and cognitive status through altered functional connectivity, although future longitudinal studies are required. Moreover, the assessment of clinical and cognitive status is difficult, but our results suggest that the frequency-specific functional connectivity within MEG resting-state networks could be used as new imaging-based biomarkers, which future studies using other cohorts now need to validate.

Table S1: Literature based RSNs: ROIs that were included in each resting-state network are listed. All RSNs consist of a unique selection of connections between ROIs in the AAL atlas.

Resting-state networks	Selection of ROIs in the AAL atlas
Auditory component	Superior temporal gyrus, heschl's gyrus, insula, postcentral gyrus
Default mode	Precuneus, posterior en anterior cingulate, inferior parietal gyrus, mesial prefrontal gyrus
Executive control	Medial frontal cortex, superior frontal gyrus, anterior cingulate
Frontoparietal (left/right)	inferior frontal gyrus pars triangularis, medial frontal gyrus, inferior parietal gyrus, superior parietal gyrus, angular gyrus
Sensorimotor	Precentral gyrus, postcentral gyrus, supplementary motor area
Temporo-parietal component	Inferior frontal gyrus pars operculis, medial temporal gyrus, superior temporal gyrus, angular gyrus
Visual component	Occipital_superior gyrus, Occipital_middle gyrus, Occipital_inferior gyrus, Calcarine gyrus, Lingual gyrus

Table S2: Regions of interest involved in functional connectivity changes

Lower alpha2 PLI in AAL regions		Higher beta PLI in AAL regions	
AAL region	T-value	AAL region	T-value
Olfactory_L	-2.6774	Olfactory_L	2.2336
Frontal_Sup_Orb_L	-2.1146	Frontal_Med_Orb_L	2.1529
Frontal_Inf_Orb_L	-2.2027	Frontal_Inf_Oper_L	2.0662
Rolandic_Oper_L	-2.2.398	Frontal_Inf_Tri_L	2.2361
Angular_L	-2.2.125	Rolandic_Oper_L	2.5095
Precuneus_L	-2.9.361	Parietal_Inf_L	2.3601
Occipital_Sup_L	-2.4559	Precuneus_L	2.0316
Occipital_Mid_L	-3.1707	Temporal_Pole_Sup_L	2.7120
Occipital_Inf_L	-2.4853	ParaHippocampal_L	2.0580
Calcarine_L	-1.9677	Cingulum_Mid_L	2.2675
Cuneus_L	-2.2252	Olfactory_R	2.1059
Lingual_L	-2.8002	Frontal_Med_Orb_R	2.8213
Fusiform_L	-3.2080	Frontal_Mid_Orb_R	3.1585
Temporal_Mid_L	-2.1673	Frontal_Inf_Orb_R	2.4659
Temporal_Inf_L	-1.9901	Frontal_Sup_R	2.1315
Temporal_Pole_Sup_L	-2.8085	Temporal_Sup_R	3.2478
Temporal_Pole_Mid_L	-3.6363		
Cingulum_Ant_L	-3.2009		
Cingulum_Post_L	-1.9896		
Rectus_R	-2.1523		
Olfactory_R	-2.0510		
Frontal_Sup_Orb_R	-2.2997		
Frontal_Sup_Medial_R	-2.2092		
Paracentral_Lobule_R	-2.0748		

Table S2: Continued

Lower alpha2 PLI in AAL regions		Higher beta PLI in AAL regions
Precentral_R	-2.3587	
Postcentral_R	-2.4734	
Precuneus_R	-3.7711	
Occipital_Sup_R	-2.2529	
Occipital_Mid_R	-1.9866	
Occipital_Inf_R	-2.1812	
Calcarine_R	-3.1729	
Cuneus_R	-3.9377	
Lingual_R	-2.3646	
Temporal_Sup_R	-2.4536	
Temporal_Inf_R	-2.4031	
ParaHippocampal_R	-2.1725	
Cingulum_Ant_R	-2.4849	
Cingulum_Mid_R	-2.5664	
Cingulum_Post_R	-2.6684	
Insula_R	-2.1395	

In 40 ROIs, PLI values in the alpha2 band were significantly lower ($p<0.05$) in MS patients compared to controls, and in 16 ROIs in the beta band the values were significantly higher ($p<0.05$). PLI values mentioned here are the average of all PLI values between a ROI and all other ROIs in the network.

Chapter 7

Functional brain network analysis using minimum spanning trees in Multiple Sclerosis: an MEG source-space study.

P. Tewarie, A. Hillebrand, M.M. Schoonheim, B.W. van Dijk, J.J.G. Geurts, F. Barkhof, C.H. Polman, C.J. Stam

Neuroimage. 2014 Mar;88:308-18

ABSTRACT

Cognitive dysfunction in Multiple Sclerosis (MS) is closely related to altered functional brain network topology. Conventional network analyses to compare groups are hampered by differences in network size, density and suffer from normalization problems. We therefore computed the Minimum Spanning Tree (MST), a sub-graph of the original network, to counter these problems. We hypothesize that functional network changes analysed with MSTs are important for understanding cognitive changes in MS and that changes in MST topology also represent changes in the critical backbone of the original brain networks. Here, resting-state magnetoencephalography (MEG) recordings from 21 early MS patients and 17 age-, gender-, and education-matched controls were projected onto atlas-based regions-of-interest (ROIs) using beamforming. The phase lag index was applied to compute functional connectivity between regions, from which a graph and subsequently the MST was constructed. Results showed lower global integration in the alpha2 (10-13 Hz) and beta (13-30Hz) band in MS patients, whereas higher global integration was found in the theta band. Changes were most pronounced in the alpha2 band where a loss of hierarchical structure was observed, which was associated with poorer cognitive performance. Finally, the MST in MS patients as well as in healthy controls may represent the critical backbone of the original network. Together, these findings indicate that MST network analyses are able to detect network changes in MS patients, which may correspond to changes in the core of functional brain networks. Moreover, these changes, such as a loss of hierarchical structure, are related to cognitive performance in MS.

INTRODUCTION

Multiple Sclerosis (MS) is an inflammatory demyelinating and neurodegenerative disease leading to both physical disability and cognitive dysfunction. It is still not fully elucidated how cognitive dysfunction and physical disability result from demyelination and neurodegeneration, given the large clinical and radiological variability of the disease. The brain is a complex network and it is widely claimed that normal cognitive function as well as cognitive dysfunction in neurological diseases cannot be fully understood without proper knowledge of the brain's topology, i.e. the spatial organization of the network (Bullmore and Sporns, 2012; Stam and van Straaten, 2012). Therefore, analysing network topology in MS in relation to cognitive dysfunction and physical disability is highly relevant.

Graph theory provides a comprehensive and sophisticated framework to characterize network topology. By applying graph theory we have gained insight in how brain networks can display features of both integration and segregation of information processing, and how networks are organized to minimize economical costs and maximize efficiency (Bullmore and Sporns, 2012; Rubinov and Sporns, 2010; Stam and van Straaten, 2012; van Straaten and Stam, 2012). An optimal topology with local clustering and strategic long distance connections (i.e. short path length) has been called a small-world network (Watts and Strogatz, 1998). Moreover, brain networks are characterized by the presence of highly important nodes that lie central in the network's flow of information, i.e. hubs (Bullmore and Sporns, 2012).

Graph theoretical analyses applied to structural and functional networks in Relapsing Remitting MS (RRMS) are scarce (Hardmeier et al., 2012; Schoonheim et al., 2011; Schoonheim et al., 2012a; Shu et al., 2011). Previous MEG studies revealed that functional networks in early RRMS patients display a more regular network, i.e. higher clustering and longer path length (Schoonheim et al., 2011) and, more specifically, temporal regions appear to lose "hubness", while parietal regions appear to become more hub-like in early RRMS patients (Hardmeier et al., 2012). Analyses in these MEG studies were performed at the sensor-level. This is difficult to interpret and may suffer from problems with functional connectivity estimation due to field spread and volume conduction. For this reason, more recent network studies have been based on analysis in source-space (Hipp et al., 2012; Palva et al., 2010), in particular using beamforming techniques (Dellen et al., 2013; Douw et al., 2013; Hillebrand et al., 2012; Ponsen et al., 2013).

Although conventional graph theoretical analyses are helpful for understanding disease mechanisms (Bullmore and Sporns, 2012), they suffer from methodological difficulties when comparing different groups or conditions (Fornito et al., 2013; van Wijk et al., 2010). For instance, graph measures are influenced by the size of the network (i.e the number of nodes), network sparsity (percentage links present) and the average degree (i.e. the number of connections per node). An often applied approach to correct for size or average degree dependence is to normalize graph metrics by random graphs. Even this normalization does not solve the dependence of size, degree and density effects and may even exuberate it. Fixing the number of nodes and average degree in the network does eliminate size effects but may introduce spurious connections or ignore

strong connections in the network (van Wijk et al., 2010). Even the use of weighted graphs instead of un-weighted graphs does not provide an optimal solution since measures computed on these graphs are influenced by (the large number of) noisy connections and by the average functional connectivity strength.

An alternative approach is to construct and compare the minimum spanning tree (MST) of the original weighted graphs (Jackson and Read, 2010a; Jackson and Read, 2010b; Wang et al., 2008). A spanning tree is a sub-graph of the original graph that does not contain circles or loops and connects all nodes in the original graph. The MST is a tree which has the minimum total weight of all possible spanning trees of the original graph (Van Mieghem and Magdalena, 2005). If the original graph contains N nodes then the MST always has N nodes and M=N-1 links, therefore enabling direct comparison of MSTs between groups and avoiding aforementioned methodological difficulties such as setting arbitrary thresholds. Furthermore, if the original network can be interpreted as a kind of transport network, and if edge weights in the original graph possess strong fluctuations, also called *the strong disorder limit,* all transport in the original graph flows over the MST (Van Mieghem and van Langen, 2005). If the *strong disorder limit* condition holds, then the union of all shortest paths coincides with the MST and the MST forms the critical backbone of the original graph (Van Mieghem and Magdalena, 2005; Wang et al., 2008).

Network analyses of functional brain networks after constructing MSTs in neurological diseases are limited (Alexander-Bloch et al., 2010; Lee et al., 2006a; Schoen et al., 2011). In epilepsy, MST network analyses allowed identification of critical nodes in a temporal network associated with seizures (Ortega et al., 2008) and characterization of different network topologies in different epilepsy types (Lee et al., 2006a). In addition, default mode network changes in Alzheimer's disease were captured by constructing MSTs based on part of the original graph (Ciftci, 2011). A recent study on functional network changes during brain maturation in children revealed that MST network analyses were sensitive for detecting changes in network topology and were related to conventional graph theoretical outcome measures on the same data (Boersma et al., 2012).

The aim of our study was three-fold. Firstly, the main question was to investigate if we could detect functional network changes in MSTs of early RRMS patients. Secondly, to what extent these changes were associated with cognitive dysfunction. Thirdly, if these changes in MST topology between MS patients and healthy controls were present, could these correspond to changes in the critical backbone of functional brain networks in RRMS?

METHODS

General study design

In this cross-sectional study, MS patients and healthy controls underwent MEG, MRI, neuropsychological assessment and neurological examination on the same day. As outcome measures we used MST metrics, cognition and neurological status. An overview of the applied methods is given in figure 1.

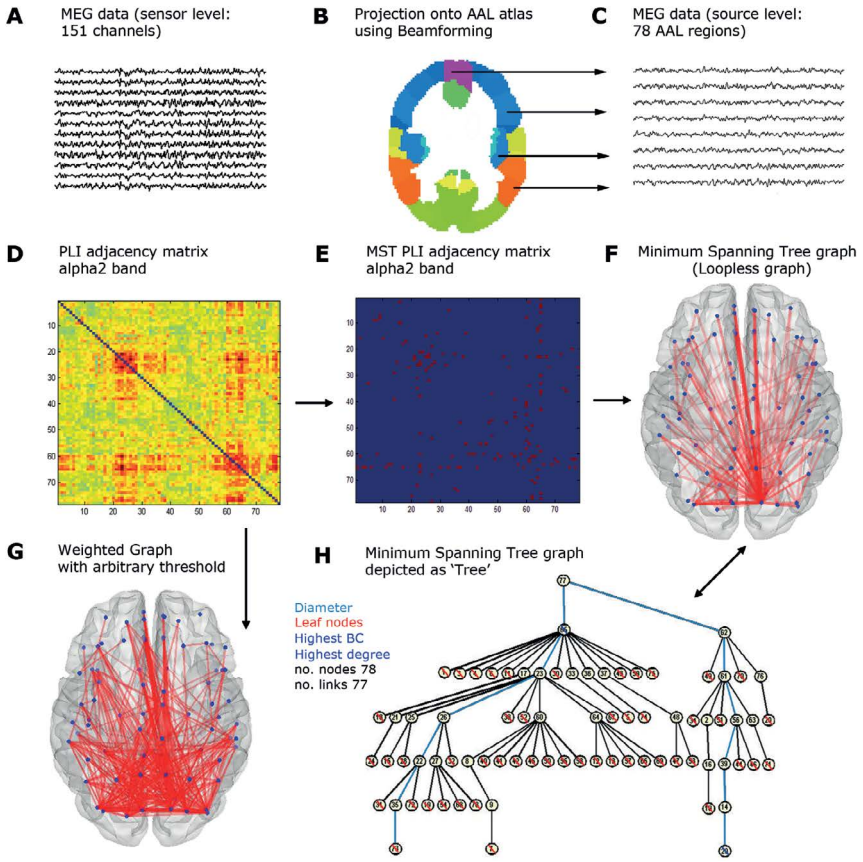

Figure 1: Overview of the applied methods. MEG data at the sensor level (A) were projected onto an AAL atlas using beamforming (B), resulting in 78 time series for each ROI (C). An 78x78 adjacency matrix is constructed for each frequency band separately based on the functional connectivity between each pair of time series (D). PLI was used as functional connectivity metric. Subsequently, Kruskal's algorithm was applied to obtain the MST matrix (E). This MST, a loopless graph, is displayed as a graph on a template (F). For illustration purposes only, a weighted graph obtained by applying an arbitraty threshold can be seen in G. This graph contains more connections and loops. F illustrates the MST as a tree structure. The node with the lowest eccentricity is placed on top. In addition, leaf nodes are depicted in red; the node with the highest degree (most connections) and BC in dark blue (node with highest BC and degree are not necessarily the same); and the diameter in light blue.

Participants

Subjects from a previous study were included (Meer et al., 2013; Tewarie et al., 2013) : 21 MS patients (mean age 41.9 ± 7.7, disease duration 6.8 ± 0.9 years) and 17 controls (mean age 39.8 ± 9.8) and were gender-, education- and age-matched. All patients were diagnosed with clinically-definite multiple sclerosis (Polman et al., 2005), specifically RRMS (Lublin and Reingold, 1996). Patients were recruited from the VU University Medical Center. All patients were part of the six-year follow-up of an early inception cohort, in which patients were included at diagnosis and subsequently

followed annually (Schoonheim et al., 2012c). Physical disability was measured using the Expanded Disability Status Scale (EDSS) (Kurtzke, 1983) and found to be relatively mild (median 2, range 0-4.5). The study was approved by the institutional ethics review board of the VUmc and all subjects gave written informed consent prior to participation. All subjects underwent a set of neuropsychological tests as described earlier (Schoonheim et al., 2011; Tewarie et al., 2013b). In summary, the brief repeatable battery for neurological disease (BRB-N), consisting of the selective reminding test (SRT), the 10/36 spatial recall test (SPART), the symbol digit modalities test (SDMT), the word list generation test (WLG), the concept shifting test (CST), the stroop color word test and the memory comparison test (MCT) were administered. An overall cognitive Z–score was calculated and used in further analyses.

Magnetic Resonance Imaging

An MRI scan was obtained from all subjects, using a 3T-MRI system (GE Signa HDXT V15m). A 2D dual-echo T2-weighted sequence (TR 9680 ms, TE 22/112 ms) and T1-weighted sequence (TR 475 ms, TE 9 ms) were obtained with 48 slices of 3 mm and 3D-T1 heavily T1-weighted sequence (FSPGR , TR 7.8 ms, TE 3.0 ms, TI 450 ms) with 1 mm, slices covering the entire brain. All scans were inspected by an experienced rater (MMS). Subsequently, lesion volumes were quantified. All lesion volumetric analyses were performed using Alice (Perceptive informatics Inc.) applying a local thresholding technique. Total gray matter (NGMV), total white matter (NWMV), and whole brain volumes (NBV), corrected for head size, were measured using the FSPGR images and SIENAX (Smith et al., 2002) version 2.5 (part of FSL 4.1, FMRIB's Software Library, http://www.fmrib.ox.ac.uk/fsl).

Magnetoencephalography

As described previously (Meer et al., 2013; Tewarie et al., 2013) , MEG data were recorded using a 151-channel whole-head MEG system (CTF systems; Port Coquitlam, BC, Canada) while participants were in a supine position in a magnetically shielded room (Vacuumschmelze, Hanau, Germany). A third-order software gradient (Vrba J, 1999) was used with a recording passband of 0– 150 Hz and a sample frequency of 625 Hz. Participants had to be free of any metal objects. Magnetic fields were recorded during a no-task, eyes-open condition for three minutes and eyes-closed condition for five consecutive minutes. At the beginning and end of each recording, the head position relative to the coordinate system of the helmet was determined by leading small alternating currents through three head position coils attached to the left and right preauricular points and the nasion. Changes in head position of <0.5 cm during a recording condition were accepted. Each original dataset consisted of a continuous resting-state recording from which artefact-free segments were subsequently selected for further analysis. Each segment or epoch had a duration of 6.555 seconds (total no. of segments or epochs was 45). Channels and epochs were visually inspected. Epochs and channels were rejected based on system related artefacts (SQUID jumps, noisy, broken or saturated channels), physiological artefacts (eye movements, eye blinks, muscle artefacts),

external artefacts (magnetized dental fillings) and environmental noise (PT, AH) (Gross et al., 2012). A minimum of 25 eyes-closed epochs was considered sufficient (Brookes et al., 2008) for further beamformer analysis. On average 5.7 channels (range: 2-14) and 8.4 epochs (range 3-20) were discarded.

Beamforming: time-series estimation for regions-of-interest

The technique used in this study was recently described (Hillebrand et al., 2012). A brief overview is given below. First, a subject's MRI was co-registered with the MEG data through identification of the same anatomical landmarks in the MRI that were also used for the placement of the MEG head-localization coils (i.e. left and right pre-auriculars and nasion). Only data from subjects where the estimated co-registration error was smaller than 0.8 cm were accepted for further analysis. The co-registered MRI was then spatially normalized to a template MRI using the SEG-toolbox in SPM8 (Friston et al., 2004). The new segmentation toolbox is an extension of the unified segmentation algorithm, which incorporates additional tissue priors for improved matching of the subject's MRI to the template (Ashburner and Friston, 2005; Weiskopf et al., 2011). The AAL atlas was used to label the voxels in a subject's normalized co-registered MRI (Tzourio-Mazoyer et al., 2002). Subcortical structures were removed, and the voxels in the remaining 78 cortical regions of interest (ROIs) were used for further analysis (Gong et al., 2009), after inverse transformation to the patient's co-registered MRI. Neuronal activity for the labeled voxels in the ROIs was reconstructed using a beamforming approach known as Synthetic Aperture Magnetometry (SAM) (Robinson and Vrba, 1999). SAM works in a sequential fashion, where the activity for each voxel is reconstructed by selectively weighting the contribution from each MEG sensor to a voxel's time-series. This weighting is done such that the activity at a voxel is reconstructed without distortion, and at the same time the contribution from external (noise) sources is minimized (Hillebrand et al., 2005; Hillebrand and Barnes, 2005). The beamformer weights are based on the covariance of the data and the forward solution (lead field) of a dipolar source at the voxel location, where data were band-pass filtered from 0.5-48 Hz. A time-window of, on average, 238 seconds (range: 164-282 sec.) was used for the computation of the data covariance matrix. The time window used for RRMS patients (170-275s) and healthy controls (164-282s) did not differ, (Mann-Whitney test, $p > 0.05$). We used broadband data for the estimation of the beamformer weights, as this avoids overestimation of covariance between channels (Barnes and Hillebrand, 2003). The sensor-level data were subsequently projected through the beamformer weights, resulting in a time-series for each voxel. Each ROI contains many voxels and the number of voxels per ROI differed. In order to represent a ROI by a single time-series, we selected, for each ROI and frequency band separately, the voxel with maximum absolute power in that frequency band (Hillebrand et al., 2012). The time-series for this voxel was used for further analysis, resulting in a total of 6 sets of 78 time-series (one for each frequency band, using six classic frequency bands: delta (0.5-4 Hz), theta (4-8 Hz), alpha1 (8-10 Hz), alpha2 (10-13Hz), beta (13-30 Hz), and gamma (30- 48 Hz)). As was done in our previous studies, we selected five artifact-

free epochs of 4096 samples (6.555 seconds) from these time-series, based on careful visual inspection (PT) to obtain stable results (Bartolomei et al., 2006; Bosma et al., 2008; Douw et al., 2008; Douw et al., 2009; Douw et al., 2010; Douw et al., 2013; Schoonheim et al., 2011; Stam et al., 2006b; Stam et al., 2009; van Dellen et al., 2013). BrainWave software was used for this purpose and also for further analyses (version 0.9.70 available from http://home.kpn.nl/stam7883/brainwave.html).

Functional Connectivity analysis

As a measure of FC, the phase lag index (PLI) was used (Stam et al., 2007), which calculates the asymmetry of the distribution of (instantaneous) phase differences between two time-series:

$$PLI=|< sign[\sin(\Delta\varphi(t_k))]>|. \quad (1)$$

Here the phase difference $\Delta\varphi$ is defined in the interval $[-\pi, \pi]$, <> denotes the mean value, sign stands for signum function and ffffl indicates the absolute value. The PLI ranges between 0 (completely symmetric phase distribution) and 1 (completely asymmetric phase distribution). The rationale behind this approach is that field spread/volume conduction causes a zero phase lag between two time-series, and that a uniform distribution of phases occurs when there is no coupling at all. The presence of a consistent, non-zero, phase lag between two time-series therefore reflects true interactions that are unaffected by field spread/volume conduction or common sources (Stam et al., 2007). Recent findings suggest that this method is capable of removing spurious coupling between ROIs at the expense of discarding any physiological interactions with zero lag (Hillebrand et al., 2012).

Table 1: MST descriptives

N	Nodes	Number of nodes in MST
M	Links	Number of links in the MST
	Degree	Number of neighbours for a given node in the MST
L	Leaf fraction	Fraction of leaf nodes in the MST where a leaf node is defined as a node with degree one
d	diameter	Longest shortest path of a network
	Eccentricity	Longest shortest path from reference node to any other node in the MST
BC	Betweenness Centrality	Fraction of all shortest paths that pass through a particular node
K	Kappa	Measure of the broadness of the degree distribution
Th	Tree hierarchy	An hierarchical metric that quantifies the trade-off between large scale integration in the MST and the overload of central nodes.

Minimum spanning tree network analyses

For each subject, each epoch and each frequency band separately we constructed the MST based on the PLI adjacency matrix by applying Kruskal's algorithm (Kruskal, 1956). In short, this algorithm

first orders the weights[1] of all links in an ascending order, then it starts the construction of the minimum spanning tree with the edge with the smallest weight and adds the following smallest edge weight until all nodes N are connected in a loopless sub-graph consisting of *M=N-1* links. If adding an edge results in formation of a cycle, this edge is skipped in the process. In our study, Kruskal's algorithm stopped when all 78 nodes were connected. After construction of the MST, all links weights are assigned a value of one.

Comparative analyses were performed between the MSTs for RRMS patients and healthy controls. Firstly, the dissimilarity between MSTs of RRMS patients and healthy controls was quantified using a measure based on information theory. This dissimilarity measure computes how much information is needed, on average, to explain MST_X given MST_Y (Lee et al., 2006a), where MST_X and MST_Y are two different MSTs with the same number of nodes. In other words the dissimilarity measure calculates the information change between two MSTs. Dissimilarity is obtained by:

$$D_{(Y|X)} = \frac{1}{N}\sum_{i=1}^{N} \log_{10}\left|\frac{D_{Y(i)}}{D_{X(i)}}\right|. \qquad (2)$$

Here $D_{X(i)}$ and $D_{Y(i)}$ are the sum of all distances from a reference node i to all of its neighbours in respectively the MST_X and the MST_Y, and N is the number of nodes in the MST. Distances refer to shortest paths based on the PLI and not to Euclidian distances. Given the sum of distances from node i to all its neighbours in MST_X, $D_{(Y|X)}$ calculates how much these distances change in the MST_Y, averaged over all nodes. See (Lee et al., 2006a) for a more detailed explanation. In our study the MST obtained from the average adjacency matrix of all healthy controls ($<MST_{HC}>$) was considered as MST_X. Subsequently for RRMS patients and individual healthy controls we calculated $D_{(Y|X)}$ with each time $<MST_{HC}>$ as a reference.

Only if MSTs between RRMS patients and controls showed different topology in a specific frequency band, i.e. were dissimilar, we calculated MST descriptives. Note that calculation of none of the MST descriptives required thresholding or any arbitrary parameter choices. The MST descriptives were degree (k), leaf number (L), diameter (d), eccentricity, betweenness centrality (BC), hierarchy (T_h), and kappa (Table 1) (Boersma et al., 2012). Degree, *BC* and eccentricity measures were calculated for each node separately. For eccentricity the mean value over all nodes was calculated as well. For betweenness centrality and degree, maximum values were listed separately. All other metrics are global measures: they characterize the MST as a whole. The number of links connected to a node is called the degree of that node. Leaf number (*L*) is the number of nodes on the tree with *k*=1. Leaf number has a lower bound of 2 and an upper bound of *M=N-1*. Here we report the leaf fraction (*=L/N)* instead of leaf number. The diameter of the tree is defined as the largest distance between any two nodes of the tree. The upper limit of the diameter is *d=M-L+2*,

1 For the construction of the MST using Kruskal's algorithm, the most important edges in the network are the ones representing a small distance (i.e. a small weight). In our case, the most important edges represent the strongest connections (i.e. a large weight). For the purpose of the computation of the MST, we therefore defined the edge weight as 1/(functional connectivity estimate), e.g. 1/PLI. The MST thus represents the sub-network with maximum connectivity.

implying that the largest possible diameter will decrease with increasing leaf number. Eccentricity of a node is defined as the longest path between that node and any other node of the tree and has a low value if this node is central in the tree. *BC* is another measure for centrality of a node ('hubness') within the network and is given by (Newman, 2010a):

$$BC_i = \frac{1}{N^2} \sum_{st} \frac{n_{st}^i}{g_{st}} . \quad (3)$$

Here n_{st}^i is 1 if the vertex i lies on a shortest path between s and t and is 0 if it does not, g_{st} is defined as the total number of shortest paths from *s* to *t* and $1/N^2$ is a normalization such that $BC_i \in [0,1]$. An important aspect in complex networks is efficient communication between all nodes, which requires a small diameter, i.e. a tree network with a star-like topology. In a star-like tree the central node might easily be overloaded since it has a high *BC*. An optimal configuration for a tree should therefore strike a balance between diameter reduction and overload prevention (Figure 2). A tree hierarchy measure that captures this trade-off was calculated (Boersma et al., 2012):

$$T_H = \frac{L}{2MBC_{\max}} . \quad (4)$$

To assure T_H ranges between 0 and 1, the denominator is multiplied by 2. If $L=2$, i.e., a line-like topology (which is called a 'path'), and *M* approaches infinity, T_H approaches 0. If $L=M$, i.e., a star-like topology, T_H approaches 0.5. Kappa, or degree divergence, which is a measure of the broadness of the degree distribution, was also calculated (Barrat et al., 2008):

$$\kappa = \frac{\langle k^2 \rangle}{\langle k \rangle} . \quad (5)$$

Here *k* is the degree.

Strong disorder limit

The weight distribution of a graph can be described by a power distribution

$$F(x) = x^{\alpha} 1_{x \in [0,1]} + 1_{x \in [1,\infty]}, \alpha > 0$$

where x represents the weights (i.e. PLI values in our case), the indicator function 1_x is one if x is true and zero otherwise and $\alpha \in [0,\infty]$ corresponds to the exponent (Van Mieghem and Magdalena, 2005). The cases $\alpha \in [1,\infty]$ do not correspond to the strong disorder limit (Van Mieghem and van Langen, 2005). If $\alpha \to 0$, this means there is a trend towards the strong disorder limit. A decreasing α corresponds with an increasing probability that that shortest paths of the original graph coincide with the MST. For regular graphs there is a critical value for $\alpha < \alpha_c$ for which the strong disorder holds (Van Mieghem and van Langen, 2005). For small world networks this critical value remains to be elucidated. From the full adjacency matrix of all subjects and epochs separately we ranked the

weights of all matrix elements in descending order and estimated α from this distribution, using a power function $F(x) = ax^{\alpha} + b$.

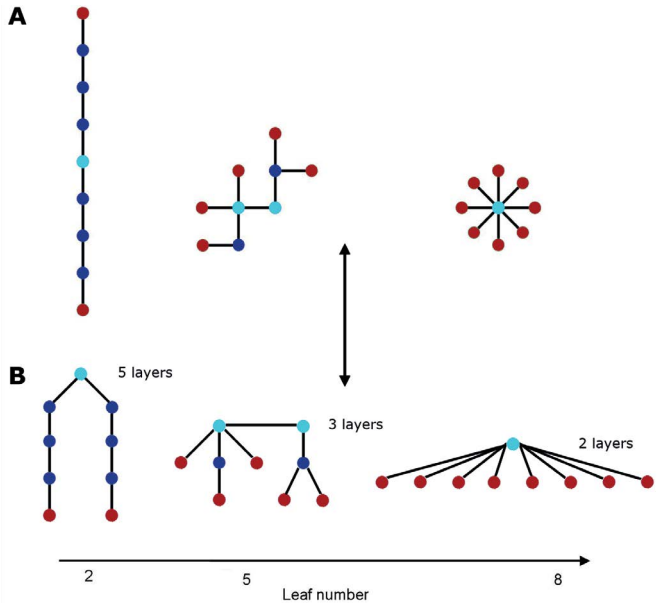

Figure 2: Tree topology and hierarchy. For illustration, trees with different topology are depicted with increasing leaf number. Leaf nodes are displayed in red. Nodes with high BC and equivalently low eccentricity are depicted in light blue. Dark blue represents nodes with no special characteristics. A) On the left, a line-like tree with a leaf number of 2 and diameter of *M-L+2=8* is depicted. On the right, a star-like tree is depicted with leaf number 8, diameter 1 and is characterized with a central node in the middle having a *BC=1*. The tree in the middle corresponds to a tree topology between aforementioned extremes. B) Identical trees as in A are depicted. Increasing leaf number is accompanied by trees having fewer layers. In each tree, nodes with lowest eccentricity are placed on top.

Statistical analyses

Firstly, dissimilarity measures were calculated for RRMS patients and healthy controls in each frequency band separately and compared with a Wilcoxon signed rank test as the data were generally not normally distributed. If there was a significant difference in dissimilarity between the MST of RRMS patients and healthy controls, then global MST descriptives between these groups were compared with the Mann-Whitney test. For each frequency band separately, graph theoretical outcome measures were corrected for multiple comparisons by the false detection rate (i.e. correcting for 7 MST measures per frequency band) (Benjamini and Hochberg, 1995). If global measures such as eccentricity, degree or BC differed between healthy controls and RRMS patients, as post-hoc analyses, we compared the nodal or regional values of these measures between groups by means of permutation analysis (Nichols and Holmes, 2002), where a null distribution

for between-group differences (independent t-test) is derived by permuting group assignment and calculating a t-statistic after each permutation. If a MST descriptive was significantly different between RRMS patients and healthy controls, only then spearman correlations were computed between these metrics and overall cognition and physical disability. Analyses were performed using SPSS for windows v.18.

Secondly, for each epoch and frequency band separately we estimated α and other parameters (*a* and *b*, see *'strong disorder limit'* section) with the nonlinear least squares method. Together with α we used goodness of fit R^2 as an outcome measure for each fit.. These analyses were done in Matlab v2011.

Table 2: Descriptive variables for controls and patients

	Controls (N=17)			Patients (N=21)			p value
	Mean	±	SD	Mean	±	SD	
Age	39.8	±	9.8	41.9	±	7.7	0.49
Education (1-7)	5.9	±	1.36	5.4	±	1.33	0.52
Gender (% female)	59%	±		57 %			
Disease Duration				6.8	±	0.9	-
NGMV (l)	0.84	±	0.05	0.81	±	0.04	0.037*
NWMV[a] (l)	0.69	±	0.03	0.66	±	0.03	.
NBV (l)	1.53	±	0.07	1.47	±	0.05	0.006*
Total thalamic volume	0.021	±	0.001	0.019	±	0.002	0.004*
Cognition	0.04		0.64	-0.19	±	0.84	0.36
EDSS (1-10)[b]				2		(0-4.5)	-
T1 lesion load (mL)				1.05	±	0.81	-
T2 lesion load (mL)				2.48	±	2.03	-

NGMV, normalized gray matter volume; NWMV, normalized white matter volume; NBV, normalized brain volume; EDSS, expanded disability status scale.[a] NWMV was not used for further analyses: lesion filling was not performed and therefore NWMV was not reliably estimated. [b] indicates median and range.* indicates significant differences between the two groups.

RESULTS

Characteristics of the included RRMS patients and healthy controls are listed in Table 1. A summary of the results is displayed in Figure 3.

Dissimilarity

MSTs were dissimilar between RRMS patients and controls in the theta band (Wilcoxon signed rank tests ($Z(36) = -2.7$, $p = 0.006$), alpha2 band ($Z(36) = -4.2$ $p < 0.001$) and beta band ($Z(36) = -3.6$ $p < 0.001$). Especially in the alpha2 band it can be visually inspected that the MST is different in RRMS patients compared to healthy controls (Figure 4): in healthy controls the strongest links (red lines)

of the MST are occipito-occipital or occipito-temporal. Even frontal nodes are mainly connected to the rest of the MST through occipital nodes. There is a shift of this direct occipital to frontal pattern in the alpha2 band in RRMS patients, with frontal nodes and occipital nodes being connected through intermediate nodes. In the theta and beta band such differences between the patterns are more difficult to observe based on visual inspection alone (Figure 4).

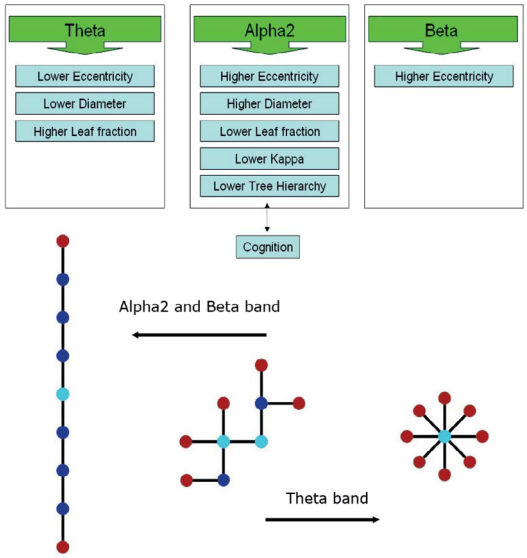

Figure 3: Summary of main results. For each frequency band we show the MST descriptives (blue rectangles) which are significantly different in early MS patients compared to healthy controls. *"higher'* and *'lower'* refer to higher or lower values in early MS patients. In the panel below the shift from the optimal tree topology to either a "path" or "star-like" topology is depicted for each frequency band for MS patients.

MST descriptives

For the theta band, diameter and mean eccentricity values were significantly lower in RRMS patients and leaf fraction was significantly higher in RRMS patients (Table 3). Regional analyses revealed that lower mean eccentricity in RRMS patients occurred widespread over the brain, but mainly in frontal and parietal areas, such as the left superior medial frontal gyrus, left middle frontal gyrus, right precentral gyrus, left inferior parietal gyrus, right superior parietal gyrus and left and right angular gyri. Lower eccentricity was also found in temporal and occipital areas and right posterior cingulate gyrus (Figure 5).

For the alpha2 band, diameter and mean eccentricity were significantly larger in RRMS patients compared to healthy controls. Other metrics such as leaf fraction, T_H, and kappa were significantly lower in RRMS patients (Table 3). Larger eccentricity at the nodal (regional) level occurred mainly at parietal and occipital areas, including the left and right calcarine gyri, left and right inferior/middle/superior occipital gyri, right cuneus, left and right precuneus and also at right anterior/middle/posterior cingulate gyri in RRMS patients (Figure 5).

For the beta band, only mean eccentricity was significantly larger in RRMS patients compared to healthy controls after correcting for multiple comparisons. Regional analyses revealed higher eccentricity in RRMS patients in mainly frontal and parietal areas such as the left superior medial frontal gyrus, left and right precuneus but also in the right and left anterior cingulated gyrus (Figure 5).

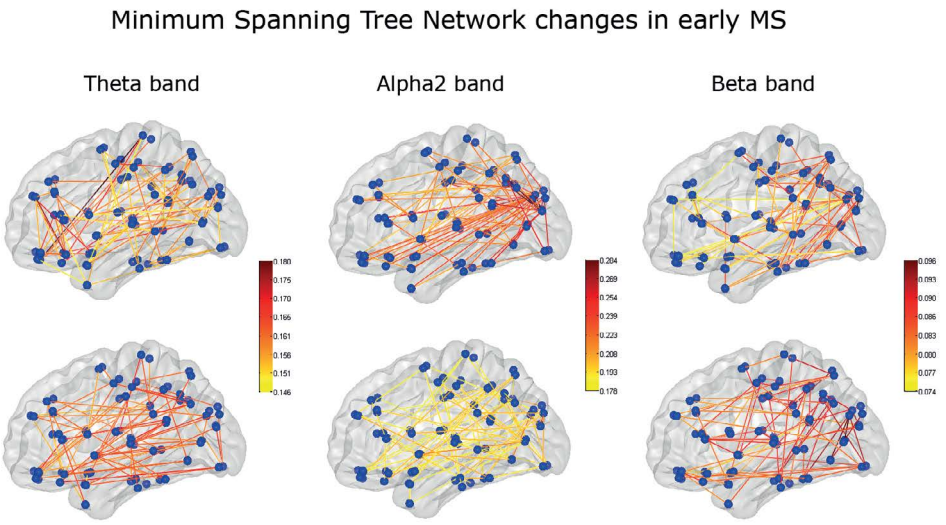

Figure 4: MST network changes in early MS. MSTs were dissimilar in the theta, alpha2 and beta band between early RRMS patients and healthy controls. The MSTs based on the average adjacency matrix of healthy controls (top) and RRMS patients (bottom) are depicted here for illustrational purposes only as there is a lot of variability in the MST for MS patients. Yet, the display of the average MST visualises some aspects that can be observed when comparing the MSTs between the groups. For example, it can be seen in the figure that the average MST in the alpha2 band in healthy controls has more leaves and a more star-like topology (with central nodes in posterior regions) than the average MST for MS patients. This is in agreement with our findings when comparing the (un-averaged) MST metrics between the MS group and healthy control group. For each frequency band, the colorbar indicates the PLI values for every link in the MST.

Correlations with cognition and physical disability

Spearman correlations with overall cognition were performed for each metric that was significantly different between RRMS patients and healthy controls for a specific frequency band. Only T_H in the alpha2 band in RRMS patients was significantly positively correlated with overall cognition ($r = 0.57$ $p = 0.007$). There were no correlations between physical disability (EDSS) and MST metrics.

Strong disorder limit

For each subject and each epoch and frequency band separately we estimated the exponent α in its weight distribution (Table 4). For all frequency bands and in RRMS patients and healthy controls α was between 0.40-0.53. This α less than 1 and may indicate that there could be a trend towards the presence of the strong disorder limit in RRMS patient data as well as in healthy controls which could have implications for the interpretation of the MST.

Table 3: MST descriptives in the theta, alpha2 and beta band in RRMS patients versus controls.

		healthy controls		**MS patients**			
		median	**range (min-max)**	**median**	**range (min-max)**	**U**	**p value**
Theta	Distance	**2.22**	**1.61-3.63**	**2.24**	**1.74-3.80↑**	**-2.7 (Z)**	**0.006**
	Betweenness Centrality (Max)	0.68	0.65-0.75	0.69	0.66-0.75	224.5	0.2
	Degree (Max)	0.15	0.10-0.19	0.14	0.11-0.18	176.5	0.9
	Diameter	**0.21**	**0.18-0.24**	**0.18**	**0.17-0.22 ↓**	**78**	**0.003**
	Eccentricity	**0.16**	**0.14-0.19**	**0.14**	**0.13-0.17 ↓**	**92**	**0.01**
	Kappa	3.6	3.14-4.44	3.69	3.17-4.36	231.5	0.3
	Leaf fraction	**0.59**	**0.56-0.65**	**0.62**	**0.57-0.68 ↑**	**270.5**	**0.006**
	Th	0.43	0.40-0.47		0.39-0.51	231.5	0.1
Alpha2	Distance	**1.88**	**0.96-3.97**	**2.05**	**0.85-4.03↑**	**-4.2 (Z)**	**<0.001**
	Betweenness Centrality (Max)	0.69	0.63-0.75	0.69	0.64-0.75	158	0.5
	Degree (Max)	0.18	0.17-0.22	0.14	0.09-0.17	140	0.2
	Diameter	**0.15**	**0.12-0.21**	**0.21**	**0.17-0.23 ↑**	**268**	**0.008**
	Eccentricity	**0.14**	**0.13-0.18**	**0.16**	**0.12-0.18 ↑**	**269**	**0.007**
	Kappa	**3.7**	**3.39-4.92**	**3.54**	**2.54-3.91 ↓**	**103**	**0.026**
	Leaf fraction	**0.62**	**0.58-0.68**	**0.59**	**0.46-0.62 ↓**	**41.5**	**<0.001**
	Th	**0.45**	**0.42-0.52**	**0.43**	**0.38-0.47 ↓**	**71.5**	**0.001**
Beta	Distance	**1.85**	**1.42-3.33**	**1.81**	**1.35-3.27↑**	**-3.6 (Z)**	**<0.001**
	Betweenness Centrality (Max)	*0.7*	*0.65-0.75*	*0.67*	*0.63-0.77 ↓*	*107*	*0.036*
	Degree (Max)	0.13	0.11-0.2	0.12	0.10-0.22	112.5	0.052
	Diameter	*0.21*	*0.19-0.22*	*0.22*	*0.18-0.24 ↑*	*260*	*0.016*
	Eccentricity	**0.16**	**0.14-0.17**	**0.17**	**0.13-0.19 ↑**	**272.5**	**0.005**
	Kappa	3.41	3.12-4.32	3.33	2.96-4.65	127	0.14
	Leaf fraction	0.58	0.56-0.61	0.58	0.53-0.62	149	0.4
	Th	0.42	0.39-0.45	0.43	0.39-0.47	219	0.24

Bold = significant after correcting for multiple comparisons by the FDR. Italic = the result is not significant anymore after correction for multiple comparisons using the FDR. Distance is defined as $\frac{1}{N}\sum_{i=1}^{N}\left|D_{Y(i)} - D_{X(i)}\right|$.

DISCUSSION

By applying minimum spanning tree analyses in MEG source-space we were able to identify functional brain network differences between early RRMS patients and healthy controls. These differences were most pronounced in the alpha2 band, where the MSTs in RRMS patients were characterised by a larger eccentricity and lower leaf fraction and 'tree hierarchy'. Clinically relevant, this lower 'tree hierarchy' in the alpha2 band was associated with poorer cognitive performance in RRMS patients. Importantly, in both RRMS patients and healthy controls there was a trend towards the presence of the strong disorder limit, indicating that changes in topology of MSTs in RRMS

patients may correspond to changes in the core of the functional networks constituted by the union of all shortest paths.

Altered functional brain network topology in early RRMS patients was found in the theta, alpha2 and beta band. Functional brain networks and its corresponding graphs are constructed based on the aggregate of all possible synchronization values between pairs of nodes in the graph. Especially theta and alpha band synchronization are associated with large scale integration and top-down processing of cortical information (Palva and Palva, 2011; von Stein A. and Sarnthein, 2000). Therefore one can hypothesize that these altered functional networks in the theta and alpha2 band in RRMS patients are indicative of large-scale changes in the functional brain network of RRMS patients. Furthermore, subsequent post-hoc analyses revealed that the MSTs in the aforementioned frequency bands differed with respect to several topological characteristics in RRMS patients. To start with global MST metrics, theta band eccentricity and diameter were lower in early RRMS patients, indicating a higher global integration of functional networks in this frequency band. As expected from the inverse relationship between leaf fraction and eccentricity, leaf fraction was higher in the theta band in RRMS patients. In contrast to the theta band, eccentricity and diameter in the alpha2 and eccentricity in the beta band were higher for patients, reflecting a lower global integration in these frequency bands. Furthermore, lower leaf fraction and hierarchy were found in the alpha2 band in RRMS patients. Nodal analyses revealed that lower eccentricity in the theta band occurred in many regions, but especially in the frontal and parietal regions. Higher eccentricity in the beta was also spread over more frontal and parietal areas whereas for the alpha2 band mainly occipital, parietal and temporal regions were affected.

Table 4: Estimated exponent α and R^2. For each frequency band and each epoch separately a power distribution was fitted to the ordered weight/PLI distribution. The table gives the mean and standard deviation of estimated exponent α and R^2.

Frequency band	Controls		MS Patients	
	Exponent α	R^2	Exponent α	R^2
Delta	0.51±0.24	0.956 ±0.018	0.53±0.20	0.956±0.017
Theta	0.51±0.19	0.950 ±0.029	0.48±0.20	0.958±0.015
Alpha1	0.51±0.25	0.957 ±0.016	0.50±0.25	0.959±0.016
Alpha2	0.53±0.20	0.957 ±0.017	0.52±0.20	0.957±0.016
Beta	0.44±0.19	0.955 ±0.015	0.45±0.19	0.955±0.016
Gamma	0.44±0.17	0.956 ±0.014	0.40±0.15	0.957±0.013

Together these findings indicate that especially in the alpha2 band (but also in the beta band) functional network topology in early RRMS tends to deviate in the direction of a more line-like topology (Figure 2), which could reflect a transition to a more regular network topology (Boersma et al., 2012). To a lesser extent, an opposite deviation towards a more star-like topology seems to be present in the theta band in early RRMS. We hypothesize that this opposite change in network topology and similarly an opposite change in global integration for the alpha/beta versus the theta

band could have several reasons: 1) pathology induces a shift from normal network topology that is different in the two frequency bands. Normal network topology in resting-state MEG tends to be highly integrated (high global efficiency) and well segregated in the theta band whereas these networks are less well integrated but highly segregated in the alpha/beta band (Stam, 2004). Therefore pathology could induce a different shift in the alpha/beta versus theta band to maintain a suboptimal trade-off between wiring cost and efficiency in early RRMS (Bullmore and Sporns, 2012). 2) A tractography study revealed that communicability, a measure of "accessibility", increases for some occipito-frontal and occipito-temporal regions, whereas it decreases for some frontal regions in RRMS (Li et al., 2012). These structural network changes could be related to the functional network changes observed in the present study (i.e. lower eccentricity in the theta band, higher eccentricity in the alpha2 band), since the MST in the alpha2 band mainly consisted of occipito-temporal and occipito-frontal connections and the MST in the theta band of frontal and fronto-parietal connections (Figure 4). Future MEG studies using cross-frequency phase coupling could elucidate whether opposing synchronization changes and subsequently network changes in the alpha2/beta vs theta band are related in RRMS. Related to this point, effects were only seen in the alpha2 band, while the alpha1 band did not change. This finding is in line with evidence that the alpha1 and alpha2 band have different functional roles or correspond to different cognitive sub-domains (Klimesch, 1999).

The present graph theoretical findings in MEG source-space in early RRMS seem to be in line with a previous MEG study at the sensor-level (Schoonheim et al., 2011). Here a tendency of a more regular / less integrated network was found, although this was observed in the alpha1 rather than the alpha2 band. Similarly, a structural network study in RRMS also found a decrease in global and nodal efficiency (Li et al., 2012). Although these findings of functional and structural network changes point in the same direction, disease duration in the functional study was relatively short whereas in the structural studies MS patients with a wide range of disease duration were included (Li et al., 2012; Schoonheim et al., 2011). It is still unknown how network changes on a functional level relate to network changes on a structural level for RRMS patients having the same disease duration, highlighting the need for combined functional and structural network studies in RRMS. The relation between structural and functional networks could also elucidate if or to what extent functional networks changes occur as a compensatory mechanism for structural network deficits in RRMS.

A clinically important finding of the present study is the association of worse cognition with lower 'tree hierarchy'. An optimal configuration for a tree should allow for large scale integration and at the same time it has to prevent overload of central nodes. The 'tree hierarchy' measure is the extent to which a tree displays this optimal configuration. Such an optimal configuration is probably somewhere between a line-like topology and a star-like topology and may constitute an optimum level of hierarchy and modularity. In many biological systems the evolution of complex networks evolves naturally towards such an optimal system which entails high modularity and

hierarchy (Simon, 1962). Here, a star-like topology corresponds with a network with few (only two) hierarchical layers (Figure 2), whereas a line line-like topology has many. Each layer lower in the hierarchy contains nodes with higher eccentricity, i.e. nodes in lower layers become less central in the functional network. In our study there seems to be a shift in early RRMS of a network with fewer layers (more star-like) to a network with more layers (more line-like). Subsequently the increase of layers in RRMS indicates that nodes become less central since they occupy lower layers. This process seems to be associated with worse cognition. This idea is strengthened by the fact that degree divergence decreases in RRMS patients. Degree divergence is proportional to the mean degree squared. Nodes in lower layers have lower degree, which could cause the mean degree to decrease with a subsequent decrease in degree divergence in RRMS patients. In future studies it will be interesting to investigate if the change in 'tree hierarchy' in RRMS is also associated with a change in modularity, since both of these properties often occur together in complex networks (Simon, 1962). Moreover it has been proven that even tree networks have high modularity (Bagrow, 2012), i.e. this characteristic can be studied in future MST studies in RRMS.

In the present study we demonstrated that the MST may tend to constitute the most important connections or the 'information highways' of the original graph, since there was a tendency of the weight distribution towards the strong disorder limit in both RRMS patients and healthy controls. This implies that the probability of MSTs of both RRMS patients and healthy controls containing the set of shortest paths is high and the MST may be considered as the critical backbone of the original networks (Van Mieghem and van Langen, 2005). Our observed differences between the MSTs of patients compared to controls might therefore correspond to changes in the critical backbone of the functional networks in RRMS patients and not to differences in irrelevant or less important connections. Furthermore, in the strong disorder limit the MST is composed of clusters interconnected by a scale-free tree (Braunstein et al., 2013). Therefore, MST network analyses could even allow one to study scale-free properties of the original network. Future theoretical studies are warranted to elucidate when the transition between the strong disorder limit and the weak disorder limit exactly occurs in small world networks before any hard claims can be made regarding to functional brain networks.

The primary rationale for using MSTs for functional network analyses is the fact that the computed outcome measures are not biased by network size, average degree or density effects. Importantly, MST usage avoids the introduction of arbitrary thresholds and normalization by random surrogates which may introduce biases in network analysis (Boersma et al., 2012; Fornito et al., 2013; van Wijk et al., 2010). The present study does have some limitations. First of all sample size was limited and therefore medication and gender effects could not be taken into account and a limited number of MST descriptives were used to analyse associations with cognition. The MST has several methodological advantages over conventional analyses, but local segregation such as clustering is not as easy to inspect as in conventional graph analyses. However, low leaf fraction and the clustering processes during the MST growth process contain information about local segregation.

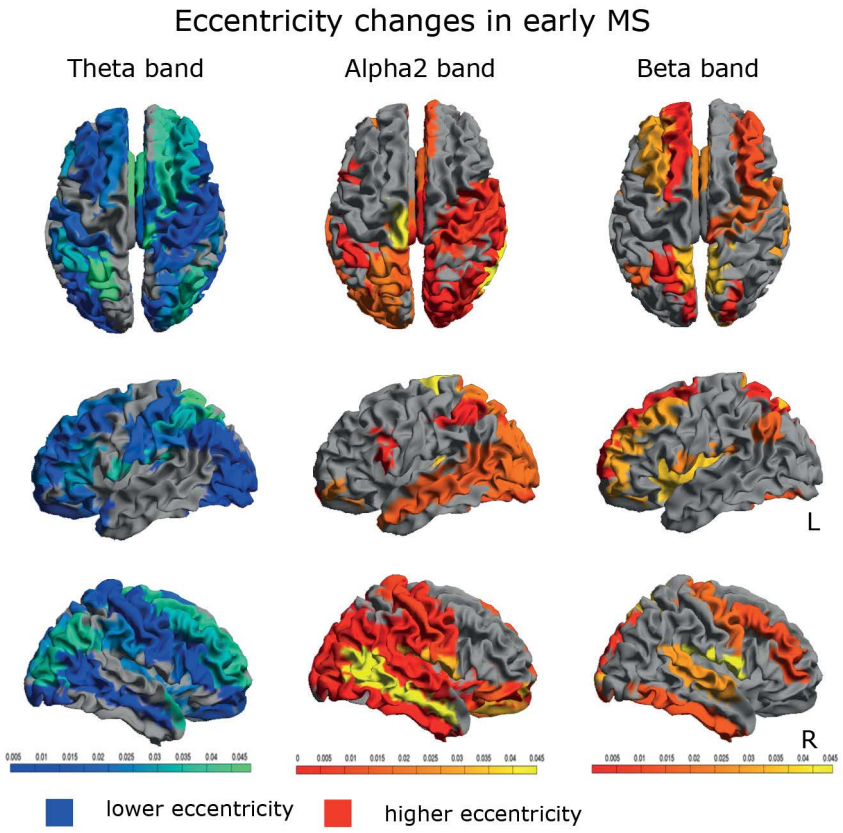

Figure 5: Eccentricity changes in early MS. Here regional eccentricity changes are shown for the theta, alpha2 and beta band in early MS patients. Colors indicate p-values. Blue indicates lower eccentricity as can be seen in the theta band in early MS. Red indicates higher eccentricity as can be inspected in the alpha2 and beta band in early MS patients. The statistical threshold was $p < 0.05$. Regional analyses were performed as post hoc analyses whenever global analyses revealed significant differences, i.e. regional analyses were not corrected for multiple comparisons.

An important methodological consideration is that the metrics used in the present study are related, such as tree hierarchy, leaf fraction, eccentricity and diameter, where diameter is in fact equal to the largest eccentricity value across all nodes. Despite the fact that MST descriptives are correlated, they do provide unique information about the MST and therefore concurrent use of these MST descriptives seems justified for post-hoc analyses. Another methodological consideration is that we calculated the MST on the basis of each epoch instead of using the PLI averaged over 5 epochs. The rationale behind this approach is the fact that the PLI distribution for one epoch tends to approach the strong disorder limit, whereas the PLI distribution averaged over five epochs approaches a Gaussian distribution, such that the interpretation of the MST as the backbone of the original network is not valid for such an average. Lastly, using the voxel with highest power as representative for every ROI

could have introduced some biases, for example for ROIs that cover a large area of cortex. Indeed, the spatial resolution that is obtainable with MEG varies from millimeters to centimeters across the brain (Hillebrand and Barnes, 2002), and depends on factors such as location of the neuronal activity, orientation of the cortex and signal-to-noise ratio (Barnes et al., 2004; Hillebrand and Barnes, 2002). Our current hypothesis is that the AAL atlas has a resolution that matches the spatial resolution of MEG resting-state data. However, future research should test whether this hypothesis is valid for all cortical regions, for example through the use of atlases with higher spatial resolution (Evans et al., 2012; Seibert and Brewer, 2011). In addition, selection of a single representative voxel might be prone to noise and outliers. However, the optimal method of dealing with multiple voxels within a ROI has not been defined yet, and using for instance an averaging method presents other biases, such as introducing artificial differences in signal-to-noise ratios for ROIs of different sizes. Similarly, one could argue that a priori selection of a target location within a ROI would speed up the computations. However, beamformer reconstructions vary most around peak activations (Barnes and Hillebrand, 2003) and as a consequence, the a priori selection of a target voxel could have the effect that the activity for a ROI is completely missed (Barnes and Hillebrand 2003) We therefore chose to adhere to methods used previously in our group.

Overall, MST network analyses cannot be considered as a total substitute for conventional analyses but for many questions or issues it offers an elegant unbiased method to compare networks. Future methodological studies in healthy controls and modelling studies are needed to further elucidate how analysis of minimum spanning trees can be used to increase our understanding of the organisation of functional brain networks. However, the present study provides a striking example of the power of this approach, namely the ability to distinguish pathological networks from healthy normal networks (Boersma et al., 2012; Olde Dubbelink et al., 2013).

To conclude, MST network analyses are not biased by commonly encountered methodological issues when reconstructing and comparing networks, such as the use of arbitrary thresholds, and are a sensitive way to characterize functional network changes in early RRMS. These functional networks show decrease in global integration and less hierarchy which is associated with reduced cognitive performance in MS. These MST network alterations in RRMS patients may tend to correspond to changes of the backbone of the original functional networks, which future theoretical studies need to clarify.

Chapter 8

Disruption of structural and functional networks in long-standing multiple sclerosis

P. Tewarie, M.D. Steenwijk, B.M. Tijms, M. Daams, L.J. Balk, C.J. Stam, B.M.J. Uitdehaag, C.H. Polman, J.J.G. Geurts, F. Barkhof, P.J.W. Pouwels, H. Vrenken, A. Hillebrand

Human brain mapping 2014 Jul: (Epub ahead of print)

ABSTRACT

Both gray matter atrophy and disruption of functional networks are important predictors for physical disability and cognitive impairment in Multiple sclerosis (MS), yet their relationship is poorly understood. Graph theory provides a modality invariant framework to analyze patterns of gray matter morphology and functional co-activation. We investigated how gray matter and functional networks were affected within the same MS sample and examined their interrelationship. Magnetic resonance imaging (MRI) and magnetoencephalography (MEG) were performed in 102 MS patients and 42 healthy controls. Gray matter networks were computed at the group-level based on cortical thickness correlations between 78 regions across subjects. MEG functional networks were computed at the subject level based on the phase-lag index between time-series of regions in source-space. In MS patients, we found a more regular network organization for structural co-variance networks and for functional networks in the theta band, whereas we found a more random network organization for functional networks in the alpha2 band. Correlation analysis revealed a positive association between co-variation in thickness and functional connectivity in especially the theta band in MS patients, and these results could not be explained by simple regional gray matter thickness measurements. This study is a first multimodal graph analysis in a sample of MS patients, and our results suggest that a disruption of grey matter network topology is important to understand alterations in functional connectivity in MS as regional gray matter fails to take into account the inherent connectivity structure of the brain.

INTRODUCTION

Multiple sclerosis (MS) is a chronic inflammatory and neurodegenerative disease of the central nervous system, often leading to a wide spectrum of clinical symptoms such as physical disability and cognitive impairment. Although the disease was initially recognized as merely a demyelinating disease, the discrepancy between classical MRI findings such as white matter lesion load and clinical dysfunction led to a search for alternative pathological substrates for clinical dysfunction (Geurts and Barkhof 2008). In this context, both gray matter atrophy and changes in neuronal activity have been reported and linked to physical disability and cognitive impairment in MS (Calabrese et al. 2007; Calabrese et al. 2010; Geurts and Barkhof 2008; Hardmeier et al. 2012; Steenwijk et al. 2014; Tewarie et al. 2013). Bridging the gap between gray matter atrophy and changes in neuronal activity may be crucial for understanding disease mechanisms that eventually lead to clinical symptoms. However, the relationship between changes in gray matter and disrupted activation patterns is still unclear and this is probably due to the fact that localized measurements fail to fully take into account the inherent connectivity structure of the brain.

Graph theory provides a framework to study brain connectivity changes in MS by representing the brain as a complex network (Stam and van Straaten 2012). Such a network consists of a set of brain regions (nodes) interconnected with links. Links can be measured based on the communication between distinct brain regions (i.e. functional connectivity); based on physical connections between these brain regions (e.g., as measured by diffusion tensor imaging, DTI) and based on co-variance of gray matter properties of these regions (i.e. structural connectivity), such as cortical thickness (Alexander-Bloch et al. 2013a). These three types of brain connectivity robustly show a non-random organization that is characterized by dense local connectivity and relatively sparse long range connections. Such a topology has been associated with a balance of integration and segregation, and a minimization of economical costs and maximization of efficiency (Bullmore and Sporns 2009; Rubinov and Sporns 2010).

Previous studies have investigated either structural co-variance or functional network organization in MS (Gamboa et al. 2013; Hardmeier et al. 2012; He et al. 2009; Schoonheim et al. 2011; Tewarie et al. 2013). Structural co-variance networks showed disrupted integration in MS, which was proportional to white matter lesion load (He et al. 2009). Functional network studies have revealed lower integration in functional networks in MS as obtained with functional magnetic resonance imaging (fMRI) and magnetoencephalography (MEG) (Gamboa et al. 2013; Hardmeier et al. 2012; Louapre et al. 2014; Schoonheim et al. 2011). However, it is still unknown how alterations of structural co-variance and functional networks in MS are related to each other. One of the hypotheses is that brain regions that show functional co-activation tend to co-vary in thickness (Alexander-Bloch et al. 2013). Therefore, disruption of structural co-variance or functional networks may influence each other. However, methodological hurdles such as differences in connectivity density impede direct comparison of networks of different studies and modalities (Fornito et al. 2013; van Wijk et al. 2010). The minimum spanning tree (MST; a sub-network containing the strongest connections,

see Methods for more details), is a promising approach that enables comparison of networks. We recently showed that in comparison to healthy controls the MSTs of MS patients are characterized by lower integration of information and loss of hierarchical structure of functional networks, and that this was related to a decline in cognitive performance (Tewarie et al. 2013). It is still unclear how these MST changes relate to other, more frequently used, graph theoretical measures.

The aim of the present study is to investigate how changes in gray matter atrophy relate to disruption of functional networks, as clarifying this relationship could give more insight in disease mechanisms in MS. To this end, we investigate how structural co-variance networks (based on cortical thickness correlations) and MEG functional networks were affected by the disease within the same MS sample. We further investigated the relationship between structural co-variance and functional networks as we hypothesized that disruption of functional networks may co-occur with disruption of structural co-variance networks. In addition, we analyzed if this relationship could merely be explained by an association between regional gray matter thickness and functional network connectivity. We obtained structural co-variances at the group level and MEG functional networks at the subject level. For all networks we computed conventional graph theoretical measures to increase the interpretability of our results within the context of previous studies. Finally, we investigated MST measures, since these minimize potential biases that might arise as a consequence of constructing networks for different imaging modalities.

METHODS

Participants

In total 120 MS patients and 44 healthy controls were recorded. Data from some subjects were excluded from analyses because of neurological comorbidity (N=10), too many artefacts or noise in the raw MEG data (N=2), or absence of MRI or MEG data (N=8). Consequently, 102 MS patients and 42 controls remained in the study. Patients were recruited from the MS database at the VUmc MS center and were part of a long disease duration cohort. The study protocol was approved by the Local Research Ethics Committee (Medical Ethical Review Committee of VU University Medical Center), whose ethics review criteria conformed to the Helsinki declaration. All subjects gave written informed consent prior to participation. An overview of the applied methods is depicted in Figure 1.

Data Acquisition

MR imaging of the brain was performed on a 3.0T whole body scanner (GE Signa HDxt, Milwaukee, WI, USA) using an eight-channel phased array headcoil. The protocol included, a three-dimensional T1-weighted fast spoiled gradient echo (FSPGR) sequence (repetition time (TR) 7.8 ms, echo time (TE) 3 ms, inversion time (TI) 450 ms, 12º flip angle (FA), sagittal 1.0 mm thick slices, 0.94 x 0.94 mm^2 in-plane resolution) for cortical segmentation, and a three-dimensional fluid attenuated inversion recovery image (FLAIR; TR 8000 ms, TE 125 ms, TI 2350 ms, sagittal 1.2 mm thick slices, 0.98 x 0.98 mm^2 in-plane resolution) for lesion detection.

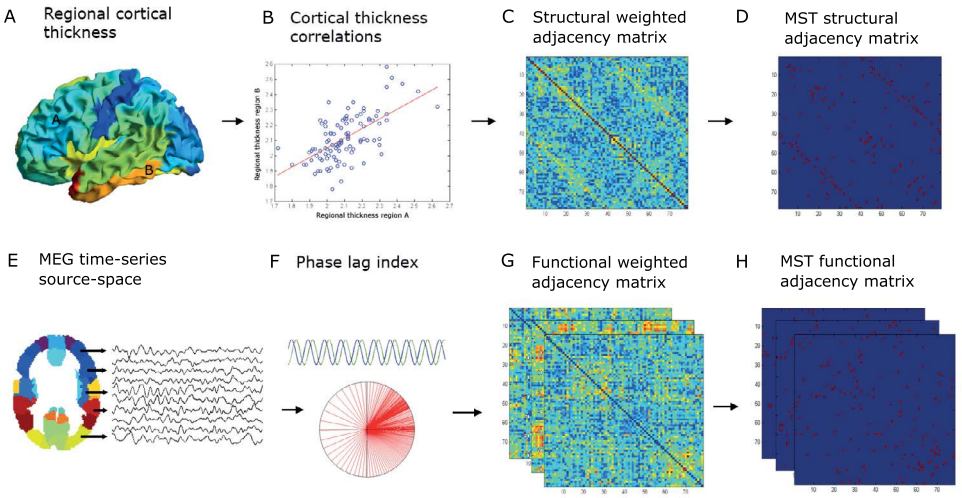

Figure 1: Overview of the applied methods: (A) regional cortical thickness was estimated by computing the distance between the surfaces of the pial and white matter layers as obtained from T1 weighted structural images. We then used the AAL atlas (78 cortical areas) to obtain an average cortical thickness value across the vertices within a region of interest (ROI). (B) Cortical thickness correlations between all possible pair of regions were subsequently computed across subjects to obtain a structural adjacency matrix at the group level (C). From this, (D) the minimum spanning tree (MST), an unique a-cyclic sub-network, was obtained. (E) MEG time-series were projected with a beamformer approach onto the same AAL atlas parcellation. (F) The phase lag index (PLI) was computed as a measure of functional connectivity between regions to obtain a frequency-dependent functional adjacency matrix (G). Subsequently, the MST was computed (H). For both structural and functional data the weighted adjacency matrices were normalized (by dividing each link weight by the mean link weight of that adjacency matrix) to minimize biases due to differences in average connectivity. Network measures were computed for the complete weighted networks and for the MSTs.

MEG data were recorded using a 306-channel whole-head MEG system (Elekta Neuromag, Oy, Helsinki, Finland) while participants were in a supine position in a magnetically shielded room (Vacuumschmelze, Hanau, Germany). Fluctuations in magnetic field strength were recorded during a no-task, eyes-open condition for three minutes (not analysed here) and eyes-closed condition for five consecutive minutes with a sample frequency of 1250 Hz. An anti-aliasing filter of 410 Hz and a high-pass filter of 0.1 Hz were applied online and other artefacts were removed offline using the temporal extension of Signal Space Separation (tSSS) in MaxFilter software with a sliding window of 10 seconds (Elekta Neuromag Oy, version 2.2.10) (Taulu and Simola 2006;Taulu and Hari 2009). Channels that were malfunctioning during the recording, for example due to excessive noise, were identified by automatic and visual inspection of the data and removed before applying tSSS. The number of excluded channels varied between one and twelve and did not differ between MS patients and healthy controls (Mann-Whitney $p>0.05$). The tSSS filter was then used to remove noise signals that SSS without temporal extension failed to discard, typically from noise sources near the head, using a subspace correlation limit of 0.9. The head position relative to the MEG sensors was recorded continuously using the signals from four head-localization coils. The head-localization coil

positions were digitized, as well as the outline of the participants scalp (~500 points), using a 3D digitizer (3SpaceFastTrack, Polhemus, Colchester, VT, USA). Scalp surfaces of all subject were co-registered to their structural MRIs using a surface-matching procedure, with an estimated resulting accuracy of 4 mm (Whalen et al. 2008). A single best fitting sphere was fitted to the outline of the scalp as obtained from the co-registered MRI, which was used as a volume conductor model for the beamformer approach described below.

Estimation of structural co-variance

Cortical thickness was measured with FreeSurfer 5.1 software after lesion filling in MS (see supplemental material for lesion filling technique) (Dale et al. 1999; Fischl et al. 1999). In short, FreeSurfer determines the pial and white matter surface of the cortex based on a T1 weighted structural image. The distance between these surfaces gives the vertex-wise cortical thickness (i.e. the perpendicular thickness at each location) of the cortex. All cortical segmentations were visually inspected for gross errors, which were manually corrected and re-run when necessary.

Subsequently, a surface-based version of the Automated Anatomical Aabeling (AAL) atlas was constructed in order to parcelate 78 identical areas for the cortical thickness and the MEG network analysis (Gong et al. 2009). To this end, the T1-weighted image of each healthy control was non-linearly registered to MNI-space using FLIRT and FNIRT (part of FSL 5.0.2; http://fsl.fmrib.ox.ac.uk/). The AAL atlas was warped to subject space using the inverse transformation of MNI registration, to obtain a subject-specific AAL parcelation. Each subject-specific volumetric atlas was subsequently sampled on the surface halfway the GM and WM, resulting in a rough AAL-parcellation containing 39 cortical areas per hemisphere for each subject. These were subsequently used to train FreeSurfer's probabilistic cortical surface classifier that makes use of the folding pattern and curvature of the surface to label cortical regions (Desikan et al. 2006). By training the classifier with a large sample of 'less-perfect' examples, 'smooth' AAL-parcellations could be obtained that are suitable for regional cortical thickness analysis. Cortical thickness was averaged across the vertices in each AAL region, resulting in 78 measures of cortical thickness per subject. Effects of age, gender, age-gender interaction and mean overall cortical thickness were removed with linear regression analyses and the resulting residuals were used for subsequent analyses (He et al. 2007).

Cortical thickness correlations were computed with Pearson correlations of average adjusted cortical thickness between AAL areas across subjects for the MS patients and healthy controls separately, resulting in two unthresholded (78 x 78) cortical thickness correlation matrices. Then, we applied a transformation of the raw correlation matrix: a value of one was added to all elements in the matrix and the result was subsequently divided by two. This transformation was performed to ensure that all matrix elements were positive since most algorithms that we used to compute topological measures require positive weights. Lastly, for descriptive purposes we also estimated white matter lesion load and whole brain atrophy using kNN-TTP and SIENAX (part of FSL 5.0.2; http://fsl.fmrib.ox.ac.uk/) (see supplementary information).

Estimation of MEG functional connectivity

A beamformer approach was adopted to map MEG data from sensor level to source space (Hillebrand et al. 2012). First the co-registered MRI was spatially normalized to a template MRI using the SEG-toolbox in SPM8 (Friston et al. 2004;Ashburner and Friston 2005;Weiskopf et al. 2011). The automated anatomical labeling (AAL) atlas was used to label the voxels in a subject's normalized co-registered MRI (Tzourio-Mazoyer et al. 2002). Subcortical structures were removed, and the voxels in the remaining 78 cortical regions of interest (ROIs) were used for further analysis (Gong et al. 2009), after inverse transformation to the patient's co-registered MRI. Next, neuronal activity in the labeled voxels was reconstructed using a scalar beamformer implementation (Elekta Neuromag Oy, beamformer, version 2.1.27) similar to Synthetic Aperture Magnetometry (Robinson and Vrba 1999).

Briefly, this beamformer sequentially reconstructs the activity for each voxel in a predefined grid covering the entire brain (spacing 2 mm) by selectively weighting the contribution from each MEG sensor to a voxel's time-series. The beamformer weights are based on the data (recorded time-series) co-variance matrix and the forward solution (lead field) of a dipolar source at the voxel location A time-window of, on average, 323 seconds (range 181-476s; range MS patients 192-476s; range healthy controls 181-349, Mann-Whitney test, $p>0.05$) was used to compute the data co-variance matrix. Singular value truncation was used when inverting the data covariance matrix, using a default setting of $1x10^{-6}$ for the ratio between the largest and smallest acceptable singular value. For each voxel in our predefined grid the pseudo-Z values, using a unity matrix as estimate for the noise covariance matrix (Hillebrand and Barnes 2005), were computed for different frequency bands (delta (0.5–4 Hz), theta (4–8 Hz), lower alpha (8–10 Hz), upper alpha (10–13 Hz), beta (13–30 Hz), and lower gamma (30–48 Hz)). Each ROI in the atlas contains many voxels, and the number of voxels per ROI differes. In order to obtain a representation of a ROI by its time-series, we selected, for each ROI and frequency band separately, the voxel with maximum pseudo-Z value in that frequency band. For this peak-voxel, we projected the broad-band (0.5-48Hz) time-series though the broad-band beamformer weights in order to obtain a time-series for a ROI (six time-series in total, i.e. 1 for each frequency band). Subsequently, the obtained time-series were downsampled 4 times. Just as in previous studies, for each subject, for each frequency band, the same five artefact free epochs of 4096 samples (13.1072 s) were selected (PT) to obtain stable results, using BrainWave software (version 0.9.101; http://home.kpn.nl/stam7883/brainwave.html) (de Haan W. et al. 2012; Douw et al. 2013; Hardmeier et al. 2012; Schoonheim et al. 2011; Tewarie et al. 2013).

Then, for each subject we filtered the selected broad-band epochs for each frequency band, where for each frequency band the time-series from the corresponding peak-voxels were used. Lastly, we computed the phase lag index (PLI) between the time-series for each pair of ROIs of the filtered data to obtain a (78 x 78) functional connectivity matrix. For this purpose, the phase is computed by taking the argument of the analytical signal (Stam et al. 2007). The PLI calculates the asymmetry of the distribution of (instantaneous) phase differences between two time-series:

$$PLI = |<sign[\sin(\Delta\varphi(t_k))]>| \quad (1)$$

where the phase difference $\Delta\varphi$ is defined in the interval $(-\pi, \pi)$, <> denotes the mean value, sign stands for signum function, || indicates the absolute value, and t_k corresponds to time with $k = 1,...,N_s$ where N_s is the number of samples. The PLI ranges between 0 (completely symmetric phase distribution) and 1 (completely asymmetric phase distribution). As field spread and volume conduction causes a zero phase lag (modulus π) between two time-series, this hardly influences the PLI since this metric captures only consistent, non-zero, phase lag between two time-series (Stam et al. 2007). For PLI analyses we averaged for each subject the five epochs, yielding one PLI matrix per subject for each frequency band.

Table 1: Demographic, clinical and MRI measures for MS patients and healthy controls

	MS patients n = 102		Healthy controls n = 42		P value
	Mean	±SD	Mean	±SD	
Age (in years)	54.23	9.76	51.14	5.98	0.023
Gender (F in %)	63.7%		61.9%		-
Disease type (RR/SP/PP)	68/22/12		-		-
Disease duration (years)	18.11	6.69	-		-
NBV (L)	1.41	0.09	1.49	0.07	<0.001
NGMV (L)	0.75	0.05	0.79	0.05	<0.001
NWMV (L)	0.66	0.04	0.69	0.03	<0.001
CT (mm)	2.48	0.10	2.56	0.08	<0.001
LV (mL)[a]	8.88	(3.37 - 17.92)		-	-
NLV (mL)[a]	10.51	(4.20 - 23.77)		-	-

Abbreviations: RR = relapsing-remitting; SP = secondary-progressive; PP = primary-progressive; NBV = normalized brain volume; NGMV = normalized GM volume; NWMV = normalized white matter volume; CT = cortical thickness; LV = lesion volume; NLV = normalized lesion volume. a: values were not normally distributed; displayed median and (interquartile range).

Network analysis

Nodes in all networks were defined by the 78 AAL regions. All networks were weighted: in structural co-variance networks links had weights corresponding to the cortical thickness correlations and in functional networks links had weights corresponding to the PLI values between AAL regions. To remove effects of differences in measuring scale, each network was normalized by dividing all link weights by the average link weight of that network (van Wijk et al. 2010). For all networks we computed weighted network properties (average connectivity, clustering, path length and their normalized versions) and the minimum spanning tree (MST; see below). This was done for each subject, epoch and frequency band for the functional networks and at group level for the structural co-variance networks.

Average structural and functional connectivity were calculated respectively as the average cortical thickness correlation and PLI value across all nodes of the network. The weighted clustering coefficient C is a measure of segregation and is defined as the geometric mean of triangles around a node (Rubinov and Sporns 2010):

$$C_w = \frac{1}{N}\sum_{i\in N}\frac{\sum_{j,h\in N}\left(w_{ij}w_{ih}w_{jh}\right)^{1/3}}{k_i(k_i-1)} \quad (2)$$

N is the number of nodes and w_{ij} is the weight between node i and nodes j, w_{ih} is the weight between j and h, and w_{lh} is the weight between nodes j and h; k refers to the degree of a node.

The average weighted shortest path length (L_w) indicates the amount of global integration. The weighted shortest paths are computed by estimating the shortest topological distance between all node pairs using Dijkstra's algorithm, where distance is defined as the inverse of the link weight. The average weighted shortest path length is computed by averaging path length over all nodes (Rubinov and Sporns 2010). Both measures were normalized by the average of the clustering and path length obtained from 500 random surrogate networks. Random surrogates were obtained by randomly shuffling the elements in the weighted fully connected networks. Preservation of the degree distribution cannot be achieved in this way, which is only feasible for unweighted networks. A large normalized clustering and shortest path length corresponds to a more regular network topology, whereas value close to 1 implies a random network topology (Watts & Strogatz, 1998). Note that for the functional networks all properties were computed for all epochs in all frequency bands and then averaged across five epochs for each subject.

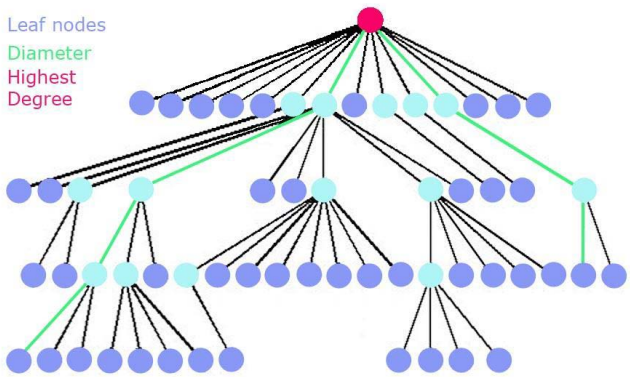

Figure 2: Explanation of the MST metrics: The MST is a sub-network of the original network that does not contain loops or triangles. Here, an MST is depicted, where the circles correspond to nodes and the (structural or functional) connections by lines. Leaf nodes, i.e. end nodes with 1 connection (a degree of 1), are colored dark blue. The pink node is the node with the highest number of connections. The diameter is the longest shortest path in the network, here depicted in green. Two other measures that were computed are degree divergence (broadness of the degree distribution) and tree hierarchy. A low tree hierarchy corresponds to a more path-like topology, whereas a high tree hierarchy to a more star-like topology (see also Table 2).

Table 2: Network properties (Definitions are based on (Stam and van Straaten 2012))

N	Nodes	Number of nodes in the network
M	Links	Number of links in the MST
C	Clustering	The unweighted clustering coefficient describes the likelihood that neighbours of a vertex are also connected, and it quantifies the tendency of network elements to form local clusters. We used the weighted equivalent of this measure to characterize local clustering.
	Path length	Measure for integration; path with lowest sum of link weights between two nodes
k	Degree	Number of neighbours for a given node in the MST or the whole network
L	Leaf fraction	Fraction of leaf nodes in the MST where a leaf node is defined as a node with degree one
D	Diameter	Longest shortest path of an MST
Th	Tree hierarchy	A hierarchical metric that quantifies the trade-off between large scale integration in the MST and the overload of central nodes.
K	Degree divergence	Measure of the broadness of the degree distribution

MSTs were constructed based on the weighted networks with Kruskal's algorithm (Kruskal 1956). In our case we started the algorithm with the largest link weights since we were interested in the strongest connections (highest PLI values) in the network. In short, this algorithm first orders the weights of all links in a descending order and starts the construction of the minimum spanning tree with the largest link weight and adds the following largest link weight until all nodes *N* are connected in a loopless (i.e. not containing triangles) sub-graph. When addition of a link forms a loop, this link is ignored. After construction of the MST, all link weights are assigned a value of one and the MST always consists of *M=N-1* links, ensuring fixed density for every network given size N. We computed the following MST properties: leaf fraction (L), diameter (d), tree hierarchy (T_h) and degree divergence (κ). Leaf number L_N is the number of nodes in the tree with only one link. Leaf number has a lower bound of 2 and an upper bound of *M=N-1*. We report the leaf fraction ($=L_N/N$), to be bounded between 0 and 1. The diameter of the tree is defined as the largest distance between any two nodes in the tree. The upper limit of the diameter is *d=M-L+2*, implying that the largest possible diameter decreases with increasing leaf number. Furthermore, we computed tree hierarchy T_H, that measures the trade-off between diameter reduction and overload prevention of the central nodes, which is necessary for efficient communication (Boersma et al. 2012):

$$T_H = \frac{L}{2MBC_{\max}}. \tag{3}$$

To assure T_H ranges between 0 and 1, the denominator is multiplied by 2. If $L=2$, i.e., a path-like topology, and M approaches infinity, T_H approaches 0. If $L=M$, i.e., a star-like topology, T_H approaches 0.5. BC_{max} refers to the maximum betweenness centrality in the tree network, where betweenness centrality is a measure for the importance of a node in the network. Finally, we computed degree divergence κ, which is a measure of the broadness of the degree distribution and also a measure of network stability (Barrat et al. 2008):

$$\kappa = \frac{\langle k^2 \rangle}{\langle k \rangle}. \tag{4}$$

Here, *k* corresponds to the degree of a node: the number of links connected to a node. See Table 2 for a brief description of all network characteristics and Figure 2 for an illustration for the MST metrics. All network characteristics were calculated with in house scripts and with the brain connectivity toolbox (https://sites.google.com/site/bctnet/) in Matlab v2012a.

Statistical analysis

Statistical analyses of the cortical thickness correlation networks and its properties were performed in Matlab v2012a. Statistical analyses of functional connectivity and MST network properties were performed in SPSS 20.0 (Chicago, IL, USA). Normality of the variables was assessed using the one-sided Kolmogorov-Smirnov test and histogram inspection. P-values<0.05 were considered statistically significant. The analyses were performed in the following three stages: Firstly, structural co-variance networks were compared between groups; secondly, functional networks were compared; finally the relationship between structural and functional networks was examined:

1. Structural co-variance networks: Raw correlation values together with all conventional and MST measures were compared using permutation analyses (1000 permutations) (Bernhardt et al. 2011; Bullmore et al. 1999; He et al. 2008). First, all conventional and MST measures were computed for structural networks of the MS and healthy control group. For each measure separately, the difference in values between healthy controls and MS patients was used as test-statistic, and significance of the test-static was determined by permutation testing: for each permutation (out of 1000), group membership was randomly permuted for all subjects and cortical thickness correlations were re-calculated for the permuted groups (see Estimation of structural co-variance). Next the test-statistic was determined for each permutation, resulting in a distribution of permuted test-statistic values. The measured test-static was evaluated against this distribution, for which the 95 percentile points were considered to be critical. No co-variance adjustment was necessary for further group comparisons as these effects were already removed before computation of cortical thickness correlations (see section "Estimation of structural co-variance").

2. Functional connectivity and functional networks: Average functional connectivity (i.e., mean PLI across nodes in the networks (before normalization)) was compared between the groups for each frequency band separately with regression analyses, including age and gender as co-variates. When mean PLI differed between groups, regional PLI values were compared between groups as a post-hoc analysis by means of permutation analysis (Nichols and Holmes 2002).

Here, a null distribution for between-group differences (independent t-test) is derived by permuting group assignment and calculating a t-statistic after each permutation. To correct for multiple comparisons, the maximum t-value across ROIs for each permutation was used to construct a distribution of maximum t-values for 1000 permutations of group membership. The threshold at the 0.05 significance level (i.e. the 95th percentile point) for the distribution permuted values was

determined. Average functional network properties (both conventional and MST) were compared between groups in each frequency band with regression analyses, including age and gender as co-variates. For all analyses within a frequency band, we corrected for multiple comparisons with the false discovery rate procedure (6 tests per frequency band) for the global tests (Benjamini and Hochberg 1995).

3. Structural co-variance versus functional networks: Thirdly, we used the nonparametric Mantel test to quantify the relationship between structural co-variance networks and MEG functional networks. To this end we constructed a group-level functional network by averaging the functional networks across epochs and subjects to obtain one 78x78 matrix per group for each frequency band. The correlation coefficient was computed between structural and functional connectivity measures across the AAL regions per group and frequency band. In addition, regional relationship between structural co-variance and functional networks was measured by calculating the difference between the rank-transformed structural co-variance ($\mathbf{SC}_R$) and the rank-transformed group-averaged functional networks ($\mathbf{FC}_R$). We computed regional similarity between structural and functional connections by:

$$similarity = \left\langle 1 - abs\left[\mathbf{SC}_R - \mathbf{FC}_R\right]\right\rangle \quad (5)$$

Here, *abs* corresponds to the absolute value, and <> corresponds to the mean over all rows of the matrix to obtain a similarity index for each ROI. To test whether a similarity value for a ROI was significant we used permutation analysis (1000 permutations) where in each permutation the elements in the ranked structural co-variance and averaged functional network matrices were randomized (Nichols and Holmes 2002).

4. Regional cortical thickness versus functional networks: Lastly, we also analyzed the relationship between regional cortical thickness and functional networks. For each subject we obtained cortical thickness values for each region. Then, we averaged each functional connectivity matrix over its rows and averaged across five epochs for each subject to obtain one functional connectivity (PLI) value for each region per subject. We then computed Pearson correlations for each region between cortical thickness and functional connectivity and corrected for the number of tests with the false discovery rate (Benjamini and Hochberg 1995).

RESULTS

Table 1 reports the subject characteristics. MS and healthy controls differed in age, but not in their gender distribution. 67% of the patient group consisted of relapsing-remitting MS patients, 21% of secondary- and 12% primary-progressive MS patients. MS patients showed significant reduction in mean cortical thickness and normalized gray matter volume (Table 1).

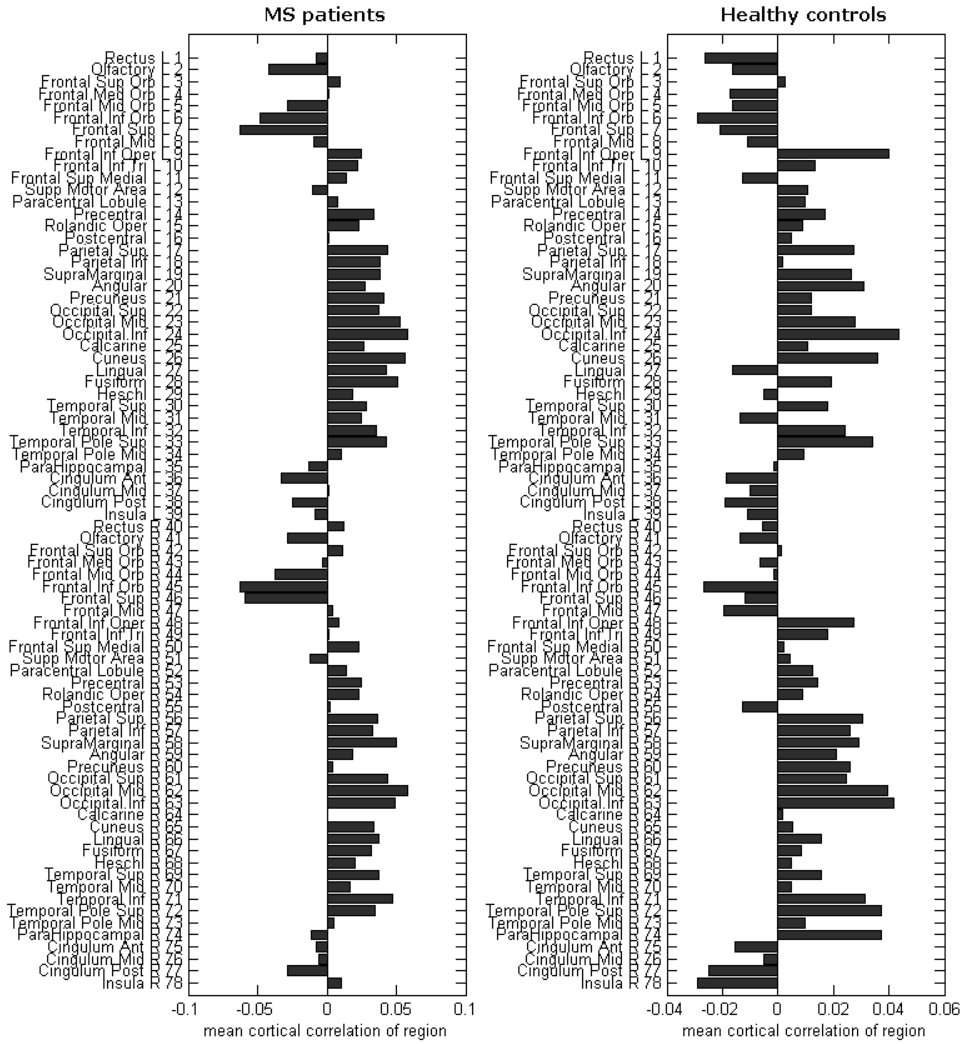

Figure 3 mean cortical correlation values: Here we show the mean raw correlation value for each region. These values are obtained by averaging over all row elements of the structural co-variance matrices in Figure S1. Depicted on the right of the horizontal bar plots are the corresponding AAL regions. The number next to each name also corresponds to the numbers in Figure S1.

Structural co-variance networks

We first compared raw cortical thickness correlation values between the two groups and these were similar for MS patients and healthy subjects (permutation test: $p = 0.8$; MS patients median R = -0.0075, range R (0.75 — -0.42), healthy controls median R = -0.0074, range R (0.62 — -0.53)). In Figure 3 we depict the mean raw cortical thickness correlation per area, where it can

be observed that these mean values are strongly affected by the large number of matrix elements with low correlations. Next, we compared network properties of the structural co-variance networks between groups. The MS group displayed a higher normalized clustering (MS patients C_w = 1.05, healthy controls C_w = 1.04, $p < 0.001$) and a higher normalized shortest path length (MS patients L_w = 0.99 healthy controls L_w = 0.98, $p < 0.001$) compared to healthy controls, which is indicative of a more regular structural co-variance network (Figure S1). Finally, we compared the structural MST between groups, but we did not find differences in MST metrics between the groups (MS patients L_n = 0.36, d = 0.14, T_H = 0.32, K = 2.47, healthy controls L_n = 0.36, d = 0.14, T_H = 0.31, K = 2.39, all p >0.05).

Functional connectivity and functional networks

In order to investigate differences in functional connectivity between the two groups we compared the mean PLI values for each frequency band between MS patients and healthy controls. First of all, MS patients showed higher mean PLI values in the delta and theta band, and lower mean PLI values in the alpha2 band than healthy controls (see Table 3). Figure 4 shows that in the delta band, higher PLI values were present in many cortical areas, except for right-temporal and occipital areas. In the theta band, MS patients showed higher PLI values in many cortical areas including occipital, temporal, parietal and frontal areas. In the alpha2 band PLI values for MS patients were lower in, among other regions, the occipital, temporal and parietal areas.

Conventional network analysis revealed a higher normalized path length in the theta band and a lower normalized clustering in the alpha2 band in MS patients (see Table 4). This indicates that network topology tends to become more regular in the theta band, in contrast to more random topology in the alpha2 band. MST analyses revealed that MST topology was only different in the alpha2 band for MS patients. This was reflected in a significantly lower leaf fraction, lower degree divergence and lower tree hierarchy in this frequency band for MS patients (see Table 4 and Figure 5).

Table 3: Comparative analyses of mean functional connectivity between MS patients and healthy controls.

	MS patients	Healthy controls	Standardized B	t value	P value
Mean PLI					
Delta	**0.113±0.004**	**0.106±0.004**	**-0.56**	**-7.90**	**<0.001**
Theta	**0.098±0.004**	**0.094±0.004**	**-0.56**	**-7.89**	**<0.001**
Alpha1	0.138±0.007	0.138±0.006	-0.10	-0.12	0.9
Alpha2	**0.112±0.006**	**0.115±0.006**	**0.22**	**2.72**	**0.007**
Beta	0.064±0.005	0.065±0.004	0.04	0.47	0.6
Gamma	0.048±0.002	0.049±0.002	0.04	0.47	0.6

Abbreviations: PLI=phase lag index, MST=minimum spanning tree.
*Values listed are mean±SD. Bold = significant after correcting for multiple comparisons by the FDR.

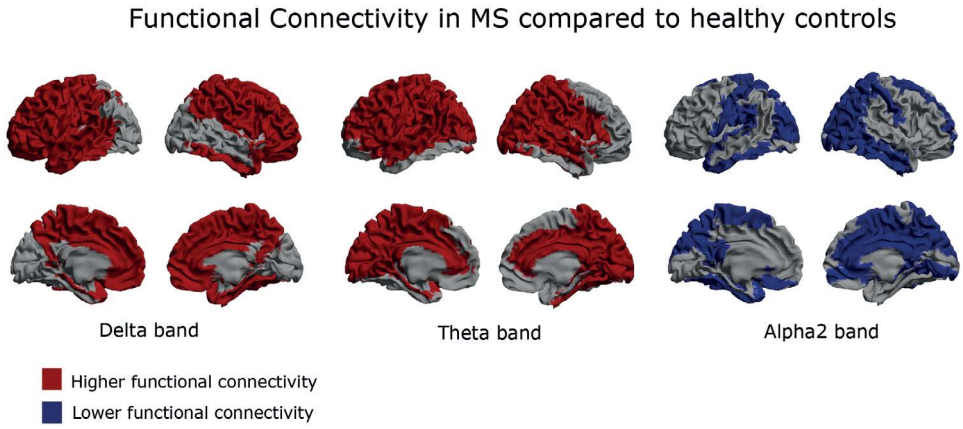

Figure 4 functional connectivity: Regional functional connectivity differences between MS patients and healthy controls in the delta, theta and alpha2 band. Here, a brain map is depicted where for each ROI the regional functional connectivity is shown, defined as the average functional connectivity between that ROI and all other ROIs. Higher functional connectivity (red color) in the MS patients is present In both the delta and theta band. Compared to the delta band, frontal cortical areas are spared in the theta band, whereas occipital, temporal and parietal areas are more affected. Lower functional connectivity (blue colour) is present in the alpha2 band, especially in temporal, occipital and parietal regions.

Structural co-variance versus functional networks

In the previous analyses we have demonstrated that both the structural co-variance and functional networks get disrupted in MS. Note that the direction of the shift in topology was the same for the structural co-variance network and the functional networks in the theta band. Both these networks were characterized by more regular organization, which was indicated by higher normalized path length and higher normalized clustering. However, functional networks in the alpha2 band showed a change in the opposite direction as these networks were characterized by a more random network organization.

To further characterize the relationship between structural co-variance and functional network alterations in MS we further performed stratified correlation analyses for the MEG frequency bands where we found significant differences in functional connectivity between MS patients and controls. We found that correlations between structural co-variance and functional networks depend on frequency band and group as there were weak but significant positive correlations between the two in the delta and alpha2 band for healthy controls and in the theta and alpha2 band for MS patients. Additional analyses revealed that these associations between the two types of networks were both driven by negative as well as positive cortical thickness correlations (see Table S2).

In order to zoom into regional relationship between structural and functional networks we computed the regional similarity between the two (Figure 6). In the delta band, we observed more regions in the healthy subject group that showed high similarity between structural co-variance and functional connectivity than in the MS patient group. In the theta band, we observed the opposite;

regional similarity was more prominent in MS patients, in particular for posterior and temporal regions. This pattern was also observed in the alpha2 band for both groups, only less prominent than in the theta band.

Table 4: Comparative analyses of functional network properties between MS patients and healthy controls

		MS patients	Healthy controls	Standardized B	t value	P value
Delta	Normalized clustering coefficient	1.0076±0.0017	1.0076±0.0013	-0.009	-1.03	0.91
	Normalized path length	1.016±0.017	1.012±0.016	-0.154	-1.83	0.069
	MST leaf fraction	0.53±0.022	0.53±0.021	0.011	0.13	0.89
	MST tree hierarchy	0.403±0.023	0.403±0.021	-0.010	-0.12	0.91
	MST degree divergence	3.1±0.17	3.16±0.17	0.12	1.41	0.16
	MST diameter	17±1.2	17±1.1	-0.032	-0.38	0.71
Theta	Normalized clustering coefficient	1.0073±0.0016	1.0068±0.0016	-0.13	-1.55	0.12
	Normalized path length	**1.016±0.013**	**1.0084±0.012**	**-0.27**	**-3.22**	**0.002**
	MST leaf fraction	0.53±0.024	0.53±0.024	-0.009	-0.11	0.91
	MST tree hierarchy	0.403±0.023	0.405±0.017	0.043	0.51	0.61
	MST degree divergence	3.1±0.15	3.1±0.19	-0.059	-0.71	0.48
	MST diameter	17±1.4	17±1.4	0.15	1.76	0.081
Alpha2	**Normalized clustering coefficient**	**1.0077±0.0019**	**1.0084±0.0018**	**0.19**	**2.24**	**0.027**
	Normalized path length	1.014±0.014	1.013±0.014	-0.061	-0.72	0.40
	MST leaf fraction	**0.53±0.021**	**0.54±0.020**	**0.23**	**2.74**	**0.007**
	MST tree hierarchy	**0.40±0.019**	**0.41±0.021**	**0.22**	**2.64**	**0.009**
	MST degree divergence	**3.1±0.18**	**3.2±0.14**	**0.17**	**2.09**	**0.039**
	MST diameter	17±1.2	17±1.1	-0.11	-1.29	0.20

Abbreviations: MST=minimum spanning tree.

*Values listed are mean±SD. Bold = significant after correcting for multiple comparisons by the FDR.

Regional cortical thickness versus functional networks

Finally, we analyzed the relationship between regional cortical thickness and functional networks by computing pair-wise correlations to investigate if the relationship between structural co-variance and functional networks can be explained by merely regional thickness values alone. We found correlations of weak strength in for example the alpha2 band, however, none of these correlations survived correction for multiple hypothesis testing (please see Table S1).

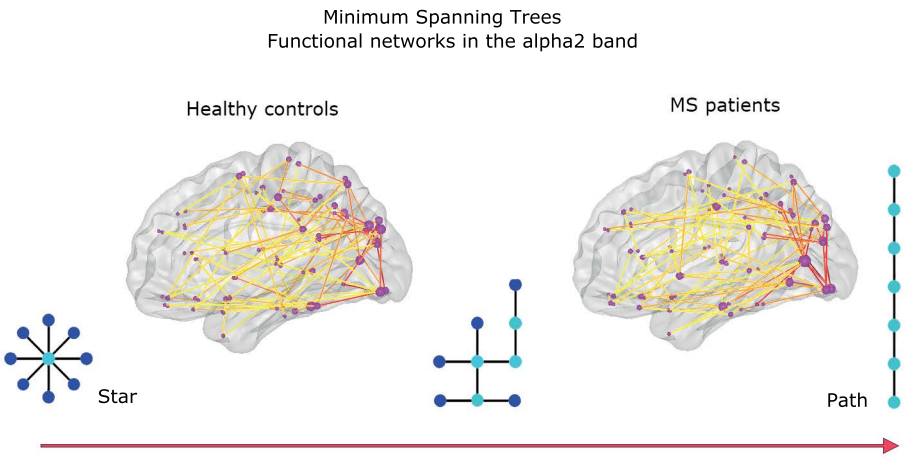

Figure 5 MST results for functional networks in the alpha2 band: For illustrative purposes the average MSTs across subjects for MS patients and healthy controls are depicted. The diameter of the circles in the glass brains is proportional to the degree of the nodes in the MST; the color of the lines connecting the circles indicates the strength of the functional connections, with warmer colors indicating stronger connections. The MST for MS patients was characterized by a shift towards a more path-like topology reflected by a lower leaf fraction, lower degree divergence and lower tree hierarchy.

DISCUSSION

The current study aimed to investigate how structural co-variance and MEG functional networks were affected by the disease within the same MS sample. Our main findings were: (1) MS patients and healthy controls showed similar average structural co-variance; (2) MS patients showed higher functional connectivity in the delta and theta band and lower functional connectivity in the alpha2 band; (3) structural co-variance networks and functional networks in the theta band in MS patients were more regularly organized than in controls (4) functional networks in the alpha2 band were more randomly organized in MS than in controls; (5) the relationship between structural co-variance and MEG functional networks was dependent on the frequency band and on group membership, particularly in the theta band.

Structural co-variance networks

Structural network analyses revealed a spatial reconfiguration of interregional cortical thickness associations in MS that did not effect the average correlation across all areas. This reconfiguration resulted in a more regular topology in the MS group, as indicated by higher normalized clustering and path length values. At this point is it still unclear as to what mechanisms underlie the existence of cortical thickness correlations. One hypothesis is that they might arise as a consequence of tension exerted by axonal connectivity between two brain areas (van Essen 1997). Another

structural co-variance study has previously reported similar findings of lower global efficiency (the inverse of path length) in MS patients, and they showed that this finding was proportional to white matter lesion load (He et al. 2009). This finding suggests that damage to white matter tracts that connect cortical areas influence the cortical thickness correlations, supporting the axonal tension hypothesis (Gong et al. 2012; Li et al. 2012; Shu et al. 2011). However, one other study demonstrated that white matter tracts explain only a part of cortical thickness correlations (30-40%) (Gong et al. 2012), suggesting that other factors are implicated in cortical thickness correlations. It has been suggested that cortical thickness correlations reflect synchronized maturation between brain areas and are not only influenced by white matter connections but also by functional co-activation (Alexander-Bloch et al. 2013a; Alexander-Bloch et al. 2013b).

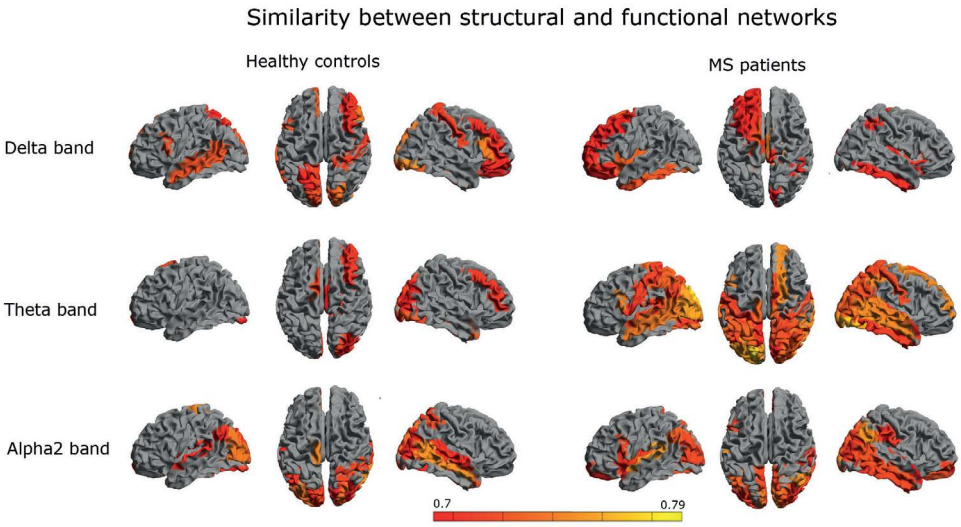

Figure 6 regional similarity: In order to quantify the regional overlap between structural and functional networks we computed a similarity measure as defined in Eq. 6 (see Methods). Colour coded maps of the similarity for each region are shown for different frequency bands. Colours were attributed to a region only if the similarity between modalities for that region was significant. Red indicates relatively low similarity and yellow indicates relatively high similarity. We observed that the similarity was especially high in temporo-posterior regions in MS patients (in the theta and alpha2 band), as well as for healthy subjects in the alpha2.

Functional connectivity and functional networks

Here we report that in comparison to healthy controls MS patients showed higher functional connectivity in the delta and theta band and lower functional connectivity in the alpha2 band. Our finding of higher functional connectivity in the theta band and lower functional connectivity in the alpha2 band in the MS group is in line with previous reports (Schoonheim et al. 2011;Tewarie et al. 2013b;Cover et al. 2006;Leocani et al. 2000). Higher functional connectivity in the delta band in MS patients has not been reported before. Possibly this increase in MS is related to the disease

duration of patients in our sample, which was longer than patients sampled in previous MEG studies (Schoonheim et al. 2011;Cover et al. 2006;Tewarie et al. 2013b). It is well known from other neurological diseases such as Parkinson's and Alzheimer's disease, that changes in the delta band are more prominent in later stages of the disease (Bosboom et al. 2009a; Bosboom et al. 2009b; de Haan W. et al. 2008). At this point it is still unclear what the relationship of higher functional connectivity in this band with cognitive functioning in MS is, but delta band oscillations in healthy subjects have been linked to decision making (Nacher et al. 2013),

Conventional functional network analyses revealed a higher path length in the theta band and lower clustering in the alpha2 band in MS patients compared to healthy controls. This indicates that functional networks in the theta band were less integrated (i.e. more regular), and in the alpha2 band less segregated (i.e. more random). MST differences between MS and control subjects were especially found in the alpha2 band, reflected by a lower MST leaf fraction, MST degree divergence and MST tree hierarchy in MS patients. An important aspect in complex networks is efficient communication between all nodes. This requires a small network diameter and simultaneous prevention of overloading of the central nodes. MST tree hierarchy measures the extent to which a tree displays this optimal configuration. In the present study, we found that functional networks in MS in the alpha2 band tend to shift away from this optimum level of hierarchy, towards a more path-like topology and thus a less integrated network. These results replicate our previous finding in an earlier MEG study of lower MST leaf fraction, MST degree divergence and MST tree hierarchy which was related to worse cognitive performance in MS patients (Tewarie et al. 2013). Here, we studied a different sample that only included relapsing remitting MS patients and patients with shorter disease duration.

Previous MEG studies using MSTs in other neurological diseases such as Parkinson's disease and neuroglioma have demonstrated that shifts towards a more path-like tree topology are signs of maladaptation and that these shifts are related to worse clinical outcome (Diessen et al. 2013; Olde Dubbelink et al. 2014; van Dellen E. et al. 2014). Our present findings seem to be in line with these results, which may suggest that neurological diseases have a final common pathway in terms of the MST. These MST findings may help to overcome contradictory findings that have been obtained with conventional network analyses in neurological diseases, as has been reported for Alzheimer's disease and epilepsy (Diessen et al. 2013; Tijms et al. 2013). These contradictory findings could be caused by the fact that conventional measures mix information about network topology and connectivity. The MST, in contrast, is insensitive to these confounds. In EEG studies, it has also been shown that the MST is sensitive to changes in network topology, rather than functional connectivity, in various cohorts and conditions, ranging from epilepsy, propofol-induced anesthesia, schizophrenia, network maturation during childhood, or changes in motor function (Boersma et al. 2012; Demuru et al. 2013; Lee et al. 2006; Lee et al. 2010; Ortega et al. 2008; Schoen et al. 2011). For a thorough review about the use of MSTs in brain network analysis we refer to (Stam et al. 2014).

Table 5: Correlations between cortical thickness correlations and functional connectivity

Frequency bands	MS patients	Healthy controls
Delta band	R = -0.01 P = 0.7	**R = 0.09** **P = 0.001**
Theta band	**R = 0.17** **P = 0.001**	R = -0.004 P = 0.6
Alpha2 band	**R = 0.13** **P = 0.001**	**R = 0.10** **P = 0.001**

Abbreviations: R = Mantel's correlation coefficient, P = p-value
Bold = significant after correcting for multiple comparisons by the FDR.

Structural co-variance versus functional networks

We observed that brain regions that co-vary in thickness were also related by functional interactions in MS. Importantly, this relationship could not be found by pairwise correlations between regional gray matter thickness and regional functional connectivity. This indicates that changes in functional connectivity to a region in MS cannot be explained by a simple process of gray matter atrophy of that same region, but only if atrophy of this region is associated with atrophy elsewhere. One of the hypothesis to explain the presence of structural co-variance is that these occur due to common and coordinated synaptogenesis in brain regions (Alexander-Bloch et al. 2013a). This coordinated synaptogenesis is probably influenced by genetics and by developmental relationships between cell-types and cortial layers. However, also synchronous firing between regions and neuronal populations can induce synaptogenesis (Katz and Shatz 1996). This process may underlie the finding that we found associations between functional interations and co-variation in cortical thickness in healthy controls as well as MS patients.

The relationship between co-variation in thickness and functional connectivity depended on group membership and frequency band. There seemed to be a shift in MS patients as within this group there was no association between the two in the delta band but appeared in the theta band. The shift of the association between functional connectivity and co-variation in thickness across frequency bands may be related to changes in the anatomy of cortical layers: from neurophysiology studies we know that infra-granular cortical layers are more involved in generation of delta oscillations and supra-granular cortical layers more in the generation of theta oscillations (Roopun et al. 2008). Although speculation, this might indicate that co-variation in thickness in MS is a process that is more associated with co-variation of supra-granular cortical layers and as a result of which the relationship between structural co-variance and theta band functional connectivity increases. If we assume that infra-granular layers are associated with delta band oscillations than factors such as retrograde axonal degeneration of infra-granular layers due to white matter lesions may lead to decrease in delta band functional connectivity. Longitudinal and animal studies are required to test these hypotheses in the future.

When examining graph theoretical findings of the structural co-variance and functional networks side by side we observed that topological changes for structural co-variance and functional networks in MS point in the same direction for the theta band, i.e. they become more regular. In contrast, we observed that functional networks in MS in the alpha2 band tend to become more random, which is in the opposite direction of the (more regular) structural co-variance network. Although this seems to be contradictory, a modeling study has revealed that the relationship between structural and functional network topology is in general non-trivial and may depend on local and global characteristics of neuronal populations.

To understand the relationship between structural co-variance and functional networks there is a need for a theoretical framework. For anatomical networks (based on physical connections rather than co-variance of cortical thickness) and functional networks such a framework has been investigated using various computational and analytical models (Deco et al. 2013; Honey et al. 2009; Tewarie et al. 2014; Zemanova et al. 2006). We recently reported that functional connectivity can be understood by taking into account the degree product between anatomically connected nodes and the Euclidean distance between brain regions (Tewarie et al. 2014). Also for structural co-variance networks there seem to be strong correlations for ROIs with short distance connections (along the diagonal of the structural connectivity matrices, see Figure S1). By using the distance vs degree model (see SI) it can be observed that both the distance between regions and the degree product in the structural co-variance networks are able to explain functional connectivity in MS patients and healthy controls (see Table S3 and S4). Together, these results suggest that nearby ROIs with similar cortical thickness variations may also be functionally related, if there is an anatomical connection present. It should be noted though that the causal direction of these relationships is as yet unclear; future empirical and theoretical studies need to investigate the relationship between structural co-variance-, structural connection-, and functional networks further.

Methodological considerations

Some limitations apply to this work. First, in the MEG source space analysis we selected the time-series of one voxel as a representation for the whole ROI. This is a reduction of data which may lead to loss of information. However, averaging over voxels in a ROI could introduce biases due to differences in ROI size leading to time-series having different signal-to-noise-ratios. Given these and other biases with averaging over sources we chose to adhere to methods used previously in our group (Hillebrand et al. 2012; Tewarie et al. 2013). Secondly, in the present study we obtained structural networks at the group-level while we obtained functional networks at the subject-level. This limits the analysis of the within subject relation between structure and function. In order to be able to interpret results within the context of previous studies, we performed group-level structural co-variance networks. For future research we will compute single-subject structural networks (Tijms et al. 2012). Thirdly, in the present study we did not analyze medication effects or potential network differences due to the disease type (relapsing remitting onset vs. progressive onset), since there was heterogeneous

use of medication and the number of progressive onset MS patients was too low to reliably estimate structural co-variance networks. We further need to mention that we did not predict clinical or cognitive dysfunction using the present data as this was not the aim of the present paper. Fourthly, in the present study we have focused on global aspects of the structural and functional networks. Future studies will also need to focus more on local properties of brain networks in MS, such as long distance correlations between individual nodes. Lastly, network analyses are accompanied with methodological difficulties such as differences in measurement scale across imaging modalities. To counter these difficulties, we removed scale effects by normalizing the weighted networks by its mean value, but this does not solve the influence of differences in the range of correlation values between two networks. The MST approach seems to be a valuable approach for the comparison of multi-modal networks, as it does not suffer from these normalization problems.

Conclusion

Both gray matter atrophy and disruption of functional brain networks are hypothesized to be important pathological substrates for physical disability and cognitive dysfunction in MS. The relationship between these pathological alterations is poorly understood, but clarifying this relationship could give more insight into disease mechanisms in MS. In the present study we aimed to bridge the gap between these two important pathological substrates of the disease. In the present cohort, we clearly demonstrated that alterations of functional connectivity in MS cannot be simply explained by regional gray matter atrophy itself as we have shown that localized measurements fail to take into account the inherent connectivity structure of the brain. Changes in functional network connectivity in MS could only be partially explained if complex and coordinated patterns of gray matter atrophy were taken into account. We have subsequently showed that there can be a complex interplay between these structural co-variance networks and functional networks in MS. Our work is a first step towards a better understanding of how differential pathological alterations are related to each other in MS.

SUPPLEMENTARY INFORMATION

Lesion segmentation.

T2 lesions were automatically segmented using a k Nearest Neighbour algorithm (Steenwijk et al., 2013). In short, this algorithm compares the brain voxels of a newly presented dataset to a collection of manually labelled examples in a feature space. The features included in this feature space are FLAIR and T1 signal intensity; normalized spatial coordinates x, y and z; and tissue type priors describing the suspected tissue class (i.e. CSF, GM or WM) to which the voxel would have belonged before the lesion developed (determined based on healthy control reference images). For every newly presented voxel, the algorithm locates the most similar examples in the training set and computes the probability of being a lesion. This probability map is subsequently thresholded to obtain a binary lesion segmentation. Importantly, the training set for automatic lesion segmentation was generated on images acquired identically (i.e. the same scanner and pulse sequences) as those in the present study.

Whole brain atrophy measures.

Normalized whole brain, GM and WM volumes were measured using the T1-weighted images and SIENAX (part of FSL 5.4, http://www.fmrib.ox.ac.uk/fsl). To minimize the impact of white matter lesions on the whole brain atrophy and cortical thickness measurements, the automated lesion-filling technique LEAP (Lesion Automated Preprocessing) was applied (Chard et al., 2010). This algorithm fills the hypo-intense lesions in the T1-weighted image with intensities comparable to the normal appearing white matter (NAWM) using the intensity histogram and the previously obtained lesion mask. After measuring normalized gray and white matter volume (NGMV and NWMV, respectively), normalized lesion volumes (NLV) were computed for all MS patients from the previously generated lesion masks. Normalization for head size was performed using the volumetric scaling factor calculated by SIENAX.

Table S1: Correlations between cortical thickness for each ROI and mean functional connectivity (PLI) for that ROI for MS patients.

	MS patients					
	Delta band		Theta band		Alpha2 band	
	R	p-value	R	p-value	R	p-value
Rectus_L	-0,05	0,62	0,02	0,84	-0,09	0,35
Olfactory_L	-0,11	0,27	0,02	0,86	0,11	0,27
Frontal_Sup_Orb_L	0,04	0,73	0,08	0,45	0,14	0,15
Frontal_Med_Orb_L	0,01	0,91	0,18	0,07	0,12	0,25
Frontal_Mid_Orb_L	0,09	0,35	-0,01	0,93	0,12	0,23
Frontal_Inf_Orb_L	0,09	0,39	-0,07	0,45	0,20	0,04
Frontal_Sup_L	0,03	0,79	0,12	0,23	0,10	0,33
Frontal_Mid_L	0,14	0,15	0,01	0,90	0,04	0,72
Frontal_Inf_Oper_L	0,13	0,18	0,00	0,99	-0,01	0,96
Frontal_Inf_Tri_L	0,21	0,04	0,09	0,38	-0,08	0,43
Frontal_Sup_Medial_L	0,02	0,82	0,04	0,69	0,09	0,35
Supp_Motor_Area_L	-0,01	0,93	-0,11	0,25	-0,07	0,49
Paracentral_Lobule_L	0,02	0,82	-0,13	0,19	0,23	0,02
Precentral_L	0,06	0,55	-0,02	0,82	0,10	0,33
Rolandic_Oper_L	0,07	0,49	0,10	0,32	0,12	0,22
Postcentral_L	0,10	0,33	-0,13	0,21	-0,01	0,90
Parietal_Sup_L	0,10	0,32	-0,06	0,52	0,06	0,53
Parietal_Inf_L	-0,03	0,76	0,05	0,59	0,22	0,03
SupraMarginal_L	0,13	0,19	-0,06	0,55	0,04	0,69
Angular_L	0,08	0,42	-0,15	0,14	0,15	0,14
Precuneus_L	0,01	0,88	-0,07	0,46	0,10	0,33
Occipital_Sup_L	0,08	0,43	0,09	0,38	0,06	0,52
Occipital_Mid_L	0,16	0,11	-0,04	0,73	0,02	0,81
Occipital_Inf_L	0,02	0,81	0,06	0,58	*0,21*	*0,04*
Calcarine_L	0,01	0,92	-0,19	0,06	0,06	0,57
Cuneus_L	0,07	0,50	-0,01	0,90	0,03	0,75
Lingual_L	-0,11	0,27	-0,08	0,42	0,02	0,82
Fusiform_L	0,12	0,23	0,11	0,29	0,18	0,07
Heschl_L	0,08	0,40	-0,05	0,62	0,10	0,31
Temporal_Sup_L	0,04	0,70	0,05	0,65	-0,05	0,60
Temporal_Mid_L	0,10	0,33	0,05	0,58	0,11	0,25
Temporal_Inf_L	0,01	0,91	0,15	0,13	0,12	0,23
Temporal_Pole_Sup_L	0,19	0,06	0,06	0,58	0,07	0,50
Temporal_Pole_Mid_L	-0,14	0,18	-0,10	0,33	*0,19*	*0,05*
ParaHippocampal_L	0,12	0,23	0,11	0,28	0,06	0,57
Cingulum_Ant_L	0,17	0,09	-0,08	0,43	0,07	0,50

Table S1: Continued

	MS patients					
	Delta band		Theta band		Alpha2 band	
	R	p-value	R	p-value	R	p-value
Cingulum_Mid_L	-0,10	0,31	0,10	0,33	0,07	0,50
Cingulum_Post_L	-0,07	0,50	-0,02	0,86	0,04	0,71
Insula_L	0,10	0,32	0,02	0,85	0,02	0,84
Rectus_R	0,06	0,54	-0,03	0,79	0,01	0,90
Olfactory_R	-0,07	0,50	0,16	0,10	0,07	0,51
Frontal_Sup_Orb_R	-0,01	0,95	-0,05	0,63	0,08	0,42
Frontal_Med_Orb_R	0,06	0,57	0,14	0,16	0,09	0,36
Frontal_Mid_Orb_R	-0,09	0,35	0,01	0,92	0,07	0,47
Frontal_Inf_Orb_R	-0,06	0,58	-0,03	0,73	0,08	0,40
Frontal_Sup_R	-0,03	0,79	-0,04	0,66	0,10	0,30
Frontal_Mid_R	0,05	0,61	0,00	1,00	0,19	0,06
Frontal_Inf_Oper_R	-0,04	0,68	-0,02	0,82	0,13	0,20
Frontal_Inf_Tri_R	-0,12	0,22	-0,14	0,16	-0,09	0,37
Frontal_Sup_Medial_R	0,14	0,16	0,09	0,37	0,16	0,11
Supp_Motor_Area_R	0,08	0,41	-0,07	0,48	0,05	0,61
Paracentral_Lobule_R	0,06	0,55	0,00	0,98	*0,22*	*0,03*
Precentral_R	-0,07	0,48	0,05	0,65	-0,01	0,92
Rolandic_Oper_R	0,18	0,07	0,10	0,31	0,03	0,78
Postcentral_R	-0,03	0,75	-0,05	0,63	0,03	0,73
Parietal_Sup_R	-0,15	0,13	-0,02	0,84	-0,06	0,55
Parietal_Inf_R	-0,01	0,89	0,00	0,97	-0,09	0,36
SupraMarginal_R	0,03	0,77	-0,11	0,27	0,00	1,00
Angular_R	0,17	0,08	-0,01	0,92	0,18	0,07
Precuneus_R	*0,22*	*0,03*	-0,05	0,61	-0,08	0,43
Occipital_Sup_R	0,02	0,83	-0,11	0,28	0,10	0,30
Occipital_Mid_R	0,06	0,57	-0,17	0,09	0,14	0,15
Occipital_Inf_R	0,03	0,77	0,04	0,71	0,06	0,52
Calcarine_R	0,07	0,49	-0,01	0,92	-0,01	0,95
Cuneus_R	0,15	0,14	0,02	0,83	*0,19*	*0,05*
Lingual_R	0,07	0,47	-0,05	0,61	0,10	0,31
Fusiform_R	0,07	0,51	0,08	0,42	-0,04	0,66
Heschl_R	-0,02	0,82	0,10	0,32	0,02	0,83
Temporal_Sup_R	0,13	0,19	-0,05	0,62	0,09	0,38
Temporal_Mid_R	-0,03	0,75	0,05	0,59	0,09	0,34
Temporal_Inf_R	0,04	0,72	0,03	0,78	0,13	0,18
Temporal_Pole_Sup_R	-0,01	0,88	0,02	0,87	*0,21*	*0,04*
Temporal_Pole_Mid_R	0,00	0,98	0,10	0,34	0,01	0,94

Table S1: Continued

	MS patients					
	Delta band		Theta band		Alpha2 band	
	R	p-value	R	p-value	R	p-value
ParaHippocampal_R	0,10	0,33	0,04	0,66	0,05	0,62
Cingulum_Ant_R	0,04	0,65	-0,11	0,28	-0,04	0,69
Cingulum_Mid_R	0,01	0,90	-0,07	0,45	0,07	0,46
Cingulum_Post_R	-0,05	0,62	-0,08	0,44	0,17	0,10
Insula_R	0,01	0,92	0,06	0,56	0,06	0,58

Table S2: Correlations between cortical thickness for each ROI and mean functional connectivity (PLI) for that ROI for healthy controls.

	Healthy controls					
	Delta band		Theta band		Alpha2 band	
	R	p-value	R	p-value	R	p-value
Rectus_L	-0,05	0,15	*0,02*	*0,04*	-0,09	0,96
Olfactory_L	-0,11	0,16	0,02	0,99	0,11	0,09
Frontal_Sup_Orb_L	0,04	0,89	0,08	0,67	0,14	0,20
Frontal_Med_Orb_L	0,01	0,50	0,18	0,77	0,12	0,97
Frontal_Mid_Orb_L	0,09	0,42	*-0,01*	*0,05*	0,12	0,89
Frontal_Inf_Orb_L	0,09	0,96	-0,07	0,19	0,20	0,58
Frontal_Sup_L	0,03	0,68	0,12	0,42	0,10	0,34
Frontal_Mid_L	0,14	0,15	0,01	0,90	0,04	0,33
Frontal_Inf_Oper_L	0,13	0,32	0,00	0,62	-0,01	0,15
Frontal_Inf_Tri_L	0,21	0,36	0,09	0,52	-0,08	0,65
Frontal_Sup_Medial_L	0,02	0,28	0,04	0,29	0,09	0,78
Supp_Motor_Area_L	-0,01	0,12	-0,11	0,07	-0,07	0,41
Paracentral_Lobule_L	0,02	0,11	-0,13	0,10	0,23	0,33
Precentral_L	0,06	0,82	-0,02	0,36	0,10	0,41
Rolandic_Oper_L	0,07	0,51	0,10	0,49	0,12	0,65
Postcentral_L	0,10	0,30	-0,13	0,85	-0,01	0,51
Parietal_Sup_L	0,10	0,76	-0,06	0,74	0,06	0,27
Parietal_Inf_L	-0,03	0,39	0,05	0,69	0,22	0,91
SupraMarginal_L	0,13	0,55	-0,06	0,44	0,04	0,32
Angular_L	0,08	0,29	-0,15	0,38	0,15	0,84
Precuneus_L	0,01	0,74	-0,07	0,94	0,10	0,49
Occipital_Sup_L	0,08	0,14	0,09	0,22	0,06	0,40
Occipital_Mid_L	0,16	0,02	-0,04	0,87	0,02	0,17
Occipital_Inf_L	0,02	0,51	0,06	0,81	0,21	0,90
Calcarine_L	*0,01*	*0,02*	-0,19	0,30	0,06	0,46
Cuneus_L	0,07	0,25	-0,01	0,30	0,03	0,41

Table S2: Continued

	Healthy controls					
	Delta band		Theta band		Alpha2 band	
	R	p-value	R	p-value	R	p-value
Lingual_L	-0,11	0,25	-0,08	0,55	0,02	0,83
Fusiform_L	0,12	0,71	0,11	0,22	0,18	0,93
Heschl_L	0,08	0,27	-0,05	0,51	0,10	0,35
Temporal_Sup_L	0,04	0,37	0,05	0,61	-0,05	0,12
Temporal_Mid_L	0,10	0,37	0,05	0,12	0,11	0,16
Temporal_Inf_L	0,01	0,96	0,15	0,72	0,12	0,36
Temporal_Pole_Sup_L	0,19	0,57	0,06	0,96	0,07	0,09
Temporal_Pole_Mid_L	-0,14	0,50	-0,10	0,45	0,19	0,77
ParaHippocampal_L	0,12	0,17	0,11	0,02	0,06	0,41
Cingulum_Ant_L	0,17	0,77	-0,08	0,62	0,07	0,41
Cingulum_Mid_L	-0,10	0,51	0,10	0,87	0,07	0,84
Cingulum_Post_L	-0,07	0,62	-0,02	0,00	0,04	0,32
Insula_L	0,10	0,74	0,02	0,76	0,02	0,11
Rectus_R	0,06	0,33	-0,03	0,89	0,01	0,06
Olfactory_R	-0,07	0,45	0,16	0,99	0,07	0,95
Frontal_Sup_Orb_R	-0,01	1,00	-0,05	0,17	0,08	0,25
Frontal_Med_Orb_R	0,06	0,92	0,14	0,29	0,09	0,12
Frontal_Mid_Orb_R	-0,09	0,49	0,01	0,59	0,07	0,25
Frontal_Inf_Orb_R	-0,06	0,84	-0,03	0,93	0,08	0,85
Frontal_Sup_R	-0,03	0,86	-0,04	0,68	0,10	0,47
Frontal_Mid_R	0,05	0,53	0,00	0,82	*0,19*	*0,01*
Frontal_Inf_Oper_R	-0,04	0,26	*-0,02*	*0,03*	0,13	0,72
Frontal_Inf_Tri_R	-0,12	0,74	-0,14	0,90	*-0,09*	*0,03*
Frontal_Sup_Medial_R	0,14	0,32	0,09	0,90	0,16	0,17
Supp_Motor_Area_R	0,08	0,55	-0,07	0,97	0,05	0,40
Paracentral_Lobule_R	0,06	0,42	0,00	0,28	0,22	0,72
Precentral_R	-0,07	0,62	0,05	0,58	-0,01	0,99
Rolandic_Oper_R	0,18	0,53	*0,10*	*0,03*	0,03	0,65
Postcentral_R	-0,03	0,42	-0,05	0,12	0,03	0,85
Parietal_Sup_R	-0,15	0,87	-0,02	0,92	-0,06	0,55
Parietal_Inf_R	-0,01	0,06	0,00	0,40	-0,09	0,55
SupraMarginal_R	0,03	0,92	-0,11	0,31	0,00	0,92
Angular_R	0,17	0,58	-0,01	0,58	0,18	0,30
Precuneus_R	0,22	0,29	-0,05	0,21	-0,08	0,12
Occipital_Sup_R	0,02	0,97	-0,11	0,13	0,10	0,79
Occipital_Mid_R	0,06	0,75	-0,17	0,62	0,14	0,22
Occipital_Inf_R	0,03	0,29	0,04	0,50	*0,06*	*0,00*

Table S2: Continued

	Healthy controls					
	Delta band		Theta band		Alpha2 band	
	R	p-value	R	p-value	R	p-value
Calcarine_R	0,07	0,33	-0,01	0,01	-0,01	0,34
Cuneus_R	0,15	0,06	0,02	0,01	0,19	0,61
Lingual_R	0,07	0,73	-0,05	0,10	0,10	0,81
Fusiform_R	0,07	0,85	0,08	0,81	-0,04	0,95
HeschI_R	-0,02	0,74	0,10	0,28	0,02	0,15
Temporal_Sup_R	0,13	0,77	-0,05	0,23	0,09	0,44
Temporal_Mid_R	-0,03	0,97	0,05	0,39	0,09	0,27
Temporal_Inf_R	0,04	0,60	0,03	0,49	0,13	0,89
Temporal_Pole_Sup_R	-0,01	0,34	0,02	0,30	0,21	0,20
Temporal_Pole_Mid_R	0,00	0,40	0,10	0,14	0,01	0,59
ParaHippocampal_R	0,10	0,09	0,04	0,96	0,05	0,20
Cingulum_Ant_R	0,04	0,99	-0,11	0,27	-0,04	0,60
Cingulum_Mid_R	0,01	0,52	-0,07	0,92	0,07	0,44
Cingulum_Post_R	-0,05	0,04	-0,08	0,32	0,17	0,48
Insula_R	0,01	0,47	0,06	0,18	0,06	0,62

Table S3: Correlations between cortical thickness correlations and functional connectivity. Analysis were performed for negative and positive cortical thickness correlations separately.

	Frequency bands	MS patients	Healthy controls
Positive thickness correlations	Delta band	R = -0.006	**R = 0.09**
		P = 0.6	**P = 0.001**
	Theta band	**R = 0.16**	R = -0.01
		P = 0.001	P = 0.7
	Alpha2 band	**R = 0.12**	**R = 0.10**
		P = 0.001	**P = 0.001**
Negative thickness correlations	Delta band	R = -0.01	**R = 0.07**
		P = 0.7	**P = 0.001**
	Theta band	**R = 0.13**	R = 0.004
		P = 0.001	P = 0.6
	Alpha2 band	**R = 0.11**	**R = 0.07**
		P = 0.001	**P = 0.001**

Abbreviations: R = Mantel's correlation coefficient, P = p-value
Bold = significant after correcting for multiple comparisons by the FDR.

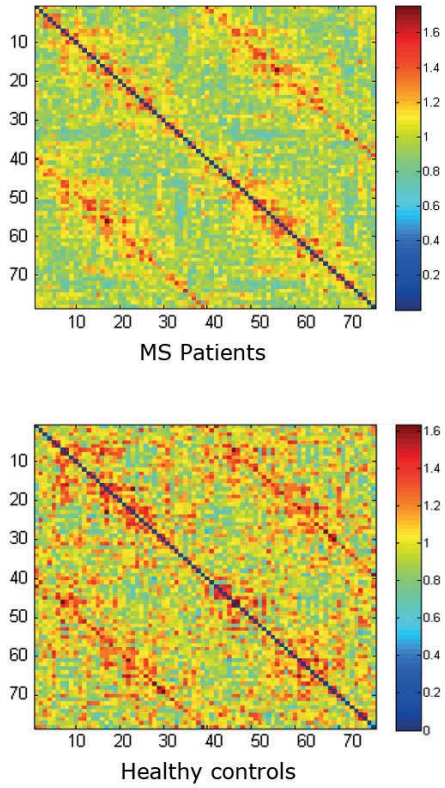

Figure S1 Structural co-variance and functional connectivity matrices: The functional connectivity matrices for the delta, theta and alpha2 band are depicted for healthy controls (first row) and MS patients (second row). Note four blocks in the functional connectivity matrices in different frequency bands corresponding to temporo-posterior regions. Structural co-variance networks for MS patients and healthy controls are depicted in the third row. Note the strong correlations near the diagonal and near two off-diagonals in MS patients as well as in healthy controls. Especially, correlations near the diagonal mainly refer to correlations between closely spaced regions. This can be confirmed by inspection of the inverse distance matrix (third row), where connections between closely spaced regions are depicted in red. The fourth row depicts the degree product matrix of MS patients and healthy controls. Note the overall high values in four large blocks which especially include frontal and parietal areas.

Chapter 9

Functional brain networks: linking thalamic atrophy to clinical disability in multiple sclerosis, a multimodal fMRI and MEG study

P. Tewarie, M.M. Schoonheim, D.I. Schouten, C.H. Polman, L.J. Balk, B.M.J. Uitdehaag, J.J.G. Geurts, A. Hillebrand, F. Barkhof, C.J. Stam

Human brain mapping 2014 Oct: (Epub ahead of print)

ABSTRACT

Thalamic atrophy is known to be one of the most important predictors for clinical dysfunction in multiple sclerosis (MS). As the thalamus is highly connected to many cortical areas, this suggests that thalamic atrophy is associated with disruption of cortical functional networks. We investigated this thalamo-cortical system to explain the presence of physical and cognitive problems in MS. Functional magnetic resonance imaging (fMRI) and magnetoencephalography (MEG) were performed in 86 MS patients and 21 healthy subjects. We computed cortical functional networks for fMRI and MEG by respectively the Pearson´s correlation coefficient and the phase lag index using the same AAL atlas for both modalities. Thalamo-cortical functional connectivity was only estimated using fMRI. We computed conventional network metrics such as clustering coefficient and path length and analyzed the minimum spanning tree (MST), a sub-network and backbone of the original network. MS patients showed reduced thalamic volumes and increased thalamo-cortical connectivity. MEG cortical functional networks showed a lower level of integration in MS in terms of the MST, whereas fMRI cortical networks did not differ between groups. Lower integration of MEG cortical functional networks was both related to thalamic atrophy as well as to increased thalamo-cortical functional connectivity in fMRI, and to worse cognitive and clinical status. The present study demonstrated for the first time that thalamic atrophy is associated with global disruption of cortical functional networks in MS and this global disruption of network activity was related to worse cognitive and clinical function in MS.

INTRODUCTION

Multiple sclerosis (MS) is a chronic demyelinating and neurodegenerative disease, leading to both cognitive impairment and physical disability. Thalamic atrophy and disruption of cortical functional networks have both been reported and found to be associated with cognitive impairment and physical disability in MS (Batista et al. 2012; Gamboa et al. 2013; Houtchens et al. 2007). Based on the widespread connectivity of the thalamus with cortical regions throughout the brain one would expect a mutual influence between thalamic atrophy and disruption of cortical functional networks in MS. However, the relationship between thalamic atrophy and cortical functional networks is largely unknown. Shedding more light on this relationship might help to understand disease mechanisms and clinical and cognitive deterioration in MS.

Cortical functional networks can be analyzed using metrics from modern network theory where a network is considered as a set of nodes and links (Bullmore and Sporns 2012; Stam and van Straaten 2012). Nodes refer to brain regions and links to communication between distinct brain regions (i.e. functional connectivity). Cortical functional networks robustly show a highly non-random organization that is characterized by dense local connectivity and relatively sparse long range connections (Bullmore and Sporns 2009). Such a topology has been associated with a balance of integration and segregation together with a minimization of wiring costs and maximization of efficiency (Bullmore and Sporns 2012). However, the quantification and comparison of functional network topology is accompanied by methodological problems as associated with differences in connectivity density or average connectivity strength (Fornito et al. 2013; van Wijk et al. 2010). Usage of conventional metrics leads to mixing of information about topology with information about functional connectivity. Even corrections for these biases by normalization procedures are not adequate (van Wijk et al. 2010). Computation of a minimum spanning tree (MST), an acyclic sub-network containing the strongest connections, enables comparison of networks without the aforementioned biases (see Methods for more details) (Lee et al. 2006; Lee et al. 2010; Schoen et al. 2011).

The organization of functional networks in MS has received relatively little attention as most studies have merely focused on changes in raw functional connectivity (Cader et al. 2006; Hawellek et al. 2011; Parisi et al. 2012; Prakash et al. 2011; Rocca et al. 2007; Rocca et al. 2012; Valsasina et al. 2011). Previous studies on the organization of functional networks in MS using either functional magnetic resonance imaging (fMRI) or magnetoencephalography (MEG) have demonstrated less integration in functional networks (Gamboa et al. 2013; Hardmeier et al. 2012; Schoonheim et al. 2011). We recently showed in an MEG study that, in comparison to healthy subjects, the MSTs of MS patients are indeed characterized by less integration of information and loss of hierarchical structure of functional networks, which was related to worse cognitive performance in MS (Tewarie et al. 2013a). Previous fMRI and MEG studies on the relationship between functional network connectivity and thalamic atrophy have revealed that abnormalities in functional connectivity between the thalamus and the cortex or even between cortical areas was associated with thalamic

atrophy, especially for occipito-parietal and motor areas (Dogonowski et al. 2013; Schoonheim et al. 2013b; Tewarie et al. 2013b; Tona et al. 2014). However, these previous studies were performed using various modalities and methodologies, hampering comparison of the results of these studies. A multi-modal imaging approach employing the same methodology on both fMRI and MEG may help to quantify functional network disruption in MS and may further increase the interpretability of these results between modalities. Furthermore, the high temporal resolution of MEG and the ability of fMRI to assess functional connectivity between the cortex and the thalamus may provide complementary information, and therefore be an advantage over uni-modal functional imaging approaches.

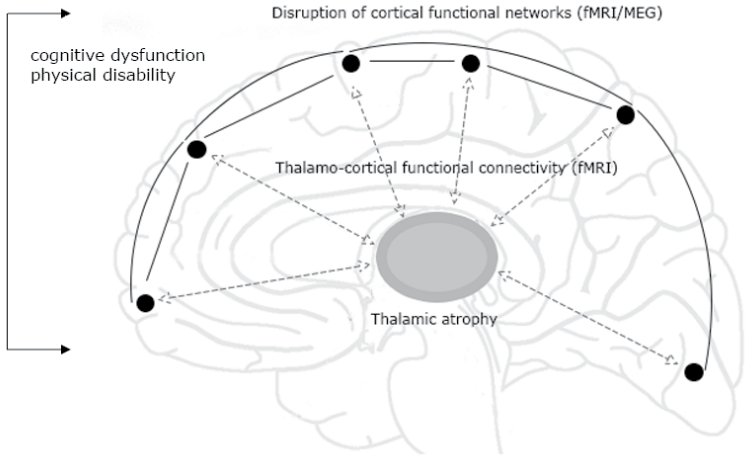

Figure 1: The thalamo-cortical loop. Depicted is our hypothesis: a loop consisting of the thalamus connected to the cortex through thalamo-cortical connections is affected. This is potentially caused by thalamic atrophy, disruption of cortical functional networks and changes in BOLD thalamo-cortical functional connectivity. We further hypothesize that these alterations are interrelated and important for explaining clinical and cognitive dysfunction.

In the present study we included subjects that have been described in previous work, where we demonstrated that thalamic atrophy and related increased thalamo-cortical functional connectivity (fMRI) were important features in MS patients (Schoonheim et al. 2014). The novel aspect of the present study is that we now link thalamic atrophy and changes in thalamo-cortical functional connectivity to the organization of cortical functional networks in MS, using both fMRI and MEG. Therefore, the aim of the present study is to test the hypothesis that thalamic atrophy and a disintegration of cortical functional networks co-occur and are linked by thalamo-cortical functional connectivity. We further hypothesize that disruption of this thalamo-cortical system is associated with clinical and cognitive dysfunction (Figure 1).

METHODS

Study design

In this cross-sectional study, we analyzed cortical functional networks, thalamic volumes, thalamo-cortical functional connectivity, neurological- and neuropsychological status in MS patients and healthy subjects. Differences in thalamic volumes and thalamo-cortical functional connectivity between MS patients and healthy subjects from this cohort (in a larger but overlapping group) have been reported before (Schoonheim et al. 2014; Schoonheim et al. 2012; Schoonheim et al. 2013b) and will be reported in this paper as descriptive information and as supplementary material. The aim of the present study was, however, to investigate if these changes were related to disruption of cortical functional networks, where we also made use of a novel atlas-based approach (not reported before). We quantified resting state cortical functional networks by using MEG and fMRI, whereas we quantified thalamo-cortical functional connectivity by using fMRI. For both MEG and fMRI obtained cortical functional networks we computed conventional graph theoretical measures such as the clustering coefficient and path length to increase the interpretability of our results within the context of previous studies. In addition, we investigated MST measures (MST leaf fraction, MST diameter, MST degree divergence and MST tree hierarchy), since these are unaffected by potential biases that may arise as a consequence of constructing networks from different imaging modalities. An overview of the applied methods is given in Figure 2.

Participants

All MS patients were part of a six-year follow-up of an early inception cohort and were also included in previous studies (Schoonheim et al. 2014; Schoonheim et al. 2012; Schoonheim et al. 2013a; Schoonheim et al. 2013b). In the present study we only included subjects who underwent both fMRI and MEG, during their most recent visit at around six years after diagnosis. Initially, 100 patients (mean age 41.6 ± 8.9 years) and 24 healthy subjects (mean age 41.8 ± 10.3 years) were included in this study and were matched for gender, age and education. 17 subjects were excluded from the present study due to absent or corrupt fMRI data (N=4), mismatch between normalized MRI and template before applying beamforming (N=2), an excess of noise and artefacts in the raw MEG data (N=5) and having a diagnosis of clinical isolated syndrome not converted to clinically definite MS (N=6). Consequently, 86 MS patients (mean age 41.6 ± 8.8 years) and 21 subjects (mean age 42.5 ± 10.3 years) remained in the present study (Table 1). Subsequently, all patients were diagnosed with clinically-definite multiple sclerosis by experienced neurologists and all patients were recruited from the VU University Medical Centre (Polman et al. 2005). Ethics approval for the present study was granted by the institutional ethics review board and written informed consent was obtained from all subjects prior to participation.

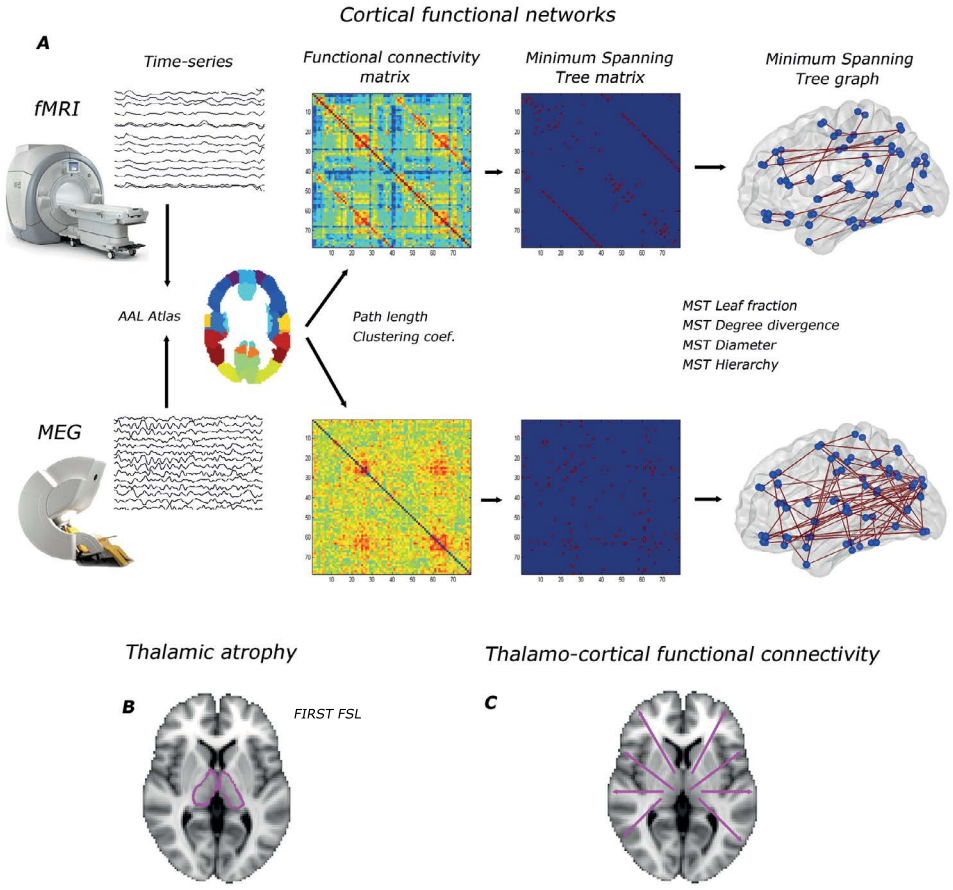

Figure 2: Overview of applied methods. A) cortical functional networks: for both fMRI and MEG, time signals were projected onto the cortical AAL atlas consisting of 78 regions. For MEG, beamforming was used as source localization method. Based on time signals in the AAL atlas we computed functional connectivity matrices (weighted networks) by the Pearson correlation coefficient and the Phase lag index for fMRI and MEG respectively. The average functional connectivity matrices over subjects are displayed (alpha2 band for MEG). Path length and clustering coefficient were computed based on these weighted networks. Subsequently, we computed the minimum spanning tree and the corresponding MST metrics; B) thalamic atrophy was computed using FIRST (FSL); C) we computed BOLD thalamo-cortical functional connectivity from all 78 cortical regions to the thalamus and averaged over hemispheres.

Neurological and neuropsychological assessment

Participants underwent a set of neurological and neuropsychological tests as described earlier (Schoonheim et al. 2012). The physical disability of MS patients was evaluated using the Expanded Disability Status Scale (EDSS) (Kurtzke, 1983). In order to assess cognitive functioning, we used an expanded version of the brief repeatable battery for neurological disease (BRB-N), which was administered to all subjects. This set of neuropsychological tests included the selective reminding

test (SRT), the 10/36 spatial recall test (SPART), the symbol digit modalities test (SDMT), the word list generation test (WLG), the concept shifting test (CST), the Stroop color-word test and the memory comparison test (MCT) (see previous studies for details (Schoonheim et al. 2011; Schoonheim et al. 2012)). Z-scores were summarized into seven cognitive domains: executive functioning (CST, WLG), verbal memory (SRT), information processing speed (SDMT), visuospatial memory (SPART), working memory (MCT), attention (Stroop) and psychomotor speed (CST, SDMT). In addition, a Z–score for overall cognition was calculated by averaging Z-scores over all separate cognitive domains. This overall cognition score was used in further analyses. The rationale behind using an overall cognition score was to reduce the number of statistical tests in order to avoid correction for a large number of tests.

Data acquisition

MRI scans were performed using a 3T-MRI system (GE SignaHDxt) with a 3D-T1 weighted fast spoiled gradient-echo (FSPGR, TR 7.8 ms, TE 3.0 ms, TI 450 ms, flip angle 12, 0.9x0.9x1 mm voxel size), 2D T2-weighted fast spin-echo (repetition time 9680 ms, echo time 22/112 ms, flip angle 90, 3 mm contiguous axial slices, in-plane resolution 0.6x0.6 mm), 2D spin-echo T1-weighted imaging (repetition time 475 ms, echo time 9.0 ms, flip angle 90, 3 mm contiguous axial slices, inplane resolution 0.7x1 mm), and a resting-state fMRI sequence containing 202 volumes, of which the first two were discarded (EPI, TR 2200 ms, TE 35 ms, flip angle 80, 3 mm contiguous axial slices covering the entire brain, in-plane resolution 3.3x3.3 mm). All lesion volumetric analyses were performed using Alice (Perceptive informatics Inc.) applying a local thresholding technique. Pre-processing was performed by an experienced rater (MMS) using FSL 5 (FMRIB's Software Library, http://www.fmrib.ox.ac.uk/fsl), and included brain extraction for the FSPGR sequence. Total gray matter (NGMV), total white matter (NWMV), and whole brain volumes (NBV), corrected for head size, were measured using SIENAX (Smith et al. 2002). Thalamic volumes were measured using FIRST (part of FSL), providing left and right volumes for the thalamus and were corrected for head size using the V-scaling factor of SIENAX. Left and right thalamic volumes were summed to give the total thalamic volume. The fMRI data was processed as part of the pipeline of MELODIC (part of FSL) using default settings, including masking, motion correction, smoothing and high-pass filtering (100s cut-off). All pre-processed fMRI images were kept in subject space; the automated anatomical labeling (AAL) atlas was non-linearly registered back to each subject using nearest-neighbour interpolation. This was done by inverting the registration steps calculated by a boundary-based registration (BBR, part of FSL) between fMRI and 3D-T1 sequences, and non-linear registration between 3D-T1 and standard space using FNIRT (part of FSL). After registration, the average time-series were calculated for each individual AAL and thalamus region, which were used for the connectivity analyses.

MEG data were recorded using a 306-channel whole-head MEG system (Elekta Neuromag, Oy, Helsinki, Finland) while participants were in a supine position in a magnetically shielded room (Vacuumschmelze, Hanau, Germany). Fluctuations in magnetic field strength were recorded during

a no-task, eyes-open condition for three minutes (not analysed here) and eyes-closed condition for five consecutive minutes with a sample frequency of 1250 Hz. An anti-aliasing filter of 410 Hz and a high-pass filter of 0.1 Hz were applied online and other artefacts were removed offline using the temporal extension of Signal Space Separation (tSSS) in MaxFilter software (Elekta Neuromag Oy, version 2.2.10) (Taulu and Hari 2009; Taulu and Simola 2006). Channels that were malfunctioning during the recording, for example due to excessive noise, were identified by automatic and visual inspection of the data and removed before applying tSSS. Automatic inspection involved Signal Space Separation (SSS) (Taulu et al., 2004). The number of excluded channels varied between one and twelve and did not differ between MS patients and healthy subjects (Mann-Whitney $U = 7.23$, $p = 0.076$). SSS and tSSS method can be explained as follows: SSS decomposes the recorded magnetic fields into those that have their origin inside the helmet (brain signals) and those that originate outside the helmet (noise signals). The noise signals are then discarded. The temporal extension of SSS was used to remove noise signals that SSS failed to discard, typically from noise sources near the head. Such noise signals have a signature in both the brain and noise signals, and can therefore be detected (and discarded) using a simple correlation approach. In this work we used a subspace correlation limit of 0.9 and a sliding window of 10 seconds, as done in previous studies (Tewarie et al. 2014b; van Dellen E. et al. 2014; van Dellen et al. 2013). The head position relative to the MEG sensors was recorded continuously using the signals from four head-localization coils. The head-localization coil positions were digitized, as well as the outline of the participants scalp (ff500 points), using a 3D digitizer (3SpaceFastTrack, Polhemus, Colchester, VT, USA). Each subject's scalp surface was co-registered to their structural MRI using a surface-matching procedure, with an estimated resulting accuracy of 4 mm (Whalen et al. 2008). A single best fitting sphere was fitted to the outline of the scalp as obtained from the co-registered MRI, which was used as a volume conductor model for the beamformer approach described below.

Estimation of functional connectivity

For fMRI we computed functional connectivity between BOLD signals of 78 cortical AAL regions by computing the Pearson correlation coefficient (Gong et al. 2009). To all functional connectivity values, based on these Pearson correlation coefficients, we added one and subsequently divided by two to avoid negative associations. This transformation was performed to ensure that all matrix elements were positive since most algorithms that we used to compute topological measures require positive weights. Subsequently, network parameters were computed on this cortical fMRI network (see below). In addition, average functional connectivity was also computed for the left and right thalamus, where we averaged over hemispheres, i,e, for each hemisphere we averaged functional connectivity values from the left or right thalamus to one of the 39 AAL regions in the corresponding hemisphere. For clarity, thalamo-cortical functional connectivity is in the rest of the paper mentioned as BOLD thalamo-cortical functional connectivity to remind the reader that this measure is exclusively estimated by fMRI.

For MEG, a beamformer approach was adopted to map MEG data from sensor level to source space (Hillebrand et al. 2012). First the co-registered MRI was spatially normalized to a template MRI using the SEG-toolbox in SPM8 (Ashburner and Friston 2005; Weiskopf et al. 2011). The cortical regions of the automated anatomical labeling (AAL) atlas were used to label the voxels in a subject's normalized co-registered MRI (Tzourio-Mazoyer et al. 2002). Subcortical structures were removed, and the voxels in the remaining 78 cortical regions of interest (ROIs) were used for further analysis (Gong et al. 2009), after a non-linear inverse transformation to the patient's co-registered MRI. Next, neuronal activity in the labeled voxels was reconstructed using a scalar beamformer implementation (Elekta Neuromag Oy, beamformer, version 2.1.27) similar to Synthetic Aperture Magnetometry (Robinson and Vrba 1999). Briefly, this beamformer sequentially reconstructs the activity for each voxel in a predefined grid covering the entire brain (spacing 2 mm) by selectively weighting the contribution from each MEG sensor to a voxel's time-series. The beamformer weights are based on the co-variance of the recorded time-series and the forward solution (lead field) of a dipolar source at the voxel location, where data were band-pass filtered from 0.5–48 Hz. A time-window of, on average, 299 seconds (range healthy subjects patients 258-297s; range MS patients 159-595s, independent t-test, $t = 1.45$, $p = 0.15$) was used to compute the co-variance matrix of the recorded time-series. Singular value truncation was used when inverting the data covariance matrix, using a default setting of 1e-06 for the ratio between the largest and smallest acceptable singular value. The sensor-level data were subsequently projected through the beamformer weights, resulting in a time series for each voxel. Each ROI contains many voxels and the number of voxels per ROI differed. In order to represent a ROI by a single time-series, we selected, for each ROI and frequency band separately, the voxel with maximum power in that frequency band. Six frequency bands were analyzed: delta (0.5–4 Hz), theta (4–8 Hz), lower alpha (8–10 Hz), upper alpha (10–13 Hz), beta (13–30 Hz), and lower gamma bands (30–48 Hz). The time-series were visually inspected for each subject and frequency band separately and the first 20 artefact-free epochs of 4096 samples (3.2768 seconds) were selected from the ROI time-series using Brainwave (version 0.9.98 available from http://home.kpn.nl/stam7883/brainwave.html).

Then, for each subject and MEG epoch separately, we computed the phase lag index (PLI) between the time-series for each pair of ROIs to obtain a (78x78) functional connectivity matrix. For this purpose, the phase was computed by taking the argument of the analytical signal (Stam et al. 2007). The PLI calculates the asymmetry of the distribution of (instantaneous) phase differences between two time-series:

$$PLI = |\langle \mathrm{sign}[\sin(\Delta\varphi(t_k))]\rangle| \quad (1)$$

where the phase difference $\Delta\varphi$ is defined in the interval $(-\pi, \pi)$, $\langle\rangle$ denotes the mean value, sign stands for signum function, $||$ indicates the absolute value, and t_k corresponds to time with $k = 1,\ldots,N_s$ where N_s is the number of samples. The PLI ranges between 0 (completely symmetric phase distribution) and 1 (completely asymmetric phase distribution). As field spread and volume

conduction causes a zero phase lag (modulus π) between two time-series, this hardly influences the PLI since this metric captures only consistent, non-zero, phase lag between two time-series (Stam et al. 2007). For PLI analyses we averaged for each subject the PLI for the twenty epochs, yielding one PLI matrix per subject for each frequency band.

Network analysis

Nodes in all networks were defined by the 78 cortical AAL regions. For fMRI this indicated that left and right thalami were not included as nodes. This was necessary to keep the size of MEG and fMRI functional networks equal to preserve comparability between modalities (see also the methodological considerations in the discussion (Fornito et al. 2013; van Wijk et al. 2010)). All networks were weighted: in fMRI functional networks links had weights corresponding to the Pearson correlation coefficient between AAL regions and in MEG functional networks links had weights corresponding to the PLI values between AAL regions. For all networks we computed weighted network properties (average connectivity, clustering coefficient, path length and their normalized versions) and the minimum spanning tree (MST; see below). This was done for each subject, epoch and frequency band for the MEG functional networks (where for each subject frequency-band specific averages over the 20 epochs were then computed), and for each subject for fMRI functional networks.

The weighted clustering coefficient C is a measure of segregation and is defined as the geometric mean of triangles around a node (Rubinov and Sporns 2010):

$$C_i = \frac{\sum_{k \neq i} \sum_{\substack{l \neq i \\ l \neq k}} w_{ik} w_{il} w_{kl}}{\sum_{k \neq i} \sum_{\substack{l \neq i \\ l \neq k}} w_{ik} w_{il}} \qquad (2)$$

where w_{ik} and w_{il} is the weight between node i and nodes k and l, respectively, and w_{kl} is the weight between nodes k and l. The average weighted clustering coefficient is computed by averaging $C_{,i}$ over all nodes.

The average weighted shortest path length indicates the amount of global integration. The weighted shortest paths are computed using Dijkstra's algorithm, where distance is defined as the inverse of the link weight and the length of a path is the sum of the inverse weights for all the edges in the path. The average weighted shortest path length is computed by averaging path length over all nodes (Rubinov and Sporns 2010). Both measures were normalized by the average weighted clustering and path length obtained from 500 random surrogate networks. A high normalized clustering and shortest path length correspond to a more regular network topology, whereas value close to 1 implies a random network topology (Watts & Strogatz, 1998).

MSTs were constructed using Kruskal's algorithm (Kruskal 1956), although in our case, we started the algorithm with the highest link weights as we were interested in the strongest connections (highest PLI values) in the network. In short, the algorithm first orders the weights of

all links in a descending order and starts the construction of the minimum spanning tree with the highest link weight and adds the following highest link weight until all *N* nodes are connected in a loopless (i.e. not containing cycles) sub-network that consists of *M=N-1* links. A link is ignored if its addition would form a loop. After construction of the MST, all link weights are assigned a value of one. We computed the following MST properties: leaf fraction (L), diameter (d), tree hierarchy (T_h) and degree divergence (κ). Leaf number L_N is the number of nodes in the tree with a degree of one, where the degree, (k), refers to the number of links connected to a node. Leaf number has a lower bound of 2 and an upper bound of *M=N-1*. We report the leaf fraction ($=L_N/M$) which is bounded between 0 and 1. The diameter of the tree is defined as the largest distance between any two nodes in the tree. The upper limit of the diameter is *d=M-L+2*, implying that the largest possible diameter decreases with increasing leaf number. Furthermore, we computed tree hierarchy T_H, that measures the trade-off between diameter reduction and overload prevention of the central nodes, which is necessary for efficient communication (Boersma et al. 2012):

$$T_H = \frac{L}{2MBC_{\max}} . \tag{3}$$

To assure T_H ranges between 0 and 1, the denominator is multiplied by 2. If $L=2$, i.e., a path-like topology, and M approaches infinity, T_H approaches 0. If $L=M$, i.e., a star-like topology, T_H approaches 0.5. BC_{max} refers to the maximum betweenness centrality in the tree network, where betweenness centrality is the fraction of all shortest paths that transverse through a specific node. Finally, we computed degree divergence κ, which is a measure of the broadness of the degree distribution (Barrat et al. 2008):

$$\kappa = \frac{\langle k^2 \rangle}{\langle k \rangle} . \tag{4}$$

Here, <> denotes the average. See Table 2 for a brief description of all network metrics. Note that all network metrics in the present study are global measures. All network metrics were calculated using Brainwave (version 0.9.98 available from http://home.kpn.nl/stam7883/brainwave.html).

Statistical analysis

Statistical analyses were performed using SPSS for windows v.20. The data were checked for normality using the Kolmogorov-Smirnov test and by visually inspecting histograms. Either independent samples t-tests or the Chi-square test were used to assess differences in gender, age and education between MS patients and healthy subjects. Structural metrics such as thalamic volumes were compared between groups by means of regression analysis with age, gender and education as covariates. We then followed a two-step approach:

1. Firstly, we first compared mean cortical functional connectivity and functional network measures between MS patients and healthy subjects for fMRI and MEG separately by using a multivariate general linear model (GLM) with age, gender and education as covariates. The used

multivariate GLM can be considered as a one-way MANOVA or a multivariate regression analysis with more than one dependent variable, mean cortical functional connectivity and functional network measures in this case. Group membership (MS patients versus healthy controls) was considered as independent variable. Since effect size in males and females may be different, effect size in each gender group was also estimated by computing the relative change within females or males between groups.

2. Secondly, only for those metrics that significantly differed between groups, we computed Spearman correlations between functional network properties on the one hand and thalamic volumes, thalamo-cortical functional connectivity, clinical disability (EDSS) and average cognition on the other hand in the MS patient group only (Rousselet and Pernet 2012). For these analyses, we used the average thalamo-cortical functional connectivity in the MS patient group.

For both steps, we corrected for the number of tests with the false discovery rate (FDR) (Benjamini and Hochberg 1995).

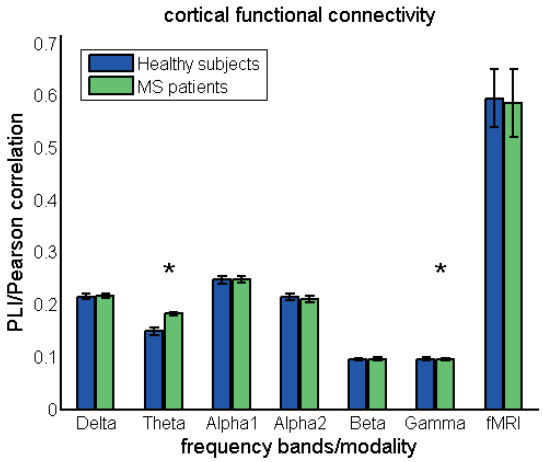

Figure 3: Cortical functional connectivity. Mean cortical functional connectivity (i.e. averaged over cortical ROIs and epochs (MEG)) is compared between groups. Note the significantly higher functional connectivity in the theta band for MS patients and lower functional connectivity in the gamma band in MS patients. Comparison for fMRI based cortical functional connectivity revealed no significant group differences.

RESULTS

Table 1 reports subject characteristics. MS patients and healthy subjects did not differ in gender or age distribution. 83% of the patient group consisted of relapsing-remitting MS patients, 6% of secondary and 11% of primary progressive MS patients. EDSS values ranged between 0 and 6.5 and average cognitive performance was significantly worse (p=..) in the MS patient group. Furthermore, MS patients showed significant reduction in thalamic volumes (Table 1).

Table 1: Demographic, clinical and MRI measures for MS patients and healthy subjects

	MS patients n = 86		Healthy subjects n = 21		P value
	Mean	±SD	Mean	±SD	
Age (in years)	41.58	8.82	42.48	10.29	>0.05
Gender (F in %)	61.9%		65.1%		>0.05
Disease duration (years)	7.15	2.11			
Disease type (RR/SP/PP)	68/5/9		-		-
EDSS (median and range)	2.5	(0-6.5)	-		-
Cognition (Z-score)	-0.83	0.76	0.06	0.48	<0.001
Thalamic volume (mL)	18.91	2.17	20.10	1.29	<0.001
NBV (L)	1.47	0.07	1.53	0.07	<0.001
NGMV (L)	0.82	0.05	0.84	0.05	<0.001
NDGMV (mL)	58.60	6.18	64.79	4.25	<0.001
T1 lesion load	2.00	2.36		-	-
T2 lesion load	4.50	5.35		-	-

Abbreviations: R relapsing-remitting; S (secondary-progressive; P (primary-progressive; NBV = normalized brain volume; NGMV = normalized GM volume; NDGMV = normalized deep gray matter volume.

Table 2: Network properties (Definitions are based on (Stam and van Straaten 2012))

N	Nodes	Number of nodes in the network
M	Links	Number of links in the MST
C	Clustering	The unweighted clustering coefficient describes the likelihood that neighbours of a node are also connected, and it quantifies the tendency of network elements to form local clusters. We used the weighted equivalent of this measure to characterize local clustering.
	Path length	Measure for integration; path with lowest sum of link weights between two nodes
k	Degree	Number of neighbours for a given node
L	Leaf fraction	Fraction of leaf nodes in the MST where a leaf node is defined as a node with degree one
D	Diameter	Longest shortest path of an MST
Th	Tree hierarchy	A hierarchical metric that quantifies the trade-off between large scale integration in the MST and the overload of central nodes.
K	Degree divergence	Measure of the broadness of the degree distribution

1a. Functional connectivity

In the first step of the analysis differences in mean cortical functional connectivity (i.e. averaged over cortical ROIs) were assessed between groups for each MEG frequency band separately and for fMRI. We found significantly higher MEG cortical functional connectivity in the theta band and significantly lower MEG cortical functional connectivity in the gamma band for MS patients (Figure 3 and Table S1). No significant differences between groups in mean fMRI functional connectivity were found at the cortical level.

However, BOLD thalamo-cortical functional connectivity was already studied region-wise in an overlapping but larger cohort, and shown to be higher with respect to especially occipital and temporal areas in MS patients (Schoonheim et al. 2014). Also in this sub-population, we demonstrate a higher BOLD thalamo-cortical functional connectivity in MS patients with especially temporal and occipital regions (see Table S2).

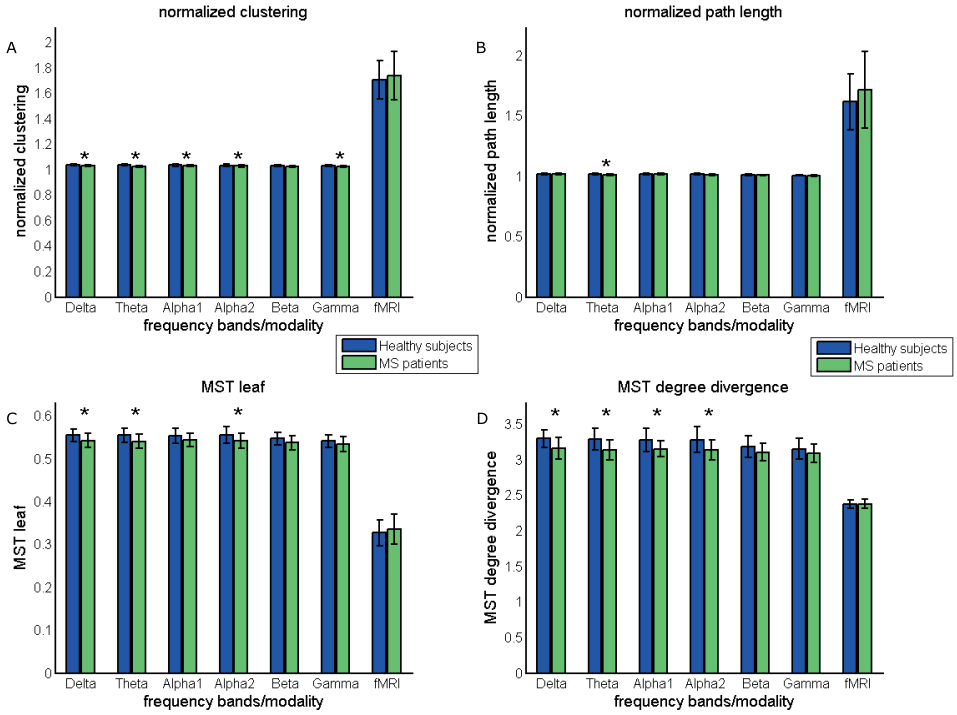

Figure 4: Conventional network and MST findings. Conventional network measures *(A)* normalized clustering and *(B)* normalized path length were compared between groups. MEG obtained cortical functional networks were characterized by significantly lower normalized clustering (delta, theta, alpha1, alpha2 and gamma band) and lower normalized path length (theta band), indicating that these networks are shifted towards random networks (Watts and Strogatz 1998). The MSTs of MS patients were characterized by *(C)* lower leaf fraction (delta, theta and alpha2 band) and *(D)* lower degree divergence (delta, theta, alpha1 and alpha2 band). This suggests that the MSTs of MS patients are shifted towards more path-like trees (Figure 5).

1b. Cortical functional networks

Conventional network analysis revealed that normalized clustering values were significantly lower in MS patients for all MEG frequency bands, except for the beta band. Normalized path length was only significantly lower in the theta band in MS patients (Figure 4 and Table S1). Together this indicates that cortical functional networks obtained by MEG are shifted towards more random network topology in MS patients, irrespective of the MEG frequency band. This was more prominent

for men than for women, as can be noted from the effect sizes for the groups (Figure 4 and Table S1). For fMRI, no differences in conventional network measures were found between the groups. However, note that within groups both clustering and path length were higher for fMRI than for MEG, indicating that the topology of fMRI obtained cortical functional networks is more regular-like.

To characterize MST topology in both groups we computed MST leaf fraction, MST degree divergence, MST diameter and MST tree hierarchy. MST analyses for MEG revealed lower leaf fraction for the delta, theta and alpha2 band in MS patients compared to healthy subjects (Figure 4 and Table S1). This was accompanied by a lower degree divergence in the delta, theta, alpha1 alpha2 bands in MS patients (Figure 4 and Table S1). Analysis of the remaining MST measures for MEG data only revealed that the diameter of MSTs was larger in the theta band in MS patients. Therefore, minimum spanning trees in MS patients obtained with MEG tended to have a more path like (less integrated) topology for the delta, theta, alpha1 and alpha2 frequency bands, however, most prominently for the theta and alpha2 band (Figure 5). In contrast to MEG, we did not find any differences between groups with respect to the MST analysis for fMRI (Figure 4 and Table S1). However, by inspecting within group differences it is clear that MSTs obtained from fMRI are characterized by lower leaf fraction and lower degree divergence, indicating a more path-like topology MST topology.

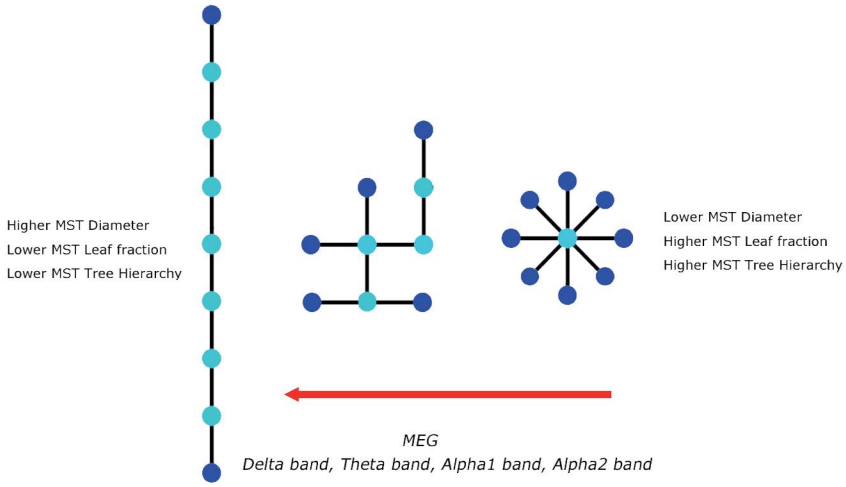

Figure 5: Main MST findings. Three MST configurations are depicted. The MST on the left is known as a path which has a high diameter ($d = 8$), low number of leaf nodes (end nodes, depicted as dark blue) and is characterized by low tree hierarchy, a measure that quantifies the trade-off between large scale integration and the overload of central nodes. The MST on the extreme right is known as a star which has a short diameter ($d = 2$), a large number of leaf nodes and is characterized by a high tree hierarchy. The MST in the middle is an intermediate configuration between these two extremes. For MEG we found a shift towards a more path-like configuration in MS patients, i.e. less efficient and less integrated. In contrast to MEG, we found a shift towards a more star-like configuration for fMRI.

2a. Cortical functional networks vs thalamic volume and BOLD thalamo-cortical functional connectivity

In the second step of the analysis we computed correlations between the network properties that significantly differed between groups and thalamic volume and BOLD thalamo-cortical functional connectivity, only for MS patients (Table 3).

- With respect to conventional network measures we observed that thalamic volume was *positively* associated with normalized clustering (alpha1, alpha2 and gamma band) and normalized path length (theta band). This suggests that decreased thalamic volumes in MS patients are associated with more random cortical functional network topology. With respect to MST measures we observed that thalamic volumes in MS patients were *positively* correlated with MST leaf fraction (theta and alpha2 band) and MST degree divergence (theta and alpha2 band). Thus, a more path-like topology in MS patients is associated with decreased thalamic volumes.
- BOLD thalamo-cortical functional connectivity was also associated with MEG obtained network measures in MS, however, only in the theta band. We found *negative* correlations between BOLD thalamo-cortical functional connectivity and clustering, MST leaf fraction and MST degree divergence in this frequency band. Again, a more random and path-like topology seemed to be associated with other disease effects in MS such as increased BOLD thalamo-cortical functional connectivity. Also note that some MST measures, especially in the theta band, such as leaf fraction and degree divergence were both associated with thalamic atrophy and BOLD thalamo-cortical functional connectivity (Figure 6).

2b. Cortical functional networks vs clinical and cognitive dysfunction

To investigate if a more random or path-like network topology in MS had clinical significance, we computed correlations between MEG network measures that significantly differed between the groups and average cognition and physical disability (EDSS). These correlations were only computed for the MS patient group (Table 3).

- With respect to average cognition, we only found a *positive* correlation between this outcome variable with MST degree divergence in the alpha1 band.
- For EDSS we found significant *negative* correlations with several MEG obtained network measures in several frequency bands: normalized clustering (delta, alpha1 and alpha2 band), MST leaf fraction (delta, theta, alpha1), MST degree divergence (delta, theta, alpha1) and MST tree hierarchy (alpha2 band). These findings demonstrate that a more random or path-like network topology in MS in several frequency bands is indeed related to clinical and cognitive status. Note that some network measures that had significant correlations with EDSS were also associated with reduced thalamic volume and increased BOLD thalamo-cortical functional connectivity. This was especially the case for MST measures in the theta band, such as the degree divergence and the leaf fraction.

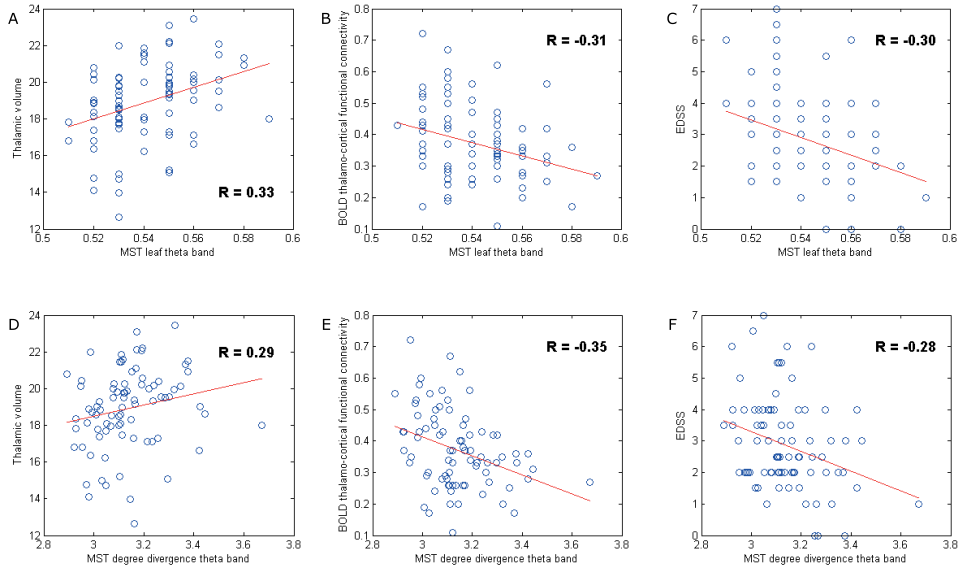

Figure 6: Correlation analysis. These scatter plots illustrate the relationship between disruption of cortical functional network topology in the theta band with other pathological characteristics of the disease, such as thalamic atrophy and increased BOLD thalamo-cortical functional connectivity, and with clinical status in MS (EDSS). Although other network measures were also related to thalamic pathology and clinical status, we illustrate that two network measures itself were related to both thalamic pathology and clinical status. MST leaf fraction in the theta band in MS patients was *positively* correlated to thalamic volume *(A)*, but *negatively* correlated to BOLD thalamo-cortical functional connectivity *(B)* and EDSS *(C)*. Similarly, MST degree divergence in the theta band in MS patients was *positively* correlated to thalamic volume *(D)*, but also negatively correlated to BOLD thalamo-cortical functional connectivity *(E)* and EDSS *(F)*, i.e. general decrease in the degree of nodes seemed to be a sign of damage.

DISCUSSION

We hypothesized that widespread disruption of the thalamocortical system, consisting of cortical functional networks connected with the thalamus, would be associated with physical disability and cognitive dysfunction (Figure 1). Our main findings were: 1) a disruption of cortical functional connectivity, as measured with MEG, and a shift towards a more random functional network topology in several MEG frequency bands in early MS. This was confirmed by MST findings that showed a less integrated (more path-like) tree topology for the same MEG frequency bands; 2) MS patients showed increased thalamocortical functional connectivity and thalamic atrophy, which 3) was associated with the shift towards a more random network topology or more path-like tree topology; 4) lastly, for only MS patients, we demonstrated that this shift in network topology was associated with worse cognitive and physical disability.

Table 3: Correlations between functional network measures. BOLD thalamo-cortical functional connectivity. thalamic atrophy and clinical cognitive measures. Values are reported as Spearman correlation values (p-value) (step 2 of the analysis).

	Thalamic volume	BOLD thalamo-cortical functional connectivity	Average Cognition	EDSS
Normalized clustering Delta	0.16 (0.15)	-0.18 (0.10)	0.09 (0.40)	**-0.40 (<0.001)**
Normalized clustering Theta	*0.23 (0.03)*	**-0.42 (<0.001)**	0.13 (0.23)	-0.17 (0.12)
Normalized clustering Alpha1	**0.32 (0.003)**	-0.17 (0.13)	0.15 (0.19)	**-0.31 (0.004)**
Normalized clustering Alpha2	**0.42 (<0.001)**	-0.09 (0.42)	0.16 (0.14)	**-0.27 (0.01)**
Normalized clustering Gamma	**0.36 (0.001)**	*-0.22 (0.05)*	0.12 (0.28)	-0.19 (0.08)
Normalized path length Theta	**0.36 (0.001)**	*-0.23 (0.04)*	*0.26 (0.02)*	-0.09 (0.40)
MST Leaf fraction Delta	0.09 (0.41)	*-0.24 (0.03)*	0.12 (0.30)	**-0.40 (<0.001)**
MST Leaf fraction Theta	**0.33 (0.002)**	**-0.31 (0.005)**	*0.22 (0.05)*	**-0.30 (0.001)**
MST Leaf fraction Alpha2	**0.28 (0.01)**	*-0.26 (0.02)*	0.06 (0.56)	-0.17 (0.13)
MST Diameter Theta	-0.14 (0.21)	0.19 (0.1)	-0.08 (0.46)	0.05 (0.65)
MST Degree divergence Delta	0.05 (0.67)	-0.14 (0.23)	0.07 (0.54)	**-0.36 (0.001)**
MST Degree divergence Theta	**0.29 (0.007)**	**-0.35 (0.001)**	0.16 (0.14)	**-0.28 (0.01)**
MST Degree divergence Alpha1	*0.23 (0.04)*	*-0.23 (0.04)*	**0.29 (0.007)**	**-0.35 (0.001)**
MST Degree divergence Alpha2	**0.34 (0.002)**	*-0.22 (0.05)*	0.16 (0.15)	-0.13 (0.23)

Bold = significant after correcting for multiple comparisons by the FDR. Italic = the result is not significant anymore after correction for multiple comparisons using the FDR (corrected for 4 x 14 tests) with FDR = p_{FDR} *i/N. Here, p_{FDR} = 0.05 (usual significance value in most statistical tests), *i* refers to the ranked index of the p-values that are computed and *N* to the number of tests.

Functional connectivity

Functional connectivity analyses revealed higher MEG functional connectivity in the theta band and lower functional connectivity in the gamma band. Higher functional connectivity in the theta band has been reported in previous studies in different disease cohorts and has been positively associated with disruption of gray matter thickness correlations in MS (Schoonheim et al. 2011; Tewarie et al. 2014a). Lower functional connectivity in the gamma band has not been a consistent finding in MEG/EEG studies so far, which makes the interpretation of this finding less straightforward, especially considering the potential for biases due to contamination by muscle activity (Pope et al. 2009). We also mention a trend of lower functional connectivity in the alpha2 band and a trend of higher functional connectivity in the beta band as these current findings, especially for the alpha2 band, have also been reported consistently in previous studies and have been linked to clinical and cognitive dysfunction (Cover et al. 2006; Leocani et al. 2000; Schoonheim et al. 2011; Tewarie et al. 2014a; Tewarie et al. 2013b).

Cortical functional networks

MEG functional network analyses revealed disruption of cortical functional networks in early MS quantified by both conventional network measures as well as MST measures. By using conventional network measures we found a shift towards a more random network topology in MS patients for several MEG frequency bands (delta, theta, alpha1, alpha2 and gamma band). A more random network topology in the alpha2 band has also been reported in a previous MEG study in an MS sample with longer disease duration (Tewarie et al. 2014a). The same study reported a more regular network topology in the theta band, which was also in agreement with one earlier MEG study analyzing an MS sample with similar disease duration as the present study (Schoonheim et al. 2011). Discrepancy between the latter studies and the present study may be caused by the use of a different functional connectivity metric, analysis at the sensor level in one of the previous study, due to biases inherent to conventional network analysis such as differences in average functional connectivity, differences in density between networks or due to difference in disease duration. Therefore, we also computed MST measures to control for these biases and we found that MSTs in MS patients displayed a less integrated, more path-like, tree topology (delta, theta, alpha1, alpha2). This type of topology was also accompanied with lower degree divergence, indicative of a loss of high degree nodes or an overall decrease in degrees of nodes in the network, which is generally observed in neurological disorders (Crossley et al. 2014). The shift towards a more path-like tree topology and thus less integrated MEG network has been a consistent finding in MS as has also been linked to worse cognitive performance (Tewarie et al. 2013a; Tewarie et al. 2014a). Other recent MEG studies involving patients with Parkinson's disease or gliomas also found that shifts towards more path-like tree topologies were signs of mal-adaptation or cognitive dysfunction (Olde Dubbelink et al. 2013; van Dellen E. et al. 2014). The hypothesis is that an optimal configuration for a tree should allow for large scale integration and at the same time it has to prevent overload of central nodes. Such an optimal configuration is probably somewhere between a path-like topology and a star-like topology and may constitute an optimum level of hierarchy and allows for efficiency. A shift towards a more path-like topology in MS could therefore also indicate a less efficient and hierarchical network which is required for integration of distinct cognitive functions.

Cortical functional networks vs thalamic pathology and disability

The thalamus plays a central role in transferring information in the brain and is one of the most important predictors for clinical and cognitive status in MS (Schoonheim et al. 2012). We therefore hypothesized that atrophy of this important structure would co-occur with widespread disintegration of functional brain connectivity. In the present study, we indeed found that thalamic atrophy was associated with a shift to a more random cortical network topology or a more path-like tree topology. We suggest that this relation between thalamic atrophy and disintegration may partially be mediated by increased BOLD thalamo-cortical functional connectivity, which might be maladaptive in this context. The clinical relevance of disruption of this thalamo-cortical system is

that less integrated functional networks were associated with worse cognitive performance and especially with worse physical disability. This indicates that physical disability is not only explained by pathology in the motor cortex or pyramidal tract alone, but is also influenced by global network damage. The correlations between network measures and clinical status were moderate, which indicates that a part of the occurring physical disability needs to be explained by other measures, such as spinal cord damage since these are not captured by brain related measures (Daams et al. 2014).

Not all frequency bands that showed an abnormal network layout were related to thalamic pathology. For example, network disruption in the delta band showed associations with worse physical disability, but not with BOLD thalamo-cortical functional connectivity or thalamic atrophy, indicating that worse physical disability may not merely be associated by changes due to thalamic atrophy, but also with cortical pathology that may be independent of thalamic atrophy. This also indicates that the relation between disintegration of cortical functional brain networks and thalamic atrophy is frequency dependent, which makes sense given the knowledge that the role of the thalamus as co-generator of brain rhythms and oscillations is frequency specific (Grossberg and Versace 2008; Hughes and Crunelli 2005; Klimesch et al. 2007; Steriade 1997).

In the present study we analyzed associations between functional networks and thalamic atrophy in early MS and therefore we have to stress that we cannot make causal claims that thalamic atrophy causes disruption of cortical functional networks. In other words: this relation might be reverse, causally bi-directional or driven by a third common source. However, in analyses of a previous study we showed that increased BOLD thalamo-cortical functional connectivity was only present in more severely cognitively impaired patients. Thalamic atrophy was worst in these patients as well, although it was also significantly present in cognitively preserved patients (Schoonheim et al. 2014). Therefore, it is likely that thalamic atrophy may precede increases in BOLD thalamo-cortical functional connectivity, and as a result may also play a causal role for disintegration of cortical functional networks. Future longitudinal studies are needed to explore this hypothesis further. However, on the other hand, increased BOLD thalamo-cortical functional connectivity itself may lead to structural damage and thus contribute to thalamic atrophy since it has been demonstrated in modelling studies that increased firing rates or functional connectivity due to disinhibition may lead to synaptic damage, especially in central regions, such as the thalamus (de Haan W. et al. 2012; Kostic et al. 2013). It is also plausible that increased thalamic connectivity might lead to increased local neurotransmitter levels, perhaps leading to excitotoxicity.

Furthermore, the thalamus is involved in feedback projections (first order relays) and in feedforward cortico-thalamo-cortical routes (higher order relays) (Sherman 2007). These feedforward routes that travel trough the thalamus may serve as parallel pathways to cortico-cortical projections and could play an important role in integration of information in functional cortical networks. Therefore, thalamic atrophy in MS could impact these parallel feedforward cortico-thalamo-cortical projections, which could eventually lead to less integrated cortical

functional networks. Lastly, we have to stress that the relationship between thalamic atrophy and disruption of cortical functional networks could also be driven by a third common global process. For example, white matter lesions or decreased white matter integrity could be associated with structural disconnection between the cortex and the thalamus (Steenwijk et al. 2013). Similarly, diffuse occurrence of gray matter lesions in both the cortex and the thalamus (Minagar et al. 2013) may lead to both thalamic atrophy and altered cortical functional networks. Future studies are needed to tease these factors apart.

Methodological considerations

We need to mention some methodological disadvantages and advantages of our approach. Firstly, in our beamforming analysis of MEG data we selected the time-series of one voxel (i.e. the voxel with the highest power) as a representation for the whole ROI. This can be regarded as a reduction of data. However, averaging over voxels in a ROI could introduce biases due to differences in ROI size leading to time-series having different signal-to-noise-ratios. Given these biases with averaging over sources we chose to adhere to methods used previously in our group (Hillebrand et al. 2012). Furthermore, we used a single sphere as a volume conductor model, which may have lead to localisation inaccuracies, particularly near temporal regions (Lalancette et al. 2011). However, we have assumed that the effects of these potential inaccuracies are negligible, given the spatial resolution of the AAL atlas in these regions. Secondly, functional network analyses revealed widespread disruption of cortical MEG functional networks, which was not reflected in cortical fMRI functional networks. This could be caused by either higher sensitivity of MEG due to its higher temporal resolution, and/or due to use of an atlas as most fMRI findings in MS have been found at the voxel level and usage of an atlas might minimize the advantage of having a high spatial resolution for fMRI (Bonavita et al. 2011; Hawellek et al. 2011; Rocca et al. 2012; Schoonheim et al. 2013b). Thirdly, MSTs mainly capture the strongest functional connections in the functional networks, which were not the same for MEG and fMRI. For fMRI we observed the highest functional connectivity in homologous interhemispheric connectivity, which was not the case for MEG. Nevertheless, the inclusion of fMRI in addition to MEG proved to provide important additional information regarding functional connectivity of the thalamus, as it enabled the observation that increased BOLD thalamo-cortical functional connectivity was related to disruption of MEG functional networks.

Fourthly, we did not include the left and right thalamus as a node in the fMRI functional network. The rationale behind this was to construct functional networks for MEG and fMRI with equal size (equal number of nodes) since differences in network size can cause biases in network comparisons (van Wijk et al. 2010). The rationale to leave out sub-cortical ROIs in the AAL atlas and therefore in the MEG functional networks is that the MEG sensitivity for activity in these ROIs is very low (Hillebrand and Barnes 2002). Estimated time-series for these regions are consequently very noisy, and the spatial resolution for these deep structures is poor. One would therefore not be sure whether an estimated source corresponding to the thalamus was only associated with thalamus activity or also

with activity from surrounding deep gray matter structures or even from the cortex. Fifthly, there was a mismatch between the numbers of MS patients and healthy subjects. A larger healthy subject group could have led to more reliable results for this group and a higher sensitivity to pick up disease effects. Sixthly, in this first multi-modal fMRI/MEG analysis in MS we omitted computation of nodal network properties in order to preserve a clear message. However, future studies could examine whether regions with different roles in the functional network are affected differentially by thalamic atrophy and thalamo-cortical interactions, and how this relates to clinical symptoms and cognition. Lastly, the main advantages of the used MEG atlas-based beamformer approach over sensor-level analyses is that it improves the signal-to-noise (SNR) of the reconstructed timeseries (Adjamian et al. 2009), eases interpretation in terms of involved anatomical structures, and the usage of an atlas allows for direct comparison of MEG with fMRI.

Conclusion

There is a need for an integrated and cross-modal framework that is able to clarify how complex pathological alterations affecting both structure and function are related to each other and how the interplay between these eventually lead to clinical and cognitive problems in MS. This study was a step towards such an integrated framework where we found that thalamic atrophy, one of the most important predictors of clinical and cognitive dysfunction in MS, was associated with less integrated cortical functional networks, possibly mediated by increased BOLD thalamo-cortical functional connectivity. This is the first multi-modal fMRI and MEG study that analyzed disintegration of functional networks in relation to thalamic atrophy in early MS, in which we have demonstrated that a multi-modal approach has an advantage over an uni-modal approach as MEG and fMRI findings were complementary. The importance of these findings is that it demonstrates how two different pathological features in early MS are indeed related and how they are associated with physical disability and cognitive dysfunction. Future studies are warranted to investigate to what extent disruption of this thalamo-cortical system occurs in latter stages of the disease or whether it is different between MS disease types.

SUPPLEMENTARY INFORMATION

THALAMO-CORTICAL FUNCTIONAL CONNECTIVITY

Statistical analyses

We compared thalamo-cortical functional connectivity (fMRI) between MS patients and healthy controls by using a multivariate generative linear model with age, gender and education as covariate. Dependent variables were the 39 thalamo-cortical functional connectivity values (i.e. averaged over hemispheres). As outcome statistic we looked at Pillai's trace test for a global test statistic and between group effects for each region. These analyses were already done in a larger cohort

Results

Thalamo-cortical functional connectivity was assessed by fMRI and compared between MS patients and healthy controls using a multivariate generative linear model. The Pillai's Trace statistic was significant ($F = 1.607$ and $p = 0.049$), indicating an overall increase of thalamo-cortical functional connectivity in MS patients. This difference was driven by increased functional connectivity from the thalamus to the rolandic operculum, cuneus, superior temporal gyrus, superior temporal pole, the insula and by functional connectivity from the thalamus to the posterior cingulated (see Table S2).

Table S1: Functional connectivity and functional network measures in MS patients versus healthy subjects for MEG data (step 1 of the analysis).

		Healthy subjects		MS patients					
		Mean	**STD**	**Mean**	**STD**	**F**	**p-value**	**Effect M**	**Effect F**
Delta	PLI	0.216	0.005	0.217	0.005	2.396	0.125	1.0%	0.6%
	Normalized clustering	**1.037**	**0.005**	**1.031↓**	**0.007**	**11.601**	**0.001**	**0.7%**	**0.5%**
	Normalized path length	1.015	0.006	1.016	0.006	.626	0.431	0.0%	0.1%
	MST leaf fraction	**0.556**	**0.014**	**0.543↓**	**0.016**	**8.542**	**0.004**	**2.8%**	**2.0%**
	MST Diameter	0.218	0.010	0.222	0.009	2.539	0.114	1.6%	1.1%
	MST degree divergence	**3.296**	**0.122**	**3.157↓**	**0.153**	**14.188**	**<0.001**	**5.1%**	**3.6%**
	MST tree hierarchy	0.416	0.011	0.411	0.013	2.699	0.104	1.3%	1.3%
Theta	**PLI**	**0.149**	**0.007**	**0.183↑**	**0.003**	**130.62**	**<0.001**	**22.8%**	**22.5%**
	Normalized clustering	**1.038**	**0.008**	**1.026↓**	**0.007**	**40.325**	**<0.001**	**1.3%**	**1.0%**
	Normalized path length	**1.014**	**0.007**	**1.010↓**	**0.005**	**9.276**	**0.003**	**0.8%**	**0.3%**
	MST leaf fraction	**0.555**	**0.017**	**0.541↓**	**0.017**	**8.366**	**0.005**	**4.2%**	**1.7%**
	MST Diameter	**0.214**	**0.006**	**0.229↑**	**0.010**	**34.326**	**<0.001**	**7.6%**	**6.6%**
	MST degree divergence	**3.291**	**0.151**	**3.136↓**	**0.140**	**16.566**	**<0.001**	**6.0%**	**3.9%**
	MST tree hierarchy	0.416	0.017	0.413	0.015	.153	0.697	3.0%	0.9%
Alpha1	PLI	0.248	0.007	0.249	0.007	.188	0.665	0.9%	0.2%
	Normalized clustering	**1.035**	**0.009**	**1.029↓**	**0.006**	**12.880**	**0.001**	**1.0%**	**0.4%**
	Normalized path length	1.017	0.006	1.016	0.005	1.237	0.269	0.4%	0.0%
	MST leaf fraction	*0.555*	*0.018*	*0.544↓*	*0.016*	*5.630*	*0.020*	*4.1%*	*0.3%*
	MST Diameter	0.225	0.010	0.229	0.0105	1.783	0.185	4.0%	1.1%
	MST degree divergence	**3.276**	**0.167**	**3.152↓**	**0.113**	**14.190**	**<0.001**	**6.8%**	**2.0%**
	MST tree hierarchy	0.419	0.013	0.415	0.013	1.093	0.298	2.7%	0.2%
Alpha2	PLI	0.215	0.006	0.211	0.006	3.282	0.073	3.5%	0.3%
	Normalized clustering	**1.034**	**0.009**	**1.028↓**	**0.008**	**9.755**	**0.002**	**1.3%**	**0.2%**
	Normalized path length	*1.017*	*0.006*	*1.013↓*	*0.006*	*5.394*	*0.022*	**0.7%**	**0.2%**
	MST leaf fraction	**0.556**	**0.019**	**0.542↓**	**0.018**	**9.845**	**0.002**	**4.6%**	**1.1%**
	MST Diameter	*0.221*	*0.013*	*0.226↑*	*0.010*	*4.449*	*0.038*	*5.9%*	*0.7%*
	MST degree divergence	**3.279**	**0.184**	**3.139↓**	**0.138**	**16.266**	**<0.001**	**8.1%**	**1.8%**
	MST tree hierarchy	*0.420*	*0.011*	*0.411↓*	*0.014*	*5.605*	*0.020*	*2.9%*	*1.6%*

Table S1: Continued

		Healthy subjects		MS patients					
		Mean	**STD**	**Mean**	**STD**	**F**	**p-value**	**Effect M**	**Effect F**
Beta	PLI	0.095	0.002	0.096	0.003	2.876	0.093	2.0%	0.9%
	Normalized clustering	1.031	0.009	1.027	0.007	3.748	0.056	1.0%	0.1%
	Normalized path length	1.009	0.005	1.007	0.005	.229	0.633	0.4%	0.0%
	MST leaf fraction	0.548	0.015	0.538	0.017	3.256	0.074	2.9%	1.1%
	MST Diameter	0.221	0.009	0.225	0.010	2.237	0.138	3.9%	0.0%
	MST degree divergence	3.181	0.152	3.105	0.126	3.708	0.057	4.8%	0.9%
	MST tree hierarchy	0.414	0.011	0.420	0.013	1.043	0.310	2.0%	0.7%
Gamma	**PLI**	**0.096**	**0.003**	**0.095↓**	**0.002**	**6.087**	**0.015**	**1.4%**	**1.3%**
	Normalized clustering	**1.029**	**0.007**	**1.023↓**	**0.007**	**8.956**	**0.004**	**0.8%**	**0.4%**
	Normalized path length	1.007	0.005	1.005	0.005	.812	0.370	0.3%	0.1%
	MST leaf fraction	0.541	0.015	0.535	0.018	2.674	0.105	3.2%	0.1%
	MST Diameter	0.221	0.008	0.225	0.009	1.995	0.161	0.4%	1.6%
	MST degree divergence	3.151	0.145	3.091	0.132	3.708	0.057	3.9%	0.7%
	MST tree hierarchy	0.408	0.012	0.404	0.013	1.687	0.197	3.7%	0.6%
fMRI	Pearson associations (FC)	0.60	0.055	0.59	0.065	0.089	0.766	3.5%	4.1%
	Normalized clustering	1.70	0.153	1.73	0.190	0.184	0.669	3.4%	4.8%
	Normalized path length	1.61	0.231	1.71	0.316	1.487	0.226	0.0%	9.7%
	MST Leaf fraction	0.33	0.030	0.34	0.035	1.352	0.248	1.4%	3.4%
	MST Diameter	0.32	0.068	0.32	0.053	0.190	0.664	8.1%	2.6%
	MST Degree divergence	2.38	0.061	2.38	0.070	0.070	0.792	0.8%	0.7%
	MST tree hierarchy	*0.26*	*0.020*	*0.27↑*	*0.029*	*5.199*	*0.025*	*5.2%*	*4.9%*

Bold = significant after correcting for multiple comparisons by the FDR. Italic = the result is not significant anymore after correction for multiple comparisons using the FDR (corrected for 7 x 7 tests) with FDR = p_{FDR} *i/N. Here, p_{FDR} = 0.05 (usual significance value in most statistical tests), *i* refers to the ranked index of the p-values that are computed and *N* to the number of tests. ↓ indicates significantly lower in MS patients. ↑indicates significantly higher in MS patients.

Table S2: Thalamo-cortical functional connectivity between each cortical region and the thalamus. averaged over hemispheres.

	Healthy controls		MS patients			
Region of interest	**Mean**	**STD**	**Mean**	**STD**	**F**	**p-value**
Rectus	0.13	0.220	0.21	0.192	1.67	0.20
Olfactory	0.14	0.227	0.24	0.227	2.62	0.10
Frontal Sup Orb	0.09	0.188	0.19	0.193	3.03	0.08
Frontal Med Orb	0.20	0.210	0.3	0.202	2.90	0.09
Frontal Mid Orb	0.43	0.166	0.45	0.176	0.00	0.98
Frontal Inf Orb	0.48	0.142	0.47	0.182	0.42	0.51
Frontal Sup	0.41	0.212	0.45	0.178	0.48	0.48
Frontal Mid	0.45	0.192	0.47	0.169	0.13	0.71
Frontal Inf Oper	0.40	0.179	0.43	0.172	0.17	0.67
Frontal Inf Tri	0.37	0.188	0.41	0.2	0.64	0.42
Frontal Sup Medial	0.28	0.205	0.36	0.192	3.28	0.07
Supp Motor Area	0.33	0.209	0.36	0.203	0.59	0.44
Paracentral Lobule	0.49	0.230	0.49	0.179	0.01	0.91
Precentral	0.29	0.243	0.34	0.204	1.42	0.23
Rolandic Oper	**0.30**	**0.165**	**0.39↑**	**0.172**	**4.00**	**0.04**
Postcentral	0.36	0.147	0.4	0.183	0.35	0.55
Parietal Sup	0.36	0.186	0.41	0.179	1.09	0.29
Parietal Inf	0.35	0.160	0.37	0.183	0.11	0.73
SupraMarginal	0.49	0.147	0.51	0.157	0.34	0.55
Angular	0.25	0.232	0.3	0.217	0.68	0.40
Precuneus	0.31	0.208	0.36	0.208	1.12	0.29
Occipital Sup	0.23	0.156	0.32	0.202	2.34	0.12
Occipital Mid	0.45	0.180	0.46	0.209	0.06	0.79
Occipital Inf	0.31	0.202	0.35	0.209	0.49	0.48
Calcarine	0.36	0.240	0.42	0.208	1.60	0.20
Cuneus	**0.25**	**0.197**	**0.37↑**	**0.192**	**5.80**	**0.01**
Lingual	0.53	0.159	0.56	0.152	0.49	0.48
Fusiform	0.51	0.177	0.53	0.189	0.26	0.60
Heschl	0.34	0.156	0.41	0.188	2.54	0.11
Temporal Sup	**0.17**	**0.180**	**0.31↑**	**0.215**	**6.03**	**0.01**
Temporal Mid	0.24	0.222	0.31	0.204	1.52	0.22
Temporal Inf	0.01	0.141	0.12	0.229	3.48	0.06
Temporal Pole Sup	**0.05**	**0.172**	**0.18↑**	**0.217**	**5.33**	**0.02**
Temporal Pole Mid	0.35	0.242	0.4	0.226	0.56	0.45
ParaHippocampal	0.51	0.154	0.47	0.203	0.68	0.41
Cingulum Ant	0.50	0.228	0.55	0.158	1.57	0.21
Cingulum Mid	0.64	0.173	0.64	0.148	0.01	0.89
Cingulum Post	**0.46**	**0.094**	**0.53↑**	**0.097**	**8.88**	**0.004**
Insula	**0.51**	**0.130**	**0.58↑**	**0.104**	**5.94**	**0.017**

Bold = Significant ($p < 0.05$). ↓ indicates significantly lower in MS patients. ↑indicates significantly higher in MS patients.

Chapter 10

Summary

SUMMARY

The aim of the present dissertation was to test the hypothesis if clinical disability in MS could be explained by disruption of functional brain networks, and subsequently if this disruption of functional brain networks was related to structural pathology in MS.

In order to investigate the role of functional network topology as a link between structural pathology and clinical disability, there is a need for theoretical framework to understand the link between structure and function under healthy physiological conditions. When such a framework is established, the resulting principles can be applied to MS functional and structural network data. In the first two chapters this framework was investigated. In **chapter 2** a computational modelling study was performed where the applicability of neural mass models for realistic conditions was studied. The rationale is that neural mass models can be used for simulating MEG-like oscillations and functional networks and thus can be used to study pathological alterations of functional networks in MS. In this study it was investigated if conventional neural mass models, based on mean-field approximations, were able to capture the underlying dynamics of a neuronal population when the underlying homogeneity of such populations, as assumed in mean-field approximations, was violated. It was demonstrated that neural mass models were able to capture the mean activity of a neuronal population only under the specific conditions of dense connectivity among neurons in the population and a network size which was well beyond 100 neurons. When these conditions were met, then neurons in the neuronal population were able to synchronize, which led to a smaller contribution of signals with higher frequencies to the mean signal of the population. The mean activity of neuronal populations that contain little of higher frequencies could be captured by conventional neural mass models, as these act as low pass filters and therefore model signals which were dominated by lower frequencies.

In **chapter 3** another part of our theoretical framework was investigated. The aim was to study the presence of modality invariant functional connections in relationship to the underlying structural network. In order to quantify these modality invariant connections both fMRI and MEG were used. A modality-invariant functional core network in temporo-posterior regions including the precuneus was reported. This modality-invariant network was found for several MEG frequency bands. Secondly, it was found that this temporo-posterior core network emerged near a modality invariant phase transition for functional connectivity. Thirdly, it was demonstrated that this modality-invariant network was not merely reflection of the connections of the structural network, but more shaped by other properties of the structural network. A simple distance vs degree model was used, consisting of a weighted sum of the distance, defined as Euclidean distance between nodes, and the product of the degrees for any two nodes in the structural network. This simple analytical model was able to explain 12% of the variance for MEG and 33% of the variance for fMRI obtained functional networks. Adding the unweighted structural network in the model did not result in significant better predictions for both modalities.

In **chapter 4** the use of the minimum spanning tree (MST, an acyclic sub-network) for characterising brain network topology was investigated. The rationale behind this study was that conventional network metrics that aim to characterize the topology of brain networks are biased by properties of the network that are not related to the topology, such as network density, average network connectivity and network size. Therefore use of these metrics could lead to incorrect or incomplete descriptions of network topology. Three fundamental research questions were studied: 1) Are MST results insensitive for biases due to differences in network density or average connectivity? 2) Is MST topology also a good reflection of the topology of the original network? 3) How robust are these MST findings? These questions were investigated by simulating small-world and scale-free networks and it was found that in contrast to conventional measures, the MST is insensitive for differences in network density or average connectivity. Secondly, a rewiring procedure for both scale-free and small-world networks was executed that gradually changed these networks into random networks. The change in topology of the MSTs during this rewiring process was in the same direction as for the original networks. This indicates that MST topology can indeed be considered as a good reflection of the topology of the underlying network as it includes the set of links that show similar topology as the original network. Lastly, the strongest links in the MST were reordered to test the robustness of the MST and it was found that these near MST spanning trees were highly similar to the MST.

In **chapter 5** it was investigated if local resting-state oscillatory brain activity in MS patients could explain the presence of clinical disability (physical disability and cognitive dysfunction). MEG time-series were both recorded in MS patients and healthy subjects and it was found that there was slowing of oscillatory activity towards lower frequencies in MS patients. Results showed less power in the alpha2 band and more power in the alpha1 band in early MS patients, which had clinical relevance as this was related to worse cognitive performance and specifically to lower information processing speed in MS patients. Regional analysis revealed that this slowing predominantly occurred in temporo-posterior regions.

In **chapter 6** the attention was shifted from the power of MEG time-series to the phase relationships between these MEG-time-series in the same population as our power study described in chapter 5. Firstly, it was investigated if functional connectivity patterns in MS were altered due to the disease. Secondly, it was investigated if these alterations in functional connectivity were related to clinical disability and thalamic atrophy (a strong predictor for clinical disability). In this context, both whole brain functional connectivity and literature based resting state networks (RSN) were analysed. Whole brain analyses revealed lower functional connectivity in the alpha2 band and higher functional connectivity in the beta band in MS patients. These findings were replicated using a RSN approach. However, functional connectivity within RSN showed stronger correlations with clinical disability than whole brain functional connectivity, which indicates that these RSNs may consist of important connections that are more involved in cognitive processes. Particularly, modulations in the default mode network in MS patients were strongly associated with both physical

disability and cognitive status in MS. In addition, it was found that lower functional connectivity in the visual RSN was related to thalamic atrophy.

Hitherto, only local activity and the strength of functional connectivity were studied in MS patients. However, by merely analyzing these properties one may miss crucial information contained in the topology or organization of these functional connections as transferring information over networks is highly dependent on their topologies. In **chapter 7** it was investigated if MS patients showed alterations in network topology and whether these changes in network topology were related to clinical disability. For this purpose, the MST was computed as it was demonstrated in chapter 4 that it is capable of overcoming methodological biases with regard to arbitrary thresholds, average connectivity and density effects. Using empirical data from MEG recordings it was demonstrated that the MSTs of MS patients were characterized by a shift towards a more path-like topology in the alpha2 band, i.e. a less integrated network. Furthermore, a shift towards a more path-like network topology corresponded to a clinical disability in MS patients, and to be more specific to worse cognitive performance in MS patients. Finally, the distribution of the weights in the original network for both MS patients and healthy subjects corresponded to a shift towards a "*strong disorder*" regime, i.e. the distribution can be described by a power distribution where the exponent tends to go to zero, indicating that most of the traffic in the network takes place on the MST.

Since it was demonstrated that in MS patients functional networks were characterized by less integration, in **chapter 8**, the aim was to investigate the relationship between these functional network alterations and structural networks in MS. Structural co-variance networks were obtained from cortical thickness correlations and functional networks from MEG recordings. For this study, a new and larger patient cohort was studied where MS patients had relatively long disease duration. For both type of networks, both MST metrics and conventional metrics were computed. Again, functional networks in MS were characterized by less integration in terms of the MST in the alpha2 band, i.e. there was a shift towards a path-like topology. Furthermore, conventional network analysis revealed that there was a shift towards a more random or regular functional network topology depending on the frequency band for MS patients. However, for the structural co-variance networks only a shift towards a more regular network topology was found. This shift was also found for functional networks in the theta band in MS patients in contrast to the alpha2 band which showed a more random network topology. Further analysis revealed that structural-covariance between two regions was positively associated with functional connectivity between two regions in especially the theta band in MS patients. Importantly, these associations were not found when correlations between regional thickness of a region and the average functional connectivity of that region were computed. These findings indicate that functional connectivity changes in MS cannot be simply explained by regional gray matter atrophy itself but only if coordinated patterns of gray matter atrophy were taken into account.

In **chapter 9**, the relationship between functional networks in MS and structural pathology was investigated and more specifically, the role of thalamic atrophy for explaining disruption of cortical

functional networks. The rationale behind this approach is that thalamic atrophy is considered to be one of the best predictors for clinical disability. As the thalamus has a central role in the brain as a relay station and even as a structure that allows for parallel cortico-thalamo-cortical routes, thalamic atrophy could be associated with disruption of cortical functional networks leading to clinical disability. In this chapter a multi-modal MEG/fMRI approach was chosen where both MEG and fMRI data were used to construct cortical functional networks. In addition, fMRI was used to compute thalamo-cortical functional connectivity. Just as in our previous study the topology of cortical functional networks was analysed by using an MST approach and by computing conventional metrics. Analysis in this chapter firstly revealed thalamic atrophy in MS patients. Secondly, it was again demonstrated that functional networks in MS were characterized by a more path-like topology in terms of the MST in several frequency bands, but especially in the alpha2 band. This shift towards a more path-like cortical functional network topology was associated with thalamic atrophy as well as higher thalamo-cortical functional connectivity (fMRI) in MS patients. These findings suggest that there is a thalamo-cortical loop consisting of the thalamus, thalamo-cortical connections and cortico-cortical connections which is affected in MS. Importantly, disruption of this thalamo-cortical system was associated with clinical disability (physical disability and cognitive impairment).

Finally the main conclusions are:

1. Neural mass models can be used to mimic oscillations originating from neuronal populations and are a good approximation of the mean activity of a neuronal population if neurons in the underlying populations synchronize.
2. There is a functional temporo-posterior core network that emerged near a modality invariant phase transition for functional connectivity and which could be predicted by especially the degree product between nodes in the underlying structural network.
3. The MST is a robust sub-network that is insensitive for network density and average connectivity effects when comparing networks and at the same time its topology is representative for the topology of the underlying network.
4. There is slowing of resting state activity in MS which is also accompanied by higher functional connectivity in especially the default mode resting state network, which were both related to worse clinical outcome in MS.
5. Changes in functional connectivity in MS can better be explained by gray matter thickness if coordinated or correlated patterns of gray matter atrophy were taken into account.
6. Functional networks in MS are consistently characterized by less integrated topology in terms of the MST. This less integrated topology is consistently associated with worse clinical outcome and thalamic atrophy/pathology.

Chapter 11

General Discussion

GENERAL DISCUSSION

There is a discrepancy between classical MRI findings, such as white matter lesion load, and clinical disability in MS. Therefore, there is a need to solve this so called 'clinico-radiological paradox'and to gain insight into mechanisms that lead to clinical disability in MS. In the present dissertation, this problem is tackled from a complex network perspective. Firstly, a theoretical framework is developed to understand how functional networks are related to the underlying structural network and how computational models, such as neural mass models, can be used to simulate functional networks under pathological conditions. Secondly, a part of this framework is applied to understand disruption of structural and functional brain networks in MS. In this context several important aspects were studied: 1) the use of neural mass models as a tool to simulate neuronal activity; 2) the relationship between structural and functional networks (in healthy conditions and in MS); 3) the minimum spanning tree (MST) as an approach to quantify network topology; 4) resting-state activity and functional connectivity in MS; and importantly, 5) the relationship between less integrated functional networks and clinical disability. In the following sections the implications and the mutual relationships between these topics will be discussed.

Neural mass modelling

Neural mass models aim to simulate the mean activity of a whole neuronal population or cortical column. These models can be used simulate EEG or MEG signals and also potentially to simulate and investigate the independent contribution and effect of several types of pathology on functional networks. Neural mass models are based on mean-field approximations that assume homogeneity of the neuronal population (excitatory or inhibitory), i.e. spatial topology is the same everywhere in the neuronal population and all neurons are considered to be identical in terms of their dynamics. However, neuronal populations are characterized by various types of inhomogeneity as they contain several types of neurons that are connected in a non-homogenous way. These non-homogenous properties of neuronal populations could even aggravate in neurological diseases such as MS, where there is axonal and neuronal loss in a neuronal population (Popescu et al., 2013). Therefore, we investigated what the error is when mean-field approximations are made in order to model the mean activity of neuronal population under inhomogenous conditions. The magnitude of the error indicates to what extent these models are useful and this can be quantified by comparing the frequency contents of the neural mass signal and mean population signal. In this context, two neural mass models were derived from a single cell neuronal model. We then demonstrated that there is indeed an error in the description of the mean activity of a neuronal population when using a mean-field approximation, but only when neurons in the neuronal population were desynchronized. Thus, the commonly used neural mass models are capable of simulating the mean activity of a neuronal population if the neurons in this population are synchronized. However, caution is needed if one intends to use neural mass models to understand empirical data, and our

results suggest that a check is needed to verify that under the specific conditions of interest there is sufficient synchronization of neurons in the neuronal population to allow for an accurate mean-field approximation. This can be achieved by comparing the average network signal of a neuronal population with its corresponding neural mass signal by computing the overlap of the corresponding spectral densities and by computing correlations or phase locking values between the neurons in the neuronal population to quantify the amount of synchronization. This exception may not hold in the case of the alpha and lower beta band. We have demonstrated that these frequency bands seem to be captured well by neural mass models irrespective of underlying network topology.

Future studies will need to investigate whether our findings were specific for the single cell neuronal model employed here, leaky integrate-and-fire neurons, or whether these findings can be generalized to mappings from other single cell neuronal models (Fitz-Hugh Nagumo neurons, Theta-neurons, Hodgkin-Huxley neurons) (Izhikevich, 2004). Apart from the neural mass models derived in the present chapter, most of the other neural mass and neural field models can also be described in terms of non-linear second-order differential equations or coupled non-linear first-order differential equations (Deco et al., 2008; Jansen and Rit, 1995; Moran et al., 2007; Rodrigues et al., 2010; Zavaglia et al., 2006). The frequency content of the signal simulated by most of these models is highly dependent on the time constants that are used in these models. The problem with these time constants is that they cannot be tuned exhaustively, otherwise they lose physiological plausibility. Therefore, these other neural mass models might as well have difficulty in capturing higher frequency contents of the mean activity of a neuronal population given the second-order differential nature of these models. Some neural mass modelling studies have claimed to have the ability to generate high frequency oscillations as the frequency content of these simulated signals resembled that of empirical data (Moran et al., 2007; Wendling et al., 2000; Zavaglia et al., 2006). However, these studies have not checked whether their simulated oscillations are a reflection of the mean activity at all. Thus, although these neural mass models may simulate high frequency oscillations, the interpretation with regard to the underlying physiological characteristics of the neuronal populations gets obscured. Therefore, in order for a neural mass model to be useful it has to satisfy two properties at the same time: 1) the neural mass signal should be a good reflection of the mean activity of the underlying neuronal population. This requires mathematical derivation of the neural mass model from the single cell neuronal model, or else comparison between mean activity of the neuronal population and the neural mass model is difficult; 2) the frequency content of the neural mass model should at least in a certain domain of interest resemble empirical EEG/MEG data. With respect to our empirical MEG findings in MS, these findings indicate that we are able to use neural mass models to explain functional connectivity changes in the alpha2 and beta band. With respect to other frequency bands, such as the theta band, a synchronization analysis is required to check whether neurons in the neuronal populations are synchronized before changes within these frequency bands can be studied.

Structural versus functional networks

Functional networks reflect communication between brain regions and are partially shaped by the underlying connections of the structural network. Communication between brain regions is crucial for proper cognitive functioning, and neuropsychiatric diseases are associated with disturbed structural and functional networks (Stam and van Straaten, 2012). Therefore, understanding the principles that determine the topology of both the structural and functional network, as well as their interdependencies is therefore crucial. Furthermore, it will allow one to understand how damage to the structural network will lead to disrupted patterns in the functional network and vice versa. This could help to distinguish between functional network changes that are due to damage to the structural network and functional network changes that are caused by changes in local dynamics or adaptation (a change in activity of neurons over time in response to input from other neurons). This will be of particular relevance in the field of MS since it is often not clear how to interpret changes in functional connectivity or functional network alterations and how this subsequently relates to clinical disability.

In the present dissertation we have demonstrated that around 20-30% of the variance of functional connectivity in healthy conditions can be explained by the product of degrees (number of connections of a brain area) in the structural network together with the Euclidean distance between different brain areas. The degree product of two nodes was the most important predictor and has the ability to also explain the presence of long range functional connections, which is a crucial characteristic of functional brain networks that cannot be explained by distance penalization alone. Our findings support the hypothesis of the importance of scale-free characteristics of structural and functional brain networks, as high degree nodes seem crucial for communication over long distances (Eguiluz et al., 2005; van den Heuvel et al., 2008). In our study we have demonstrated that these high degree nodes do not only have importance for the structural network, but also for the functional networks as we demonstrated that these "highways" are also accompanied with a high amount of traffic (functional connectivity).

Since our analytical model suggested that the degree product has the predictive power to explain functional connectivity, we now could speculate how this could help us with explaining altered functional connectivity in MS. Structural network studies in MS are limited (Li et al., 2012; Shu et al., 2011). Only one previous study analyzed hubness in structural networks in MS and reported that several regions such as the precuneus, premotor cortex, cingulated gyri, inferior parietal cortex and cuneus showed reduction in the amount of degree (Shu et al., 2011). Based on this reduction in high degree nodes, one of the possible explanations for the frequently observed reduced functional connectivity in MS could be due to the reduction in the degree as we have demonstrated that this is proportional to a reduction in functional connectivity (Cruz Gomez et al., 2013; Richiardi et al., 2012; Tecchio et al., 2008). We have also repeatedly found reduction of functional connectivity between brain regions in the alpha2 band in our MEG studies. MEG studies show consistently reductions in functional connectivity between regions that are located far from each other (Cover et al., 2006;

Schoonheim et al., 2011). Given that the product of high degree nodes is required to uphold long range connections, reduction in high degree nodes could therefore also impact the presence of long range connections which also seems to be the case in MS. Although our analytical model is capable of explaining functional connectivity, its explanation is only tested for stationary patterns of functional connectivity averaged over long periods of time and probably less sensitive to fast changes in functional connectivity. Models that describe the fast neuronal dynamics are necessary for this purpose, such as neural mass models, neural field models, Kuramoto models or even epidemic spreading models together with functional connectivity metrics that can be computed for short time scales.

Therefore, apart from the analytical model, we have also used neural mass models to explain the emergence of functional connections. Here, we used neural masses at node locations and connected them through a literature based structural network. We demonstrated that there was an optimal structural connectivity strength for which the emergent simulated functional networks provided the best fit, for both MEG and fMRI. This finding is in line with previous studies which have all shown that the best fit for empirical functional connectivity is near a bifurcation or phase transition (Deco et al., 2009; Deco et al., 2011; Deco et al., 2012; Deco et al., 2013a; Deco et al., 2013b; Nakagawa et al., 2013). The finding that the best fit for functional connectivity is near a bifurcation has important implications, as it explains why functional connectivity is not static but a very dynamic process that can modulate very fast over time. If the optimal structural connectivity strength had been lower, this would indicate that synchronization between regions is very hard to achieve and highly influenced by noise. In contrast, if the optimal structural connectivity strength would have been higher than this would indicate that regions can become highly synchronized, but lose the ability to desynchronize in order to permit flexibility for communication with other regions. Therefore, the optimal structural connectivity strength allows for synchronization between brain regions and at the same time for flexibility which permits interplay between de-synchronization (decoupling) and synchronization (coupling). The question that follows and needs to be addressed is how this optimal structural connectivity strength is achieved in the brain. Is it an emergent property or optimization of a self-organizing process? (Plenz and Thiagarajan, 2007)

Another important finding with regard to our neural mass modelling is the emergence of topological features of functional networks. Weak global structural connectivity leads to a more random functional network topology. Increasing the global structural connectivity strength leads to a network that better resembles the structural network. This has also been found in other modelling studies that used graph metrics such as clustering and global efficiency to characterise the topology of functional networks (Cabral et al., 2012; Ponten et al., 2010). An important finding in these studies was that increasing the global structural connectivity strength led to a more small-world network topology, whereas decreasing this parameter led to a random network. Interestingly, the same behaviour was found when the structural network was damaged by random removal of links. Also in MS it is a recurring finding that the integrity of structural connections decreases and that

there is structural disconnection (link damage) due to lesional damage (Rocca et al., 2012; Rocca and Filippi, 2007). These structural changes could explain why in two of our MS studies we have found that functional network topology tends to have more random characteristics in all frequency bands except the theta band. However, in the theta band there seemed to be a discrepancy since both a shift towards a more random network and towards a more regular network were found. This could either be caused by normalization biases (see discussion minimum spanning tree) or by differences in disease duration of the cohorts.

The importance of understanding the relationship between structural and functional networks was also demonstrated in chapter 7 where we analyzed the co-variance in regional thickness. In MS regional cortical thickness is decreased probably due to neurodegeneration, which is an important marker for cognitive and clinical dysfunction (Filippi et al., 2012; Popescu et al., 2013). Several studies have demonstrated that there is a relationship between thickness of regions and functional connectivity (Alexander-Bloch et al., 2013b). For example, taxi drivers showed increased functional connectivity between temporal regions involved in semantic memory and at the same time these temporal regions showed increased thickness (Alexander-Bloch et al., 2013a). This also suggests that coordinated maturation of thickness may be an important property to understand functional connectivity and not the absolute value of thickness of a region. In our study we also found that the absolute value of regional thickness itself was not associated with functional connectivity in healthy controls or MS patients. A relationship between functional connectivity and thickness was only found if we took into account the mutual influence of thickness between regions, i.e. cortical thickness *correlations*. By examining the network topological results we reported that structural co-variance networks tend to become more regular, which was also the case for functional networks in the theta band. However, in contrast to these networks functional networks in the alpha2 band displayed a more random network topology. The discrepancy between the differences with respect to the alpha2 and theta band is not fully understood, but could be related to the layer specificity for the generation of these oscillations(Roopun et al., 2008). From neurophysiology studies we know that infra-granular cortical layers are more involved in generation of alpha oscillations and supra-granular cortical layers more in the generation of theta oscillations (Bollimunta et al., 2008; Roopun et al., 2008). As there might be retrograde axonal degeneration in especially infra-granular layers (layers with relatively more cortico-fugal projections through white matter) due to white matter lesions in connected tracts this could impact alpha oscillations more than theta oscillations and therefore lead to different behaviour of functional networks in these frequency bands. These present findings are an example where we may have reached a limit for empirical research without a proper theoretical framework as merely empirical research will probably fail to elucidate these findings. We will sketch a computational approach that could help here.

Consider a number of neuronal populations consisting of individual neurons. We further assume that the number of neurons and connections in a population is proportional to the thickness of regions based on empirical findings in MS. We then also have to take into account the physical

connections between populations, based on empirical data. After simulating activity for all neurons, the mean activity of all populations can computed such that functional connectivity can be calculated between neuronal populations. Then, by decreasing regional thickness (based on the number of neurons or connections in a population) one can investigate what the influence is on functional network topology and if there will be a discrepancy between the alpha2 and the theta band. The opposite effect could also be studied, the effect of functional connectivity on regional thickness. Now, one could start with the same model, but for the initial conditions, the number of neurons in each population is equal. We then disconnect some nodes in the network as a surrogate for white matter lesions and then simulate the activity of neurons in the network. Subsequently, the number of neurons/thickness of each region is updated in relation to the strength of the functional connectivity between these regions. Further modelling approaches could use more realistic neuronal populations where more details are included about individual neuron types and layer specificity. In this situation, by selectively decreasing the number of connections and/or neurons it may expected that functional network topology in the alpha band would diverge from structural co-variance network topology.

In one of the previous paragraphs we have stated that the absolute value of regional thickness itself was not sufficient to explain functional connectivity, however, we found that there is one exception to this rule, the thalamus. We have demonstrated that decrease of integration in cortical functional networks was associated with thalamic atrophy in MS. The reason why the thalamus differs in its role in functional connectivity compared to cortical regions could be due to its ubiquitous structural and functional connectivity. There is no other structure in the brain that is so strongly connected to so many other areas as the thalamus (Minagar et al., 2013; Sherman, 2007; van den Heuvel and Sporns, 2011). Furthermore, the thalamus is involved in feedback projections (first order relays) and in feedforward cortico-thalamo-cortical routes (higher order relays) (Sherman, 2007). Feedback projections correspond to projections originating from sensory organs and systems that are transmitted to the cortex. Feedforward routes are pathways that connect two cortical areas with the thalamus as intermediate node. It is hypothesized that these feedforward routes may serve as parallel pathways to cortico-cortical projections and could play an important role in integration of information in functional cortical networks. Therefore, thalamic atrophy in MS could impact these parallel feedforward cortico-thalamo-cortical projections, which could eventually lead to less integrated cortical functional networks. Other scenarios that explain the association between disruption of functional networks and thalamic atrophy are also possible as both may be driven by a third independent process such as global neurodegeneration.

To summarize, we can explain functional connectivity in terms of properties of the structural network such as the structural degree product between nodes. In addition, we need models of neural oscillations to study dynamical changes in functional connectivity. By using these models we have demonstrated that functional network connectivity emerges near a bifurcation when the global structural connectivity is altered. These findings are important as they can explain the

observed more random network topology in MS. Thirdly; we have reported that the relationship between regional thickness and functional connectivity can only be understood if the coordinated patterns of regional thickness are taken into account, except for the thalamus, possibly due to its ubiquitous connectivity.

The minimum spanning tree

It is increasingly acknowledged that quantification of either structural or functional network topology is important for the understanding of efficient information transfer in brain networks and optimal cognitive functioning. However, the quantification and comparison of network topology is accompanied by methodological issues such as differences in network size, network density or average connectivity. In chapter 4 it was demonstrated that the MST is able to overcome many of these methodological issues, except network size. Furthermore, it was demonstrated that the topology of the MST accurately captures the underlying network topology in terms of the clustering coefficient and path length. Empirical studies that have used conventional network measures have led to more confusion in the field than clarity as for several diseases there is no clear pattern what happens in terms of network topology during the disease course (Diessen et al., 2013; Tijms et al., 2013). As long as a standard atlas with fixed size is used the MST could help in this context as it assures that it only captures information about network topology and not other properties of the network such as average connectivity, average density or average degree.

However, it may be the case that the MST is not suitable for more advanced network analysis such as diffusion processes on networks, searching and routing, or epidemic spreading. For example, diffusion processes are shown to be relevant for understanding the relationship between structural and functional brain networks (Abdelnour et al., 2014). However, there needs to be redundancy in networks for understanding diffusion processes, a set of paths from node A to node B, and not just one path, which is the case for the MST. This lack of redundancy would make the study of these processes too trivial, which may not be a good representation of actual processes on the underlying network. Taken together, this indicates that the MST seems to be a good intermediate step in the development of an unbiased approach to compare networks. Future unbiased approaches should therefore be able to reconstruct a larger sub-network characterised by more redundancy and include the backbone of the original network. A potential candidate for this purpose could be the union of shortest path trees (USPT) ((Meier et al., 2014) in preparation). This is a sub-network of the original network that contains the set of shortest paths of the original network. Although the construction of the USPT depends on the choice for link transformation and a tuning parameter alpha, the links that are included in the USPT are not arbitrary, but always have a topological meaning. Furthermore, the MST is always contained in the USPT irrespective of the tuning parameter alpha. If the tuning parameter alpha becomes high, there is convergence between the USPT and the MST. Therefore, the MST can be considered as a special case of the USPT.

Functional connectivity

Both higher functional connectivity and lower functional connectivity in MS patients in different frequency bands using MEG were found. In addition, higher functional connectivity from the thalamus to cortical regions in MS patients was also demonstrated. Previous fMRI and MEG studies have also found increases as well as decreases in functional connectivity (Cader et al., 2006; Cruz Gomez et al., 2013; Greicius et al., 2009; Hardmeier et al., 2012; Hawellek et al., 2011; Parisi et al., 2012; Richiardi et al., 2012; Tona et al., 2014; Valsasina et al., 2011). Both decreased and increased functional connectivity has been related to clinical and cognitive dysfunction. Especially increased functional connectivity within resting state networks, such as the default mode network, seems to be of clinical relevance as was demonstrated in our MEG study and in several fMRI studies (Bonavita et al., 2011; Richiardi et al., 2012; Rocca et al., 2010; Rocca et al., 2012). We found that especially lower functional connectivity in the alpha2 band was an important hallmark for MS since this was a consistent finding for different MS patient cohorts. However, a problem with many functional connectivity findings is that the MS community does not have a clear grip what these findings actually mean: is an increase in functional connectivity a sign of damage or a compensatory mechanism? In one of our previous studies we found that increased functional connectivity was only found in a group of MS patients who were cognitively impaired and not in the group of MS patients with preserved cognition (Schoonheim et al., 2014). This suggested that this increase could be a sign of pathology or damage. However, these findings may also fit in the hypothesis of cognitive degeneracy: several cortical systems can support a process corresponding to a cognitive domain, i.e. there is redundancy (Price and Friston, 2002). In cognitively preserved MS patients it could well be the case that there is still sufficient redundancy such that increases in functional connectivity are not yet necessary to maintain a process necessary for cognitive functioning. However, within this line of reasoning and speculation it could be argued that in case of failure of redundancy there is a need for increased functional connectivity as observed in cognitively impaired MS patients. Here, an increase in functional connectivity may implicate a partially restoration of the cortical system involved in cognitive functioning. However, the mentioned hypotheses above are both merely speculation.

Therefore, correlating functional connectivity changes in MS to cognitive changes only, will by no means give us an answer to what these changes mean and if these functional connectivity changes are beneficial or maleficent for maintaining cognitive functioning. As stated earlier, for MS, the empirical findings indicate that there could be both an increase and decrease in functional connectivity where both have been linked to structural pathology and clinical disability. This could as well indicate that the shape of the curve for functional connectivity vs clinical status could be described by an inverted U-curve suggesting that any shift from this optimum (or maximum) is maladaptive and related to clinical disability.

An alternative way to understand these functional connectivity changes is to study their relationship with the underlying structural network. As discussed above, given the changes on the

structural network of MS patients decreased functional connectivity in MS could be explained, in for example the alpha2 band, based on our distance versus degree model. However, an increase in functional connectivity seems to be difficult to explain by our model as our model suggests that an increase in functional connectivity should be observed due to an increase in degree for nodes in the structural network. However, this has (yet) not been reported in empirical studies. One previous modelling study suggested that only part of the functional connectivity can be explained by taking into account structural network properties and that a significant part could be explained by local brain dynamics (Messe et al., 2014). Therefore, in future studies computational models that capture the local dynamics in more detail could be used to study the appearance of increased functional connectivity in MS. In these models, the role and influence of several pathological features of MS on functional connectivity should be studied, such as an excessive amount of glutamate (consistently found in MS) and an up or down regulation of NMDA receptors or a decrease in connections in the neuronal population (Geurts et al., 2003; Kostic et al., 2013; Pampliega et al., 2011; Voulgari-Kokota et al., 2012). One earlier neural mass modelling study for Alzheimer's disease demonstrated that by decreasing the connection strength in a neuronal population there can be an initial increase in activity and functional connectivity followed by a gradual decrease in activity and functional connectivity (de Haan W. et al., 2012). This observation may also be generalized to other diseases such as MS where there is also loss of connectivity within a neuronal population. However, the error due to mean-field approximations was not studied here as in these conditions decreasing network density may lead to a discrepancy between the mean activity of a neuronal population and the corresponding neural mass signal which indicates that the interpretation with regard to the underlying physiological characteristics of the neuronal population becomes difficult (see section neural mass modelling).

Functional network topology

In this dissertation we have investigated how functional network topology alters in MS patients. With respect to conventional metrics, such as the clustering coefficient and path length, we reported that functional brain networks in MS tend to become more random in several frequency bands and irrespective of disease duration. Only in the theta band and in the MS cohort with longer disease duration we found that functional network topology becomes more regular, which resembled the topological change in structural co-variance between regions. Two previous studies have also reported more regular functional network topology in early MS (Schoonheim et al., 2011; Schoonheim et al., 2012). However, the latter studies were either performed using a different modality (fMRI) or did their analyses in sensor-space using a functional connectivity metric that is sensitive to the effects of volume conduction/field spread. Nevertheless, the fact that there is no consistent shift in topology using conventional network metrics, e.g. some studies report higher clustering in contrast to other studies that report lower clustering (Diessen et al., 2013; Tijms et al., 2013), there is a need for a new framework for understanding and characterizing functional network topology. Thorough

reviews have reported that there is large discrepancy of network topological findings between studies and centers (Diessen et al., 2013; Stam et al., 2014; Tijms et al., 2013).

In the present dissertation, we have used an MST approach to counter several methodological biases and we consistently found a more path-like topology in MS patients irrespective of the disease duration when compared to healthy subjects. In contrast to conventional network metrics, we did not find a discrepancy between studies in network topological changes when using the MST. We also repeatedly found that a shift towards a more path-like topology was associated with cognitive and clinical dysfunction. Similar findings have also been reported for Parkinson's disease and neuroglioma, where a shift towards a more path-like topology was associated with measures of disability (Olde Dubbelink et al., 2014; van Dellen E. et al., 2014). Together these findings may indicate that a shift towards a more path-like topology could be a final common pathway in neurological diseases that is always as sign of damage. More path-like trees are characterized by lower efficiency due to longer path lengths between nodes and decrease of hierarchy. Also selective damage to high degree nodes, repeatedly found in neuropsychiatric diseases, could lead to more path-like topology (Bullmore and Sporns, 2012). However, to maintain a flexible an optimal configuration for flow on a network all these mentioned features are necessary (Bullmore and Sporns, 2012).

One of the advantages of the MST approach is that our results with respect to network topology for MS patients seem to be robust and at the same time we can interpret them in terms of conventional network measures. In one of our methodological studies we demonstrated that there seems to be a continuous spectrum with regard to MST topology when networks are rewired from either a scale free to random or from regular to random. Scale-free networks correspond to MSTs with star-like topology, whereas regular networks correspond to a path-like topology. In between those two extremes we find both small-world networks and random networks. In all our MS studies we found that MST network topology shifted towards more path-like topologies. This was characterized by higher eccentricity and diameter and lower leaf fraction but also by a decrease in degree divergence. This degree divergence especially decreases when the average degree also decreases, i.e. this measure is able to capture changes in scale-free characteristics of the underlying network. This could indicate that functional network topology in MS loses its scale-free characteristics. This indicates that high degree nodes in the functional networks in MS are also, and perhaps even preferentially, damaged. This could support the present hypothesis that damage to high degree nodes is a final common pathway in many neurological diseases due to its sensitivity to damage (Bullmore and Sporns, 2012; de Haan W. et al., 2012).

Methodological considerations

There are several methodological issues that need to be addressed to make progress in the field of complex brain networks. These include consensus on the definition of nodes and links, functional connectivity metrics which are not biased by negative values (Pearson's correlations coefficients) (Pritchard et al., 2014), functional connectivity metrics for MEG/EEG that are not sensitive to

volume conduction/field spread and at the same time sensitive for short distance interactions, reliable measures for cross-frequency phase-coupling, and unbiased method to compare networks. Also more practical methodological points with regard to MEG recordings and post-processing need to be addressed in order to allow for a reliable basis for further network analyses. Below follows a discussion about these points in detail.

First of all, data selection forms the basis for functional connectivity and network analysis. As MEG data is often contaminated by artefacts and noise, careful selection and inspection of the data is required prior to further analysis. Until now, mostly semi-automatic techniques have been adopted, such as temporal signal-space separation (tSSS), to (spatially) filter the data and remove artefacts (Taulu and Hari, 2009; Taulu and Simola, 2006). However, tSSS is not able remove all artefacts and especially drowsiness cannot be checked for yet. Therefore, the gold standard is still to use semi-automatic techniques in combination with thorough visual inspection (Gross et al., 2012). The problem with this visual inspection is that this entails subjectivity that can lead to different epoch selection for different researchers and eventually to different results. Therefore, there is a need to improve the completely automatic artefact rejection methods as these are currently not able to ensure robust performance (Gross et al., 2012).

Secondly, the development of functional connectivity metrics should result in metrics that are also sensitive for short distance connections and at the same time insensitive to volume conduction/field spread. There are several measures that are sensitive for short distance connections, however, in these cases it is often difficult to separate the contribution of volume conduction/field spread from actual physiological functional connectivity (Pereda et al., 2005). In our work we have consequently used the PLI, which calculates the asymmetry of the instantaneous phase differences between signals. This metric has proven to be robust and less sensitive to volume conduction/field spread. However, the disadvantage is that its correction for volume conduction/field spread maybe too strong which leads to insensitivity to small-distance connections since these correspond to two time-series with very small and stable phase differences. This decreased sensitivity could subsequently also influence the topology of functional networks. For the MST this could indicate that there is lower probability that short distance links are included, which could lead to less segregation and thus a less path-like tree topology. In terms of conventional networks, this was also found using the PLI as these networks obtained by this metric showed more random topology compared to networks obtained from metrics more sensitive to volume conduction/field spread (Peraza et al., 2012).

Another challenge in this area is to have metrics that can reliably describe functional coupling and decoupling between brain regions as both properties are important to maintain efficient communication between brain regions. This functional coupling and decoupling is especially interesting when the temporal evolution of brain networks needs to be studied. There is increasing evidence that this temporal evolution of functional brain networks is important for the understanding of normal brain functioning (de Pasquale F. et al., 2010; Jirsa and Kelso, 2000; Roopun et al., 2008).

Another point related to metrics that quantify functional connectivity is cross-frequency phase coupling. In many empirical MEG and EEG studies (also in our work) it is found that there can be simultaneous increase in functional connectivity in one frequency band together with a decrease in another frequency band. These simultaneous changes in functional connectivity allow us to investigate whether these simultaneous changes in functional connectivity are related. Until now, the main problem with respect to cross-frequency phase coupling metrics is that they are sensitive to volume conduction/field spread and thus not reliably applicable to MEG/EEG data.

Future directions

One of the most important aims in the research field of MS should be to achieve a quantitative theory that explains the relationships between the most important pathological characteristics of the disease in order to give insights into mechanisms that lead to neurological symptoms. Such a quantitative theory for disease mechanisms in MS should preferably describe a hierarchical system consisting of a structural network superimposed by a functional network, and where the impact of classical structural pathology is understood in terms of alterations with respect to both the structural and functional networks (see figure 1 in the introduction). However, a quantitative theory is still far out of reach due to limited cross-talk between quantitative models and experimental findings. This has led to a large number of experimental findings that may not easily be understood in terms of the present qualitative ideas about disease mechanisms in MS.

A complex network perspective should be an essential part of the theory as it is crucial for the understanding of the relationships between structure and function and the occurrence of cognitive and clinical dysfunction. Either rewiring or growth models may be suited to simulate structural networks, where specific learning rules should be able to capture the change in the structural networks due to lesions, atrophy, or changes in the integrity of gray/white matter. Subsequently, quantitative models should elucidate the interrelationship between structural and functional networks such that the effect of lesions or atrophy on communication between brain regions can be elucidated. At the same time, such models may also explain how disturbed communication between brain regions affects structural network connectivity or structural pathology. Such models eventually need to explain the clinical status of the patient, given the knowledge of the structural and functional pathology of the patient, i.e. such a quantitative theory needs to solve the 'clinico-radiological' paradox. Other clinically relevant issues that also need to be addressed by a quantitative theory are the difference in disease severity between males and females and the occurrence of disease subtypes.

In the future, a quantitative theory should not only be of use for neurobiologists who are interested in disease mechanisms, but also for the neurologist in the outpatient-clinic. It is not expected that it will help to diagnose MS patients, but to give an objective measure of the 'clinico-pathological' status of the patient. A measure for 'clinico-pathological' status in this context means

an objective measure for the neurological deficits of the patient together with an objective measure for the observed pathology in the brain of the patient. An objective measure for the 'clinico-pathological' status of the patient could also help to judge treatment response of an individual patient. Furthermore, if one understands the dynamics of a system one might also make better predictions about how the system will behave in the near future and therefore it could help to give an individualised prognosis.

Appendix

Abbott, L., van Vreeswijk, C., 1993. Asynchronous states in networks of pulse-coupled neuron. Phys.Rev.A 48, 1483-1490.

Abdelnour, F., Voss, H.U., Raj, A., 2014. Network diffusion accurately models the relationship between structural and functional brain connectivity networks. Neuroimage 90, 335-347.

Aertsen, A.M.H.J., Preissl, H., 1991. Dynamics of activity and connectivity in physiological neuronal networks. Non linear dynamics and neuronal networks, 281-302.

Alexander-Bloch, A., Giedd, J.N., Bullmore, E., 2013a. Imaging structural co-variance between human brain regions. Nat.Rev.Neurosci. 14, 322-336.

Alexander-Bloch, A., Raznahan, A., Bullmore, E., Giedd, J., 2013b. The convergence of maturational change and structural covariance in human cortical networks. J.Neurosci. 33, 2889-2899.

Alexander-Bloch, A.F., Gogtay, N., Meunier, D., Birn, R., Clasen, L., Lalonde, F., Lenroot, R., Giedd, J., Bullmore, E.T., 2010. Disrupted modularity and local connectivity of brain functional networks in childhood-onset schizophrenia. Front Syst.Neurosci. 4, 147.

Alexander-Bloch, A.F., Vertes, P.E., Stidd, R., Lalonde, F., Clasen, L., Rapoport, J., Giedd, J., Bullmore, E.T., Gogtay, N., 2013c. The anatomical distance of functional connections predicts brain network topology in health and schizophrenia. Cereb.Cortex 23, 127-138.

Amari, S.I., 1972. Characteristics of Random Nets of Analog Neuron-Like Elements. IEEE Trans.Syst.Man Cybern 2, 643-657.

Amari, S.-I., Yoshida, K., Kanatani, K.-I., 1977. A mathematical foundation for statistical neurodynamics. SIAMJ. Appl.Math 33, 95-126.

Ashburner, J., Friston, K.J., 2005. Unified segmentation. Neuroimage. 26, 839-851.

Audoin, B., Zaaraoui, W., Reuter, F., Rico, A., Malikova, I., Confort-Gouny, S., Cozzone, P.J., Pelletier, J., Ranjeva, J.P., 2010. Atrophy mainly affects the limbic system and the deep grey matter at the first stage of multiple sclerosis. J.Neurol.Neurosurg.Psychiatry 81, 690-695.

Bagrow, J.P., 2012. Communities and bottlenecks: trees and treelike networks have high modularity. Phys. Rev.E.Stat.Nonlin.Soft.Matter Phys. 85, 066118.

Baladron, J., Fasoli, D., Faugeras, O., Touboul J., 2012. Mean-field description and propagation of chaos in networks of Hodgkin-Huxley and FitzHugh-Nagumo neurons. J Math Neurosci 2, 2190-8567.

Barabasi, A.L., Albert, R., 1999. Emergence of scaling in random networks. Science 286, 509-512.

Barahona, M., Pecora, L., 2002. Synchronization in Small-World Systems. Phys.Rev.Lett. 89, 054101-1-054101-4.

Barkhof, F., 2002. The clinico-radiological paradox in multiple sclerosis revisited. Curr.Opin.Neurol. 15, 239-245.

Barnes, G.R., Hillebrand, A., 2003. Statistical flattening of MEG beamformer images. Hum.Brain Mapp. 18, 1-12.

Barnes, G.R., Hillebrand, A., Fawcett, I.P., Singh, K.D., 2004. Realistic spatial sampling for MEG beamformer images. Hum.Brain Mapp. 23, 120-127.

Barrat, A., Barthelemy, M., Vespignani, A., 2008. Networks and complexity. Dynamical processes on complex networks, pp. 24-49.

Barrat, A., Barthelemy, M., Pastor-Satorras, R., Vespignani, A., 2004. The architecture of complex weighted networks. Proc.Natl.Acad.Sci.U.S.A 101, 3747-3752.

Bartolomei, F., Bosma, I., Klein, M., Baayen, J.C., Reijneveld, J.C., Postma, T.J., Heimans, J.J., van Dijk, B.W., de Munck, J.C., de, J.A., Cover, K.S., Stam, C.J., 2006. Disturbed functional connectivity in brain tumour patients: evaluation by graph analysis of synchronization matrices. Clin.Neurophysiol. 117, 2039-2049.

Batista, S., Zivadinov, R., Hoogs, M., Bergsland, N., Heininen-Brown, M., Dwyer, M.G., Weinstock-Guttman, B., Benedict, R.H., 2012. Basal ganglia, thalamus and neocortical atrophy predicting slowed cognitive processing in multiple sclerosis. J.Neurol. 259, 139-146.

Belykh, I., de, L.E., Hasler, M., 2005. Synchronization of bursting neurons: what matters in the network topology. Phys.Rev.Lett. 94, 188101.

Benjamini, Y., Hochberg, Y., 1995. Controlling the false discovery rate: a practical and powerful approach to multiple testing. Journal of the Royal Statistical Society 57, 289-300.

Bernhardt, B.C., Chen, Z., He, Y., Evans, A.C., Bernasconi, N., 2011. Graph-theoretical analysis reveals disrupted small-world organization of cortical thickness correlation networks in temporal lobe epilepsy. Cereb.Cortex 21, 2147-2157.

Bhattacharya, B.S., Coyle, D., Maguire, L.P., 2011. A thalamo-cortico-thalamic neural mass model to study alpha rhythms in Alzheimer's disease. Neural Netw. 24, 631-645.

Blondel, V.D., Gajardo, A., Heymans, M., Senellart, P., van Dooren, P., 2006. A measure of similarity between graph vertices: applications to synonym extraction and web searching. SIAM Rev. 46, 647-666.

Bo, L., 2009. The histopathology of grey matter demyelination in multiple sclerosis. Acta Neurol.Scand. 120, 51-57.

Boersma, M., Smit, D.J., Boomsma, D.I., Geus, E.J., Delemarre-van de Waal HA, Stam, C., 2012. Growing trees in child brains: Graph theoretical analysis of EEG derived minimum spanning tree in 5 and 7 year old children reflects brain maturation. Brain Connect. 3, 50-60.

Boersma, M., Smit, D.J., de Bie, H.M., Van Baal, G.C., Boomsma, D.I., de Geus, E.J., Delemarre-van de Waal HA, Stam, C.J., 2011. Network analysis of resting state EEG in the developing young brain: structure comes with maturation. Hum.Brain Mapp. 32, 413-425.

Bollimunta, A., Chen, Y., Schroeder, C.E., Ding, M., 2008. Neuronal mechanisms of cortical alpha oscillations in awake-behaving macaques. J.Neurosci. 28, 9976-9988.

Bonavita, S., Gallo, A., Sacco, R., Corte, M.D., Bisecco, A., Docimo, R., Lavorgna, L., Corbo, D., Costanzo, A.D., Tortora, F., Cirillo, M., Esposito, F., Tedeschi, G., 2011a. Distributed changes in default-mode resting-state connectivity in multiple sclerosis. Mult.Scler. 17, 411-422.

Bonavita, S., Gallo, A., Sacco, R., Corte, M.D., Bisecco, A., Docimo, R., Lavorgna, L., Corbo, D., Costanzo, A.D., Tortora, F., Cirillo, M., Esposito, F., Tedeschi, G., 2011b. Distributed changes in default-mode resting-state connectivity in multiple sclerosis. Mult.Scler. 17, 411-422.

Borgers, C., Epstein, S., Kopell, N.J., 2005. Background gamma rhythmicity and attention in cortical local circuits: a computational study. Proc.Natl.Acad.Sci.U.S.A 102, 7002-7007.

Bosboom, J.L., Stoffers, D., Stam, C.J., Berendse, H.W., Wolters, E.C., 2009a. Cholinergic modulation of MEG resting-state oscillatory activity in Parkinson's disease related dementia. Clin.Neurophysiol. 120, 910-915.

Bosboom, J.L., Stoffers, D., Stam, C.J., van Dijk, B.W., Verbunt, J., Berendse, H.W., Wolters, E.C., 2006. Resting state oscillatory brain dynamics in Parkinson's disease: an MEG study. Clin.Neurophysiol. 117, 2521-2531.

Bosboom, J.L., Stoffers, D., Wolters, E.C., Stam, C.J., Berendse, H.W., 2009b. MEG resting state functional connectivity in Parkinson's disease related dementia. J.Neural Transm. 116, 193-202.

Bosma, I., Stam, C.J., Douw, L., Bartolomei, F., Heimans, J.J., van Dijk, B.W., Postma, T.J., Klein, M., Reijneveld, J.C., 2008. The influence of low-grade glioma on resting state oscillatory brain activity: a magnetoencephalography study. J.Neurooncol. 88, 77-85.

Boucsein, C., Nawrot, M., Schnepel, P., Aertsen, A., 2011. Beyond the cortical column: abundance and physiology of horizontal connections imply a strong role for inputs from the surround. Frontiers in neuroscience 5, 32.

Braunstein, L., Wu, Z., Chen, Y., Buldyrev, S., Kalisky, T., Sreenivasan, S., Cohen, R., Lopez, E., Havlin, S., Eugene Stanley, H., 2013. Optimal path and minimum spanning trees in random weighted networks . Int.J.Bifurcation Chaos 17, 2215-2284.

Breakspear, M., Terry, J.R., Friston, K.J., 2003. Modulation of excitatory synaptic coupling facilitates synchronization and complex dynamics in a biophysical model of neuronal dynamics. Network. 14, 703-732.

Brookes, M.J., Hale, J.R., Zumer, J.M., Stevenson, C.M., Francis, S.T., Barnes, G.R., Owen, J.P., Morris, P.G., Nagarajan, S.S., 2011a. Measuring functional connectivity using MEG: methodology and comparison with fcMRI. Neuroimage. 56, 1082-1104.

Brookes, M.J., Vrba, J., Robinson, S.E., Stevenson, C.M., Peters, A.M., Barnes, G.R., Hillebrand, A., Morris, P.G., 2008. Optimising experimental design for MEG beamformer imaging. Neuroimage. 39, 1788-1802.

Brookes, M.J., Woolrich, M., Luckhoo, H., Price, D., Hale, J.R., Stephenson, M.C., Barnes, G.R., Smith, S.M., Morris, P.G., 2011b. Investigating the electrophysiological basis of resting state networks using magnetoencephalography. Proc.Natl.Acad.Sci.U.S.A 108, 16783-16788.

Brookes, M.J., Woolrich, M.W., Barnes, G.R., 2012a. Measuring functional connectivity in MEG: a multivariate approach insensitive to linear source leakage. NeuroImage 63, 910-920.

Broyd, S.J., Demanuele, C., Debener, S., Helps, S.K., James, C.J., Sonuga-Barke, E.J., 2009. Default-mode brain dysfunction in mental disorders: a systematic review. Neurosci.Biobehav.Rev. 33, 279-296.

Brunel, N., Hakim, V., 1999. Fast global oscillations in networks of integrate-and-fire neurons with low fi ring rates. Neural Comput 11, 1621-1671.

Brunetti, M., Belardinelli, P., Caulo, M., Del, G.C., Della, P.S., Ferretti, A., Lucci, G., Moretti, A., Pizzella, V., Tartaro, A., Torquati, K., Olivetti, B.M., Romani, G.L., 2005. Human brain activation during passive listening to sounds from different locations: an fMRI and MEG study. Hum.Brain Mapp. 26, 251-261.

Brunetti, M., Della, P.S., Ferretti, A., Del, G.C., Cianflone, F., Belardinelli, P., Caulo, M., Pizzella, V., Olivetti, B.M., Romani, G.L., 2008. A frontoparietal network for spatial attention reorienting in the auditory domain: a human fMRI/MEG study of functional and temporal dynamics. Cereb.Cortex 18, 1139-1147.

Bullmore, E., Sporns, O., 2009. Complex brain networks: graph theoretical analysis of structural and functional systems. Nat.Rev.Neurosci. 10, 186-198.

Bullmore, E., Sporns, O., 2012. The economy of brain network organization. Nat.Rev.Neurosci. 13, 336-349.

Bullmore, E.T., Suckling, J., Overmeyer, S., Rabe-Hesketh, S., Taylor, E., Brammer, M.J., 1999. Global, voxel, and cluster tests, by theory and permutation, for a difference between two groups of structural MR images of the brain. IEEE Trans.Med.Imaging 18, 32-42.

Buxton, R.B., Wong, E.C., Frank, L.R., 1998. Dynamics of blood flow and oxygenation changes during brain activation: the balloon model. Magn Reson.Med. 39, 855-864.

Byrd, R.h., Schnabel, R.B., Schultz, G.A., 1987. A trust region algorithm for nonlienarly constrained optimization. SIAM J.Numer.Anal. 24, 1152-1170.

Cabral, J., Hugues, E., Kringelbach, M.L., Deco, G., 2012. Modeling the outcome of structural disconnection on resting-state functional connectivity. Neuroimage. 62, 1342-1353.

Cabral, J., Hugues, E., Sporns, O., Deco, G., 2011. Role of local network oscillations in resting-state functional connectivity. Neuroimage. 57, 130-139.

Cabral, J., Luckhoo, H., Woolrich, M., Joensson, M., Mohseni, H., Baker, A., Kringelbach, M.L., Deco, G., 2013. Exploring mechanisms of spontaneous MEG functional connectivity: How delayed network interactions lead to structured amplitude envelopes of band-pass filtered oscillations. Neuroimage. 90, 423-435.

Cader, S., Cifelli, A., Abu-Omar, Y., Palace, J., Matthews, P.M., 2006. Reduced brain functional reserve and altered functional connectivity in patients with multiple sclerosis. Brain 129, 527-537.

Calabrese, M., Atzori, M., Bernardi, V., Morra, A., Romualdi, C., Rinaldi, L., McAuliffe, M.J., Barachino, L., Perini, P., Fischl, B., Battistin, L., Gallo, P., 2007. Cortical atrophy is relevant in multiple sclerosis at clinical onset. J.Neurol. 254, 1212-1220.

Calabrese, M., Filippi, M., Gallo, P., 2010. Cortical lesions in multiple sclerosis. Nat.Rev.Neurol. 6, 438-444.

Cessac, B., 1995. Increase in complexity in random neural networks. J.Phys.I (France) 5, 409-432.

Cessac, B., 2008. A discrete time neural network model with spiking neurons: rigorous results on the spontaneous dynamics. J.Math.Biol. 56, 311-345.

Cessac, B., Vieville T, 2013. On dynamics of integrate-and-fire neural networks with adaptive conductance based synapses. Front.Neurosci 2.

Chard, D.T., Jackson, J.S., Miller, D.H., Wheeler-Kingshott, C.A., 2010. Reducing the impact of white matter lesions on automated measures of brain gray and white matter volumes. J.Magn Reson.Imaging 32, 223-228.

Cheriton, D., Tarjan, R.E., 1976. Finding minimum spanning trees. SIAM Journal on Computing 5, 724-742.

Chiaravalloti, N.D., DeLuca, J., 2008. Cognitive impairment in multiple sclerosis. Lancet Neurol. 7, 1139-1151.

Ciftci, K., 2011. Minimum spanning tree reflects the alterations of the default mode network during Alzheimer's disease. Ann.Biomed.Eng 39, 1493-1504.

Collin, G., Sporns, O., Mandl, R.C., van den Heuvel, M.P., 2013. Structural and Functional Aspects Relating to Cost and Benefit of Rich Club Organization in the Human Cerebral Cortex. Cereb.Cortex.

Colon, E., Hommes, O.R., de Weerd, J.P., 1981. Relation between EEG and disability scores in multiple sclerosis. Clin.Neurol.Neurosurg. 83, 163-168.

Compston, A., Coles, A., 2008. Multiple sclerosis. Lancet 372, 1502-1517.

Cottrell, D.A., Kremenchutzky, M., Rice, G.P.A., Koopman, W.J., Hader, W., Baskerville, J., Ebers, G.C., 1999. The natural history of multiple sclerosis: a geographically based study 5. The clinical features and natural history of primary progressive multiple sclerosis. Brain 122, 625-639.

Cover, K.S., Vrenken, H., Geurts, J.J., van Oosten, B.W., Jelles, B., Polman, C.H., Stam, C.J., van Dijk, B.W., 2006a. Multiple sclerosis patients show a highly significant decrease in alpha band interhemispheric synchronization measured using MEG. Neuroimage. 29, 783-788.

Creutzfeldt, O., Ito, M., 1968. Functional synaptic organization of primary visual cortex neurones in the cat. Exp. Brain Res. 6, 324-352.

Cruz Gomez, A.J., Ventura, C.N., Belenguer, A., Avila, C., Forn, C., 2013. Regional brain atrophy and functional connectivity changes related to fatigue in multiple sclerosis. PLoS.One. 8, e77914.

Daams, M., Geurts, J.J., Barkhof, F., 2013. Cortical imaging in multiple sclerosis: recent findings and 'grand challenges'. Curr.Opin.Neurol. 26, 345-352.

Dale, A.M., Fischl, B., Sereno, M.I., 1999. Cortical surface-based analysis. I. Segmentation and surface reconstruction. Neuroimage. 9, 179-194.

Dale, A.M., Liu, A.K., Fischl, B.R., Buckner, R.L., Belliveau, J.W., Lewine, J.D., Halgren, E., 2000. Dynamic statistical parametric mapping: combining fMRI and MEG for high-resolution imaging of cortical activity. Neuron 26, 55-67.

Damoiseaux, J.S., Rombouts, S.A., Barkhof, F., Scheltens, P., Stam, C.J., Smith, S.M., Beckmann, C.F., 2006. Consistent resting-state networks across healthy subjects. Proc.Natl.Acad.Sci.U.S.A 103, 13848-13853.

David, O., Garnero, L., Cosmelli, D., Varela, F.J., 2002. Estimation of neural dynamics from MEG/EEG cortical current density maps: application to the reconstruction of large-scale cortical synchrony. IEEE Trans.Biomed. Eng 49, 975-987.

de Haan W., Mott, K., van Straaten, E.C., Scheltens, P., Stam, C.J., 2012a. Activity dependent degeneration explains hub vulnerability in Alzheimer's disease. PLoS.Comput.Biol. 8, e1002582.

de Haan W., Stam, C.J., Jones, B.F., Zuiderwijk, I.M., van Dijk, B.W., Scheltens, P., 2008. Resting-state oscillatory brain dynamics in Alzheimer disease. J.Clin.Neurophysiol. 25, 187-193.

de Haan W., van der Flier, W.M., Wang, H., Van Mieghem, P.F., Scheltens, P., Stam, C., 2012b. Disruption of functional brain networks in Alzheimer's disease: what can we learn from graph spectral analysis of resting-state MEG? Brain Connect. 2, 45-55.

De Luca M., Beckmann, C.F., De, S.N., Matthews, P.M., Smith, S.M., 2006. fMRI resting state networks define distinct modes of long-distance interactions in the human brain. Neuroimage. 29, 1359-1367.

de Munck, J.C., Goncalves, S.I., Huijboom, L., Kuijer, J.P., Pouwels, P.J., Heethaar, R.M., Lopes da Silva, F.H., 2007. The hemodynamic response of the alpha rhythm: an EEG/fMRI study. Neuroimage. 35, 1142-1151.

de Pasquale F., Della, P.S., Snyder, A.Z., Lewis, C., Mantini, D., Marzetti, L., Belardinelli, P., Ciancetta, L., Pizzella, V., Romani, G.L., Corbetta, M., 2010. Temporal dynamics of spontaneous MEG activity in brain networks. Proc.Natl. Acad.Sci.U.S.A 107, 6040-6045.

de Pasquale F., Della, P.S., Snyder, A.Z., Marzetti, L., Pizzella, V., Romani, G.L., Corbetta, M., 2012. A cortical core for dynamic integration of functional networks in the resting human brain. Neuron 74, 753-764.

de Waal H., Stam, C.J., de, H.W., van Straaten, E.C., Scheltens, P., van der Flier, W.M., 2012. Young Alzheimer patients show distinct regional changes of oscillatory brain dynamics. Neurobiol.Aging 33, 1008-1031.

Deco, G., Jirsa, V., Robinson, P., Breakspear, M., Friston, K., 2008. The dynamic brain: from spiking neurons to neural masses and cortical fields. Plos Comput Biol 4, e1000092.

Deco, G., Jirsa, V., McIntosh, A.R., Sporns, O., Kotter, R., 2009. Key role of coupling, delay, and noise in resting brain fluctuations. Proc.Natl.Acad.Sci.U.S.A 106, 10302-10307.

Deco, G., Jirsa, V.K., 2012. Ongoing cortical activity at rest: criticality, multistability, and ghost attractors. J.Neurosci. 32, 3366-3375.

Deco, G., Jirsa, V.K., McIntosh, A.R., 2011. Emerging concepts for the dynamical organization of resting-state activity in the brain. Nat.Rev.Neurosci. 12, 43-56.

Deco, G., Jirsa, V.K., McIntosh, A.R., 2013a. Resting brains never rest: computational insights into potential cognitive architectures. Trends Neurosci. 36, 268-274.

Deco, G., Ponce-Alvarez, A., Mantini, D., Romani, G.L., Hagmann, P., Corbetta, M., 2013b. Resting-State Functional Connectivity Emerges from Structurally and Dynamically Shaped Slow Linear Fluctuations. J.Neurosci. 33, 11239-11252.

Deco, G., Senden, M., Jirsa, V., 2012. How anatomy shapes dynamics: a semi-analytical study of the brain at rest by a simple spin model. Front Comput.Neurosci. 6, 68.

Dell'Acqua, M.L., Landi, D., Zito, G., Zappasodi, F., Lupoi, D., Rossini, P.M., Filippi, M.M., Tecchio, F., 2010. Thalamocortical sensorimotor circuit in multiple sclerosis: an integrated structural and electrophysiological assessment. Hum.Brain Mapp. 31, 1588-1600.

Demuru, M., Fara, F., Fraschini, M., 2013. Brain network analysis of EEG functional connectivity during imagery hand movements. Journal of integrative neuroscience 12, 441-447.

Desikan, R.S., Segonne, F., Fischl, B., Quinn, B.T., Dickerson, B.C., Blacker, D., Buckner, R.L., Dale, A.M., Maguire, R.P., Hyman, B.T., Albert, M.S., Killiany, R.J., 2006. An automated labeling system for subdividing the human cerebral cortex on MRI scans into gyral based regions of interest. Neuroimage. 31, 968-980.

Destexhe, A., Sejnowski, T.J., 2001. Thalamocortical Assemblies: How Ion Channels, Single Neurons and Large-Scale Networks Organize Sleep Oscillations. Oxford University Press.

Diessen, E., Diederen, S.J., Braun, K.P., Jansen, F.E., Stam, C.J., 2013. Functional and structural brain networks in epilepsy: What have we learned? Epilepsia 54, 1855-1865.

Dobrin, R., Duxbury, P.M., 2001. Minimum spanning trees on random networks. Phys.Rev.Lett. 86, 5076-5079.

Dogonowski, A.M., Siebner, H.R., Sorensen, P.S., Wu, X., Biswal, B., Paulson, O.B., Dyrby, T.B., Skimminge, A., Blinkenberg, M., Madsen, K.H., 2013. Expanded functional coupling of subcortical nuclei with the motor resting-state network in multiple sclerosis. Mult.Scler. 19, 559-566.

Douw, L., Baayen, H., Bosma, I., Klein, M., Vandertop, P., Heimans, J., Stam, K., de, M.J., Reijneveld, J., 2008. Treatment-related changes in functional connectivity in brain tumor patients: a magnetoencephalography study. Exp.Neurol. 212, 285-290.

Douw, L., Baayen, J.C., Klein, M., Velis, D., Alpherts, W.C., Bot, J., Heimans, J.J., Reijneveld, J.C., Stam, C.J., 2009. Functional connectivity in the brain before and during intra-arterial amobarbital injection (Wada test). Neuroimage. 46, 584-588.

Douw, L., de, G.M., van, D.E., Aronica, E., Heimans, J.J., Klein, M., Stam, C.J., Reijneveld, J.C., Hillebrand, A., 2013. Local MEG networks: The missing link between protein expression and epilepsy in glioma patients? Neuroimage.

Douw, L., van, D.E., Baayen, J.C., Klein, M., Velis, D.N., Alpherts, W.C., Heimans, J.J., Reijneveld, J.C., Stam, C.J., 2010. The lesioned brain: still a small-world? Front Hum.Neurosci. 4, 174.

Dussert, C., Rasigni, G., Rasigni, M., Palmari, J., Llebaria, A., 1986. Minimal spanning tree: A new approach for studying order and disorder. Phys.Rev.B Condens.Matter 34, 3528-3531.

Eguiluz, V.M., Chialvo, D.R., Cecchi, G.A., Baliki, M., Apkarian, A.V., 2005. Scale-free brain functional networks. Physical Review Letters 94, 018102.

Engel, A.K., Fries, P., 2010. Beta-band oscillations--signalling the status quo? Curr.Opin.Neurobiol. 20, 156-165.

Engel, A.K., Fries, P., Singer, W., 2001. Dynamic predictions: oscillations and synchrony in top-down processing. Nat.Rev.Neurosci. 2, 704-716.

Erdos, P., Renyi, A., 1959. On random graphs. Publicationes Mathematicae Debrecen 6, 290-297.

Evans, A.C., Janke, A.L., Collins, D.L., Baillet, S., 2012. Brain templates and atlases. Neuroimage. 62, 911-922.

Facchetti, D., Mai, R., Colombo, A., Capra, R., Marciano, N., Gasparotti, R., Poloni, M., 1994. Limited clinical significance of traditional and quantitative EEG in multiple sclerosis. Acta Neurol.Belg. 94, 245-250.

Faivre, A., Rico, A., Zaaraoui, W., Crespy, L., Reuter, F., Wybrecht, D., Soulier, E., Malikova, I., Confort-Gouny, S., Cozzone, P.J., Pelletier, J., Ranjeva, J.P., Audoin, B., 2012. Assessing brain connectivity at rest is clinically relevant in early multiple sclerosis. Mult.Scler. 18, 1251-1258.

Faugeras, O., Touboul, J., Cessac, B., 2009. A constructive mean-fi eld analysis of multi-population neural networks with random synaptic weights and stochastic inputs. front.in comp.neuroscience 3, 1-28.

Feng, Y.K., 1981. Clinico-electroencephalographic studies of multiple sclerosis. Clin.Exp.Neurol. 17, 47-57.

Filippi, M., Rocca, M.A., Barkhof, F., Bruck, W., Chen, J.T., Comi, G., DeLuca, G., De, S.N., Erickson, B.J., Evangelou, N., Fazekas, F., Geurts, J.J., Lucchinetti, C., Miller, D.H., Pelletier, D., Popescu, B.F., Lassmann, H., 2012. Association between pathological and MRI findings in multiple sclerosis. Lancet Neurol. 11, 349-360.

Fischl, B., Sereno, M.I., Dale, A.M., 1999. Cortical surface-based analysis. II: Inflation, flattening, and a surface-based coordinate system. Neuroimage. 9, 195-207.

Fornito, A., Zalesky, A., Breakspear, M., 2013. Graph analysis of the human connectome: Promise, progress, and pitfalls. Neuroimage. 80C, 426-444.

Fornito, A., Zalesky, A., Bullmore, E.T., 2010. Network scaling effects in graph analytic studies of human resting-state FMRI data. Front Syst.Neurosci. 4, 22.

Foster, D.V., Kauffman, S.A., Socolar, J.E., 2006. Network growth models and genetic regulatory networks. Physical Review E 73, 031912.

Freeman, W., 1975. Mass action in the nervous system.

Friston, K.J., 1994. Functional and effective connectivity in neuroimaging: A synthesis. Human Brain Mapping 2, 56-78.

Friston, K.J., Holmes, P., Worsley, K.J., Poline, J.P., Frith, C.D., Frackowiak, R.S.J., 2004. Statistical parametric maps in functional imaging: A general linear approach. Human Brain Mapping 2, 189-210.

Gallo, A., Esposito, F., Sacco, R., Docimo, R., Bisecco, A., Della, C.M., D'Ambrosio, A., Corbo, D., Rosa, N., Lanza, M., Cirillo, S., Bonavita, S., Tedeschi, G., 2012. Visual resting-state network in relapsing-remitting MS with and without previous optic neuritis. Neurology 79, 1458-1465.

Gamboa, O.L., Tagliazucchi, E., von, W.F., Jurcoane, A., Wahl, M., Laufs, H., Ziemann, U., 2013. Working memory performance of early MS patients correlates inversely with modularity increases in resting state functional connectivity networks. Neuroimage.

Gerstner, W., Kistler, W., 2002. Spiking neuron models: single neurons, populations, plasticity. Cambridge University Press, Cambridge.

Geurts, J.J., Barkhof, F., 2008. Grey matter pathology in multiple sclerosis. Lancet Neurol. 7, 841-851.

Geurts, J.J., Wolswijk, G., Bo, L., van, d., V, Polman, C.H., Troost, D., Aronica, E., 2003. Altered expression patterns of group I and II metabotropic glutamate receptors in multiple sclerosis. Brain 126, 1755-1766.

Ghosh, A., Rho, Y., McIntosh, A.R., Kotter, R., Jirsa, V.K., 2008. Noise during rest enables the exploration of the brain's dynamic repertoire. PLoS.Comput.Biol. 4, e1000196.

Girvan, M., Newman, M.E., 2002. Community structure in social and biological networks. Proceedings of the National Academy of Sciences 99, 7821-7826.

Gong, G., He, Y., Chen, Z.J., Evans, A.C., 2012. Convergence and divergence of thickness correlations with diffusion connections across the human cerebral cortex. Neuroimage. 59, 1239-1248.

Gong, G., He, Y., Concha, L., Lebel, C., Gross, D.W., Evans, A.C., Beaulieu, C., 2009. Mapping anatomical connectivity patterns of human cerebral cortex using in vivo diffusion tensor imaging tractography. Cereb.Cortex 19, 524-536.

Grabska-Barwinska, A., Latham, P.E., 2013. How well do mean field theories of spiking quadratic-integrate-and-fire networks work in realistic parameter regimes? J.Comput.Neurosci.

Graham, R.L., Hell, P., 1985. On the history of the minimum spanning tree problem. Annals of the History of Computing 7, 43-57.

Gross, J., Baillet, S., Barnes, G.R., Henson, R.N., Hillebrand, A., Jensen, O., Jerbi, K., Litvak, V., Maess, B., Oostenveld, R., Parkkonen, L., Taylor, J.R., van, W., V, Wibral, M., Schoffelen, J.M., 2012. Good practice for conducting and reporting MEG research. Neuroimage. 65C, 349-363.

Grossberg, S., Versace, M., 2008. Spikes, synchrony, and attentive learning by laminar thalamocortical circuits. Brain Res. 1218, 278-312.

Grummich, P., Nimsky, C., Pauli, E., Buchfelder, M., Ganslandt, O., 2006. Combining fMRI and MEG increases the reliability of presurgical language localization: a clinical study on the difference between and congruence of both modalities. Neuroimage. 32, 1793-1803.

Haacke, E.M., Brown, R.W., Thompson, M.R., Venkatesan, R., 1999. Magnetic resonance imaging. Physical principles and sequence design.

Hafkemeijer, A., van der Grond, J., Rombouts, S.A., 2012. Imaging the default mode network in aging and dementia. Biochim.Biophys.Acta 1822, 431-441.

Hagmann, P., Cammoun, L., Gigandet, X., Meuli, R., Honey, C.J., Wedeen, V.J., Sporns, O., 2008. Mapping the structural core of human cerebral cortex. PLoS.Biol. 6, e159.

Haimovici, A., Tagliazucchi, E., Balenzuela, P., Chialvo, D.R., 2013. Brain organization into resting state networks emerges at criticality on a model of the human connectome. Phys.Rev.Lett. 110, 178101.

Hamalainen, M., Hari, R., Ilmoniemi R.J., Knuutila J., Lounasmaa O.V., 1993. Magnetoencephalography-theory, instrumentation, and applications to noninvasive studies of the working human brain. Reviews of modern physics 65, 413-505.

Hansen, P., Kringelbach, M., Salmelin, R., 2010. MEG: An introduction to methods. Oxford university press.

Hardmeier, M., Schoonheim, M.M., Geurts, J.J., Hillebrand, A., Polman, C.H., Barkhof, F., Stam, C.J., 2012. Cognitive dysfunction in early multiple sclerosis: altered centrality derived from resting-state functional connectivity using magneto-encephalography. PLoS.One. 7, e42087.

Harel, O., 2009. The estimation of R 2 and adjusted R 2 in incomplete data sets using multiple imputation. Journal of Applied Statistics 36, 1109-1118.

Hawellek, D.J., Hipp, J.F., Lewis, C.M., Corbetta, M., Engel, A.K., 2011. Increased functional connectivity indicates the severity of cognitive impairment in multiple sclerosis. Proc.Natl.Acad.Sci.U.S.A 108, 19066-19071.

He, Y., Chen, Z., Evans, A., 2008. Structural insights into aberrant topological patterns of large-scale cortical networks in Alzheimer's disease. J.Neurosci. 28, 4756-4766.

He, Y., Chen, Z.J., Evans, A.C., 2007. Small-world anatomical networks in the human brain revealed by cortical thickness from MRI. Cereb.Cortex 17, 2407-2419.

He, Y., Dagher, A., Chen, Z., Charil, A., Zijdenbos, A., Worsley, K., Evans, A., 2009. Impaired small-world efficiency in structural cortical networks in multiple sclerosis associated with white matter lesion load. Brain 132, 3366-3379.

Helekar, S.A., Shin, J.C., Mattson, B.J., Bartley, K., Stosic, M., Saldana-King, T., Montague, P.R., Hutton, G.J., 2010. Functional brain network changes associated with maintenance of cognitive function in multiple sclerosis. Front Hum.Neurosci. 4, 219.

Helmholtz, H., 1853. Ueber einige Gesetze der Vertheilung elektrischer Strome in koperliche Leitern, mit Anwendung suf die thierischen elektrischen Versuche. Ann.Physik u.Chem. 2, 211-233.

Hermundstad, A.M., Bassett, D.S., Brown, K.S., Aminoff, E.M., Clewett, D., Freeman, S., Frithsen, A., Johnson, A., Tipper, C.M., Miller, M.B., Grafton, S.T., Carlson, J.M., 2013. Structural foundations of resting-state and task-based functional connectivity in the human brain. Proc.Natl.Acad.Sci.U.S.A 110, 6169-6174.

Hillebrand, A., Barnes, G.R., 2002. A quantitative assessment of the sensitivity of whole-head MEG to activity in the adult human cortex. Neuroimage. 16, 638-650.

Hillebrand, A., Barnes, G.R., 2005. Beamformer analysis of MEG data. Int.Rev.Neurobiol. 68, 149-171.

Hillebrand, A., Barnes, G.R., Bosboom, J.L., Berendse, H.W., Stam, C.J., 2012. Frequency-dependent functional connectivity within resting-state networks: an atlas-based MEG beamformer solution. Neuroimage. 59, 3909-3921.

Hillebrand, A., Singh, K.D., Holliday, I.E., Furlong, P.L., Barnes, G.R., 2005. A new approach to neuroimaging with magnetoencephalography. Hum.Brain Mapp. 25, 199-211.

Hipp, J.F., Hawellek, D.J., Corbetta, M., Siegel, M., Engel, A.K., 2012. Large-scale cortical correlation structure of spontaneous oscillatory activity. Nat.Neurosci. 15, 884-890.

Hlinka, J., Palus, M., Vejmelka, M., Mantini, D., Corbetta, M., 2011. Functional connectivity in resting-state fMRI: is linear correlation sufficient? Neuroimage. 54, 2218-2225.

Honey, C.J., Kotter, R., Breakspear, M., Sporns, O., 2007. Network structure of cerebral cortex shapes functional connectivity on multiple time scales. Proc.Natl.Acad.Sci.U.S.A 104, 10240-10245.

Honey, C.J., Sporns, O., Cammoun, L., Gigandet, X., Thiran, J.P., Meuli, R., Hagmann, P., 2009. Predicting human resting-state functional connectivity from structural connectivity. Proc.Natl.Acad.Sci.U.S.A 106, 2035-2040.

Houtchens, M.K., Benedict, R.H., Killiany, R., Sharma, J., Jaisani, Z., Singh, B., Weinstock-Guttman, B., Guttmann, C.R., Bakshi, R., 2007. Thalamic atrophy and cognition in multiple sclerosis. Neurology 69, 1213-1223.

Hughes, S.W., Crunelli, V., 2005. Thalamic mechanisms of EEG alpha rhythms and their pathological implications. Neuroscientist. 11, 357-372.

Hui, H.B., Pantazis, D., Bressler, S.L., Leahy, R.M., 2010. Identifying true cortical interactions in MEG using the nulling beamformer. Neuroimage. 49, 3161-3174.

Izhikevich, E.M., 2004. Which model to use for cortical spiking neurons? IEEE transactions on neural networks 15, 1063-1070.

Jackson, T.S., Read, N., 2010. Theory of minimum spanning trees. I. Mean-field theory and strongly disordered spin-glass model. Phys.Rev.E.Stat.Nonlin.Soft.Matter Phys. 81, 021130.

Jansen, B., Rit, V., 1995. Electroencephalogram and visual evoked potential generation in a mathematical model of coupled cortical columns. Biol.Cybern. 73, 357-366.

Jensen, O., Goel, P., Kopell, N., Pohja, M., Hari, R., Ermentrout, B., 2005. On the human sensorimotor-cortex beta rhythm: sources and modeling. Neuroimage. 26, 347-355.

Jeong, J., 2004. EEG dynamics in patients with Alzheimer's disease. Clin.Neurophysiol. 115, 1490-1505.

Jirsa, V.K., Kelso, J.A., 2000. Spatiotemporal pattern formation in neural systems with heterogeneous connection topologies. Phys.Rev.E.Stat.Phys.Plasmas.Fluids Relat Interdiscip.Topics. 62, 8462-8465.

Katz, L.C., Shatz, C.J., 1996. Synaptic activity and the construction of cortical circuits. Science 274, 1133-1138.

Kawakami, O., Kaneoke, Y., Maruyama, K., Kakigi, R., Okada, T., Sadato, N., Yonekura, Y., 2002. Visual detection of motion speed in humans: spatiotemporal analysis by fMRI and MEG. Hum.Brain Mapp. 16, 104-118.

Kim, D.H., Noh, J.D., Jeong, H., 2004. Scale-free trees: the skeletons of complex networks. Phys.Rev.E.Stat. Nonlin.Soft.Matter Phys. 70, 046126.

King, B.M., Tidor, B., 2009. MIST: Maximum Information Spanning Trees for dimension reduction of biological data sets. Bioinformatics. 25, 1165-1172.

Klein, M., Engelberts, N.H., van der Ploeg, H.M., Kasteleijn-Nolst Trenite, D.G., Aaronson, N.K., Taphoorn, M.J., Baaijen, H., Vandertop, W.P., Muller, M., Postma, T.J., Heimans, J.J., 2003. Epilepsy in low-grade gliomas: the impact on cognitive function and quality of life. Ann.Neurol. 54, 514-520.

Klemm, K., Eguiluz, V.M., 2002. Highly clustered scale-free networks. Physical Review E 65, 036123.

Klimesch, W., 1999. EEG alpha and theta oscillations reflect cognitive and memory performance: a review and analysis. Brain Res.Brain Res.Rev. 29, 169-195.

Klimesch, W., Sauseng, P., Hanslmayr, S., 2007. EEG alpha oscillations: the inhibition-timing hypothesis. Brain Res.Rev. 53, 63-88.

Kostic, M., Zivkovic, N., Stojanovic, I., 2013. Multiple sclerosis and glutamate excitotoxicity. Rev.Neurosci. 24, 71-88.

Kruskal, J., 1956. On the Shortest Spanning Subtree of a Graph and the Traveling Salesman Problem. Proceedings of the American Mathematical Society, 48-50.

Kumar, S., Rao, S.L., Chandramouli, B.A., Pillai, S.V., 2009. Reduction of functional brain connectivity in mild traumatic brain injury during working memory. J.Neurotrauma 26, 665-675.

Kurtzke, J.F., 1983. Rating neurologic impairment in multiple sclerosis: an expanded disability status scale (EDSS). Neurology 33, 1444-1452.

Landau, L.D., Lifshitz, E.M., 1968. Statistical Physics. Course in Theoretical Physics, pp. 1-28.

Le van Quyen, M., 2003. Disentangling the dynamic core: a research program for a neurodynamics at the large-scale. Biological Research 36, 67-88.

Leavitt, V.M., Wylie, G., Genova, H.M., Chiaravalloti, N.D., DeLuca, J., 2012. Altered effective connectivity during performance of an information processing speed task in multiple sclerosis. Mult.Scler. 18, 409-417.

Lee, U., Kim, S., Jung, K.Y., 2006b. Classification of epilepsy types through global network analysis of scalp electroencephalograms. Physical Review E 73, 041920.

Lee, U., Oh, G., Kim, S., Noh, G., Choi, B., Mashour, G.A., 2010. Brain networks maintain a scale-free organization across consciousness, anesthesia, and recovery: evidence for adaptive reconfiguration. Anesthesiology 113, 1081.

Leocani, L., Locatelli, T., Martinelli, V., Rovaris, M., Falautano, M., Filippi, M., Magnani, G., Comi, G., 2000. Electroencephalographic coherence analysis in multiple sclerosis: correlation with clinical, neuropsychological, and MRI findings. J.Neurol.Neurosurg.Psychiatry 69, 192-198.

Li, C., Wang, H., De Haan, W., Stam, C.J., Van Mieghem, P., 2011. The correlation of metrics in complex networks with applications in functional brain networks. Journal of statistical mechanics: theory and experiment 2011, 11018.

Li, Y., Jewells, V., Kim, M., Chen, Y., Moon, A., Armao, D., Troiani, L., Markovic-Plese, S., Lin, W., Shen, D., 2012. Diffusion tensor imaging based network analysis detects alterations of neuroconnectivity in patients with clinically early relapsing-remitting multiple sclerosis. Hum.Brain Mapp. 34, 3376-3391.

Liao, X.H., Xia, M.R., Xu, T., Dai, Z.J., Cao, X.Y., Niu, H.J., Zuo, X.N., Zang, Y.F., He, Y., 2013. Functional brain hubs and their test-retest reliability: A multiband resting-state functional MRI study. Neuroimage.

Licker, M.D., 2002. Dictionary of Physics, 3th ed.

Liley, D.T., Cadusch, P.J., Gray, M., Nathan, P.J., 2003. Drug-induced modification of the system properties associated with spontaneous human electroencephalographic activity. Phys.Rev.E.Stat.Nonlin.Soft.Matter Phys. 68, 051906.

Liu, A.K., Belliveau, J.W., Dale, A.M., 1998. Spatiotemporal imaging of human brain activity using functional MRI constrained magnetoencephalography data: Monte Carlo simulations. Proc.Natl.Acad.Sci.U.S.A 95, 8945-8950.

Liu, Z., Ding, L., He, B., 2006. Integration of EEG/MEG with MRI and fMRI. IEEE Eng Med.Biol.Mag. 25, 46-53.

Lloret-Climent, M., Nescolarde-Selva, J., 2014. Data analysis using circular causality in networks. Complexity 19, 15-19.

Lodder, S.S., van Putten, M.J., 2013. Quantification of the adult EEG background pattern. Clin.Neurophysiol. 124, 228-237.

Logothetis, N.K., 2008. What we can do and what we cannot do with fMRI. Nature 453, 869-878.

Logothetis, N.K., Pauls, J., Augath, M., Trinath, T., Oeltermann, A., 2001. Neurophysiological investigation of the basis of the fMRI signal. Nature 412, 150-157.

Lopes da Silva F., 1991. Neural mechanisms underlying brain waves: from neural membranes to networks. Electroencephalogr.Clin.Neurophysiol. 79, 81-93.

Lopes da Silva, F., Hoeks, A., Smits, H., Zetterberg, L., 1974. Model of brain rhythmic activity. The alpha-rhythm of the thalamus. Kybernetik 15, 27-37.

Louapre, C., Perlbarg, V., Garcia-Lorenzo, D., Urbanski, M., Benali, H., Assouad, R., Galanaud, D., Freeman, L., Bodini, B., Papeix, C., Tourbah, A., Lubetzki, C., Lehericy, S., Stankoff, B., 2014. Brain networks disconnection in early multiple sclerosis cognitive deficits: An anatomofunctional study. Hum.Brain Mapp.

Lublin, F.D., Reingold, S.C., 1996. Defining the clinical course of multiple sclerosis: results of an international survey. National Multiple Sclerosis Society (USA) Advisory Committee on Clinical Trials of New Agents in Multiple Sclerosis. Neurology 46, 907-911.

Lublin, F.D., Reingold, S.C., Cohen, J.A., Cutter, G.R., Sorensen, P.S., Thompson, A.J., Wolinsky, J.S., Balcer, L.J., Banwell, B., Barkhof, F., Bebo, B., Jr., Calabresi, P.A., Clanet, M., Comi, G., Fox, R.J., Freedman, M.S., Goodman, A.D., Inglese, M., Kappos, L., Kieseier, B.C., Lincoln, J.A., Lubetzki, C., Miller, A.E., Montalban, X., O'Connor, P.W., Petkau, J., Pozzilli, C., Rudick, R.A., Sormani, M.P., Stuve, O., Waubant, E., Polman, C.H., 2014. Defining the clinical course of multiple sclerosis: The 2013 revisions. Neurology.

Mantini, D., Perrucci, M.G., Del, G.C., Romani, G.L., Corbetta, M., 2007. Electrophysiological signatures of resting state networks in the human brain. Proc.Natl.Acad.Sci.U.S.A 104, 13170-13175.

Mardia, K.V., 1975. Statistics of directional data. Journal of the Royal Statistical Society.Series B (Methodological), 349-393.

Maslov, S., Sneppen, K., 2002. Specificity and stability in topology of protein networks. Science 296, 910-913.

Mattia, M., Del Giduice, P., 2002. Population dynamics of interacting spiking neurons. Phys.Rev.E Stat.Nonlin. Soft Matter Phys. 66, 51917.1-51917.19.

Meer, v.d.M., Tewarie, P., Schoonheim, M., Douw, L., Barkhof, F., Polman, C., Stam, C., Hillebrand, A., 2013. Clinical disability in MS correlates with resting-state oscillatory brain activity: an MEG source-space study. NeuroImage: Clinical 2, 727-734.

Meier, J., Tewarie, P., Wang, H., Stam, C.J., Van Mieghem, P., 2014. The Union of Shortest Path Trees of Functional Brain Networks. in preparation.

Messe, A., Rudrauf, D., Benali, H., Marrelec, G., 2014. Relating Structure and Function in the Human Brain: Relative Contributions of Anatomy, Stationary Dynamics, and Non-stationarities. PLoS computational biology 10, e1003530.

Meunier, D., Lambiotte, R., Fornito, A., Ersche, K.D., Bullmore, E.T., 2009. Hierarchical modularity in human brain functional networks. Front Neuroinform. 3, 37.

Michailidis, G., 2005. Minimum Spanning Tree. Encyclopedia of Statistics in Behavioral Science.

Minagar, A., Barnett, M.H., Benedict, R.H., Pelletier, D., Pirko, I., Sahraian, M.A., Frohman, E., Zivadinov, R., 2013. The thalamus and multiple sclerosis: modern views on pathologic, imaging, and clinical aspects. Neurology 80, 210-219.

Molgedey, L., Schuchardt, J., SChuster, H., 2013. Suppressing chaos in neural networks by noise. Phys.Rev.Lett. 69, 3717-3719.

Moran, R.J., Kiebel, S.J., Stephan, K.E., Reilly, R.B., Daunizeau, J., Friston, K.J., 2007. A neural mass model of spectral responses in electrophysiology. Neuroimage. 37, 706-720.

Moreno-Bote, R., Parga, N., 2005. Simple model neurons with AMPA and NMDA filters: role of synaptic time scales. Neurocomputing 65-66, 441-448.

Moret, B.M.E., Shapiro, H.D., 1993. An empirical assessment of algorithms for constructing a minimum spanning tree. In: Dean, N., Shannon, G.E. (Eds.), Computational support for discrete mathematics, pp. 99-117.

Mori, S., van Zijl, P., 2002. Fiber tracking: principles and strategiesGÇôa technical review. NMR in Biomedicine 15, 468-480.

Moynot, O., Samuelides, M., 2002. Large deviations and mean-field theory for asymmetric random recurrent neural networks. Probab.Theory Relat.Fields 123, 41-75.

Murakami, S., Okada, Y., 2006. Contributions of principal neocortical neurons to magnetoencephalography and electroencephalography signals. The Journal of physiology 575, 925-936.

Muthukumaraswamy, S.D., Edden, R.A., Jones, D.K., Swettenham, J.B., Singh, K.D., 2009. Resting GABA concentration predicts peak gamma frequency and fMRI amplitude in response to visual stimulation in humans. Proc.Natl.Acad.Sci.U.S.A 106, 8356-8361.

Muthukumaraswamy, S.D., Singh, K.D., 2011. A cautionary note on the interpretation of phase-locking estimates with concurrent changes in power. Clin.Neurophysiol. 122, 2324-2325.

Nacher, V., Ledberg, A., Deco, G., Romo, R., 2013. Coherent delta-band oscillations between cortical areas correlate with decision making. Proc.Natl.Acad.Sci.U.S.A 110, 15085-15090.

Nakagawa, T.T., Jirsa, V.K., Spiegler, A., McIntosh, A.R., Deco, G., 2013. Bottom up modeling of the connectome: Linking structure and function in the resting brain and their changes in aging. Neuroimage. 80, 318-329.

Newman, M.E., 2002. Assortative mixing in networks. Phys.Rev.Lett. 89, 208701.

Newman, M.E., Strogatz, S.H., Watts, D.J., 2001. Random graphs with arbitrary degree distributions and their applications. Physical Review E 64, 026118.

Newman, M., 2010a. Betweenness centrality. Networks, an introduction, pp. 142-146.

Newman, M., 2010b. The configuration model. Networks: an introduction, 1st ed, pp. 323-329.

Nichols, T.E., Holmes, A.P., 2002. Nonparametric permutation tests for functional neuroimaging: a primer with examples. Hum.Brain Mapp. 15, 1-25.

Nikulin, V.V., Brismar, T., 2006. Phase synchronization between alpha and beta oscillations in the human electroencephalogram. Neuroscience 137, 647-657.

Nolte, G., Ziehe, A., Nikulin, V.V., Schlogl, A., Kramer, N., Brismar, T., Muller, K.R., 2008. Robustly estimating the flow direction of information in complex physical systems. Phys.Rev.Lett. 100, 234101.

Nunez, P.L., Srinivasan, R., Westdorp, A.F., Wijesinghe, R.S., Tucker, D.M., Silberstein, R.B., Cadusch, P.J., 1997. EEG coherency: I: statistics, reference electrode, volume conduction, Laplacians, cortical imaging, and interpretation at multiple scales. Electroencephalography and clinical neurophysiology 103, 499-515.

Ogawa, S., Tank, D.W., Menon, R., Ellermann, J.M., Kim, S.G., Merkle, H., Ugurbil, K., 1992. Intrinsic signal changes accompanying sensory stimulation: functional brain mapping with magnetic resonance imaging. Proceedings of the National Academy of Sciences 89, 5951-5955.

Ohki, K., Chung, S., Ch'ng, Y.H., Kara, P., Reid, R.C., 2005. Functional imaging with cellular resolution reveals precise micro-architecture in visual cortex. Nature 433, 597-603.

Ojemann, G.A., Ojemann, J., Ramsey, N.F., 2013. Relation between functional magnetic resonance imaging (fMRI) and single neuron, local field potential (LFP) and electrocorticography (ECoG) activity in human cortex. Frontiers in human neuroscience 7.

Olde Dubbelink, K.T., Hillebrand, A., Stoffers, D., Deijen, J.B., Twisk, J.W., Stam, C.J., Berendse, H.W., 2014. Disrupted brain network topology in Parkinson's disease: a longitudinal magnetoencephalography study. Brain 137, 197-207.

Olde Dubbelink, K.T., Stoffers, D., Deijen, J.B., Twisk, J.W., Stam, C.J., Berendse, H.W., 2012. Cognitive decline in Parkinson's disease is associated with slowing of resting-state brain activity: a longitudinal study. Neurobiol. Aging.

Ortega, G.J., Sola, R.G., Pastor, J., 2008. Complex network analysis of human ECoG data. Neurosci.Lett. 447, 129-133.

Palva, J.M., Palva, S., Kaila, K., 2005. Phase synchrony among neuronal oscillations in the human cortex. J.Neurosci. 25, 3962-3972.

Palva, S., Palva, J.M., 2007. New vistas for alpha-frequency band oscillations. Trends Neurosci. 30, 150-158.

Pampliega, O., Domercq, M., Soria, F.N., Villoslada, P., Rodriguez-Antiguedad, A., Matute, C., 2011. Increased expression of cystine/glutamate antiporter in multiple sclerosis. J.Neuroinflammation. 8, 63.

Parisi, L., Rocca, M.A., Valsasina, P., Panicari, L., Mattioli, F., Filippi, M., 2012. Cognitive rehabilitation correlates with the functional connectivity of the anterior cingulate cortex in patients with multiple sclerosis. Brain Imaging Behav.

Peraza, L.R., Asghar, A.U., Green, G., Halliday, D.M., 2012. Volume conduction effects in brain network inference from electroencephalographic recordings using phase lag index. J.Neurosci.Methods 207, 189-199.

Pereda, E., Quiroga, R.Q., Bhattacharya, J., 2005. Nonlinear multivariate analysis of neurophysiological signals. Prog.Neurobiol. 77, 1-37.

Peter, R., 1979. Synaptic density in human frontal cortexGÇödevelopmental changes and effects of aging. Brain research 163, 195-205.

Pikovsky, A., Rosemblum, M., Kurths, J., 2001. Mutual synchronization of two interacting periodic oscillators. Synchronization A universal concept in nonlinear sciences.

Pinotsis, D.A., Hansen, E., Friston, K.J., Jirsa, V.K., 2013. Anatomical connectivity and the resting state activity of large cortical networks. Neuroimage. 65, 127-138.

Pirko, I., Lucchinetti, C.F., Sriram, S., Bakshi, R., 2007. Gray matter involvement in multiple sclerosis. Neurology 68, 634-642.

Plenz, D., Thiagarajan, T.C., 2007. The organizing principles of neuronal avalanches: cell assemblies in the cortex? Trends in neurosciences 30, 101-110.

Polman, C.H., Reingold, S.C., Edan, G., Filippi, M., Hartung, H.P., Kappos, L., Lublin, F.D., Metz, L.M., McFarland, H.F., O'Connor, P.W., Sandberg-Wollheim, M., Thompson, A.J., Weinshenker, B.G., Wolinsky, J.S., 2005. Diagnostic criteria for multiple sclerosis: 2005 revisions to the "McDonald Criteria". Ann.Neurol. 58, 840-846.

Ponsen, M., Stam, C., Bosboom, J., Berendse, H., Hillebrand, A., 2013. A three dimensional anatomical view of oscillatory resting-state activity and functional connectivity in Parkinson's disease related dementia: An MEG study using atlas-based beamforming . Neuroimage:clinical 2, 95-102.

Ponten, S.C., Daffertshofer, A., Hillebrand, A., Stam, C.J., 2010. The relationship between structural and functional connectivity: graph theoretical analysis of an EEG neural mass model. Neuroimage. 52, 985-994.

Pope, K.J., Fitzgibbon, S.P., Lewis, T.W., Whitham, E.M., Willoughby, J.O., 2009. Relation of gamma oscillations in scalp recordings to muscular activity. Brain topography 22, 13-17.

Popescu, V., Klaver, R., Galis-deGraaf, Y., Voorn, P., Knol, D., Versteeg, A., Schenk, G., Barkhof, F., de Vries, H., Vrenken, H., Geurts, J., 2013. Pathological substrate of MRI-derived cortical atrophy in multiple sclerosis. submitted.

Power, J.D., Schlaggar, B.L., Lessov-Schlaggar, C.N., Petersen, S.E., 2013. Evidence for hubs in human functional brain networks. Neuron 79, 798-813.

Prakash, R.S., Patterson, B., Janssen, A., Abduljalil, A., Boster, A., 2011. Physical activity associated with increased resting-state functional connectivity in multiple sclerosis. J.Int.Neuropsychol.Soc. 17, 986-997.

Price, C.J., Friston, K.J., 2002. Degeneracy and cognitive anatomy. Trends in cognitive sciences 6, 416-421.

Prim, R.C., 1957. Shortest connection networks and some generalizations. Bell system technical journal 36, 1389-1401.

Pritchard, W.S., Laurienti, P.J., Burdette, J.H., Hayasaka, S., 2014. Functional brain networks formed using cross-sample entropy are scale-free. Brain Connect.

Quattrini, A., Paggi, A., Ortenzi, A., Di, B.P., Cianci, F., Forastieri, L., 1981. CT and EEG investigations in 100 patients with multiple sclerosis (MS). Ital.J.Neurol.Sci. 2, 25-34.

Rao, S.M., Leo, G.J., Bernardin, L., Unverzagt, F., 1991. Cognitive dysfunction in multiple sclerosis. I. Frequency, patterns, and prediction. Neurology 41, 685-691.

Richiardi, J., Gschwind, M., Simioni, S., Annoni, J.M., Greco, B., Hagmann, P., Schluep, M., Vuilleumier, P., Van, D., V, 2012. Classifying minimally disabled multiple sclerosis patients from resting state functional connectivity. Neuroimage. 62, 2021-2033.

Robinson, P.A., 2012. Interrelating anatomical, effective, and functional brain connectivity using propagators and neural field theory. Phys.Rev.E.Stat.Nonlin.Soft.Matter Phys. 85, 011912.

Robinson, S.E., Vrba, J., 1999. Functional neuroimaging by synthetic aperture magnetometry . In: Yoshimoto, M., Kotani, S., Kuriki, H., Karibe, N., Nakatato, E. (Eds.), Recent advances in biomagnetism. Tohoku University Press, Sendai, pp. 302-305.

Rocca, M.A., Filippi, M., 2007. Functional MRI in multiple sclerosis. J.Neuroimaging 17 Suppl 1, 36S-41S.

Rocca, M.A., Pagani, E., Absinta, M., Valsasina, P., Falini, A., Scotti, G., Comi, G., Filippi, M., 2007. Altered functional and structural connectivities in patients with MS: a 3-T study. Neurology 69, 2136-2145.

Rocca, M.A., Valsasina, P., Absinta, M., Riccitelli, G., Rodegher, M.E., Misci, P., Rossi, P., Falini, A., Comi, G., Filippi, M., 2010. Default-mode network dysfunction and cognitive impairment in progressive MS. Neurology 74, 1252-1259.

Rocca, M.A., Valsasina, P., Martinelli, V., Misci, P., Falini, A., Comi, G., Filippi, M., 2012. Large-scale neuronal network dysfunction in relapsing-remitting multiple sclerosis. Neurology 79, 1449-1457.

Rodrigues, S., Chizhov, A., Marten, F., terry, J., 2010. Mappings between a macroscopic neural-mass model and a reduced conductance-based model. Biol.Cybern., 361-371.

Roopun, A.K., Kramer, M.A., Carracedo, L.M., Kaiser, M., Davies, C.H., Traub, R.D., Kopell, N.J., Whittington, M.A., 2008. Temporal Interactions between Cortical Rhythms. Front Neurosci. 2, 145-154.

Rosazza, C., Minati, L., 2011. Resting-state brain networks: literature review and clinical applications. Neurol. Sci. 32, 773-785.

Rousselet, G.A., Pernet, C.R., 2012. Improving standards in brain-behavior correlation analyses. Front Hum. Neurosci. 6, 119.

Rubinov, M., Sporns, O., 2010. Complex network measures of brain connectivity: uses and interpretations. Neuroimage. 52, 1059-1069.

Rudolph-Lilith, M., Dubois, M., Destexhe, A., 2012. Analytical integrate-and-fire neuron models with conductance-based dynamics and realistic postsynaptic potential time course for event-driven simulation strategies. Neural Comput. 24, 1426-1461.

Samuelides, m., Cessac, B., 2007. Random recurrent neural networks. Eur.Phys.J.Spec.Top 142, 7-88.

Schnitzler, A., Gross, J., 2005. Normal and pathological oscillatory communication in the brain. Nat.Rev. Neurosci. 6, 285-296.

Schoen, W., Chang, J.S., Lee, U., Bob, P., Mashour, G.A., 2011. The temporal organization of functional brain connectivity is abnormal in schizophrenia but does not correlate with symptomatology. Conscious.Cogn 20, 1050-1054.

Schoonheim, M., Hulst, H.E., Roemer, B., Strik, M., Wink, A.M., Uitdehaag, B.M.J., Barkhof, F., Geurts, J.G., 2014. Thalamus structure and function determines severity of cognitive impairment in multiple sclerosis. Brain submitted.

Schoonheim, M.M., Geurts, J.J., Barkhof, F., 2010. The limits of functional reorganization in multiple sclerosis. Neurology 74, 1246-1247.

Schoonheim, M.M., Geurts, J.J., Landi, D., Douw, L., van der Meer, M.L., Vrenken, H., Polman, C.H., Barkhof, F., Stam, C.J., 2011. Functional connectivity changes in multiple sclerosis patients: A graph analytical study of MEG resting state data. Hum.Brain Mapp. 34, 52-61.

Schoonheim, M.M., Hulst, H.E., Landi, D., Ciccarelli, O., Roosendaal, S.D., Sanz-Arigita, E.J., Vrenken, H., Polman, C.H., Stam, C.J., Barkhof, F., Geurts, J.J., 2012a. Gender-related differences in functional connectivity in multiple sclerosis. Mult.Scler. 18, 164-173.

Schoonheim, M.M., Popescu, V., Rueda Lopes, F.C., Wiebenga, O.T., Vrenken, H., Douw, L., Polman, C.H., Geurts, J.J., Barkhof, F., 2012b. Subcortical atrophy and cognition: sex effects in multiple sclerosis. Neurology 79, 1754-1761.

Schoonheim, M.M., Popescu, V., Rueda Lopes, F.C., Wiebenga, O.T., Vrenken, H., Douw, L., Polman, C.H., Geurts, J.J., Barkhof, F., 2012c. Subcortical atrophy and cognition: Sex effects in multiple sclerosis. Neurology.

Schoonheim, M.M., Vigeveno, R.M., Lopes, F.C., Pouwels, P.J., Polman, C.H., Barkhof, F., Geurts, J.J., 2013a. Sex-specific extent and severity of white matter damage in multiple sclerosis: Implications for cognitive decline. Hum.Brain Mapp.

Schoonheim, M., Geurts, J., Wiebenga, O., de Munck, J., Polman, C., Stam, C., Barkhof, F., Wink, A., 2013b. Decreased functional network centrality in early multiple sclerosis: relations with cognitive dysfunction and physical disability. Neuroimage in press.

Seibert, T.M., Brewer, J.B., 2011. Default network correlations analyzed on native surfaces. J.Neurosci.Methods 198, 301-311.

Shanahan, M., 2012. The brain's connective core and its role in animal cognition. Philosophical Transactions of the Royal Society B: Biological Sciences 367, 2704-2714.

Sherman, S.M., 2007. The thalamus is more than just a relay. Curr.Opin.Neurobiol. 17, 417-422.

Shu, N., Liu, Y., Li, K., Duan, Y., Wang, J., Yu, C., Dong, H., Ye, J., He, Y., 2011. Diffusion tensor tractography reveals disrupted topological efficiency in white matter structural networks in multiple sclerosis. Cereb.Cortex 21, 2565-2577.

Simon, H., 1962. The architecture of complexity . Proceedings of the American Philosophical Society, 106, 467-482.

Singh, K.D., 2012. Which "neural activity" do you mean? fMRI, MEG, oscillations and neurotransmitters. Neuroimage. 62, 1121-1130.

Skudlarski, P., Jagannathan, K., Calhoun, V.D., Hampson, M., Skudlarska, B.A., Pearlson, G., 2008. Measuring brain connectivity: diffusion tensor imaging validates resting state temporal correlations. Neuroimage. 43, 554-561.

Smith, S.M., Zhang, Y., Jenkinson, M., Chen, J., Matthews, P.M., Federico, A., De, S.N., 2002. Accurate, robust, and automated longitudinal and cross-sectional brain change analysis. Neuroimage. 17, 479-489.

Song, S., Miller, K.D., Abbott, L.F., 2000. Competitive Hebbian learning through spike-timing-dependent synaptic plasticity. Nat.Neurosci. 3, 919-926.

Sotiropoulos, S.N., Bai, L., Morgan, P.S., Constantinescu, C.S., Tench, C.R., 2010. Brain tractography using Q-ball imaging and graph theory: Improved connectivities through fibre crossings via a model-based approach. Neuroimage 49, 2444-2456.

Stam, C.J., 2004. Functional connectivity patterns of human magnetoencephalographic recordings: a 'small-world' network? Neurosci.Lett. 355, 25-28.

Stam, C.J., Breakspear, M., van Cappellen van Walsum AM, van Dijk, B.W., 2003. Nonlinear synchronization in EEG and whole-head MEG recordings of healthy subjects. Hum.Brain Mapp. 19, 63-78.

Stam, C.J., de, H.W., Daffertshofer, A., Jones, B.F., Manshanden, I., van Cappellen van Walsum AM, Montez, T., Verbunt, J.P., de Munck, J.C., van Dijk, B.W., Berendse, H.W., Scheltens, P., 2009. Graph theoretical analysis of magnetoencephalographic functional connectivity in Alzheimer's disease. Brain 132, 213-224.

Stam, C.J., Jones, B.F., Manshanden, I., van Cappellen van Walsum AM, Montez, T., Verbunt, J.P., de Munck, J.C., van Dijk, B.W., Berendse, H.W., Scheltens, P., 2006a. Magnetoencephalographic evaluation of resting-state functional connectivity in Alzheimer's disease. Neuroimage. 32, 1335-1344.

Stam, C.J., Nolte, G., Daffertshofer, A., 2007. Phase lag index: assessment of functional connectivity from multi channel EEG and MEG with diminished bias from common sources. Hum.Brain Mapp. 28, 1178-1193.

Stam, C.J., Pijn, J.P., Suffczynski, P., Lopes da Silva, F.H., 1999. Dynamics of the human alpha rhythm: evidence for non-linearity? Clin.Neurophysiol. 110, 1801-1813.

Stam, C.J., Tewarie, P., van, D.E., van Straaten, E.C., Hillebrand, A., Van, M.P., 2014. The trees and the forest: Characterization of complex brain networks with minimum spanning trees. Int.J.Psychophysiol. 92, 129-138.

Stam, C.J., van Straaten, E.C., 2012a. The organization of physiological brain networks. Clin.Neurophysiol 123, 1067-1087.

Steenwijk, M.D., Daams, M., Pouwels, P.J., Balk, L.J., Tewarie, P.K., Killestein, J., Uitdehaag, B.M., Geurts, J.J., Barkhof, F., Vrenken, H., 2014. What Explains Gray Matter Atrophy in Long-standing Multiple Sclerosis? Radiology, 132708.

Steriade, M., 1997. Synchronized activities of coupled oscillators in the cerebral cortex and thalamus at different levels of vigilance. Cereb.Cortex 7, 583-604.

Stoffers, D., Bosboom, J.L., Deijen, J.B., Wolters, E.C., Berendse, H.W., Stam, C.J., 2007. Slowing of oscillatory brain activity is a stable characteristic of Parkinson's disease without dementia. Brain 130, 1847-1860.

Stys, P.K., Zamponi, G.W., van, M.J., Geurts, J.J., 2012. Will the real multiple sclerosis please stand up? Nat.Rev. Neurosci. 13, 507-514.

Tao, G., Datta, S., He, R., Nelson, F., Wolinsky, J.S., Narayana, P.A., 2009. Deep gray matter atrophy in multiple sclerosis: a tensor based morphometry. J.Neurol.Sci. 282, 39-46.

Taulu, S., Hari, R., 2009. Removal of magnetoencephalographic artifacts with temporal signal-space separation: demonstration with single-trial auditory-evoked responses. Hum.Brain Mapp. 30, 1524-1534.

Taulu, S., Simola, J., 2006. Spatiotemporal signal space separation method for rejecting nearby interference in MEG measurements. Phys.Med.Biol. 51, 1759-1768.

Tecchio, F., Zito, G., Zappasodi, F., Dell' Acqua, M.L., Landi, D., Nardo, D., Lupoi, D., Rossini, P.M., Filippi, M.M., 2008. Intra-cortical connectivity in multiple sclerosis: a neurophysiological approach. Brain 131, 1783-1792.

Tewarie, P., Hillebrand, A., Schoonheim, M.M., van Dijk, B.W., Geurts, J.J.G., Barkhof, F., Polman, C.H., Stam, C.J., 2013a. Functional brain network analysis using minimum spanning trees in Multiple Sclerosis: an MEG source-space study. Neuroimage 88, 308-318.

Tewarie, P., Steenwijk, M., Tijms, B., Daams, M., Balk, L., Stam, C., Uitdehaag, B., Polman, C., Geurts, J., Barkhof, F., Pouwels, P., Vrenken, H., Hillebrand, A., 2014a. Disruption of structural and functional networks in long-standing multiple sclerosis. Human Brain Mapping submitted.

Tewarie, P., Hillebrand, A., van, D.E., Schoonheim, M.M., Barkhof, F., Polman, C.H., Beaulieu, C., Gong, G., van Dijk, B.W., Stam, C.J., 2014b. Structural degree predicts functional network connectivity: A multimodal resting-state fMRI and MEG study. Neuroimage.

Tewarie, P., Schoonheim, M.M., Stam, C.J., van der Meer, M.L., van Dijk, B.W., Barkhof, F., Polman, C.H., Hillebrand, A., 2013d. Cognitive and clinical dysfunction, altered MEG resting-state networks and thalamic atrophy in multiple sclerosis. PLoS.One. 8, e69318.

Thomas, R., 2006. Circular causality. Syst.Biol.(Stevenage.) 153, 140-153.

Tijms, B.M., Series, P., Willshaw, D.J., Lawrie, S.M., 2012. Similarity-based extraction of individual networks from gray matter MRI scans. Cereb.Cortex 22, 1530-1541.

Tijms, B.M., Wink, A.M., de, H.W., van der Flier, W.M., Stam, C.J., Scheltens, P., Barkhof, F., 2013. Alzheimer's disease: connecting findings from graph theoretical studies of brain networks. Neurobiol.Aging 34, 2023-2036.

Tona, F., Petsas, N., Sbardella, E., Prosperini, L., Carmellini, M., Pozzilli, C., Pantano, P., 2014. Multiple Sclerosis: Altered Thalamic Resting-State Functional Connectivity and Its Effect on Cognitive Function. Radiology, 131688.

Tononi, G., Edelman, G.M., Sporns, O., 1998. Complexity and coherency: integrating information in the brain. Trends Cogn Sci. 2, 474-484.

Touboul, J.D., Ermentrout, G.B., 2011. Finite-size and correlation-induced effects in mean-field dynamics. J.Comput.Neurosci. 31, 453-484.

Treves, A., 1993. Mean-field analysis of neuronal spike dynamics. Netw.Comput.Neural Syst 4, 259-284.

Tzourio-Mazoyer, N., Landeau, B., Papathanassiou, D., Crivello, F., Etard, O., Delcroix, N., Mazoyer, B., Joliot, M., 2002. Automated anatomical labeling of activations in SPM using a macroscopic anatomical parcellation of the MNI MRI single-subject brain. Neuroimage. 15, 273-289.

Uhlhaas, P.J., Singer, W., 2006. Neural synchrony in brain disorders: relevance for cognitive dysfunctions and pathophysiology. Neuron 52, 155-168.

Valsasina, P., Rocca, M.A., Absinta, M., Sormani, M.P., Mancini, L., De, S.N., Rovira, A., Gass, A., Enzinger, C., Barkhof, F., Wegner, C., Matthews, P.M., Filippi, M., 2011. A multicentre study of motor functional connectivity changes in patients with multiple sclerosis. Eur.J.Neurosci. 33, 1256-1263.

van Dellen E., Douw, L., Hillebrand, A., de Witt Hamer, P.C., Baayen, J.C., Heimans, J.J., Reijneveld, J.C., Stam, C.J., 2014. Epilepsy surgery outcome and functional network alterations in longitudinal MEG: A minimum spanning tree analysis. Neuroimage. 86, 354-363.

van Dellen E., Hillebrand, A., Douw, L., Heimans, J.J., Reijneveld, J.C., Stam, C.J., 2013. Local polymorphic delta activity in cortical lesions causes global decreases in functional connectivity. Neuroimage. 83C, 524-532.

van Dellen, E., de Witt Hamer, P.C., Douw, L., Klein, K., Heimans, J.J., Stam, C.J., Reijneveld, J.C., Hillebrand, A., 2013. Connectivity in MEG resting-state networks increases after resective surgery for low-grade glioma and correlates with improved cognitive performance. Neuroimage:clinical 2, 1-7.

van den Heuvel, M.P., Hulshoff Pol, H.E., 2010. Exploring the brain network: a review on resting-state fMRI functional connectivity. Eur.Neuropsychopharmacol. 20, 519-534.

van den Heuvel, M.P., Kahn, R.S., Goni, J., Sporns, O., 2012. High-cost, high-capacity backbone for global brain communication. Proc.Natl.Acad.Sci.U.S.A 109, 11372-11377.

van den Heuvel, M.P., Mandl, R.C., Kahn, R.S., Hulshoff Pol, H.E., 2009a. Functionally linked resting-state networks reflect the underlying structural connectivity architecture of the human brain. Hum.Brain Mapp. 30, 3127-3141.

van den Heuvel, M.P., Sporns, O., 2011. Rich-club organization of the human connectome. J.Neurosci. 31, 15775-15786.

van den Heuvel, M.P., Stam, C.J., Kahn, R.S., Hulshoff Pol, H.E., 2009b. Efficiency of functional brain networks and intellectual performance. J.Neurosci. 29, 7619-7624.

van den Heuvel, M.P., Stam, C.J., Boersma, M., Hulshoff Pol, H.E., 2008. Small-world and scale-free organization of voxel-based resting-state functional connectivity in the human brain. Neuroimage 43, 528-539.

Van Mieghem, P., Magdalena, S.M., 2005. Phase transition in the link weight structure of networks. Phys. Rev.E.Stat.Nonlin.Soft.Matter Phys. 72, 056138.

Van Mieghem, P., van Langen, S., 2005. Influence of the link weight structure on the shortest path. Phys. Rev.E.Stat.Nonlin.Soft.Matter Phys. 71, 056113.

van Putten, M.J., Tavy, D.L., 2004. Continuous quantitative EEG monitoring in hemispheric stroke patients using the brain symmetry index. Stroke 35, 2489-2492.

van Wijk, B.C., Stam, C.J., Daffertshofer, A., 2010. Comparing brain networks of different size and connectivity density using graph theory. PLoS.One. 5, e13701.

Vazquez-Marrufo, M., Gonzalez-Rosa, J.J., Vaquero, E., Duque, P., Borges, M., Gomez, C., Izquierdo, G., 2008. Quantitative electroencephalography reveals different physiological profiles between benign and remitting-relapsing multiple sclerosis patients. BMC.Neurol. 8, 44.

Vertes, P.E., Alexander-Bloch, A.F., Gogtay, N., Giedd, J.N., Rapoport, J.L., Bullmore, E.T., 2012. Simple models of human brain functional networks. Proc.Natl.Acad.Sci.U.S.A 109, 5868-5873.

Vindiola, M.M., Vettel, J.M., Gordon, S.M., Franaszczuk, P.J., McDowell, K., 2014. Applying EEG phase synchronization measures to non-linearly coupled neural mass models. Journal of Neuroscience Methods 226, 1-14.

Vogels, T.P., Abbott, L.F., 2005. Signal propagation and logic gating in networks of integrate-and-fire neurons. J.Neurosci. 25, 10786-10795.

Voulgari-Kokota, A., Fairless, R., Karamita, M., Kyrargyri, V., Tseveleki, V., Evangelidou, M., Delorme, B., Charbord, P., Diem, R., Probert, L., 2012. Mesenchymal stem cells protect CNS neurons against glutamate excitotoxicity by inhibiting glutamate receptor expression and function. Exp.Neurol. 236, 161-170.

Vrba J, A.G.B.K., 1999. 151-Channel whole-cortex MEG system for seated or supine positions. Recent Advances in Biomagnetism.Sendai, Japan: Tohoku University Press.

Wang, H., Hernandez, J.M., Van, M.P., 2008. Betweenness centrality in a weighted network. Phys.Rev.E.Stat. Nonlin.Soft.Matter Phys. 77, 046105.

Watts, D.J., Strogatz, S.H., 1998. Collective dynamics of 'small-world' networks. Nature 393, 440-442.

Weiskopf, N., Lutti, A., Helms, G., Novak, M., Ashburner, J., Hutton, C., 2011. Unified segmentation based correction of R1 brain maps for RF transmit field inhomogeneities (UNICORT). Neuroimage. 54, 2116-2124.

Wendling, F., Bellanger, J.J., Bartolomei, F., Chauvel, P., 2000. Relevance of nonlinear lumped-parameter models in the analysis of depth-EEG epileptic signals. Biological cybernetics 83, 367-378.

Whalen, C., Maclin, E.L., Fabiani, M., Gratton, G., 2008. Validation of a method for coregistering scalp recording locations with 3D structural MR images. Hum.Brain Mapp. 29, 1288-1301.

Winter, W.R., Nunez, P.L., Ding, J., Srinivasan, R., 2007. Comparison of the effect of volume conduction on EEG coherence with the effect of field spread on MEG coherence. Stat.Med. 26, 3946-3957.

Wong, K.F., Wang, X.J., 2006. A recurrent network mechanism of time integration in perceptual decisions. J.Neurosci. 26, 1314-1328.

Wu, Y., Bhat, P.R., Close, T.J., Lonardi, S., 2008. Efficient and accurate construction of genetic linkage maps from the minimum spanning tree of a graph. PLoS.Genet. 4, e1000212.

Wu, Z., Braunstein, L.A., Havlin, S., Stanley, H.E., 2006. Transport in weighted networks: Partition into superhighways and roads. Physical Review Letters 96, 148702.

Yeo, B.T., Krienen, F.M., Sepulcre, J., Sabuncu, M.R., Lashkari, D., Hollinshead, M., Roffman, J.L., Smoller, J.W., Z+Âllei, L., Polimeni, J.R., 2011. The organization of the human cerebral cortex estimated by intrinsic functional connectivity. Journal of neurophysiology 106, 1125-1165.

Yger, P., El, B.S., Destexhe, A., Fregnac, Y., 2011. Topologically invariant macroscopic statistics in balanced networks of conductance-based integrate-and-fire neurons. J.Comput.Neurosci. 31, 229-245.

Yook, S.H., Jeong, H., Barabasi, A.L., 2002. Modeling the Internet's large-scale topology. Proc.Natl.Acad.Sci.U.S.A 99, 13382-13386.

Zavaglia, M., Astolfi, L., Babiloni, F., Ursino, M., 2006. A neural mass model for the simulation of cortical activity estimated from high resolution EEG during cognitive or motor tasks. J.Neurosci.Methods 157, 317-329.

Zemanova, L., Zhou, C., Kurths, J., 2006. structural and functional clusters of complex brain networks. Physica D: Nonlinear phenomena 224, 202-212.

Zetterberg, L.H., Kristiansson L., Mossberg, K., 1978. Performance of a model for a local neuron population. Biol. Cybern. 31, 15-26.

Zhou, C., Zemanova, L., Zamora, G., Hilgetag, C.C., Kurths, J., 2006. Hierarchical organization unveiled by functional connectivity in complex brain networks. Phys.Rev.Lett. 97, 238103.

Zumer, J.M., Brookes, M.J., Stevenson, C.M., Francis, S.T., Morris, P.G., 2010. Relating BOLD fMRI and neural oscillations through convolution and optimal linear weighting. Neuroimage. 49, 1479-1489.

Appendix

Het doel van dit proefschrift was om te onderzoeken of klinische verschijnselen (fysieke beperkingen en cognitieve stoornissen) bij MS verklaard konden worden door verstoring van functionele hersenennetwerken en vervolgens of verstoring van functionele hersenennetwerken een brug kon vormen tussen structurele pathologie en klinische verschijnselen bij MS patiënten. Een belangrijke motivatie hiervoor is dat tot op heden nog niet goed begrepen wordt waardoor er klinische verschijnselen ontstaan bij patiënten met MS. Het is bekend dat bij MS patiënten littekens ontstaan in de hersenen, zogenoemde witte stof laesies. Er blijkt echter een discrepantie te zijn tussen het aantal witte stof laesies en de klinische verschijnselen van de patiënt: het kan namelijk heel goed voorkomen dat mensen met weinig laesies veel klachten hebben en vice-versa. Om die reden is er de afgelopen decennia veel onderzoek gedaan naar alternatieve verklaringen voor het ontstaan van klinische verschijnselen bij MS patiënten. Het centraal thema in dit proefschrift is het idee dat hersenactiviteit, en in het bijzonder de communicatie tussen hersengebieden, beide cruciaal zijn voor motoriek en cognitie en dat een verstoring hiervan zou kunnen leiden tot klinische verschijnselen bij MS patiënten. Daarbij is het idee dat elke vorm van structurele schade tot gevolg zou moeten hebben dat er verstoring optreedt van hersenactiviteit of communicatie tussen hersengebieden. Hierbij is de verwachting dat de mate waarin dit optreedt, afhangt van de locatie van de structurele schade. Structurele schade op een niet centrale plek in het functionele netwerk zal waarschijnlijk weinig effect hebben op de rest van het functionele netwerk en dus ook weinig invloed op klinische verschijnselen, en vice versa.

Om de rol van functionele netwerk organisatie als brug tussen structurele pathologie en klinische verschijnselen te begrijpen, is er behoefte aan een theoretisch kader van waaruit het verband tussen structuur en functie verklaard kan worden. Wanneer een dergelijk kader wordt opgesteld, kunnen de daaruit volgende formules of principes toegepast worden om de relatie tussen structurele en functionele netwerk veranderingen bij MS te begrijpen. De eerste twee hoofdstukken vormen de basis voor een dergelijk kader.

In **hoofdstuk 2** is een simulatie studie uitgevoerd waarbij het achterliggend doel was om te onderzoeken of zogeheten 'neural mass' modellen gebruikt kunnen worden om hersenactiviteit of functionele netwerken te simuleren onder pathofysiologische omstandigheden zoals bij MS. Indien dit het geval is zou onderzocht kunnen worden in hoeverre structurele schade zoals corticale atrofie, thalamus atrofie, witte stof lesies en afname in witte stof integriteit van invloed zijn op locale en globale eigenschappen van functionele netwerken bij MS. Neural mass modellen simuleren de gemiddelde activiteit van een neuronale populatie, zonder dat de activiteit van de afzonderlijke individuele neuronen in acht wordt genomen. Om te bewerkstelligen dat de activiteit van een neuronale populatie beschreven kan worden door slechts de gemiddelde activiteit van een populatie zijn een aantal aannames vereist. Een van de aannames is dat neuronen in de neuronale populatie identiek zijn en dat de activiteit van elk neuron beschreven kan worden door middel van dezelfde statistiek. Door deze aanname kan de activiteit van alle neuronen vervangen worden door het gemiddelde, de zogeheten gemiddelde-veld benadering. Echter realistische neuronale populaties en

neuronale populaties bij ziektes zoals bij MS zijn niet homogeen (niet alle neuronen zijn hetzelfde en het aantal verbindingen van elk neuron varieert). Daarom is in dit hoofdstuk onderzocht of neural mass modellen ook onder inhomogene omstandigheden nog steeds een goede weergave zijn voor de gemiddelde activiteit van een neuronale populatie. De resultaten van deze studie laten zien dat de neural mass modellen alleen onder specifieke omstandigheden, zoals een hoge verbindingsdichtheid en een minimale netwerk omvang, in staat zijn om de gemiddelde activiteit van een neuronale populatie weer te geven. Wanneer aan deze voorwaarden wordt voldaan, dan zijn neuronen in de neuronale populatie in staat om te synchroniseren, waardoor de bijdrage van hoog frequente signalen aan het gemiddelde signaal afneemt. Gezien het feit dat neural mass modellen beschouwd kunnen worden als laag-doorlaat filters kunnen ze onder dergelijke omstandigheden het gemiddelde van een neuronale populatie goed weergeven.

In **hoofdstuk 3** is een ander deel van het theoretisch kader onderzocht. Het doel was om modaliteits-invariante functionele verbindingen aan te tonen en de relatie met het onderliggend structureel netwerk te onderzoeken. Om deze modaliteits-invariante functionele verbindingen te kwantificeren werden functionele MRI (fMRI) en magnetoencephalografie (MEG) metingen verricht. Voor beide modaliteiten werden functionele netwerken geconstrueerd, waarbij gebruik werd gemaakt van dezelfde atlas (een 'kaart' die de grootte en locatie van hersenregio's definieert). Vervolgens werd gekwantificeerd tussen welke regio's beide modaliteiten gekenmerkt werden door sterke functionele interacties. Bij deze analyse werd een modaliteits-invariant functioneel netwerk gevonden in temporo-posterieure gebieden, waaronder de precuneus, een regio die centraal gelegen is in het functionele hersennetwerk. Met behulp van neural mass modellen, werd vast gesteld dat dit modaliteits-invariant functioneel netwerk ontstaat na een fase overgang voor globale functionele connectiviteit. Met een fase overgang wordt een snelle verandering van een eigenschap in een systeem verstaan. Vervolgens werd ontdekt dat dit modaliteits-invariant functioneel netwerk geen één op één weerspiegeling was van het onderliggende structurele netwerk. Een eenvoudig analytisch model dat gebruik maakt van eigenschappen van het structureel netwerk was in staat tot op ongeveer 30% van de bestaande functionele verbindingen en de sterkte daarvan te verklaren. Dit model houdt in dat op basis van de Euclidische afstand tussen twee hersengebieden en het product van de degree tussen de gebieden functionele verbindingen verklaard kunnen worden. Hierbij refereert degree naar het aantal verbindingen dat een hersengebied heeft met alle andere hersengebieden. Met andere woorden, hoe dichter twee gebieden bij elkaar liggen en des te groter de degree van die twee gebieden, des te groter de functionele interactie tussen die twee gebieden is. Het is gebleken dat voornamelijk het product van de degrees tussen twee gebieden cruciaal is om te voorspellen hoe sterk de functionele interactie is tussen hersengebieden, ongeacht of fMRI of MEG gebruikt wordt als techniek om de functionele verbindingen te meten.

In **hoofdstuk 4** is onderzocht hoe een 'minimum spanning tree' (MST), een sub-netwerk dat geen lussen bevat, gebruikt kan worden om de organisatie of topologie van structurele of functionele hersennetwerken te karakteriseren. De motivatie voor deze studie is dat conventionele

netwerkmaten gevoelig zijn voor eigenschappen van het netwerk die niet direct gerelateerd zijn aan topologie, zoals netwerkdichtheid, netwerkgrootte en de gemiddelde sterkte van de verbindingen. Hierdoor kunnen resultaten die verkregen worden met behulp van deze conventionele maten een vertekende weergave geven van de topologie van het netwerk. In deze studie hebben we daarom de volgende hypotheses opgesteld: 1) de MST is ongevoelig voor eigenschappen van het netwerk die niet direct te maken hebben met de topologie; 2) de topologie van de MST is een goede weergave van de topologie van het onderliggend netwerk; 3) verkregen resultaten met behulp van de MST zijn robuust. In het kader van de eerste hypothese zijn er simulaties uitgevoerd waarbij netwerkdichtheid en gemiddelde sterkte van de verbindingen stapsgewijs zijn bijgesteld om het effect hiervan op conventionele netwerk maten en de MST te onderzoeken. Hieruit bleek dat in tegenstelling tot de MST alleen de conventionele netwerk maten gevoelig waren voor veranderingen van deze netwerk eigenschappen. In het kader van de tweede hypothese zijn reguliere netwerken (netwerken waarbij de degree voor elke node hetzelfde is) en scale-free netwerken (netwerken gekenmerkt door de aanwezigheid van gebieden met een hoge degree) stapsgewijs gerandomiseerd tot 'random' netwerken (netwerken waarbij de aanwezigheid van een verbinding gebaseerd is op een kans). Uit deze analyse bleek dat de topologie veranderingen van de MST sterk gerelateerd waren aan de topologie veranderingen van het onderliggend netwerk. Het belang van deze bevinding is dat de MST dus relevante eigenschappen van het onderliggend netwerk weet te behouden en dus een goede weergave is van de topologie van het onderliggend netwerk. Ten slotte bleek dat door modificaties aan te brengen aan de MST, de topologie lang stabiel en robuust blijft.

In de volgende hoofdstukken hebben we de opgedane kennis uit de eerste hoofdstukken toegepast op sructurele en functionele hersennetwerken bij MS. Tevens zijn er analyses gedaan naar lokale hersenactiviteit bij MS. Bij verschillende neurodegeneratieve ziekten zoals de ziekte van Parkinson en de ziekte van Alzheimer blijkt er een toename te zijn van trage hersenactiviteit. Dit is vaak gerelateerd is aan klinische verschijnselen. Gezien de recente aanwijzingen dat MS ook een neurodegeneratieve ziekte is, is in **hoofdstuk 5** onderzocht of er ook een vertraging optreedt van hersenactiviteit bij MS patiënten en of dit in verband staat met klinische verschijnselen. In het kader hiervan zijn er bij een groep MS patiënten met een relatief korte ziekteduur MEG metingen verricht. Hierbij vonden wij dat er een ook vertraging optreedt van hersenactiviteit bij patiënten met MS. Deze vertraging werd voornamelijk gevonden in achterste hersengebieden. Ten slotte vonden we dat vertraging van hersenactiviteit een klinisch relevante bevinding bleek te zijn bij MS patiënten, omdat deze vertraging samenhing met slechtere cognitieve functies en in het bijzonder met tragere informatie verwerkingssnelheid.

In **hoofdstuk 6** hebben we onderzocht of de sterkte van de communicatie (=functionele connectiviteit) tussen hersengebieden verstoord raakt bij MS en of dit van klinische relevantie is. Wederom zijn MEG metingen verricht om in dit geval functionele connectiviteit tussen hersengebieden te schatten. In dit hoofdstuk is functionele connectiviteit op twee manieren onderzocht. Ten eerste is functionele connectiviteit geschat tussen alle hersengebieden in de gebruikte atlas. Ten tweede

is functionele connectiviteit geschat tussen gebieden die behoren bij zogeheten 'resting-state' netwerken (RSNs). RSNs kunnen beschouwd worden als clusters van gebieden die onderling een hoge mate van communicatie vertonen. Uit de analyses bleek dat afhankelijk van de frequentie band er een toename of afname was van de functionele connectiviteit tussen hersengebieden bij MS. Deze veranderingen werden voornamelijk gevonden voor de RSNs. Het bleek verder dat in het bijzonder toename of afname van functionele connectiviteit in deze RSNs van klinische relevantie was. Verhoging van de functionele connectiviteit in het zogeheten 'default mode netwerk' in de beta band was geassocieerd met een toename van fysieke beperkingen en cognitieve stoornissen bij MS patiënten. Verder werd ontdekt dat verdunning van een centrale hersenstructuur, de thalamus, gerelateerd was aan een afname van functionele connectiviteit in het visueel netwerk in de alpha2 band bij MS patiënten.

Na het onderzoeken van hersenactiviteit en functionele connectiviteit bij MS was de volgende stap om functionele netwerk topologie bij MS in kaart te brengen. De reden hiervoor is dat informatie over de hersennetwerken gemist kan worden wanneer alleen naar de sterkte van de netwerk verbindingen gekeken wordt zonder te kijken naar de organisatie hiervan. In **hoofdstuk 7** is onderzocht of de topologie van functionele hersennetwerken verstoord raakt bij MS door middel van het construeren van de MST. Voor het schatten van de functionele hersennetwerken zijn eveneens MEG metingen gebruikt. Bevindingen toonden minder geïntegreerd functionele netwerken bij MS patiënten aan. Dit houdt in dat de communicatie tussen twee willekeurige hersengebieden over een langere afstand gaat en dat er een afname is van hersengebieden met veel verbindingen bij MS. Deze minder geïntegreerde functionele netwerken bleken geassocieerd te zijn met cognitieve stoornissen bij MS patiënten. Dit toont aan dat verstoring van functionele hersennetwerken van klinisch belang is.

In de laatste hoofdstukken (**hoofdstuk 8 en 9**) werd onderzocht in hoeverre het fenomeen van minder geïntegreerde functionele netwerken bij MS een reproduceerbare bevinding was. Verder werd onderzocht in hoeverre deze bevindingen gerelateerd waren aan structurele pathologie bij MS, en in het bijzonder atrofie (verlies van hersenvolume). In **hoofdstuk 8** werd onderzocht in hoeverre veranderingen in functionele hersennetwerken bij MS samenhingen met veranderingen van structurele netwerken op basis van corticale dikte correlaties. De motivatie voor deze studie is dat atrofie één van de belangrijkste indicatoren is voor progressie van de ziekte en dat patronen van verdunning ook invloed kunnen hebben op, of in ieder geval gecorreleerd zijn aan de communicatie tussen hersengebieden. Een van de aannames is immers dat uit activiteit van een groot aantal dendrieten (signaal ontvangers van neuronen) tezamen informatie afgeleid kan worden over de communicatie tussen hersengebieden. Atrofie kan leiden tot afname van (volume van) dendrieten en daardoor tot een verstoring van de communicatie of functionele connectiviteit. Voor deze studie zijn MEG metingen en dikte metingen van de hersenschors met behulp van MRI verricht bij MS patiënten met een langere ziekte duur. Uit de stapsgewijze analyses is gebleken dat er ten eerste wederom een afname was van functionele connectiviteit in de alpha2 band en een toename van

functionele connectiviteit in de delta en theta band. Ten tweede werd gevonden dat functionele netwerk topologie, op basis van de MST, opnieuw gekenmerkt werd door minder integratie. Ten derde bleek dat een verstoring van functionele hersennetwerken gepaard ging met een verstoring van structurele netwerken. De relevantie van deze bevindingen is dat er uitsluitend een relatie bestaat tussen functionele netwerken en atrofie als we de anatomie of structuur van de hersenen beschouwen als complex netwerk.

In het laatste **hoofdstuk (9)** is de hypothese opgesteld dat er een wederzijdse beïnvloeding is tussen verstoring van functionele hersennetwerken en thalamus atrofie bij MS. Verder werd verondersteld dat verstoring van dit thalamo-corticaal systeem geassocieerd is met klinische verschijnselen. In het kader van deze studie zijn zowel MEG als fMRI metingen verricht en is bovendien ook het volume van de thalamus gekwantificeerd. Uit dit onderzoek bleek dat er een verhoging optrad van functionele connectiviteit (MEG) in de theta band en een verlaging van functionele connectiviteit in de alpha2 band. Verder werd een verhoging geobserveerd van functionele connectiviteit (fMRI) vanuit de thalamus naar de rest van de hersenen. Op basis van de MST (MEG) werd opnieuw een minder geïntegreerd functioneel netwerk waargenomen. Dit minder geïntegreerd functioneel netwerk was zowel met thalamus atrofie als met verhoogde functionele connectiviteit vanuit de thalamus naar de rest van de hersenen gerelateerd. Bovendien bleek dat minder geïntegreerde functionele netwerken ook samenhingen met zowel fysieke beperkingen als cognitieve stoornissen. Concluderend hebben we kunnen bevestigen dat schade aan de thalamus gepaard gaat met globale netwerk verstoring van de gehele hersenen en dat dit klinisch relevant is.

Appendix

LJ Balk
Department of Neurology,
VU University medical center
Amsterdam, The Netherlands

F Barkhof
Department of Radiology and
Nuclear medicine, VU University medical center,
Amsterdam, The Netherlands

C. Beaulieu
Department of Biomedical Engineering,
University of Alberta, Edmonton, Alberta,
Canada

M Daams
Department of Radiology and
Nuclear medicine, VU University medical center,
Amsterdam, The Netherlands

A Daffertshofer
MOVE research institute, VU University,
Amsterdam, The Netherlands

E van Dellen
Department of Psychiatry, Brain Center Rudolf
Magnus, University Medical Center Utrecht,
Utrecht, the Netherlands.

BW van Dijk
Department of Clinical Neurophysiology,
Department of Physics and medical
technology, VU University medical center,
Amsterdam, The Netherlands

L Douw
Martinos Center for Biomedical Imaging,
Massachusetts General Hospital, Boston,
Massachusetts, USA, Department of anatomy
and neurosciences, VU University, Amsterdam,
The Netherlands

JJG Geurts
Department of anatomy and neurosciences,
VU University, Amsterdam, The Netherlands

G Gong
National Key Laboratory of Cognitive
Neuroscience and Learning, School of Brain
and Cognitive Sciences, Beijing Normal
University, Beijing, China

A Hillebrand
Department of Clinical Neurophysiology,
VU University medical center, Amsterdam,
The Netherlands

ML van der Meer
Department of Neurology, Amstelland
ziekenhuis, Amstelveen, The Netherlands

CH Polman
Department of Neurology, VU University
medical center Amsterdam, The Netherlands

PJW Pouwels
Department of Physics and medical echnology,
VU University medical center, Amsterdam,
The Netherlands

MM Schoonheim
Department of anatomy and neurosciences,
VU University, Amsterdam, The Netherlands

MD Steenwijk
Department of Radiology and
Nuclear medicine, VU University medical center,
Amsterdam, The Netherlands

CJ Stam
Department of Clinical Neurophysiology,
VU University medical center, Amsterdam,
The Netherlands

BMJ Uitdehaag
Department of Neurology, VU University
medical center, Amsterdam, The Netherlands

H Vrenken
Department of Physics and medical
technology, Department of Radiology and
Nuclear medicine, VU University medical center,
Amsterdam, The Netherlands

Appendix

Prejaas K.B. Tewarie, geboren op 8 februari 1985 te Amsterdam, rondde zijn VWO af aan het Comenius Lyceum te Amsterdam in 2003 en startte daarna de opleiding Geneeskunde aan de Vrije Universiteit in Amsterdam. Door interesse in de Natuurkunde besloot hij om naast Geneeskunde te starten met de bachelor opleiding Natuurkunde in 2006 aan de Vrije Universiteit in Amsterdam. Zijn interesse in de neurologie werd gewekt tijdens het keuzevak neurowetenschappen in het derde jaar van de studie Geneeskunde wat verder heeft geleid tot een keuze-coschap bij de Neurochirurgie in het VUmc, een keuze-coschap Neurologie in het Neurologie en Neurochirurgie instituut (UCL, Queen Square) in Londen en tot een wetenschappelijke stage over transcraniele magnetische stimulatie bij Parkinson patienten onder begeleiding van dr. Y. Van der Werf. Na het behalen van zijn artsexamen in 2010 startte hij met wetenschappelijk onderzoek naar functionele hersennetwerken bij MS, onder begeleiding van prof. dr. C.H. Polman, prof.dr. C.J. Stam, dr. ir. A. Hillebrand en prof. dr. F. Barkhof, hetgeen heeft geleid tot dit proefschrift. Na het behalen van zijn bachelordiploma Natuurkunde in 2012 startte hij met de master Natuurkunde eveneens aan de Vrije Universiteit in Amsterdam. In het kader hiervan heeft hij keuzevakken over computational neuroscience gevolgd aan de Radboud Universiteit in Nijmegen. Zijn masterproject heeft hij verricht bij de Fysica en medische technologie in het VUmc onder begeleiding van dr. B.W. van Dijk en prof.dr. A. Daffertshofer. De master Natuurkunde heeft hij begin 2014 afgerond en zijn masterscriptie is tevens opgenomen als hoofdstuk 2 in dit proefschrift .

Prejaas K.B. Tewarie was born on February 8th 1985, in Amsterdam. After finishing high school at the Comenius Lyceum in Amsterdam he started Medical School at the VU University in Amsterdam in 2003. Due to strong interest in Physics, he also decided to start a Bachelor's program in Physics at the VU University in Amsterdam in 2006, which he completed in 2012. His interest in Neurology started during an elective course on Neuroscience in his third year of Medical School. This interest subsequently resulted into a clinical elective at the Neurosurgery department at the VUmc, a clinical elective at the Neurology and Neurosurgery Institute (UCL, Queen Square) in London and an internship on transcranial magnetic stimulation in Parkinson's disease patients. The latter was done under the supervision of dr. Y. Van der Werf. After receiving his medical degree in 2010, he began his research on functional brain networks in MS under the supervision of prof. dr. C.H. Polman, prof. dr. C.J. Stam, dr. A. ir. Hillebrand and prof. dr. F. Barkhof. In 2012 he started a Master's program in Physics also at the VU University in Amsterdam. For his Master education, he followed elective courses on computational neuroscience at the Radboud University in Nijmegen. He did his master project at the department of Physics and Medical Technology at the VUmc under supervision of dr. B.W. van Dijk and prof. A. Daffertshofer. He completed his MSc in Physics in the beginning of 2014. His Master thesis is included as a chapter in this dissertation (Chapter 2).

Appendix

Bij dezen wil ik niet alleen degenen bedanken die bijgedragen hebben aan dit proefschrift, maar iedereen die mij geholpen heeft met het traject dat ik nu achter de rug heb: proefschrift en studie Natuurkunde. Hoewel het niet altijd aan me te zien was, is dit is een loodzwaar en uitputtend traject geweest. Als ik terug kijk, vraag ik mezelf weleens af waar ik de energie vandaan heb gehaald, want als ik het *nu* weer opnieuw zou moeten doen, was het me zeker niet gelukt. Vanwege het besef dat jullie hulp onmisbaar is geweest in deze uitputtingsslag, wil ik jullie mijn dank betuigen. Alhoewel ik mijn proefschrift heb afgerond, heb ik eigenlijk niet het idee dat ik 'iets' daadwerkelijk heb afgerond, dus eigenlijk komt dit dankwoord naar mijn idee ook te vroeg...

Allereerst wil ik alle MS patienten, hun families en alle vrijwilligers bedanken voor de moeite die ze hebben genomen om deel te nemen aan onze vele onderzoeken. Zonder jullie inbreng en hulp was dit onderzoek niet mogelijk geweest. Ik wil jullie ook erg bedanken voor de fijne en inspirerende gesprekken die ik met jullie heb gehad tijdens jullie vele bezoeken.

Promotoren en co-promotoren:
Aan jullie wil ik als eerste dit zeggen: 'Dit proefschrift is alleen en ook alleen tot stand gekomen, omdat ik stond op de schouders van reuzen'. Uiteraard valt mijn werk in het niet vergeleken met degene die ik hier citeer!

De eerste reus, beste Chris, de basis en het fundament voor dit proefschrift heb jij gelegd. In de tijd dat aan mij getwijfeld werd over de haalbaarheid van mijn plannen (Natuurkunde en Geneeskunde), heb jij mij niet alleen de kans geboden om onderzoek te doen, maar ook de vrijheid gegeven en de ruimte geboden om mijn eigen weg in te slaan. Vanaf het eerste moment heb je er vertrouwen in gehad dat het allemaal goed zou komen. Mijn dank hiervoor is niet in woorden uit te drukken, omdat dit vertrouwen mij de rust heeft gegeven wat essentieel was om zowel mijn onderzoek als mijn studie succesvol af te ronden.

De tweede reus, beste Kees, als er een fundament staat moet er nog gebouwd worden. Dat bouwen heb ik onder jouw begeleiding gedaan en ik ben je ontzettend dankbaar dat jij mij hierbij blijvend hebt kunnen inspireren. Anders was dat bouwen heel saai geweest. Ik heb de afgelopen jaren met bewondering staan kijken hoe je in staat bent geweest om nieuwe ideeen te genereren en hoe je die op mij heb weten over te brengen. Die nieuwe ideeen vinden hun oorsprong dan ook in de indrukwekkende visie die je hebt op de hersenen, een visie waarnaar ik altijd met alle plezier heb geluisterd. De combinatie van jouw strakke begeleiding en het tegelijkertijd bieden van ruimte, is denk ik het meest essentieel geweest voor de afronding van mijn proefschrift. Echter, waarvoor ik je het meest dankbaar ben is iets dat dit proefschrift overstijgt. Voordat ik in aanraking was gekomen met jouw onderzoek, heb ik lang getobd of de kennis die ik zou opdoen met beide studies ooit samen zou kunnen komen. Gelukkig heb jij een 'boek' voor mij opengeslagen dat illustreert hoe ik wis- en natuurkunde kan gebruiken om de hersenen beter te begrijpen. Ik hoop dat ik dit boek nooit meer hoef dicht te slaan.

De derde reus, beste Arjan, hoewel dat nooit aan je te merken is, ben je ook een reus in de MEG wereld. Ik wil je bedanken voor de vele dingen die ik van je geleerd heb, waarbij er toch één onderwerp centraal staat: 'beamforming'. De introductie van beamforming door jou heeft het allergrootste gedeelte van mijn onderzoek mogelijk gemaakt, in het bijzonder het 'multi-modal imaging' onderzoek. Ondanks dat je het altijd ontzettend druk had, kon ik altijd bij je langs lopen en je storen voor vragen. Soms waren dit ook stomme vragen (hierbij mijn excuses) over scriptjes die maar niet wilde werken, uitleg over post-processen van MEG data welke je al eerder gegeven had, maar ondanks dat bleef je altijd kalm en behulpzaam. Jij was voor mij het slot achter de deur voor elk artikel, want na jouw kritische blik wist ik dat er geen analyse fouten in een artikel konden zitten, dat de kromme Engelse zinnen waren omgebuigd tot goed Engels, en dat mijn interpretatie van de resultaten een behoorlijke mate van kritiek kon doorstaan.

De vierde reus, beste Frederik, het is niet alleen jouw onbetwiste kennis over neuroradiologie dat mij opgevallen is de afgelopen jaren, maar ook jouw translationele blik en ideeen op het onderzoek binnen onze groep. Jouw input over 'multi-modal imaging' is dan ook erg belangrijk geweest voor de afronding van mijn laatste artikelen over MEG/MRI. Ik wil je verder bedanken voor de steun die ik van je heb gehad in de loop der jaren en de steun die ik nog steeds van je krijg bij nieuwe projecten.

Beste Bob, jij bent verreweg degene van wie ik het meest heb geleerd de afgelopen jaren; van begeleiding van mijn bachelorproject tot begeleiding van mijn masterproject. Waar Kees een boek voor mij heeft opengeslagen, heb jij laten zien hoe ik dat boek moet gebruiken en heb jij uitleg gegeven over dat boek: van quasi-statische Maxwell vergelijkingen, de kabelvergelijking, Hogdkin-Huxley vergelijkingen tot SQUIDs en 'Josephson junctions' en ga zo maar door. Naast deze bagage heb je mij ook nog de nodige programmeervaardigheden bijgebracht. Ook bij jou kon ik te allen tijde terecht voor vragen. Mijn dank is groot.

Beste Andreas, ook jou wil ik heel erg bedanken. Wanneer ik bij jou in de kamer kwam, kreeg ik altijd de indruk dat ik bij de slimste man van de wereld op bezoek was. Iedere keer weer heb ik genoten van je scherpe analyses en uitleg over complexe onderwerpen. Daarnaast heb jij mij een voorproefje gegeven over de moeilijke hoofdstukken van het 'boek' en elke keer dat ik jouw kamer verliet ging ik daarom weg met ontzettend veel inspiratie. Het lijkt me ontzettend leuk om in de toekomst nog veel van je te leren, zodat ik deze moeilijke hoofdstukken kan verkennen. Om dat te doen realiseer ik mij inmiddels heel goed dat mijn aandacht niet meer verstrooid mag zijn, maar juist gefocust moet zijn.

Ik wil graag de leden van de leescommissie hartelijk bedanken voor het beoordelen van mijn proefschrift en het zitting nemen als opponent tijdens mijn verdediging: prof.dr. A. Daffertshofer, prof.dr. B.M.J. Uitdehaag, prof.dr.ir. M.J.A.M. van Putten, prof.dr. R.Q. Hintzen, dr. E.C.W. van Straaten en dr. H. Vrenken.

Beste Bernard, nadat jij het roer van Chris hebt overgenomen, heb jij, net als hem, mij de volledige ruimte en steun gegeven voor mijn onderzoek. Ik hoop dat ik nog lang mijn wetenschappelijke bijdrage kan leveren aan onderzoek binnen het MS centrum. Joep en Bob, zonder jullie beide had ik hier niet gestaan, want ik ben op deze plek terecht gekomen via jullie. Verder wil ik jullie alle drie bedanken voor de leerzame tijd en voor de feedback tijdens het voorbereiden van presentaties voor bijeenkomsten en congressen.

En dan de MS collega's, de thuisbasis: Judith, Anke, Lisanne, Jessica, Joram, Eva, Libertje, Marieke, en nu ook Marloes en Cyra. Eva, dank je wel voor je begeleiding in het begin van mijn onderzoekstijd, dat was wel echt nodig. Judith en Anke, wat is het toch fijn om zorgzame kamergenoten te hebben die je voorzien van lekker eten en je herinneren aan afspraken. Lisanne en Jessica, dank jullie wel voor jullie grote mate van flexibiliteit in de samenwerking met deze chaotische collega. Zonder jullie hulp met het plannen, jullie inhoudelijke input, het overnemen van EDSSsen en het inspringen bij andere werkzaamheden had ik het waarschijnlijk niet gered. Ook alle andere MS collega's, ik wil jullie bedanken voor jullie hulp en de gezellige tijd.

Edwin, ik wil je bedanken voor de leuke en vruchtbare (inhoudelijke) discussies die we samen hebben gehad. Ik denk dat we allebei erg blij zijn dat ons grootste gezamenlijke project eindelijk is afgerond, op naar de volgende projecten! Menno, het is maar dat jij het prima vond dat ik met de 'presto' data aan de slag kon, anders was meer dan de helft van dit proefschrift er niet geweest! Martijn, je weet, we zijn allebei 'hooggeleid G', dus het gaat helemaal goedkomen met onze nieuwe projecten.

Ndedi, Karin, Nico en Peter Jan, heel erg bedankt voor de honderden MEG metingen die jullie hebben verricht. Daarbij wil ik Ndedi nog extra bedanken voor haar hulp bij de vele stappen die verricht moesten worden om de MEG data te projecteren naar 'source-space'. Ook Sandra wil ik erg bedanken voor haar hulp bij de logistiek en planning. Natasja, Jos, Laura, Josca en Niels, jullie zijn onmisbaar geweest in de hele schakel van onderzoek dat plaats gevonden heeft bij ons. Dankzij jullie inspanning heb ik mij veel meer kunnen richten op de inhoud van mijn onderzoek. Ontzettend bedankt! Danielle en Gianina, ondanks de complexe schema's van de trial patienten en de vele agenda's waar jullie rekening mee moesten houden, hebben jullie alsnog dusdanig weten te plannen zodat ik tussendoor nog naar mijn werkcolleges en practica op de Universiteit kon gaan. Dit heb ik zeer gewaardeerd.

Verder wil ik uiteraard alle netwerkonderzoekers bij de KNF bedanken voor de vele discussies, de feedback en de leerzame momenten: Marjolein, Meichen, Gwenda, Ida, Dagmar, Linda, Niels, Alida, maar ook Sophie, Willem, Hanneke, Bernadette, Kim en Betty.

Alhoewel onze gezamenlijke projecten geen deel uitmaken van mijn proefschrift wil ik toch Jil en Piet Van Mieghem heel erg bedanken voor de vele leerzame momenten over de prachtige wiskunde en de prettige samenwerking.

Onderzoekers van de anatomie en neurowetenschappen wil ik graag ook bedanken: Marita, Geert, Antoine, Oliver, Hanneke en uiteraard ook Jeroen Geurts. Daarnaast wil ik ook Ysbrand bedanken, omdat hij degene is geweest die me enthiousiast heeft weten te maken over onderzoek binnen de neurowetenschappen.

Verder wil ik ook alle natuurkunde en wiskunde docenten bedanken die mij gedurende studie gesteund hebben, vaardigheden hebben bijgebracht en mij de ruimte hebben geboden om naast mijn studie volop bezig te zijn met onderzoek. In het bijzonder wil ik hierbij bedanken: Ivo van Stokkum, Wim Sterrenburg, Jaap Buning, Piet Blankert, Tjonnie Li, Ben Bakker, Klaas Allaart, Paul Tiesinga, Bert Kappen, Jan de Munck, Hugo Vrenken, Piet Mulders, Gerhard Raven en Fred MacKintosh.

Meester Jose, *Sabumnim*, discipline, geduld, doorzettingsvermogen en wilskracht zijn belangrijke eigenschappen die mij hier doorheen gesleept hebben. Deze heeft u mij bijgebracht, Kiap!

Bij dezen wil ook al mijn vrienden, neven en nichten, neefjes en nichtjes, zwagers en bhaujis, ooms en tantes bedanken voor hun steun de afgelopen jaren. Neem mij niet kwalijk dat ik niet al jullie namen noem, want dat zijn er echt heel veel!

In het bijzonder wil ik al mijn grootouders bedanken en jullie graag dit zeggen: '*mere liye bahut garv ki baat hai, ki main aap logo ka pota aur nati hun. Yeh 'proefschrift' sirf aapke ashirwaad se puri hogayi hai. Isliye, main sir jhukake aap logo ka dhanyavaad karta hun, pranaam'.*

Swamiji, '*apareyam itas tvaneyaam, prakritim viddhi me paraam, jeeva bhootaam mahaa baaho, yayedam dhaaryate jagat'.*

Dan mijn broers en zussen. Minyandi en Rema, voor jullie schiet ik woorden tekort, maar hiebij een poging. Minyandi *'brother in, brother out'*, Rema '.....' (Safafitisch), Prewien *'what you wanna say broer?'* Sweta *'fijn om zo'n zorgzame zus te hebben!'*, Kirna *'no mind'*, Vyasa *'Boyka, Oess!'*, Prewesh *'we schieten de pijlen en knallen sowieso als vulkanen!'*, dank je wel voor het mij bijbrengen van photoshop-skills. Zonder jouw hulp had ik geen enkele figuur van mijn proefschrift kunnen maken. Uiteraard wil ik ook bedanken: Shafira, Bauji, Shivan en de nieuwe generatie!

Ook mijn tweede vader en moeder, oom Kesho en Mousi wil ik graag bedanken voor hun steun, liefde en zorg.

Ma en Pa, voor jullie heb ik eigenlijk helemaal geen woorden, dit is voor jullie...